Development of A Microfluidic-Based Artificial Placenta Type Neonatal Lung Assist Device for Preterm Neonates

By

MOHAMMADHOSSEIN DABAGHI

B.Sc., M.Sc.

A Thesis

Submitted to the School of Graduate Studies

in Partial Fulfilment of the Requirements for the Degree of

Doctor of Philosophy in School of Biomedical Engineering

McMaster University

Development of A Microfluidic-Based Artificial Placenta Type Neonatal Lung Assist Device for Preterm Neonates

McMaster University DOCTOR OF PHILOSOPHY (2019)
Hamilton, Ontario, Canada

TITLE: Development of a microfluidic-based artificial placenta type neonatal lung assist device for preterm neonates

AUTHOR: Mohammadhossein Dabaghi

B.Sc. (Sharif University of Technology)

M.Sc. (Sharif University of Technology)

SUPERVISOR: Professor P. Ravi Selvaganapathy

CO-SUPERVISOR: Professor Christoph Fusch

NUMBER OF PAGES: xxii, 212

ABSTRACT

Among all organs, lungs are the last ones to grow and develop fully. As a result, extreme premature neonates may suffer from respiratory failure due to their immature lungs and will require respiratory support in the form of mechanical ventilation or extracorporeal membrane oxygenation (ECMO). In addition, extreme prematurity is recognized as the primary cause of neonatal morbidity and mortality. The conventional standard of care for respiratory support of preterm neonates with respiratory failure are invasive and may lead to long-term morbidities and complications. Hence, a non-invasive respiratory support technique named "Artificial Placenta" has been developed to address the issues and challenges associated with the current technologies. An artificial placenta type device is one designed to provide required oxygenation in room air via non-invasive access to the umbilical vessels without the need of any external pump. In this thesis, microfluidic and microfabrication technologies have been employed in the development of a pumpless neonatal lung assist device (LAD) for preterm neonates in two approaches: 1) design and develop novel microfabrication techniques to fabricate advanced microfluidic blood oxygenators with high gas exchange capacity and reduced form factor and 2) design and construct several modular LADs based on the oxygenators that were developed to fulfill the required gas transfer needs for these babies. The new microfluidic blood oxygenators with double-sided gas transfer channels were found to enhance oxygenation up to 343 % in room air and be easily scaled-up to achieve higher gas exchange capacities without a noticeable increase in priming volume. Furthermore, this microfabrication method has been utilized to make the largest all PDMS ultra-thin double-sided blood oxygenator with higher gas exchange capabilities. Also, a novel composite material made of PDMS and PTFE was introduced that conferred high flexibility to the oxygenator to decrease the form factor of such devices. This device was one of the first microfluidic blood oxygenators with enough flexibility to be deformed, bent, or rolled without limitation and losing its functionality. In order to satisfy the gas transfer need of these preterm neonates, few microfluidic-based modular LADs were constructed to support different birth weights up to 2 kg. The main design criteria for such a LAD in this research was low pressure drops (capable of being operated by a baby's heart), an oxygen transfer of 1.3 – 1.9 mL min^{-1} kg^{-1} of body weight (or an increase in oxygen saturation level from ~ 75 % to ~ 100 % and ideally in room air), and low priming volume (less than 10 % of the total blood volume of a baby). These LADs first were evaluated in vitro to measure their gas exchange capacities and those which could meet needed oxygenation would be tested in vivo. For the first time, it was shown that a pumpless microfluidic-based LAD could support a newborn piglet and provide adequate oxygenation in room air or the oxygen-rich environment. The application of these microfluidic blood oxygenators was not only limited to preterm neonates but also can be used to develop LADs for adult patients.

ACKNOWLEDGMENT

First, I would like to express my deepest and sincerest appreciation to my advisor, Professor Ponnambalam Ravi Selvaganapathy, for giving me an opportunity to work on this amazing project as well as his constant support and guidance during the past four years. His valuable advice has not been only guided me throughout my entire research, but also prepared me for my next journey. His passion for science and knowledge inspired me to read and learn more. Truly, his patience and vast knowledge was one of the main reasons helping this project successfully move forward.

Second, I would like to thank my co-supervisor, Professor Christoph Fusch, for helping me to understand another aspect of this project by his unconditional support for this research. Without doubt, his passion for this project has always encouraged me to work harder. His interest in this project not only gave me motivation, but also inspired me to embrace any challenge.

I am grateful to all people involved in this project, who have supported and helped me through any steps of the project, especially Dr. John L. Brash for sharing his wonderful knowledge and experience. I would like to thank Dr. Gerhard Fusch for his unconditional help and support throughout all my experiments; literally, he was always around even in Christmas days! I am also grateful to Dr. Niels Rochow for sharing his experience and help in different aspects of the project. It was my honor to work with these wonderful people and I am looking forward to our future collaboration.

In my entire research, I have been blessed with a friendly and amazing group of fellow students, researchers in CAMEF: Reza, Aliakbar, Shayan, Harpreet, Darren, Leo, Ali, Juncong, Alireza, Kevon, and so many others.

Last but not the least, I would like to thank my parents for their constant support and unconditional love throughout my life and my entire education. I am also grateful to my dear sister, Ghazal, for her love and support.

My special thanks go to my wife, Neda Saraei, for her love and her encouragement throughout my research. She had not only supported me, but also worked beside me days and nights. She was to me like “Sam to Frodo in the lord of the rings”; without her I could have not been here and had any of my accomplishments. She sacrificed a lot to let me succeed what I have been seeking. There is no word to appreciate such a support.

TABLE OF CONTENTS

LIST OF FIGURES

LIST OF TABLES

1 Chapter 1

Motivation and Organization

1.1 Introduction

Preterm neonates do not have fully developed lungs and may suffer respiratory distress syndrome (RDS) due to lack of pulmonary surfactant, leading to neonatal mortality and morbidity. This situation is even more severe for extreme preterm neonates born at less than 28 weeks of gestational age leading to a low survival rate [1], [2]. Every year in the United States, premature births count to around 10 % of the total births (4 million) showing the seriousness of this situation [3], [4]. The standard of care for respiratory support of preterm neonates suffering from RDS is mechanical ventilation [5]. Although this technique has saved many lives over the years, it is an invasive method as an endotracheal tube should be inserted via mouth or nose and it could cause several complications such as pulmonary injury, bronchopulmonary dysplasia, and retinopathy of prematurity involving with possible long-term side effects[6]–[8]. When mechanical ventilation is not adequate, the other technique called extracorporeal membrane oxygenation (ECMO) can be used. In this method, blood is withdrawn from a baby's body and sent to an external device for oxygenation. Due to safety issues and complexity of the extracorporeal circuit, conventional ECMO devices which are designed for older children or adults may not be a suitable option for treating preterm neonates with RDS. These devices and their blood circuit typically have a large priming volume that is comparable to the total volume of blood in a neonate. Therefore, use of these devices requires filling the oxygenator with donor blood to prevent hemodilution, a process that has its own complications. Additionally, a non-uniform and non-physiological blood distribution are other areas of concern for these devices which can create dead zones or high shear stress regions with the possibility of hemolysis or clot formation. To avoid

these complications, a high concentration of anticoagulation should be used [9]. Hollow fiber membrane oxygenators (HFMO) are typical devices for ECMO purposes. HFMOs consist of a bundle of porous or non-porous fibers packed inside of a plastic shell [10]. Oxygen is introduced through fibers and blood flows around these fibers where gas transfer happens as shown in Figure 1.1. Although HFMOs have undergone remarkable modifications and improvements, they still carry some of the limitations involved with conventional ECMO devices such as plasma leakage [11]. Therefore, an alternative method with minimum side effects has been sought called as an artificial placenta (AP) [1], [12].

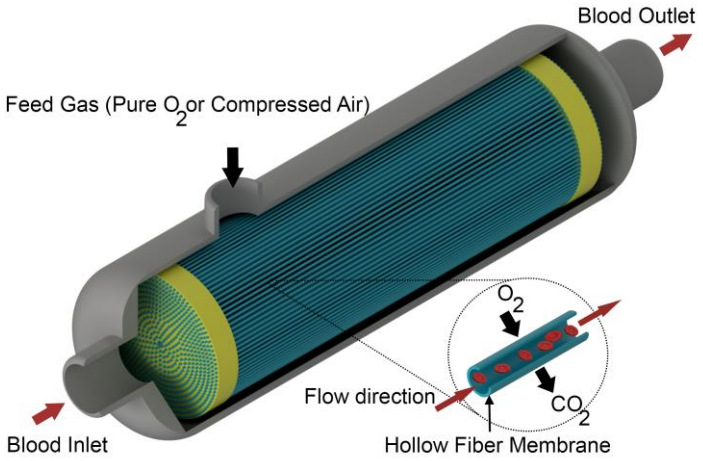

Figure 1.1: a 3D schematic view of a conventional hollow fiber membrane oxygenator.

An AP type device aims to provide sufficient oxygenation to preterm neonates while their lungs are growing and developing. Such a device is designed to be connected to the umbilical cord as the vascular access (a non-invasive or less invasive approach) and be perfused by a baby's heart without the need of any external pump while having the gas exchange in room air. To avoid other complications and simplify its operation, an AP type device should have low priming volume to eliminate the need of any blood transfusion [12].

In an attempt to satisfy these criteria, microfabrication techniques have been employed to miniaturize AP type blood oxygenators [13]. Early designs of these microfluidic artificial placenta type blood oxygenator focused on developing a proof-of-concept that

demonstrated smaller priming volume, reduced pressure drop to allow pumpless operation, and showed gas transfer in room air [5], [13]. As a result, a microfluidic-based single oxygenator unit (SOU) was developed by Wu et al. [13] as a lung assist device (LAD) for preterm newborn neonates. SOUs consisted of a blood flow path, named as "blood vascular network," and a gas-permeable membrane. The blood vascular network was a square-shape chamber with a width of 43 mm and a height of 80 µm having an array of micropillar (500 µm × 500 µm) for supporting a thin gas-permeable membrane on the top (Figure 1.2). The inlet and outlet were diagonally placed at the vertices of the microchamber. This design was chosen to reach the maximum possible gas transfer efficiency while minimizing hydraulic pressure resistance and shear stress to the blood flow. In this work, the effect of various gas-permeable membranes including non-porous and porous polydimethylsiloxane (PDMS) membranes and two hole-through porous polycarbonate (PC) membranes on the gas exchange efficiency of an SOU was investigated. PDMS is a silicone-based material with a high gas-permeability [14] which was found as the best option to fabricate a non-porous gas permeable membrane.

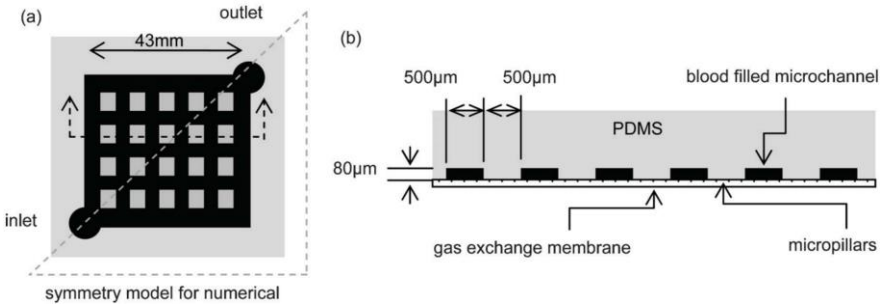

Figure 1.2: Single oxygenator unit (SOU) developed by Wu et al. in 2013 [13].

As it was discussed by Wu et al. [14], an SOU was not sufficient to support required oxygenation for preterm infants. Therefore, several SOUs were assembled in a parallel configuration to form a modular device as a LAD for these infants. Rochow et al. [5] constructed a LAD by connecting 10 SOUs using custom-made manifolds and interconnections as seen in Figure 1.3. Each SOU had a priming volume of 0.12 mL, and the total priming volume of the LAD was 4.8 mL. In vitro and in vivo experiments were conducted to investigate the gas exchange efficiency of the LAD. In overall, an ideal

LAD is supposed to provide enough gas exchange in room air for preterm neonates with RDS in a passive operation and have low priming volume without the need of blood transfusion.

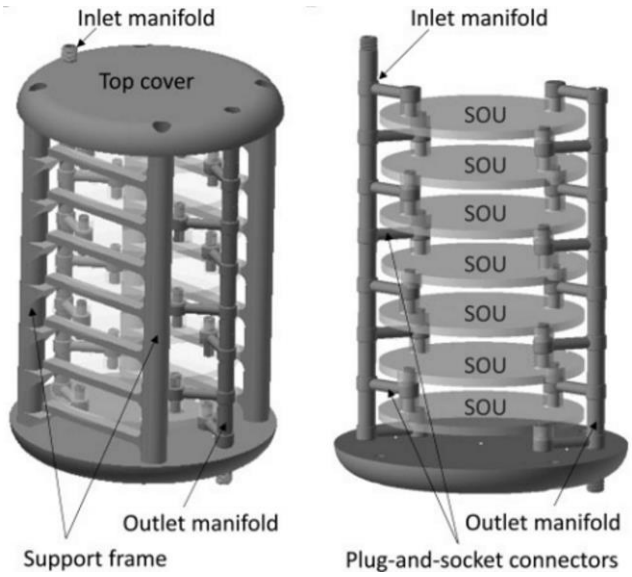

Figure 1.3: the LAD designed and developed by Rochow et al. in 2014 [5].

1.2 Research objectives and aims

The main objective of this thesis is to develop an artificial placenta type microfluidic blood oxygenator which can be used in the construction of a neonatal lung assist device (LAD). Such a device was introduced by Wu et al. [13], but their gas exchange capacities were low resulting in low gas transfer for the LAD developed by Rochow et al. [5]. Therefore, an improvement in SOU's gas transfer was needed to be able to construct a modular LAD which could fulfill requirements for an artificial placenta type LAD. The objective was accomplished by addressing the following aims:

I. Assemble the existing single-sided SOUs into a modular LAD and demonstrate oxygenation characteristics of the LAD.
II. Improve the design and develop new fabrication methods to enhance the gas transfer of the microfluidic blood oxygenators by introducing a double-sided device and modifying their characteristics.

III. Develop new LADs using the new designed microfluidic blood oxygenators with double-sided gas transfer microchannels to improve the gas exchange capacity and achieve the required oxygenation for preterm neonates.

IV. Introduce a new type of microfluidic blood oxygenator with high flexibility to reduce the form factor and the overall build-up volume.

1.3 Thesis outline

This thesis consists of 8 chapters presented in a "sandwich thesis" format. A motivation and organization chapter (Chapter 1) is shown at the beginning to elucidate the need of this work. In the final chapter (Chapter 8), an overall conclusion is made, and the possible future works are presented. Chapters 2 – 7 are based on either published or ready-to-submit articles. The summary of these chapters are as follows:

Chapter 2: This chapter presents a review of microfluidic blood oxygenators and compares the performance of these devices. In the first part of this chapter, the need for miniaturization of blood oxygenators has been discussed, and the overview of an ideal microfluidic-based oxygenator with portability has been described. Then, it was shown that microfluidic blood oxygenators could be categorized based on the ventilation gas that they use (either oxygen or air). In the next part, the devices using air as the sweep gas are further categorized based on their operation into pump-driven and heart-driven groups which has been emphasized as an essential step toward the realization of microfluidic blood oxygenators as a simple and portable device. The next challenge for microfluidic blood oxygenators has been highlighted by sub-dividing the heart-driven microfluidic blood oxygenators to the devices with air channels and the devices capable of being exposed directly to room air which is recommended as an ideal approach for simplifying blood oxygenators to a portable and easy-to-operate device. Finally, the challenges in front of microfluidic blood oxygenators are reviewed and discussed based on the manufacturing obstacles and hemocompatibility needs. The current limitations in the manufacturing of microfluidic blood oxygenators have been comprehensively discussed to understand what further development is required.

Chapter 3: As mentioned in the previous section, the microfluidic blood oxygenators need to be scaled up to be used in a real application. This chapter describes the use of a newly developed single-sided microfluidic blood oxygenator with a composite membrane which was made of ultra-thin stainless-steel mesh and PDMS, for the construction a LAD. The new LAD was designed by assembling 32 microfluidic blood oxygenators including 16 parallel branches with two devices in series to increase the gas exchange capacity. This LAD was evaluated using bovine blood in vitro as well as being tested in an in-vivo experiment by a newborn piglet. Although this LAD design demonstrated that modular assembly of single-sided SOUs was possible to achieve a better oxygenation and be used in vivo, it did not have sufficient capacity to fully oxygenate the blood which could be caused because of low efficiency of the current single-sided SOU in gas transfer.

Chapter 4: In order to improve the poor oxygenation capacity of single-sided SOU identified in the previous chapter, a new microfluidic blood oxygenator with double-sided microchannels for gas transfer was developed and described in this chapter. In single-sided SOUs, only one side of the blood vascular network contributed to gas transfer while the other side was passive in gas exchange resulting in inadequate oxygenation. For this reason, a new layer-by-layer microfabrication technique was developed to reduce the thickness of the passive layer low enough to involve this side of the blood vascular network in gas exchange as well. Additionally, it was shown that a double-sided microfluidic blood oxygenator could perform much better up to 343 % compared to single-sided devices. Later, an attempt was made to increase the capacity of a microfluidic blood oxygenator by fabricating a device with a larger gas exchange surface area without compromising its gas exchange efficiency. In the end, four of these large double-sided devices were connected in two different parallel flow configurations. In vitro results confirmed that the LAD in this work could meet all artificial placenta requirements when the LAD was using oxygen as the sweep gas. Even though this was an important step toward the development of a pumpless microfluidic blood oxygenator for an artificial placenta application, further improvements would be needed to achieve the same level of oxygenation in room air. This happened as the overall gas exchange surface

area of the current double-sided SOUs was not fully effective in gas transfer due to the fact that the half of this area was blocked by the mesh.

Chapter 5: To overcome the limitation described in the previous chapter, a solution was found to fabricate a large surface area microfluidic blood oxygenator without using a reinforcement material such ultra-thin stainless-steel mesh by coating a permanent perfluoro silane layer on the mold. This coating was beneficial in easily peeling off a thin layer of all PDMS microfluidic network from a mold without tearing. The mechanical assessment was performed to show that these thin PDMS-based microfluidic devices are reliable to be used in a LAD production. Also, a new tapered inlet configuration was developed to access the blood vascular network avoiding any sudden change in blood flow paths and eliminating high shear stress regions and thrombosis formation. As a result, a new LAD was constructed by assembling 8 of these devices and tested in an enriched oxygen environment and room air. This LAD was designed in such a way to ensure that blood would experience a physiological flow path. Although the results revealed that this LAD ,which has low priming volume and pressure drop, could reach acceptable oxygenation in room air for the first time, it had a significant form factor and not sufficient oxygenation in room air for preterm neonates weighing more than one kg.

Chapter 6: The issue identified in the previous part is addressed in this chapter by introducing the first ultra-thin flexible microfluidic blood oxygenator. Polytetrafluoroethylene (PTFE) was employed in this study as a scaffold to reinforce PDMS while maintaining the flexible nature of PDMS. Thanks to the flexibility of these ultra-thin devices, the overall build-up volume and the form factor of a microfluidic blood oxygenator were significantly reduced. To illustrate the stability and functionality of this flexible device, hydraulic and blood experiments were done without impacting their performances. Even, these devices were twisted and deformed in very complex shapes and perfused without failure suggesting that they were versatile and robust.

Moreover, a flower-shape design oxygenator was fabricated to combine some connectors and devices in one bigger format to decrease the total priming volume. In the end, a large

ultra-thin flexible microfluidic blood oxygenator was rolled in a cylindrical geometry to form a compact device for preterm neonates with extremely low birth-weights. Though it was shown that this rolled device could provide enough oxygenation for these infants weighing up to 675 g using oxygen as the sweep gas, a modular LAD would be needed to support preterm infants with various weight.

Chapter 7: To address the limitations described in chapters 5 and 6, the ultra-thin microfluidic blood oxygenator developed in the previous section was integrated by the tapered inlet/outlet designed in part 5 and was used to make a compact LAD consisting blood flow distributors with a biomimetic design. The height of microchannels was increased, and 16 devices were connected in parallel to form a pumpless LAD. In vitro studies were conducted to asses the gas transfer efficiency of this LAD in an enriched oxygen environment and room air resulting in the highest gas exchange achieved by a microfluidic-based oxygenator till now. Further, a newborn piglet was used to test this LAD in a pumpless manner. First, the inner surface of the LAD was coated by an easy and simple coating to improve its hemocompatibility. This coating was done by circulating a mixture of heparin and normal saline solution for 4 – 5 hours before the experiment. The stability and effectiveness of this coating were evaluated in vitro revealing that this coating was stable on PDMS surfaces for at least 20 hours and could reduce fibrinogen adsorption significantly compared to non-coated PDMS surfaces. Then, the LAD with this coating was attached to a newborn piglet. A hypoxic condition was simulated for the piglet same as the situation that a preterm neonate with RDS may experience. Different clinical and gas exchange measurements were conducted during the experiment to investigate the performance of this LAD in vivo. Despite the fact that this LAD was designed for neonates weighing around 1 kg, it could provide enough respiratory support for the piglet while was supplied by pure oxygen. These results suggested that a LAD with a higher number of microfluidic blood oxygenators could provide sufficient oxygenation for an animal with the same weight in room air.

Chapter 8: This chapter provides a summary of all achievements in this thesis concluding that microfluidic blood oxygenators have a great potential to be used as an

artificial placenta type device for blood oxygenation following by recommendations for the future works. The future works are focused on two approaches: (i) using the current microfabrication technologies to improve the gas exchange of a microfluidic blood oxygenator and (ii) using the new fabrication techniques such as 3D printing to 3D print an artificial lung.

1.4 Contribution

The contributions made in this thesis are mainly in the development of novel microfabrication techniques and its application in the design and development of microfluidic blood oxygenators. In this thesis, a new microfabrication process has been introduced to develop ultrathin large-area microfluidic devices with gas-permeable membranes on both sides of the microchannels featuring robust, repeatable, and reliable devices thanks to using a spin-coating process to precisely control the fabrication of the different layers of these devices. This new technique has been employed to demonstrating a microfluidic blood oxygenator with double-sided gas transfer channels which could be exposed directly to room air resulting in enhancing the gas exchange compared to single-sided microfluidic blood oxygenators. In contrast to the existing double-sided microfluidic blood oxygenator, the new microfabrication process did not rely on stabilizer layers on each side of the blood channels to fabricate a device with larger gas exchange surface area. Besides, a surface treatment has been applied to the mold, which was made by the conventional photolithography, to increase the water contact angle of the surface and reduce the stickiness of the mold to fabricate a large ultra-thin PDMS microfluidic device with double-sided gas transfer channels. In this thesis, a new inlet/outlet with tapered configuration was designed and integrated to microfluidic blood oxygenators to eradicate dead zones and high shear stress regions to eschew clot formations. In addition, flow distributors (dividers) with biomimetic blood flow paths were designed to uniformly distribute blood in a modular LAD while the pressure drop and the priming volume were minimized. Moreover, one of the main challenges for microfluidic blood oxygenators, which was lack of flexibility and a large form factor, has been addressed in this thesis by

developing an ultra-thin flexible microfluidic device with reinforced PDMS membranes capable of bending and rolling to complex shapes to reduce the form factor.

At the application level, various pumpless artificial placenta type LADs for preterm infants were developed and assessed in vitro and in vivo. In the first attempt, 32 single-sided SOUs were used to construct a LAD which could achieve the highest oxygenation (the maximum oxygen uptake of 0.9 mL min^{-1}) in room air at a reasonable blood flow rate (40 mL min^{-1}) and a low pressure drop (40 mm Hg) among all microfluidic-based oxygenators at that time. The next modular LAD in this thesis was developed by connecting four large-area double-sided microfluidic blood oxygenators with ultra-thin stainless-steel mesh and became the first passive oxygenator, which could support preterm infants weighing up to 2 kg, with a low priming volume of 8 mL and a desirable oxygenation (1.96 mL min^{-1} at a pressure drop of 30 mm Hg) using pure oxygen as the sweep gas. In the next phase, eight ultra-thin PDMS-based double-sided microfluidic blood oxygenators with large gas-exchange-surface-area and tapered-shape inlets were used in the fabrication of the third generation of LADs in this thesis. This LAD was the first pumpless modular oxygenator as an artificial placenta with low priming volume and adequate oxygenation (the maximum oxygen uptake of 1.24 mL min^{-1}) in room air for preterm neonates weighing up to one kg. Moreover, this LAD was the first of its kind to support a high blood flow rate of 150 mL min^{-1} (equal to an increase of 27 % in oxygen saturation level) while reaching an oxygen transfer of 4.54 mL min^{-1} in an oxygen-rich environment. Finally, the most advanced microfluidic-based LAD was introduced in this thesis to meet all design criteria for an artificial placenta type blood oxygenator for preterm neonates with RDS. This LAD for the first time could provide enough oxygenation for preterm infants weighing more than 1 kg in room air while had a low priming volume and low pressure drop suited for a pumpless operation. Further, this LAD was connected to a newborn piglet to demonstrate the superior performance of the LAD in oxygenation required for supporting preterm newborns with RDS.

Chapters 2 – 7 are based on my contributions to the articles which can be divided into a review paper under preparation for submission, two regular articles published in

Biomicrofluidics, one regular article published in *Lab on a Chip (LOC)*, one ready regular article for submission, and one regular article under preparation for submission. The authors and the title of these articles are as follows:

1. Mohammadhossein Dabaghi, Niels Rochow, Rupesh Kumar Mahendran, Neda Saraei, Gerhard Fusch, John L. Brash, Christoph Fusch, and Ponnambalam Ravi Selvaganapathy. "***Miniaturization of artificial lungs toward portability***," under preparation for submission.

2. Harpreet Matharoo*, Mohammadhossein Dabaghi*, Niels Rochow, Gerhard Fusch, Neda Saraei, Mohammed Tauhiduzzaman, Stephan Veldhuis, John L. Brash, Christoph Fusch, and Ponnambalam Ravi Selvaganapathy. "***Steel reinforced composite silicone membranes and its integration to microfluidic oxygenators for high performance gas exchange***," Biomicrofluidics, vol. 12, no. 1, 2018.

3. Mohammadhossein Dabaghi, Gerhard Fusch, Neda Saraei, Niels Rochow, John L. Brash, Christoph Fusch, and Ponnambalam Ravi Selvaganapathy. "***An artificial placenta type microfluidic blood oxygenator with double-sided gas transfer microchannels and its integration as a neonatal lung assist device***," Biomicrofluidics, vol. 12, no. 3, 2018.

4. Mohammadhossein Dabaghi, Neda Saraei, Gerhard Fusch, Niels Rochow, John L. Brash, Christoph Fusch, and Ponnambalam Ravi Selvaganapathy. "***An ultra-thin PDMS-based microfluidic lung assist device with biomimetic blood flow paths***," ready for submission.

5. Mohammadhossein Dabaghi, Neda Saraei, Gerhard Fusch, Niels Rochow, John L. Brash, Christoph Fusch, and Ponnambalam Ravi Selvaganapathy. "***An ultra-thin***

* Both authors contributed equally to this work.

highly flexible microfluidic device for blood oxygenation," Lab on a Chip, 2018, 18, 3780-3789.

6. Mohammadhossein Dabaghi, Niels Rochow, Neda Saraei, Gerhard Fusch, Shelley Monkman, Kevin Da, Alireza Shahin-Shamsabadi, Devon Jones, John L. Brash, Kathleen Delaney, Christoph Fusch, and Ponnambalam Ravi Selvaganapathy. "***A pumpless microfluidic neonatal lung assist device for artificial placenta applications***," under preparation for submission.

References

[1] J. T. Church *et al.*, "The artificial placenta: Continued lung development during extracorporeal support in a preterm lamb model," *J. Pediatr. Surg.*, vol. 53, no. 10, pp. 1896–1903, 2018.

[2] E. A. Partridge *et al.*, "An extra-uterine system to physiologically support the extreme premature lamb," *Nat. Commun.*, vol. 8, p. 15112, 2017.

[3] B. E. Hamilton, J. A. Martin, and M. J. K. S. Osterman, "Births: Preliminary Data for 2015 National Vital Statistics Reports," *Natl. Vital Stat. Reports*, vol. 65, no. 3, pp. 1–15, 2015.

[4] J. A. Martin, B. E. Hamilton, M. J. K. Osterman, S. C. Curtin, and T. J. Mathews, "Births: Final Data for 2015," *Natl. Vital Stat. Reports*, vol. 66, no. 1, pp. 1–70, 2017.

[5] N. Rochow *et al.*, "An Integrated Array of Microfluidic Oxygenators as a Neonatal Lung Assist Device: In Vitro Characterization and In Vivo Demonstration," *Artif. Organs*, vol. 38, no. 10, pp. 856–866, Oct. 2014.

[6] A. G. S. Philip, "Bronchopulmonary dysplasia: then and now.," *Neonatology*, vol. 102, no. 1, pp. 1–8, 2012.

[7] M. A. Attar and S. M. Donn, "Mechanisms of ventilator-induced lung injury in premature infants," *Semin. Neonatol.*, vol. 7, no. 5, pp. 353–360, Oct. 2002.

[8] H. M. Chambers and D. van Velzen, "Ventilator-related pathology in the extremely immature lung," *Pathology*, vol. 21, no. 2, pp. 79–83, Jan. 1989.

[9] A. A. Gimbel, E. Flores, A. Koo, G. García-Cardeña, and J. T. Borenstein, "Development of a biomimetic microfluidic oxygen transfer device," *Lab Chip*, vol. 16, no. 17, pp. 3227–3234, 2016.

[10] L. Lequier, S. B. Horton, D. M. McMullan, and R. H. Bartlett, "Extracorporeal membrane oxygenation circuitry.," *Pediatr. Crit. care Med.*, vol. 14, pp. S7-12, Jun. 2013.

[11] J. P. Montoya, C. J. Shanley, S. I. Merz, and R. H. Bartlett, "Plasma leakage through microporous membranes. Role of phospholipids.," *ASAIO J.*, vol. 38, no. 3, pp. M399-405, 1992.

[12] N. Rochow *et al.*, "Artificial placenta -Lung assist devices for term and preterm newborns with respiratory failure," *Int J Artif Organs*, vol. 36, pp. 377–391, 2013.

[13] W.-I. Wu *et al.*, "Lung assist device: development of microfluidic oxygenators for preterm infants with respiratory failure," *Lab Chip*, vol. 13, no. 13, p. 2641, 2013.

[14] W. L. Robb, "THIN SILICONE MEMBRANES-THEIR PERMEATION PROPERTIES AND

SOME APPLICATIONS," *Ann. N. Y. Acad. Sci.*, vol. 146, no. 1 Materials in, pp. 119–137, Jan. 1968.

2 Chapter 2

MINIATURIZATION OF ARTIFICIAL LUNGS TOWARD PORTABILITY

Complete citation:

Mohammadhossein Dabaghi, Niels Rochow, Rupesh Kumar Mahendran, Gerhard Fusch, Neda Saraei, John Brash1, Christoph Fusch and P. Ravi Selvaganapathy. *"Miniaturization of Artificial Lungs Toward Portability."* Under preparation to be submitted.

Contribution:

My contributions include reviewing the literature and writing the manuscript.

2.1 Abstract

Artificial lungs have been used to support patients in open-heart surgery by providing required gas transfer with an extracorporeal circuit. Nonetheless, some patients need extended support for a few weeks or months even after the surgery. Therefore, a portable or wearable lung assist device which could be operated for several weeks with a minimum maintenance would be ideal. Miniaturization of blood oxygenators, using microfluidic technology, has been a promising avenue for the realization of such portable artificial lungs. Microfluidic blood oxygenators (MBO) are also suitable for neonates with respiratory failure due to their low priming volume and pressure drop. This review discusses the history of microfluidic oxygenator development, the need for miniaturization and recent progress in miniaturized artificial lungs. MBOs have made significant advances in: 1) reducing device size; 2) providing biomimetic blood flow paths for cells and platelets to experience more physiological pressures and shear stresses; 3) enabling operation in room air; and, 4) operating without the need of an external pump. Research has focused on two primary directions: investigating new designs of microfluidic channels and membranes to enhance the gas exchange or scaling up the size of the device to reach higher throughput. Up to now, the highest achieved blood flow rate by an MBO is 60 mL/min (an oxygen transfer of 47.64 mL O_2/L_{Blood}) which would be enough to be used for neonates while using oxygen as the sweep gas. This review also discusses the challenges faced by this technology in practical applications as well as required future improvements to meet the requirements for older neonates and even adults.

2.2 Introduction

Extracorporeal membrane oxygenation (ECMO) is a method of life support that provides oxygen and removes the carbon dioxide from the blood. Blood is extracted from the body and flowed through a device with a high surface area membrane which oxygen or air on the other side that allows the exchange of gases (oxygen and carbon dioxide) between the blood and the external gas. The blood is then sent back into the body, thereby maintaining healthy levels of oxygen saturation.

The first blood oxygenator which was a disc-based device with a direct contact between blood and the external gas dates all the way back to 1885 by *Von Frey, and Gruber*[1] and was the basis for many other devices that were later developed until the late 1970s. Several versions including surface and bubble type direct contact oxygenators were developed with a number of design improvements and were evaluated in-vitro as well as in-vivo. Direct contact between air surfaces and blood caused several complications such as damage to red blood cells and platelets, blood coagulation, and protein denaturation which limited the performance of these types of oxygenators and led to the origin of the next generations[2]. In the early 1970s, hollow fiber membranes (HFM) were adopted from renal dialyzers for use in blood oxygenators[3]. Since then, HFMs have experienced steady improvements in various aspects such as materials, fabrication, blood pumps and device circuitry.

HFM based devices are the current state-of-art devices for blood oxygenation in the clinical settings. They consist of bundles or sheets of hollow fibers (porous or non-porous), which can be twisted in different configurations and packed in a plastic shell. Even though these devices have been continuously modified to have more physiological blood flow paths and achieve better gas transfer rates, they still have some limitations due to the complexity of the blood flow path and the gas exchange efficiency. High priming volume is one of the main concerns for these devices which necessitates blood transfusion to avoid hemodilution. Moreover, this volume of blood which is in contact with synthetic surfaces inside HFMs requires a significant amount of anticoagulants to prevent clot and

thrombus formations. The other issue with HFMs is their complicated blood flow paths which could lead to creations of regions with low or extremely high shear stresses.

There are various motivations behind miniaturization of blood oxygenators: 1) minimizing priming volume, 2) the reduction of stagnation zones, 3) ability to support thinner membranes and the ability to achieve smaller dimension channels, thereby enhancing gas exchange efficiency. In the case of HFMs, blood oxygenators with their circuits should be primed by: a saline solution resulting in the dilution of blood after being connected to patients or donor blood to maintain the optimal hematocrit level during the treatment. Furthermore, complicated blood flow path inside HFMs and their circuits which is prone to stagnation zones and the need of an external pump for achieving a stable blood flow are the other limitations of the current HFMs. More importantly, the challenges involved in fabricating hollow fibers with thinner membranes may limit their performance. As a result, miniaturization of these devices can be considered as a solution to introduce an easy-to-operate device with portability and minimum complications.

These motivations led to developing more compact HFMs such as the one introduced by Federspiel's research group[4]–[6] (a pressure drop of ~ 80 mm Hg at a blood flow rate of ~ 4 L min^{-1}) with a reduced priming volume (the priming volume of the device and the loop was around 200 mL) or the one designed to miniaturize the size of HFMs for preterm neonates by integrating a rotary blood pump inside an oxygenator yielding to decreasing the overall priming volume[7]–[11]. NeonatOx[12] can be considered as one of the most advanced HFM oxygenators for premature neonates so that this device could be operated in a pumpless manner with a low priming volume of ~ 20 mL.

The adaptation of microfabrication methods which were initially developed for the microelectronics industry to fabricate micromechanical structures has enabled the development of microfluidic devices with microchannels capable of handling small fluid volume (of the order of µL to pL)[13]. Lungs which comprise of millions micro-scale capillaries and alveoli have an incredibly high gas exchange surface area[14]. As

Federspiel and Svitek[14] anticipated, the future of artificial lungs would be to mimic the micro-scale of alveoli and capillaries which could be achieved by fabricating micro-blood-channels to decrease not only diffusion resistance but also to fabricate such a miniaturized device with high surface-area-to-blood-volume ratios[14]. These devices could then be suitably designed so that their pressure drop is in a range that could be perfused by the patient's heart, without the need for an external pump. Due to its miniaturized nature, these devices would automatically be small in form factor, all of which are factors that enable portability of these devices. Any oxygenator device having a blood channel with the laminar flow can be categorized as a microfluidic blood oxygenator[15]. Based on this definition, the first miniaturized oxygenator was introduced by Kolobow and Bowman in 1963[16] where they coated a sheet of vinyl fiberglass screen with silastic (silicone rubber) to be used as "alveolar membrane." This silicone-coated membrane had a thickness of 127 µm and was wrapped around a supporting cylinder that formed different parallel layers with 80 µm spacing. Blood was flowed among these separated layers to let gas transfer occur. Kolobow and Bowman blood oxygenator could be considered as the first generation of the current commercial silicone-based oxygenators. Later in 1977, Hung et al. improved oxygenation of such a device by etching an array of parallel channels onto both sides of a stainless-steel plate to make a flat-plate membrane blood oxygenator for neonates by maximizing the number of channels per plate (1130 channels per each plate)[17].

An MBO mainly consists of three components[15]: a blood side flow manifold, a gas side flow manifold, and a thin gas permeable membrane. The blood side manifold could be an array of microfluidic channels (called as "vascular network") which would be designed in a way to mimic the natural lung as shown in Figure 2.1. The gas side manifold is designed such that there is a uniform delivery of gases (oxygen or air) in the vicinity of the gas permeable membrane. Microfluidic oxygenators allow the flexibility to design suitable flow manifolds to be optimized for lower pressure drop and priming volume by suitably positioning air chamber or channels adjacent to the blood vascular network for gas exchange. In some oxygenators, the gas side manifold is eliminated so that ambient

air or oxygen exposure is possible. In oxygenators, membranes play an important role and are responsible for separating the blood side from the gas side physically while still allowing gas exchange to occur rapidly. Polydimethylsiloxane (PDMS) is the first choice for fabricating membranes for MBOs thanks to its high permeability and ease of use[18], [19].

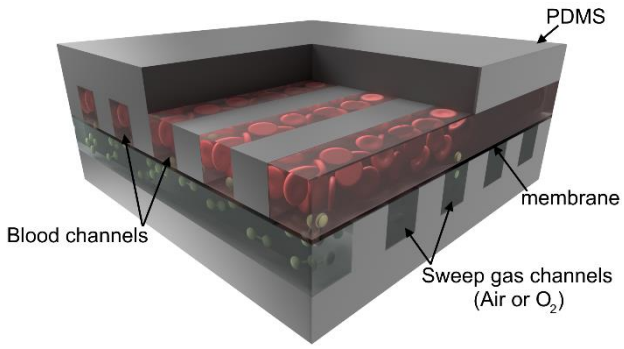

Figure 2.1: Schematic 3D image of an MBO.

2.3 Classification of MBOs

In this review, MBOs are distinguished based on the gas that they use for oxygenation and further subdivided based on their perfusion method into pump-driven and heart-driven as shown in Figure 2.2. Finally, ideal devices, which do not need a pump and can be exposed directly to room air for gas exchange, are highlighted for their suitability for an application as portable artificial lungs.

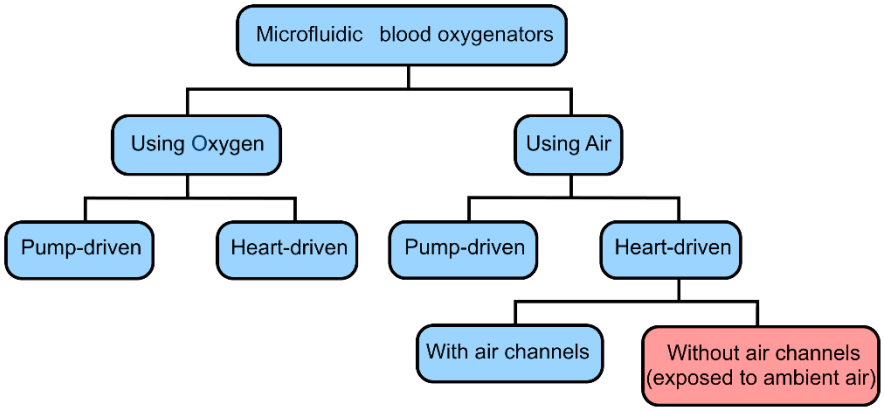

Figure 2.2: Classification of miniaturized blood oxygenators with a focus on portability.

A heart-driven MBO is defined as a device which can be operated by the pressure differential (the difference between artery and vein) provided by a heart (the pressure is usually around 80 mm Hg[20] for a normal adult and 20 – 60 mm Hg[21] for preterm and term neonates).

2.4 MBOs using Oxygen

The first generation of microfluidic blood oxygenators, like their predecessors (hollow fiber membranes), required oxygen to provide adequate oxygenation to blood. They incorporated gas and blood manifolds constructed of microchannels sandwiching a gas permeable membrane. Lee *et al.*[22] introduced theoretical models to study the suitability of different designs for MBOs with various heights and geometries. Some of these designs were later fabricated and experimentally validated including designs that consisted of an array of straight rectangular microchannels and the second one with microscale support posts placed in a wide rectangular channel. The main advantage of using pillars was to increase the effective gas exchange surface area for such a device with the same size. These devices were operated at low pressure drop but could not fully oxygenate blood at a reasonable blood flow rate. Also, using pure oxygen as a ventilation source makes these designs more complicated to build a portable artificial lung[23], [24].

MBOs using oxygen as their gas supply can be categorized based on their hydraulic driving source to devices that require an external pump for operation or those which can be operated in a pumpless configuration.

2.4.1 Pump-driven MBOs using oxygen

At the initial stage development of MBOs, most of the research and development focused on introducing new designs for a better blood vascular network to achieve the highest possible gas exchange. As a result, the operation of these devices was depended on an external pump and oxygen supply. For instance, *Burgess et al.*[25] fabricated a small-scale multilayer PDMS MBO by stacking two blood and four gas channel layers to improve the overall gas transfer efficiency of their MBO by presenting microchannels

with double-sided gas diffusion. The blood side of the device had an array of 56 blood channels with 100 µm width, and the gas side was a chamber with micropillars to support the gas-permeable membranes. For a module with 112 microchannels with a length of 1.8 cm, the total gas exchange surface area was 4.72 cm^2 and the total priming volume was 4.56 µl. This work was the first attempt to build such an MBO with the diffusion of oxygen occurring from both sides of the blood channels. Although this approach was promising, no gas transfer data was reported using blood to investigate the gas exchange capabilities of this device[25].

Vacanti's group[26] presented results for a miniaturized microfluidic artificial lung having a 200 µm-tall microvascular network which was consisted of a branching network with different widths from several millimeters to micrometers to mimic the flow distribution network of the natural lungs (Figure 2.3). In this study, two silicone semi-permeable gas membranes with a thickness of 63 µm, and a 12 µm-thick porous polycarbonate membrane with 1 µm pore size were used. The total gas exchange surface area was 30.8 cm^2 including all branching channels and micro-capillaries and was just 18 cm^2 for micro-capillaries where had the highest contribution in gas transfer. The operating blood flow rate varied from 0.6 mL/min to 8 mL/min at which the pressure drop of 19.8 – 123.1 mmHg was reached. Their microcapillaries experienced shear stresses ranged between 1 to 26.6 dynes/cm^2 at a blood flow rate of 4 mL/min. The maximum oxygen uptake of 0.24 mL/min (mean) happened at a blood flow rate of 8 mL/min for devices with the silicone-based membrane. They found that the gas transfer for all three membranes was in the same range and limited by diffusion in blood microchannels, which was also recognized before as one of the limitations for commercial hollow fiber oxygenators. Also, pure oxygen was used to supply the gas chamber. They suggested that a device with 357 layers would be needed to increase pO_2 from 57 to 79 mmHg. However, adding several layers to adopt this system for an adult lung assist device would lead to a large device which may not be clinically useful.

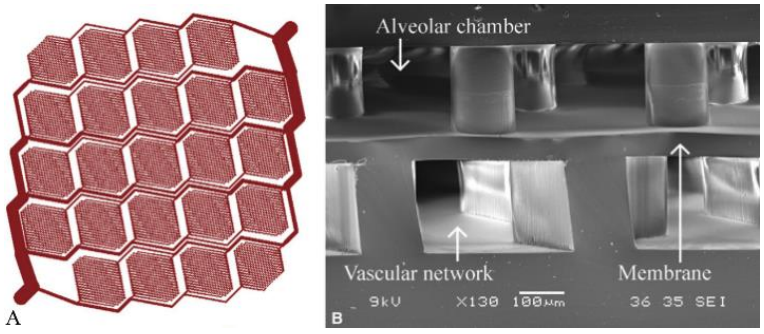

Figure 2.3: (A) top-view of the microvascular network designed in this study and (B) SEM image of cross-sectional of the device. Reproduced with permission from Elsevier [26].

Kniazeva et al.[27] developed a multilayer MBO inspired by the physiological vasculature to mimic a physiological flow path for blood (Figure 2.4). In this work, few different membranes thickness of 11, 26, 46, 59, 83, and 120 µm were tested to select the best membrane thickness. Several devices with 3, 5 or 10 bilayers, which consisted of a blood vascular microchannel network and an oxygen channel separated by a thin membrane, were constructed. Instead of blood, Phosphate Buffered Saline (PBS) was used to evaluate the gas transfer efficiency[27].

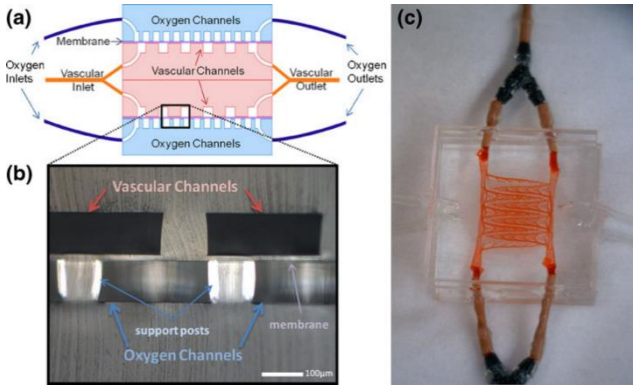

Figure 2.4: A single modular MBO developed. Reproduced with permission from Springer Nature[27].

The same research group led by Borenstein then tested a ten-bilayer configuration (called "transfer modules") of the device that they had previously developed [27] with bovine blood in 2012 [28]. Each of these ten transfer modules with their inlets and outlets was connected to the central vertical channels to provide access for blood and gas inflows and outflows. The tested devices in this study had 50 or 100 µm-tall channels and 30 or 117

µm-thick membranes. All devices were tested by whole bovine blood varying blood flow rates from 1 – 10 mL/min. The maximum oxygen uptake of 0.275 mL/min was reached at a blood flow rate of 10 mL/min for ten-transfer-modules devices with 50 µm-tall blood channels and 30 µm-thick membranes. They found that a higher number of layers, thinner membranes, and shorter blood vascular networks would increase gas transfer. Also, decreasing the height of blood vascular networks would lead to lower priming volume but higher pressure drops. In this study, the resistance of the vascular networks for single and 10-layers transfer modules was measured using DI water, and no pressure drop was reported once devices perfused by blood [28]. However, the pressure drop with water was still high which made this device not suitable for a portable application.

Gimbel et al.[29] from Borenstein's research group presented results for a multilayer MBO with the same design for the vascular network which was introduced by Kniazeva in 2012 [28]. The size of the vascular network was increased, and 14 transfer modules were stacked in parallel to reach a higher active gas exchange surface area of 46.2 cm^2 (Figure 2.5)[30].

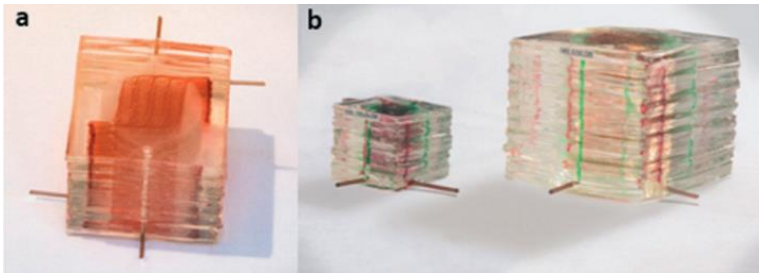

Figure 2.5: (a) 10-layers MBO with the original size for the vascular network and (b) comparing 10-layers device with 14-layers device with the expanded vascular network. Reproduced with permission from The Royal Society of Chemistry [29].

Gas transfer in both devices was evaluated using heparinized bovine blood. The expanded device could achieve an oxygen uptake of 1.2 mL/min at a blood flow rate of 25 mL/min. Although their device achieved such a high oxygen transfer, no pressure drop was reported in this study which is a critical factor for any pumpless blood oxygenator. Additionally, human endothelial cells were coated in the blood vascular network to improve the hemocompatibility of the device. They found less blood clot formation in

cells-coated devices compared to those without cell coating. Additionally, they showed that coating endothelial cells did not attenuate the oxygen uptake [30].

Sreenivasan et al. [31] developed new ultra-thin, polymeric free-standing membranes (FSMs) and composite membranes (CMs) with large surface area using initiated Chemical Vapor Deposition (iCVD) for artificial lungs. Five µm-thick FSMs achieved 1.3 times higher CO_2 transfer compared to an eight µm-thick silicone-based membrane[31]. Even though these new membranes showed high permeability, they were not tested by blood to show their real gas transfer potential as the gas transfer may be limited by channels thickness, not the membrane thickness. Although an advanced membrane would enhance gas transfer throughout the membrane, the overall gas exchange will not be improved significantly as the resistance to oxygen diffusion in blood is the most significant factor in oxygenation, especially for channels whose heights are more significant than the red blood cells dimensions.

Femmer et al.[32] developed a microfluidic device that used passive micromixers and chaotic advection principles to mix the fluid as it travels through a channel to demonstrate that these structures could enhance oxygen uptake in water. An array of 28 mm-long parallel channels which were 500 µm wide and 50 µm tall was designed as the contractor chip for the liquid and gas sides. Staggered herringbone micromixers (SHM) structures with 50 µm depth and 125 µm width were patterned on channels in groups of six (12 groups per channel). A 127 µm-thick PDMS membrane was sandwiched between the liquid and the gas sides. Specifically, SHMs were introduced in liquid channels to promote mixing (Figure 2.6). The main idea was to add some turbulence inside the blood channel and let red blood cells from different layers mixed to improve the overall gas exchange. They demonstrated that the device with SHMs achieved higher oxygen uptake up to 66 % compared to the device without SHMs. They also found that the pressure drops reduced for channels with SHMs compared to those without SHMs.

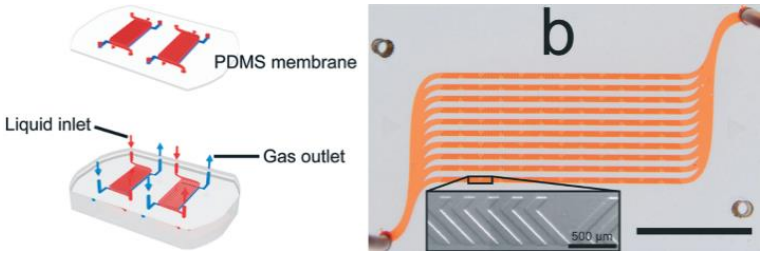

Figure 2.6: The microfluidic gas-liquid-contacting device with staggered herringbone structures as micromixers for enhancing mixing in blood. Reproduced with permission from The Royal Society of Chemistry [32].

They envisioned microchannels with SHMs would be useful for miniaturized blood oxygenators in the future[32]. Although it is an exciting solution to avoid the high diffusional resistance of gases in the plasma by mixing different layers of blood, thereby enhancing oxygenation, issues associated with shear stresses encountered by the blood in some areas of the channels and stagnation of blood in others have not been considered and could potentially lead to thermogenesis in realistic conditions which acquire more investigations.

Rieper et al.[33] developed a microfluidic multilayers extracorporeal gas exchange device with double-sided gas diffusion by stacking ten blood and 11 air layers (Figure 2.7). An array of 40 parallel microchannels, which were 1 mm wide and separated by 500 µm wide bars, formed the blood compartment. A 90 µm-thick PDMS membrane separated the blood side from the gas side. The total gas exchange surface area for their device was 120 cm^2 per layer with a priming volume of around 0.7 mL. Pure oxygen or air was used as the ventilation gas. A seven-layers device was tested by porcine blood. One layer of oxygen compartment achieved oxygen uptakes of 0.3 mL/min and 0.156 mL/min for pure oxygen and air at a blood flow rate of 5 mL/min, respectively. At a blood flow rate of 15 mL/min, the pressure drop was 80 mmHg. They estimated that 833 blood compartments would be needed to provide an oxygen transfer of 250 mL/min for adult artificial lungs. Such a device with 833 blood compartment layers will have a priming volume of 580 mL[33]. Although this was the first time that such a high blood flow rate of 50 mL/min was achieved with an MBO, wire electrical discharge machining which was used to fabricate the blood compartment out of a steel sheet may not be appropriate to produce

smooth channel walls that are required to prevent hemolysis and thrombotic reactions on surfaces. Furthermore, the device design was not optimized by flow distribution analysis and shear stress analysis to identify stagnation and high shear zones above the blood coagulation threshold (10 Pa[34], [35]).

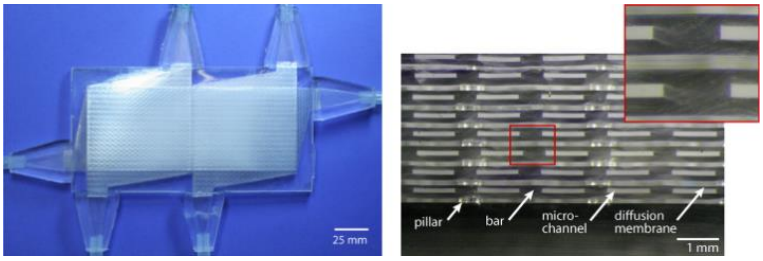

Figure 2.7: The microfluidic multilayers extracorporeal gas exchange device designed by Rieper et al. Reproduced with permission from Springer Nature[33].

Potkay research group developed a miniaturized rolled-membrane MBO[36] as depicted in Figure 2.8. This was the first representation of an MBO in a rolled shaped configuration which could be beneficial in order to reduce the building volume and the form factor. The rolled microfluidic device consisted of a blood vascular network with 5450 microcapillaries, which were 10 µm tall, 40 µm wide, and 1014 µm long, a 66 µm-thick PDMS membrane, a 100 µm-tall gas chamber, and a capping layer. The total priming volume of the device excluding the inlet and the outlet was 27 µL. Air or oxygen was supplied to the gas chamber as the ventilation gas. Whole bovine blood was used to test the device with varying blood flow rates from 0.1 mL/min to 1.25 mL/min. The rolled device could increase oxygen saturation level from ~ 65% to 95 % at a blood flow rate of 0.5 mL/min and 0.2 mL/min using pure oxygen and air as the ventilation gas, respectively. At this blood flow rate, the pressure drop was around 80 mmHg. They predicted that they could achieve the same oxygen transfer at a blood flow rate of 1.5 L/min by increasing the diameter of device and having 219 or 355 gas exchange units for oxygen or air as the ventilating gas, respectively. Such a scaled-up device with 219 or 355 gas exchange units would have a priming volume of around 41 mL or 71 mL, respectively. However, experimental testing was only performed at low blood flow rates

(0.1 mL/min to 1.25 mL/min), and the high pressure drop observed make this design unsuitable for a portable pumpless blood oxygenator.

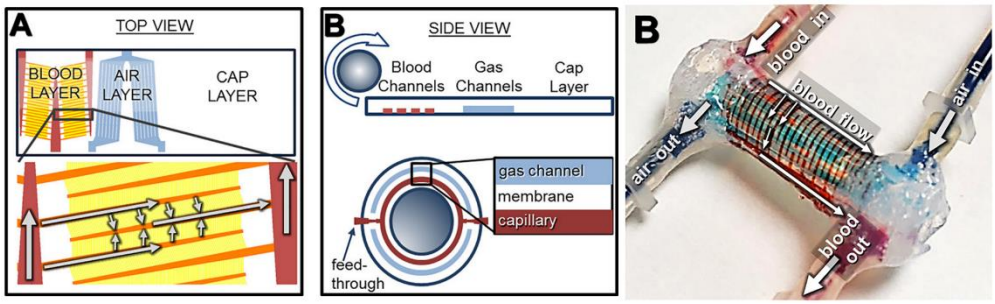

Figure 2.8: the rolled MBO designed by Thompson et. al. Reproduced with permission from AIP publishing[36].

Potkay's group[37] later optimized their device dimension using numerical simulation, and fabricated a device with 9870 artificial capillaries which were 3.2 mm in length, 120 µm in width and an optimum height of 30 µm. Bovine blood was used to test this optimized device at various blood flow rates from 5 mL/min to 25 mL/min. A maximum oxygen transfer of ~ 0.4 mL/min was achieved at a blood flow rate of 25 mL/min which is the highest blood flow rate handled by an MBO up to now. Moreover, the pressure drops varied from ~ 30 mm Hg to ~ 90 mm Hg over the tested blood flow rates. Similar to their previous work, they used a biomimetic approach to design the blood flow path that can minimize shear stress and avoid thrombotic reaction as well as damage to red blood cells. However, the lithographic process that was used for fabrication is essentially a 2D patterning process and results in formation of abrupt steps in regions where the distribution channel meets with the artificial capillaries which serve as stagnation zones that could result in thrombotic reaction. In addition, the design and the fabrication process used may not be suitable to embed membranes on both sides of the flow network which can significantly improve the oxygenation performance and consequently allow higher flow rates of operation.

2.4.2 Heart-driven MBO using oxygen

In an attempt to eliminate the need of an external pump, MBOs have been modified in such a way to achieve the same level of oxygenation at hydraulic resistance that is tuned to produce the required flow rate when operating at the arterio-venous pressure difference provided by the heart (~80 mm Hg[20] for a normal adult and 20 – 60 mm Hg[21] for preterm and term neonates). One way to achieve a lower operating pressure is to increase the height of the blood channel. However, the gas transfer could be compromised while the blood channels height is increased because the resistance to oxygen molecules diffusion would be dramatically increased. Double-sided gas diffusion for blood channels has been proposed as a solution to overcome this issue. In this section, heart-driven MBOs that are using oxygen as the sweep gas are reviewed.

Vacanti's research group developed a miniaturized microfluidic lung assist device[38] with a tissue-engineered architectural approach to simulate physiological blood flow rates of natural lungs in the blood channels of the vascular network (Figure 2.9). The vascular network consisted of microchannels with 100 µm height and a branching network, which was designed to mimic natural branching and sizing of blood vessels in natural lungs as explained by Murray in 1926 [39], [40] and was bonded to a 9-µm-thick gas permeable membrane. A computational calculation was done to design microchannel network that had uniform flow distribution at bifurcations, low shear stress of 14 – 56 dynes/cm^2 to avoid damaging red blood cells (the physiologic arterial range is 10 – 70 dynes/cm^2 [41]), and low pressure drop to be driven by the pressure differential provided by a heart [38].

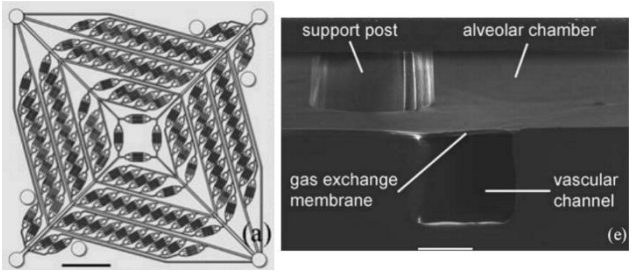

Figure 2.9: The microfluidic lung assist device with a biomimetic design which had been fabricated and tested with blood. Reproduced with permission from The Royal Society of Chemistry[38].

The total gas exchange surface area of their device was 23.1 $cm^{2,}$ but only 30 % of this area was active in gas transfer as the vascular channels. The oxygen uptake of 41 $mL/min/m^2$ at a blood flow rate of 6.3 mL/min was achieved while the pressure drop was around 20 mmHg and the pure oxygen was used as the ventilation gas. They also suggested to stack several layers to provide sufficient oxygen for an adult patient. Based on their calculations, 115 layers would be needed to achieve the required gas transfer and the gas exchange surface area would be 0.26 m^2. However, a 115-layers device would be too large to be used as a portable or clinical lung assist device [38]. Later, they studied the effect of channel dimensions, oxygen exposure length, and blood shear rate on the amount of the oxygen uptake and the carbon dioxide removal using a small-scale MBO. They demonstrated that blood in smaller channels would be more oxygenated compared to the larger channels at the same shear stress. They also showed that to achieve fully oxygenated blood for 50 and 100 µm channels, the residence time should be equal or greater than ~0.8 and ~1.1 seconds respectively [42].

2.5 MBOs Using Air:

Portability of the oxygenator is significantly enhanced when it uses air as the exchange gas instead of pure oxygen. Using atmospheric air could also avoid some complications because of using oxygen[43], [44]. In this part, MBOs are categorized based on their abilities to be operated by a pump or be heart-driven. Further, all heart-driven devices are further sub-divided into two groups: those with air channels that require pumping of air through them and those without air channels which are exposed directly to ambient air. The existence of air channels also limits the portability of these devices since a compressed air source is needed to supply air to the channels with small dimensions to always provide fresh air adjacent to membranes. In other words, not flowing fresh air to the channels can cause to the accumulation of carbon dioxide adjacent to membranes, thereby deteriorating oxygenation. Consequently, those devices that can be directly exposed to room air are more suitable for portable applications.

2.5.1 Pump-driven MBOs using air

Replacing pure oxygen with air could be considered as another step toward portability as it obviates the need of an external oxygen source. Since the use of air does not provide as much oxygen flux through the membrane, it requires device geometries that usually have significant pressure drop across them necessitating the use of a external pump.

One of the earliest such microfluidic devices was developed by Potkay *et al*.[45] which featured a non-porous PDMS membrane with 15 µm thickness and microcapillaries with 20 and 10 µm height using air as the sweep gas. To mimic the branching of the natural lungs, microchannels in the blood compartment were fabricated with different heights of 140, 60 and 20 or 10 µm. Artificial microcapillaries in blood side were 88 µm wide and spaced 88 µm apart. Support posts were used in the gas side to avoid the membrane collapsing, thereby reducing the effective surface area by 20%. Larger channels with (140 and 60 µm in height) were responsible for blood distribution (produced lower pressure drop), and smaller channels (10 or 20 µm in height) were used for efficient gas exchange. The total surface area including all branching channels and microcapillaries was 24 cm^2. Devices with 20 µm-tall and 10 µm-tall microcapillaries had the active gas exchange surface areas of 2.34 cm^2 and 1.67 cm^2 respectively[45] (Figure 2.10).

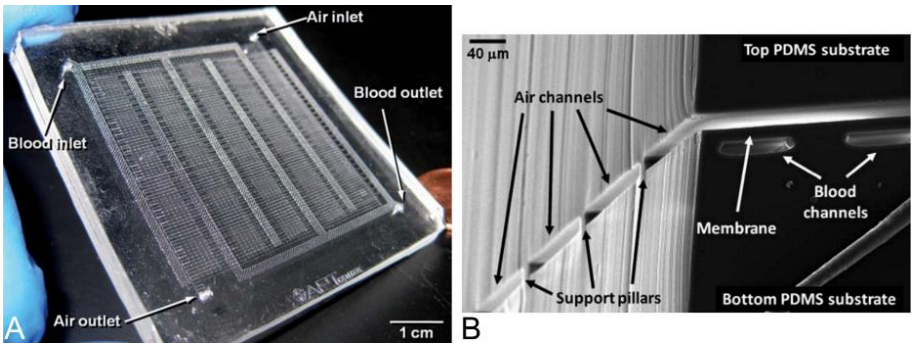

Figure 2.10: (A) A photograph of the device made by Potkay et al. (b) SEM image of the cross-sectional of the device. Reproduced with permission from The Royal Society of Chemistry[45].

In this study, porcine blood was used to test all devices while air was supplied as the ventilating gas. The highest oxygen uptake achieved in this experiment was around 0.04 mL/min at a blood flow rate of 1.5 mL/min with the corresponding pressure drop of ~ 500

mmHg. They observed that the pressure drop on the blood side increased over time which was due to clot formation in the small artificial capillaries. After ~3 hours running the blood into the device, they found that less than 10 % of the artificial microcapillaries were clogged. Also, they claimed that despite using air instead of pure oxygen, their device had a similar or better efficiency compared to other available artificial lungs[45].

The work done by Rieper[33] could also be categorized here as they also tested their device with air. Their device efficiency was decreased by around 50 % by using air as the ventilation gas which was expected since the oxygen concentration was lower in the air and the oxygen concentration differential was lower.

2.5.2 Heart-driven MBOs using Air

After replacing pure oxygen by compressed or atmospheric air as a ventilation gas, the next step would be to reduce the hydraulic resistance of these devices to the desired level (20 – 60 mm Hg[12], [46]–[48] for neonates and ~ 80 mm Hg[15] for adults) such that blood could be perfused in them solely from the arterio-venous pressure difference supplied by the heart. This was the next step towards portability by eliminating the need of an external pump for perfusing blood to the oxygenators. Some of the devices developed with this aim had air channels for gas exchange which required a compressed air line or cylinder as the gas source. Others only needed exposure to ambient air and were more suitable for portable operations.

2.5.2.1 With Air Channels

Potkay's group [49] developed a small-scale MBO with biomimetic blood flow which could promote uniform wall shear rate and minimize blood trauma (Figure 2.11). The blood microvascular network consisted of 200 µm-tall microchannels at the entrance of the device, 60 µm-tall microchannels as branching channels, and 8897 of 10 µm-tall microcapillaries, which were 60 µm wide and 370 µm long, for gas transfer. A 15 µm-thick silicone-based membrane and the biomimetic vascular network were bonded together by means of oxygen plasma. Also, polyethylene-glycol (PEG) was coated inside

of the vascular network to improve hemocompatibility [49]. Whole bovine blood was used to test PEG-coated and uncoated devices while compressed air was supplied to the gas chamber as the ventilating gas. Uncoated devices could increase oxygen saturation from ~ 60 % to 80 – 100 % at blood flow rates of 0.2 – 1 mL/min and the pressure drop of 2 – 10 mmHg. They also showed that changing air flows did not influence gas transfer significantly. Their results confirmed that PEG-coated device could operate at a longer time with minimal clotting comparing to uncoated devices whose exiting oxygen saturation significantly dropped after 60 minutes due to coagulating in microcapillaries [49].

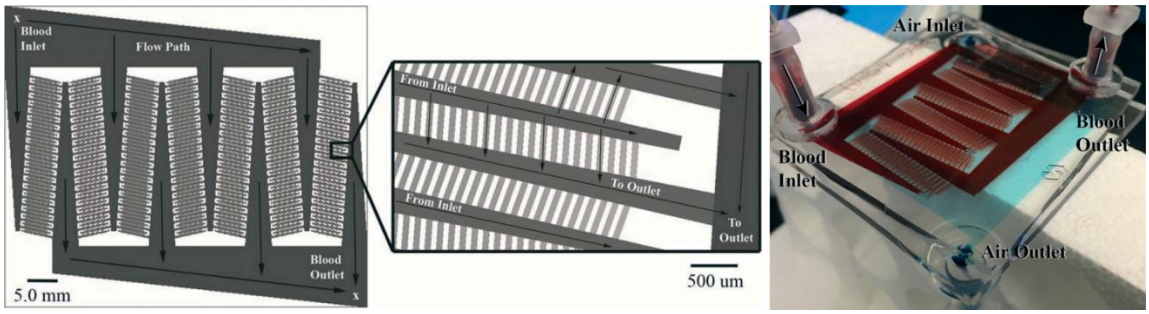

Figure 2.11: The MBO blood vascular network's design (the left picture) and the fabricated MBO by Kovach et al. Reproduced with permission from The Royal Society of Chemistry[49].

2.5.2.2 Without Air Channels

Ideal portable artificial lungs would be as simple as lungs to operate; They should not need an external pump to perfuse blood or gases such as oxygen and air for operation. One method to achieve these goals would be to use the individual's heart itself as the pump and to expose the blood through a thin membrane to the ambient air for gas exchange. Such a device will be the closest mimic of the natural lungs, simple in design and robust to operate. In this section, the progress of these devices is highlighted.

Wu et al.[48], [50] developed one such miniaturized MBO unit which was designed to be used specifically as a LAD for preterm and term neonates with respiratory failure. The device which consisted of a microfluidic vascular network and a gas permeable membrane was exposed directly to the ambient air. This unique design could eliminate

the need of a ventilating gas supply and add portability to the device. An 80 µm-tall microvascular network with 500 µm square pillars was bonded to four different membranes: a 20 µm-thick non-porous PDMS membrane, a porous PDMS membrane, and 6 µm-thick porous polycarbonate membranes with two pore sizes of 0.1 and 0.05 µm. (Figure 2.12). Moreover, they introduced a new interconnection design with a tapered configuration for the inlet and outlet to reduce the pressure drop which was generated because of a sharp bend in flow direction[48], [50]. The total gas exchange surface area was 15.26 cm^2 and the priming volume was 0.122 mL which led to a surface-to-volume ratio of 125.082 cm^{-1}. The porous PDMS membrane had the highest gas transfer among all four membranes. A maximum oxygen uptake of ~ 2 µL/min/cm^2 was achieved at a blood flow rate of 4 mL/min for the porous PDMS membrane once the pressure drop was ~30 mmHg. They claimed that oxygen and carbon dioxide transfer were 367% and 233% more efficient compared to hollow fiber-based oxygenators, respectively[48], [50]. They found that very thin non-porous PDMS membranes (1– 5 µm) were too delicate to be easily handled and be bonded to the vascular network without any failure. Additionally, pinholes were observed for ultra-thin PDMS membranes with large surface area. Finally, they suggested that several oxygenator units should be stacked to support the required gas exchange.

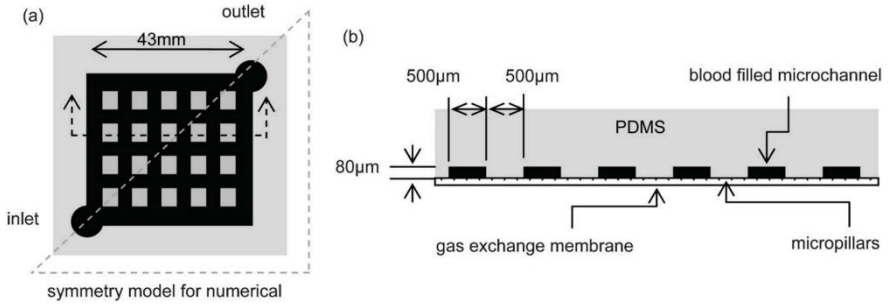

Figure 2.12: The top and cross-sectional view of the blood vascular network with micro-pillars. Reproduced with permission from The Royal Society of Chemistry[48].

Rochow et. al.[47], [51] developed a modular LAD by stacking several small-scale MBOs developed by Wu et. al.[48] to supplement the gas transfer deficiency for one-Kg neonates. Ten small-scale microfluidic oxygenators were connected to each other in a

parallel configuration using 3D-printed manifolds (Figure 2.13). This LAD had a priming volume of 4.8 mL and was tested *in vitro* and *in vivo*. Blood flow rates varied from 5 to 40 mL/min to test the LAD *in vitro* under two different conditions: air ambient and a pure oxygen environment by placing the LAD under a hood with flowing oxygen. A maximum oxygen uptake of 10.4 µL/min/cm^2 was reached at a blood flow rate of 40 mL/min and an average pressure drop of 60 mmHg for the LAD tested by pure oxygen. The total gas exchange surface area for the LAD with 10 microfluidic oxygenators was 152.6 cm^2.

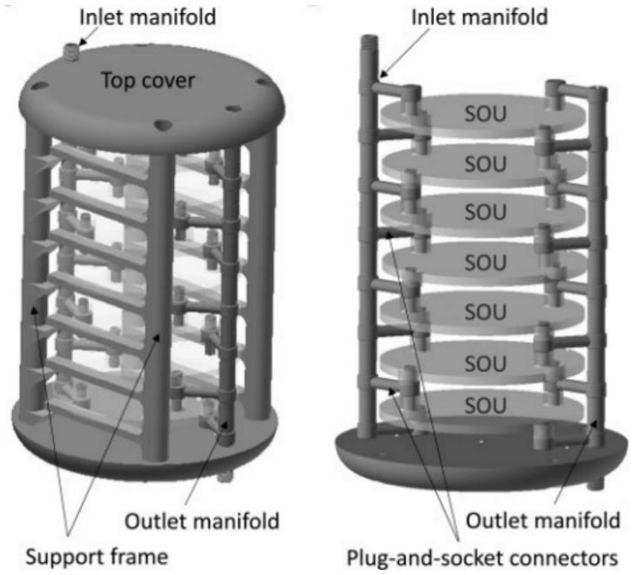

Figure 2.13: The modular LAD with 10 MBOs designed to provide required oxygenation for preterm neonates with respiratory failure. Reproduced with permission from Wiley[47].

Later, baby piglets were used to measure gas transfer of the LAD while being perfused solely by the animal's heart. Two different experimental setups for animal tests were used: (i) the LAD was attached to the left carotid artery, and the right jugular vein (5 piglets) and (ii) the LAD was connected between the umbilical artery and the umbilical vein (2 piglets). This study was the first of its kind for an MBO to be able to achieve high gas transfer with low priming volume, low pressure drops and the elimination of an external pump for perfusion. However, this LAD could not fully oxygenate blood due to short residence time of blood in the device.

Table 2.1 compares the performance of all MBOs in the literature that have been developed till now. Here, four parameters of which are priming volume, oxygen transfer, blood flow rate, and pressure drop are represented as the main criteria to compare these devices. Oxygen transfer is reported as mL of oxygen per liters of blood to show the real capacity of each device. As shown in this table, most MBOs do not support high blood flow rates (usually a blood flow rate lower than 10 mL/min) to fulfill the gas transfer need for patients. The highest oxygen transfer (60 mL O_2/L_{Blood} using oxygen and 32 mL O_2/L_{Blood} using air) was achieved by the double-sided MBO developed by Rieper et al.[33] at the highest blood flow rate (50 mL min^{-1}) reported for a microfluidic-based oxygenator. Also, their device has the highest gas exchange surface area among all MBOs. The superior performance of their device shows that blood channels with double-sided gas exchange are the best option to improve the overall gas transfer capacity of an MBO. However, even such a device cannot provide required gas transfer for clinical applications and should be significantly scaled up to meet patients' needs.

Table 2.1: A summary of previous studies in MBOs. This table includes only devices which have been tested by blood. The oxygen uptake data represents the maximum reported results at achieved blood flow rates for that oxygen uptake.

Source	H [µm]	Surface Area [cm^2]	Priming Volume [mL]	Max O_2 Transfer [mL O_2/L_{Blood}]	Blood Flow [mL/min]	ΔP [mm Hg]	Supply Gas
Lee[24] 2008	15	0.83	0.00124	10.5	1.9	4	O_2
	15	0.83	0.00124	3.33	1.9	4	Air
Hoganson[26] 2010	200	18	N/A	40.18	4	67	O_2
Potkay[45] 2011	20	2.34	0.00585	21.4	1.5	500	Air
	10	1.67	0.00208	25	1.5	N/A	Air
Hoganson[38] 2011	100	23.1	N/A	15.03	6.3	20	O_2
Kniazeva[52] 2012	100	N/A	N/A	26.5	10	N/A	O_2
Wu[48] 2013	80	15.26	0.122	7.05	4	25	Air
Rochow[47] 2014	80	152.6	4.8	40	40	63	O_2
	80	152.6	4.8	7.63	40	63	Air
Rieper[33] 2015	100	1200	7	60	50	80	O_2
	100	1200	7	32	50	80	Air
Gimbel[29] 2016	100	33.02	0.165	48	25	N/A	O_2
Thompson[36] 2017	10	2.21	0.027	N/A	1.25	120	O_2
	10	2.21	0.027	N/A	0.5	75	Air
Thompson[37]	30	31.5	0.47	16	25	83	O_2

2.6 Future Challenges

Up to now, several MBOs have been developed and tested. MBOs achieved high gas exchange efficiencies thanks to their high surface-area-to-volume ratios. Furthermore, low priming volume, a biomimetic blood vascular network which provides uniform blood distribution, and feasibility of working with ambient air make them promising alternatives for current commercial oxygenators. Even though significant effort was made to minimize the priming volume and pressure drop for these MBOs while reaching the maximum oxygenation, further improvements can still be made to enhance their gas exchange performance, especially at higher blood flow rates. For instance, unlike hollow fiber membranes where the gas exchange occurs from all sides, microfluidic oxygenators still only allow gas exchange on one or two sides of their network. The challenges involved with these devices can be categorized to scale-up and manufacturing challenges, surface modification of PDMS devices to improve hemocompatibility, and large-bore access for artificial placenta applications.

2.6.1 Scale-Up and Manufacturing Challenges

The primary challenge for MBOs to meet clinical needs and to meet some of the capabilities of the hollow fiber membrane oxygenators is low throughput. To address this issue, two approaches have been taken: 1) fabricating devices with larger gas exchange surface area to enhance the gas exchange capacity in a single layer device and 2) stacking several layers in parallel to increase the overall throughput. Practically, both of these approaches must be combined to overcome this challenge. First, the size of MBO should be expanded to provide higher gas transfer at higher blood flow rates. For instance, Thompson et al.[37] could fabricate a single layer device capable of standing a high blood flow rate of 25 mL/min to employ a reasonable oxygen transfer. However, there were manufacturing limitations that prevents the expansion of the device size; the photolithography facilities can only support small wafers around 8 - 12 inches. However, Thompson et al.[37] work proved that it would be feasible to achieve better efficiency

with suitable modifications like increasing the number of blood channels per device for increasing the gas exchange capacity and optimizing blood channel's height to minimize pressure drop while achieving a good oxygenation. With the current microfabrication technologies, it may be possible to achieve a maximum blood flow rate of 40-50 mL for a single layer device. Next, several such units can be connected in parallel to achieve higher capacities. The biggest challenge to parallelization of single layer devices is the interconnections of these layers as these connectors occupy a considerable portion of the total priming volume[47]. To avoid using a signifcant number of connectors which results in a high priming volume, these single layers should be brought very close to each other, or the fabrication process can integrate both the oxygenator as well as the connectors and the flow distributors in one single process.

As it was reported in several works[36]–[38], [49], the flow distributor channels, which do not have a contribution in gas exchange and are only responsible for blood distribution, and main blood channels ,which are involved in gas exchange, should be designed and fabricated with different heights to avert high shear stress and pressure drop generation. Nevertheless, the conventional photolithography technique is restricted in 2D designs resulting in manufacturing microfeatures with a sharp and sudden change in blood flow which could lead to creating dead zones with a great chance of hemolysis. The promising solution to this problem is to use other manufacturing processes which are capable of fabrication in microscale. Computer Numerical Control (CNC) machining has shown a great potential to construct master molds with micro-scale features for MBOs[33]. CNC machining has more freedom in size and 3D designs which make it very useful for mass production. However, a mold fabricated by this method would have a rough surface (at least around 1 µm). Therefore the manufactured devices would be more prone to clot formation.

As mentioned above, the future of microfluidic blood oxygenators are tied to the available manufacturing technologies. In order to overcome the limitations associated with these conventional manufacturing technologies, Additive Manufacturing (AM) can be used in the fabrication of microfluidic blood oxygenators to realize the advantage of real 3D

micro structures. AM has the potential to construct a complex 3D network of microchannels at a large scale with an acceptable repeatibilty[53]. This 3D network can be fabricated by either directly printing PDMS or a silicone-based material[54], [55] or casting PDMS around a sugar-based construction which can be dissolved later by water[56], [57]. Consequently, a large-scale MBO with 3D structures will be manufactured without the need of stacking several single-layer devices.

2.6.2 Surface Modification of PDMS Devices to Improve Hemocompatibility

The LAD including the catheters and lines are in contact with the patient's blood and vessels. For instance, it has been identified that in neonates who received ECMO, several factors alter the clotting system and induce inflammatory responses[58]. The events in this chain are hemodilution, dilutional coagulopathy, contact factor pathway activation, thrombin generation, platelet activation, platelet dysfunction, and inflammatory responses including complement activation and cytokine release. To prevent the circuit from clotting, systemic anticoagulation is necessary. The aim is to achieve biocompatibility to prevent thrombosis and coagulation of the LAD's channel, to preserve platelet functions, and to avert bleeding and inflammation[59], [60]. Several approaches to accomplish on the biocompatibility of the medical devices by surface modification has been proposed[60]. Ideally, the surface modifications should cover the entire area which is in contact with blood and the body. The surface modification should be stable while the device is performing as well as the manufacturing should be feasible and economic[60]. PDMS is widely used for the fabrication of MBOs as it has high gas permeability, transparency, and flexibility. Nonetheless, PDMS has an intrinsic hydrophobic nature and is more likely to adsorb proteins on its surface[61]. For instance, hydrophobic surfaces are more attractive to fibrinogen which is widely found in plasma and involved in blood coagulation[62]–[64]. Therefore, it is critical to treat any blood contact surfaces inside these devices with an appropriate coating to be able to use them in long-term applications. To date, different coating strategies[65]–[73] have been applied to PDMS surfaces to enhance its hemocompatibility. Polyethylene glycol[49], [70], [72] (PEG) and antithrombin heparin[65], [66] (ATH) have been used specifically for MBOs by using

polydopamine as a bioglue[74], [75]. In addition, surface passivation and biomimetic surface functionalization have been described for PDMS[71], [73], [76]–[78]. Another promising approach to achieve biocompatibility is endothelialization of all inner surfaces. This approach adopts the natural properties of the endothelium and aims to create a monolayer of endothelial cells which controls all hemostatic and anti-inflammatory function. Currently there are two major concepts to produce endothelization: First, is the in vitro pre-endothelialization of the circuit[79] and second the self endothelialization ("in situ capture" or "fallout seeding") of circulating endothelial progenitor cells to surfaces[80]–[82]. This type of surface modification is done for PDMS surfaces[29], [83] and MBOs, showing that the gas exchange can also be promoted[83].

In conclusion, the application of the LAD requires an approach for surface modification to achieve biocompatibility of the PDMS device. Currently, there are several methods for surface modification for PDMS under development. Biometric surface functionalization with covalent ATH complex linked with polydopamine on PDMS seems to be promising as ATH has higher activity and a longer half-life compared to heparin. In addition to surface modification of blood contact surfaces, the blood flow path should be adequately designed to ensure that platelets and different cells will not be damaged because of high shear stress regions and they will experience smooth travel through the blood vascular network without activating of platelets and thrombus formations[84], [85]. This should be considered in designing of each component from the blood vascular network to all connectors to assure that platelet activation, protein adsorption, inflammation, and thrombosis are avoided.

2.6.3 Large-Bore Access for Artificial Placenta Applications

To use microfluidic-based LADs as an artificial placenta device, the access to the umbilical vessels is necessary. However, these vessels start constricting immediately after birth, and the catheters explicitly designed for umbilical have very small inner diameters with a long length which can introduce significant resistance to blood flow, thereby reducing the achieved blood flow rate by such a LAD[86], especially in a passive device

that is pumped just by the arterio-venous pressure difference. If a sufficient blood flow rate is not achieved (~ 30 mL/min/kg[47], [48]), then the systemic oxygen saturation may not reach the levels required to serve a lung assist function. The umbilical artery and vein have a large diameter of 4 ± 2 mm and 9 ± 5 mm, respectively, at 36 weeks of gestation, suggesting that these vessels have the capability of reopening to these dimensions after birth[86]. Therefore, an optimal solution would be to reopen these vessels to provide the required blood flow rates for an artificial placenta type LAD.

An interesting approach is to design a catheter with high flexibility to insert into these vessels while being expanded by reaching to its designated location. Such a catheter can have a smaller outer diameter of ~ 2 mm to easily be inserted to the vessels, then be inflated or expanded to the maximum diameter to provide the required blood flow rate. Different advanced technologies such as shape memory polymers[87]–[95], soft robotics[46], [96]–[100], microfluidic-based soft robotics[98], [101]–[104], and inflatable or expandable stents[105] can be adopted here to develop such an expandable catheter for the access through umbilical vessels.

2.7 Summary

In this review, miniaturization of blood oxygenators is considered as an essential key toward portability. Hollow fiber membranes are widely used in clinical settings, but they have high priming volume and need an external pump (most scenarios) and an oxygen source. In the last few years, some effort has been made to reduce the size of these devices and increase their gas exchange efficiencies. However, there is a trade-off between priming volume and pressure drop for hollow fiber membranes. Microfluidics blood oxygenators are another type of blood oxygenators which still under research improvement. Although few microfluidic-based oxygenators have been introduced as an artificial placenta device for preterm infants, they still cannot provide all gas exchanges required for an adult patient due to their small size. Nonetheless, microfluidics blood oxygenators have shown high gas transfer efficiency at small scale which can make them a promising replacement for hollow fiber membranes in the future. The shortcoming of the current microfabrication methods is recognized as the principal limitation in the scale-up process of these devices. This challenge can be addressed by using additive manufacturing which can facilitate the fabrication of 3D features at a larger scale. Hemocompatibility and large bore-access to umbilical vessels for an artificial placenta application are considered as others area of concerns for these devices.

References

[1] H. Iwahashi, K. Yuri, and Y. Nosé, "Development of the oxygenator: Past, present, and future," *J. Artif. Organs*, vol. 7, no. 3, pp. 111–120, 2004.

[2] M. W. Lim, "The history of extracorporeal oxygenators," *Anaesthesia*, vol. 61, no. 10, pp. 984–995, 2006.

[3] T. Yeager and S. Roy, "Evolution of Gas Permeable Membranes for Extracorporeal Membrane Oxygenation," *Artif. Organs*, vol. 41, no. 8, pp. 700–709, 2017.

[4] S. P. Madhani *et al.*, "In Vivo 5 Day Animal Studies of a Compact, Wearable Pumping Artificial Lung," *ASAIO J.*, p. 1, 2017.

[5] S. P. Madhani, B. J. Frankowski, and W. J. Federspiel, "Fiber Bundle Design for an Integrated Wearable Artificial Lung," *ASAIO J.*, vol. 63, no. 5, pp. 631–636, 2017.

[6] S. P. Madhani *et al.*, "In vitro and in vivo evaluation of a novel integrated wearable artificial lung," *J. Hear. Lung Transplant.*, vol. 36, no. 7, pp. 806–811, 2017.

[7] J. Arens *et al.*, "The aachen MiniHLM - A miniaturized heart-lung machine for neonates with an integrated rotary blood pump," *Artif. Organs*, vol. 34, no. 9, pp. 707–713, 2010.

[8] R. Kopp *et al.*, "A miniaturized extracorporeal membrane oxygenator with integrated rotary blood pump: Preclinical in vivo testing," *ASAIO J.*, vol. 57, no. 3, pp. 158–163, 2011.

[9] P. C. Schlanstein, R. Borchardt, I. Mager, T. Schmitz-Rode, U. Steinseifer, and J. Arens, "Gas exchange efficiency of an oxygenator with integrated pulsatile displacement blood pump for neonatal patients," *Int. J. Artif. Organs*, vol. 37, no. 1, pp. 88–92, 2014.

[10] R. Borchardt, P. Schlanstein, I. Mager, J. Arens, T. Schmitz-Rode, and U. Steinseifer, "In vitro performance testing of a pediatric oxygenator with an integrated pulsatile pump," *ASAIO J.*, vol. 58, no. 4, pp. 420–425, 2012.

[11] K. Stang *et al.*, "First in vivo results of a novel pediatric oxygenator with an integrated pulsatile pump," *ASAIO J.*, vol. 61, no. 5, pp. 574–582, 2015.

[12] J. Arens *et al.*, "NeonatOx: A Pumpless Extracorporeal Lung Support for Premature Neonates," *Artif. Organs*, vol. 35, no. 11, pp. 997–1001, 2011.

[13] H. A. Stone and S. Kim, "Microfluidics: Basic issues, applications, and challenges," *AIChE J.*, vol. 47, no. 6, pp. 1250–1254, 2001.

[14] W. J. Federspiel and K. A. Henchir, “Lung, Artificial: Basic Principles and Current Applications,” *Encyclopedia of Biomaterials and Biomedical Engineering, edited by G.L. Bowlin and G. Wnek (Marcel 49 Dekker, New York, 2004)*. Marcel Dekker, Inc, New York, pp. 910–921, 2004.

[15] J. a Potkay, “The promise of microfluidic artificial lungs.,” *Lab Chip*, vol. 14, no. 21, pp. 4122–4138, 2014.

[16] R. L. Kolobow, Theodor; Bowman, “CONSTRUCTION AND EVALUATION OF AN ALVEOLAR MEMBRANE ARTIFICI... : ASAIO Journal,” *Am. Soc. Artif. Intern. Organs*, vol. 9, no. 1, pp. 238–243, 1963.

[17] H. S. B. and M. H. W. T.-K. Hung, “Transport and Flow Phenomena in a Microchannel Membrane Oxygenator,” *Ann. Biomed. Eng*, vol. 5, no. 4, pp. 343–361, 1977.

[18] A. Lamberti, S. L. Marasso, and M. Cocuzza, “PDMS membranes with tunable gas permeability for microfluidic applications,” *RSC Adv.*, vol. 4, no. 106, pp. 61415–61419, 2014.

[19] G. Firpo, E. Angeli, L. Repetto, and U. Valbusa, “Permeability thickness dependence of polydimethylsiloxane (PDMS) membranes,” *J. Memb. Sci.*, vol. 481, pp. 1–8, 2015.

[20] J. E. Hall, *Guyton and Hall textbook of medical physiology*. Elsevier Health Sciences, 2015.

[21] N. Rochow *et al.*, “Artificial placenta -Lung assist devices for term and preterm newborns with respiratory failure,” *Int J Artif Organs*, vol. 36, pp. 377–391, 2013.

[22] J. K. Lee, H. H. Kung, and L. F. Mockros, “Microchannel technologies for artificial lungs: (1) theory.,” *ASAIO J.*, vol. 54, no. 4, pp. 372–82, 2008.

[23] M. C. Kung, J.-K. Lee, H. H. Kung, and L. F. Mockros, “Microchannel technologies for artificial lungs: (2) screen-filled wide rectangular channels.,” *ASAIO J.*, vol. 54, no. 4, pp. 383–9, 2008.

[24] L. M. JK Lee, MC Kung, HH KUng, “Microchannel Technologies for Artificial Lungs: (3) Open Rectangular Channels,” *ASAIO J. NIH Public Access*, vol. 54, no. 4, pp. 390–395, 2008.

[25] K. A. Burgess, H. H. Hu, W. R. Wagner, and W. J. Federspiel, “Towards microfabricated biohybrid artificial lung modules for chronic respiratory support,” *Biomed. Microdevices*, vol. 11, no. 1, pp. 117–127, 2009.

[26] D. M. Hoganson *et al.*, “Branched vascular network architecture: a new approach to lung assist device technology.,” *J. Thorac. Cardiovasc. Surg.*, vol. 140, no. 5, pp. 990–995, 2010.

[27] T. Kniazeva, J. C. Hsiao, J. L. Charest, and J. T. Borenstein, “A microfluidic respiratory assist

device with high gas permeance for artificial lung applications," *Biomed. Microdevices*, vol. 13, no. 2, pp. 315–323, 2011.

[28] T. Kniazeva *et al.*, "Performance and scaling effects in a multilayer microfluidic extracorporeal lung oxygenation device," *Lab Chip*, vol. 12, no. 9, pp. 1686–1695, 2012.

[29] A. A. Gimbel, E. Flores, A. Koo, G. García-Cardeña, and J. T. Borenstein, "Development of a biomimetic microfluidic oxygen transfer device," *Lab Chip*, vol. 16, no. 17, pp. 3227–3234, 2016.

[30] A. A. Gimbel, E. Flores, A. Koo, G. García-Cardeña, and J. T. Borenstein, "Development of a biomimetic microfluidic oxygen transfer device," *Lab Chip*, vol. 10, no. 17, p. 1047, 2016.

[31] R. Sreenivasan, E. K. Bassett, D. M. Hoganson, J. P. Vacanti, and K. K. Gleason, "Ultra-thin, gas permeable free-standing and composite membranes for microfluidic lung assist devices," *Biomaterials*, vol. 32, no. 16, pp. 3883–3889, 2011.

[32] T. Femmer, M. L. Eggersdorfer, A. J. Kuehne, and M. Wessling, "Efficient gas-liquid contact using microfluidic membrane devices with staggered herringbone mixers," *Lab Chip*, vol. 15, no. 15, pp. 3132–3137, 2015.

[33] T. Rieper, C. Muller, and H. Reinecke, "Novel scalable and monolithically integrated extracorporeal gas exchange device," *Biomed. Microdevices*, vol. 17, no. 5, pp. 1–10, 2015.

[34] A. S. and J. M. MH Kroll, JD Hellums, LV McIntire, "Platelets and Shear Stress," *Blood*, vol. 88, no. 5, pp. 1525–1541, 1996.

[35] A. M. Malek, "Hemodynamic Shear Stress and Its Role in Atherosclerosis," *Jama*, vol. 282, no. 21, pp. 2035–2042, 1999.

[36] A. J. Thompson, L. H. Marks, M. J. Goudie, A. Rojas-Pena, H. Handa, and J. A. Potkay, "A small-scale, rolled-membrane microfluidic artificial lung designed towards future large area manufacturing," *Biomicrofluidics*, vol. 11, no. 2, 2017.

[37] A. J. Thompson, L. J. Ma, T. J. Plegue, and J. A. Potkay, "Design Analysis and Optimization of a Single Layer PDMS Microfluidic Artificial Lung," *Trans. Biomed. Eng.*, 2018.

[38] D. M. Hoganson, H. I. Pryor, E. K. Bassett, I. D. Spool, and J. P. Vacanti, "Lung assist device technology with physiologic blood flow developed on a tissue engineered scaffold platform.," *Lab Chip*, vol. 11, no. 4, pp. 700–707, 2011.

[39] C. D. Murray, "the Physiological Principle of Minimum Work Applied To the Angle of Branching of Arteries," *J. Gen. Physiol.*, vol. 9, no. 6, pp. 835–841, 1926.

[40] C. D. Murray, “The physiological principle of minimum work.I. The vascular system and the cost of blood volume,” *Proc.Natl. Acad. Sci. U. S. A.*, vol. 12, no. 3, pp. 207–214, 1926.

[41] A. M. Malek, S. L. Alper, and S. Izumo, “Hemodynamic Shear Stress and Its Role in Atherosclerosis,” *JAMA*, vol. 282, no. 21, p. 2035, Dec. 1999.

[42] E. K. Bassett, D. M. Hoganson, J. H. Lo, E. J. N. Penson, and J. P. Vacanti, “Influence of vascular network design on gas transfer in lung assist device technology.,” *ASAIO journal (American Society for Artificial Internal Organs : 1992)*, vol. 57, no. 6. pp. 533–8, 2011.

[43] S. Perrone, C. Bracciali, N. Di Virgilio, and G. Buonocore, “Oxygen Use in Neonatal Care: A Two-edged Sword,” *Front. Pediatr.*, vol. 4, no. January, pp. 1–7, 2017.

[44] B. Weinberger, D. L. Laskin, D. E. Heck, and J. D. Laskin, “Oxygen Toxicity in Premature Infants,” *Toxicol. Appl. Pharmacol.*, vol. 181, no. 1, pp. 60–67, May 2002.

[45] J. A. Potkay, M. Magnetta, A. Vinson, and B. Cmolik, “Bio-inspired, efficient, artificial lung employing air as the ventilating gas.,” *Lab Chip*, vol. 11, no. 17, pp. 2901–2909, 2011.

[46] J. Shintake, V. Cacucciolo, D. Floreano, and H. Shea, “Soft Robotic Grippers,” *Adv. Mater.*, vol. 30, no. 29, 2018.

[47] N. Rochow *et al.*, “An Integrated Array of Microfluidic Oxygenators as a Neonatal Lung Assist Device: In Vitro Characterization and In Vivo Demonstration,” *Artif. Organs*, vol. 38, no. 10, pp. 856–866, Oct. 2014.

[48] W.-I. Wu *et al.*, “Lung assist device: development of microfluidic oxygenators for preterm infants with respiratory failure.,” in *Lab on a chip*, 2013, vol. 13, no. 13, pp. 2641–50.

[49] K. M. Kovach *et al.*, “In vitro evaluation and in vivo demonstration of a biomimetic, hemocompatible, microfluidic artificial lung.,” *Lab Chip*, vol. 15, no. 5, pp. 1366–75, 2015.

[50] W. Wu *et al.*, “Development of Microfluidic Oxygenators as Lung Assisting Devices for Preterm Infants,” in *15th International Conference on Miniaturized Systems for Chemistry and Life Sciences*, 2011, pp. 550–552.

[51] N. Rochow *et al.*, “Integrated microfluidic oxygenator bundles for blood gas exchange in premature infants,” *Proc. IEEE Int. Conf. Micro Electro Mech. Syst.*, no. February, pp. 957–960, 2012.

[52] T. Kniazeva *et al.*, “Performance and scaling effects in a multilayer microfluidic extracorporeal lung oxygenation device,” *Lab Chip*, vol. 12, no. 9, pp. 1686–1695, 2012.

[53] F. Liravi and E. Toyserkani, "Additive manufacturing of silicone structures: A review and prospective," *Addit. Manuf.*, vol. 24, no. January, pp. 232–242, 2018.

[54] S. Zheng, M. Zlatin, P. R. Selvaganapathy, and M. A. Brook, "Multiple modulus silicone elastomers using 3D extrusion printing of low viscosity inks," *Addit. Manuf.*, vol. 24, no. May, pp. 86–92, 2018.

[55] N. Bhattacharjee, C. Parra-Cabrera, Y. T. Kim, A. P. Kuo, and A. Folch, "Desktop-Stereolithography 3D-Printing of a Poly(dimethylsiloxane)-Based Material with Sylgard-184 Properties," *Adv. Mater.*, vol. 30, no. 22, pp. 1–7, 2018.

[56] A. Farzin *et al.*, "3D-Printed Sugar-Based Stents Facilitating Vascular Anastomosis," *Adv. Healthc. Mater.*, vol. 1800702, pp. 1–9, 2018.

[57] A. Bégin-Drolet *et al.*, "Design of a 3D printer head for additive manufacturing of sugar glass for tissue engineering applications," *Addit. Manuf.*, vol. 15, pp. 29–39, 2017.

[58] A. Kamdar, N. Rintoul, and L. Raffini, "Anticoagulation in neonatal ECMO," *Semin. Perinatol.*, vol. 42, no. 2, pp. 122–128, 2018.

[59] X. Liu *et al.*, "Blood compatible materials: State of the art," *J. Mater. Chem. B*, vol. 2, no. 35, pp. 5718–5738, 2014.

[60] D. Eytan, Y. Bitterman, and G. M. Annich, "VV extracorporeal life support for the Third Millennium: Will we need anticoagulation?," *J. Thorac. Dis.*, vol. 10, no. Suppl 5, pp. S698–S706, 2018.

[61] W.-I. Wu, K. N. Sask, J. L. Brash, and P. R. Selvaganapathy, "Polyurethane-based microfluidic devices for blood contacting applications," *Lab Chip*, vol. 12, no. 5, p. 960, Feb. 2012.

[62] T. A. Horbett and P. K. Weathersby, "Adsorption of proteins from plasma to a series of hydrophilic-hydrophobic copolymers. I. Analysis with thein situ radioiodination technique," *J. Biomed. Mater. Res.*, vol. 15, no. 3, pp. 403–423, May 1981.

[63] S. Tunc, M. F. Maitz, G. Steiner, L. Vázquez, M. T. Pham, and R. Salzer, "In situ conformational analysis of fibrinogen adsorbed on Si surfaces," *Colloids Surfaces B Biointerfaces*, vol. 42, no. 3–4, pp. 219–225, May 2005.

[64] C. F. W. and and † Maria M. Santore*, "Fibrinogen Adsorption on Hydrophilic and Hydrophobic Surfaces: Geometrical and Energetic Aspects of Interfacial Relaxations," 2001.

[65] J. M. Leung, L. R. Berry, A. K. C. Chan, and J. L. Brash, "Surface modification of

polydimethylsiloxane with a covalent antithrombin–heparin complex to prevent thrombosis," *J. Biomater. Sci. Polym. Ed.*, vol. 25, no. 8, pp. 786–801, May 2014.

[66] J. M. Leung *et al.*, "Surface modification of poly(dimethylsiloxane) with a covalent antithrombin–heparin complex for the prevention of thrombosis: use of polydopamine as bonding agent," *J. Mater. Chem. B*, vol. 3, no. 29, pp. 6032–6036, Jul. 2015.

[67] L. Yang, Y. Okamura, and H. Kimura, "Surface modification on polydimethylsiloxane-based microchannels with fragmented poly(l -lactic acid) nanosheets," *Biomicrofluidics*, vol. 9, no. 6, p. 064108, Nov. 2015.

[68] D. C. Leslie *et al.*, "A bioinspired omniphobic surface coating on medical devices prevents thrombosis and biofouling," *Nat. Biotechnol.*, vol. 32, no. 11, pp. 1134–1140, Nov. 2014.

[69] P. Xue *et al.*, "Surface Modification of Poly(dimethylsiloxane) with Polydopamine and Hyaluronic Acid To Enhance Hemocompatibility for Potential Applications in Medical Implants or Devices," *ACS Appl. Mater. Interfaces*, vol. 9, no. 39, pp. 33632–33644, Oct. 2017.

[70] T. J. Plegue, K. M. Kovach, A. J. Thompson, and J. A. Potkay, "Stability of Polyethylene Glycol and Zwitterionic Surface Modifications in PDMS Microfluidic Flow Chambers," *Langmuir*, vol. 34, no. 1, pp. 492–502, Jan. 2018.

[71] K. Nagahashi, Y. Teramura, and M. Takai, "Stable surface coating of silicone elastomer with phosphorylcholine and organosilane copolymer with cross-linking for repelling proteins," *Colloids Surfaces B Biointerfaces*, vol. 134, pp. 384–391, Oct. 2015.

[72] K. M. Kovach, J. R. Capadona, A. Sen Gupta, and J. A. Potkay, "The effects of PEG-based surface modification of PDMS microchannels on long-term hemocompatibility," *J. Biomed. Mater. Res. Part A*, vol. 102, no. 12, p. n/a-n/a, Jan. 2014.

[73] Z. Zhang, J. Borenstein, L. Guiney, R. Miller, S. Sukavaneshvar, and C. Loose, "Polybetaine modification of PDMS microfluidic devices to resist thrombus formation in whole blood," *Lab Chip*, vol. 13, no. 10, p. 1963, Apr. 2013.

[74] H. Lee, S. M. Dellatore, W. M. Miller, and P. B. Messersmith, "Mussel-inspired surface chemistry for multifunctional coatings.," *Science*, vol. 318, no. 5849, pp. 426–30, Oct. 2007.

[75] Y. Tokura, S. Harvey, C. Chen, Y. Wu, D. Y. W. Ng, and T. Weil, "Fabrication of Defined Polydopamine Nanostructures by DNA Origami-Templated Polymerization," *Angew. Chemie - Int. Ed.*, vol. 57, no. 6, pp. 1587–1591, 2018.

[76] T. J. Plegue, K. M. Kovach, A. J. Thompson, and J. A. Potkay, "Stability of Polyethylene Glycol and Zwitterionic Surface Modifications in PDMS Microfluidic Flow Chambers," *Langmuir*, vol. 34, no. 1, pp. 492–502, 2018.

[77] T. Yabuta, K. Tsuru, S. Hayakawa, and A. Osaka, "Synthesis of blood compatible PDMS-based organic-inorganic hybrid coatings," *J. Sol-Gel Sci. Technol.*, vol. 31, no. 1–3 SPEC.ISS., pp. 273–276, 2004.

[78] H. Chen *et al.*, "Fibrinolytic poly(dimethyl siloxane) surfaces," *Macromol. Biosci.*, vol. 8, no. 9, pp. 863–870, 2008.

[79] T. Liu, S. Liu, K. Zhang, J. Chen, and N. Huang, "Endothelialization of implanted cardiovascular biomaterial surfaces: The development from in vitro to in vivo," *J. Biomed. Mater. Res. - Part A*, vol. 102, no. 10, pp. 3754–3772, 2014.

[80] M. Avci-Adali, G. Ziemer, and H. P. Wendel, "Induction of EPC homing on biofunctionalized vascular grafts for rapid in vivo self-endothelialization - A review of current strategies," *Biotechnol. Adv.*, vol. 28, no. 1, pp. 119–129, 2010.

[81] J. H. Pang *et al.*, "In situ Endothelialization: Bioengineering Considerations to Translation," *Small*, vol. 11, no. 47, pp. 6248–6264, 2015.

[82] I. Adipurnama, M. C. Yang, T. Ciach, and B. Butruk-Raszeja, "Surface modification and endothelialization of polyurethane for vascular tissue engineering applications: A review," *Biomater. Sci.*, vol. 5, no. 1, pp. 22–37, 2017.

[83] S. Menzel *et al.*, "Towards a Biohybrid Lung: Endothelial Cells Promote Oxygen Transfer through Gas Permeable Membranes," *Biomed Res. Int.*, vol. 2017, pp. 1–8, 2017.

[84] M. B. Gorbet and M. V. Sefton, "Biomaterial-associated thrombosis: roles of coagulation factors, complement, platelets and leukocytes," *Biomaterials*, vol. 25, no. 26, pp. 5681–5703, Nov. 2004.

[85] X. Liu *et al.*, "Blood compatible materials: state of the art," *J. Mater. Chem. B*, vol. 2, no. 35, pp. 5718–5738, Aug. 2014.

[86] J. Peng *et al.*, "Postnatal dilatation of umbilical cord vessels and its impact on wall integrity: Prerequisite for the artificial placenta," *Int. J. Artif. Organs*, vol. 41, no. 7, pp. 393–399, Jul. 2018.

[87] Y. Zhang *et al.*, "Radiopaque Highly Stiff and Tough Shape Memory Hydrogel Microcoils for Permanent Embolization of Arteries," *Adv. Funct. Mater.*, vol. 28, no. 9, pp. 1–11, 2018.

[88] K. Kratz, U. Voigt, and A. Lendlein, "Temperature-memory effect of copolyesterurethanes and

their application potential in minimally invasive medical technologies," *Adv. Funct. Mater.*, vol. 22, no. 14, pp. 3057–3065, 2012.

[89] M. Behl, M. Y. Razzaq, and A. Lendlein, "Multifunctional shape-memory polymers," *Adv. Mater.*, vol. 22, no. 31, pp. 3388–3410, 2010.

[90] H. Xu, C. Yu, S. Wang, V. Malyarchuk, T. Xie, and J. A. Rogers, "Deformable, programmable, and shape-memorizing micro-optics," *Adv. Funct. Mater.*, vol. 23, no. 26, pp. 3299–3306, 2013.

[91] W. Voit *et al.*, "High-strain shape-memory polymers," *Adv. Funct. Mater.*, vol. 20, no. 1, pp. 162–171, 2010.

[92] A. Balasubramanian, R. Morhard, and C. J. Bettinger, "Shape-memory microfluidics," *Adv. Funct. Mater.*, vol. 23, no. 38, pp. 4832–4839, 2013.

[93] Z. Zhao, K. Zhang, Y. Liu, J. Zhou, and M. Liu, "Highly Stretchable, Shape Memory Organohydrogels Using Phase-Transition Microinclusions," *Adv. Mater.*, vol. 29, no. 33, pp. 1–8, 2017.

[94] C. M. Yakacki, R. Shandas, D. Safranski, A. M. Ortega, K. Sassaman, and K. Gall, "Strong, tailored, biocompatible shape-memory polymer networks," *Adv. Funct. Mater.*, vol. 18, no. 16, pp. 2428–2435, 2008.

[95] H. Yang *et al.*, "3D Printed Photoresponsive Devices Based on Shape Memory Composites," *Adv. Mater.*, vol. 29, no. 33, pp. 1–7, 2017.

[96] B. Gorissen, D. Reynaerts, S. Konishi, K. Yoshida, J. W. Kim, and M. De Volder, "Elastic Inflatable Actuators for Soft Robotic Applications," *Adv. Mater.*, vol. 29, no. 43, pp. 1–14, 2017.

[97] S. M. Mirvakili and I. W. Hunter, "Artificial Muscles: Mechanisms, Applications, and Challenges," *Adv. Mater.*, vol. 30, no. 6, pp. 1–28, 2018.

[98] L. Hines, K. Petersen, G. Z. Lum, and M. Sitti, "Soft Actuators for Small-Scale Robotics," *Adv. Mater.*, vol. 29, no. 13, 2017.

[99] R. V. Martinez, A. C. Glavan, C. Keplinger, A. I. Oyetibo, and G. M. Whitesides, "Soft actuators and robots that are resistant to mechanical damage," *Adv. Funct. Mater.*, vol. 24, no. 20, pp. 3003–3010, 2014.

[100] B. Mosadegh *et al.*, "Pneumatic networks for soft robotics that actuate rapidly," *Adv. Funct. Mater.*, vol. 24, no. 15, pp. 2163–2170, 2014.

[101] T. Ranzani, S. Russo, N. W. Bartlett, M. Wehner, and R. J. Wood, "Increasing the Dimensionality of Soft Microstructures through Injection-Induced Self-Folding," *Adv. Mater.*, vol. 30, no. 38, pp. 1–6, 2018.

[102] T. N. Do, H. Phan, T. Q. Nguyen, and Y. Visell, "Miniature Soft Electromagnetic Actuators for Robotic Applications," *Adv. Funct. Mater.*, vol. 28, no. 18, pp. 1–11, 2018.

[103] E. Diller and M. Sitti, "Three-dimensional programmable assembly by untethered magnetic robotic micro-grippers," *Adv. Funct. Mater.*, vol. 24, no. 28, pp. 4397–4404, 2014.

[104] V. Magdanz, M. Medina-Sánchez, L. Schwarz, H. Xu, J. Elgeti, and O. G. Schmidt, "Spermatozoa as Functional Components of Robotic Microswimmers," *Adv. Mater.*, vol. 29, no. 24, pp. 1–18, 2017.

[105] A. A. Amiri Moghadam *et al.*, "Toward Development of Inflatable Stents with Application in Endovascular Treatments," *Adv. Funct. Mater.*, vol. 1804147, pp. 1–9, 2018.

3 Chapter 3

STEEL REINFORCED COMPOSITE SILICONE MEMBRANES AND ITS INTEGRATION TO MICROFLUIDIC OXYGENATORS FOR HIGH PERFORMANCE GAS EXCHANGE

Complete citation:

Harpreet Matharoo*, Mohammadhossein Dabaghi*, Niels Rochow, Gerhard Fusch, Neda Saraei, Mohammed Tauhiduzzaman, Stephen Veldhuis, John Brash, Christoph Fusch, and P. Ravi Selvaganapathy. *"Steel reinforced composite silicone membranes and its integration to microfluidic oxygenators for high performance gas exchange."* Biomicrofluidics 12, no. 1 (2018): 014107.

Copyright:

Contribution:

My contributions include designing and fabricating the lung assist device for in vitro and in vivo experiments, planning and performing the related experiments, interpretation and analysis of data and results, and writing the manuscript.

* Both authors contributed equally to this work.

3.1 Abstract

Respiratory distress syndrome (RDS) is one of the main causes of fatality in newborn infants, particularly in neonates with low birth-weight. Commercial extracorporeal oxygenators have been used for low-birth-weight neonates in neonatal intensive care units (NICU). However, these oxygenators require high blood volumes to prime. In the last decade, microfluidics oxygenators using enriched oxygen have been developed for this purpose. Some of these oxygenators use thin polydimethylsiloxane (PDMS) membranes to facilitate gas exchange between the blood flowing in the microchannels and the ambient air outside. However, PDMS is elastic and the thin membranes exhibit significant deformation and delamination under pressure which alters the architecture of the devices causing poor oxygenation or device failure. Therefore, an alternate membrane with high stability, low deformation under pressure, and high gas exchange was desired. In this paper, we present a novel composite membrane consisting of an ultra-thin stainless-steel mesh embedded in PDMS, designed specifically for a microfluidic single oxygenator unit (SOU). In comparison to homogeneous PDMS membranes, this composite membrane demonstrated high stability, low deformation under pressure, and high gas exchange. In addition, a new design for oxygenator with sloping profile and tapered inlet configuration has been introduced to achieve the same gas exchange at lower pressure drops. SOUs were tested by bovine blood to evaluate gas exchange properties. Among all tested SOUs, the flat design SOU with composite membrane has the highest oxygen exchange of 40.32 mL/min/m2. The superior performance of the new device with composite membrane was demonstrated by constructing a lung assist device (LAD) with a low priming volume of 10 mL. The LAD was achieved the oxygen uptake of 0.48 – 0.90 mL/min and the CO2 release of 1.05 – 2.27 mL/min at blood flow rates of ranging between 8 – 48 mL/min. This LAD was shown to increase the oxygen saturation level by 25 % at the low pressure drop of 29 mmHg. Finally, a piglet was used to test the gas exchange capacity of the LAD in vivo. The animal experiment results were in accordance with in-vitro results which shows that the LAD is capable of providing sufficient gas exchange at a blood flow rate of ~24 mL/min.

3.2 Introduction

RDS is a significant cause of infant mortality even in developed countries. For instance, it has been shown to be the second highest (16%) cause for mortality of infants, who were born with low-weight and suffering from RDS, between the age of one and eighteen years in England and Wales [1]. Respiratory failure under severe RDS is usually treated by mechanical ventilation, or extracorporeal membrane oxygenation (ECMO). Intensive mechanical ventilation can cause necrotizing bronchiolitis and alveolar septal injury with inflammation and scarring [2]. As a result chronic long term complications, i.e. bronchopulmonary dysplasia (BPD) can develop which often require prolonged hospitalization and home oxygen support [3]. ECMO has been shown to significantly reduce mortality in situations where mechanical ventilation is not sufficient. However, the main disadvantage of ECMO is that it requires surgery to connect the device to central blood vessels. Furthermore, ECMO requires systemic anticoagulation, placing the patient at high risk for hemorrhage, in particular intracranial hemorrhage with related neurological complications [4]. Additionally, the current ECMO devices have a high filling volume requiring priming with donor blood and veno-venous as well as veno-arterial ECMO systems need support by external pumps [5].

To design such an oxygenator, it should be noted that neonates typically have the arterio venous pressure difference in the range of 20 – 60 mmHg (~30 mmHg on average), a typical weight of 500 up to 2000 g. A neonate of about 1 kg with RDS will require about 15 to 45 mL/min of their blood to be oxygenated through an external device such as an oxygenator in order to be sustained [6]. Therefore, an ideal oxygenation device for use with preterm infants will have low priming volume, can be pumpless and use the arterio-venous pressure difference to perfuse, have a high surface to volume ratio for high gas exchange and exchanges gases with the ambient environment, obviating the need for an enriched oxygen atmosphere [6]. A prototype of such an device based on microfluidic oxygenating units was recently described [2], [6]. Among reported microfluidic oxygenators [2], [7], [16]–[18], [8]–[15], only those of Wu [18] and Rochow [2] were designed for operation at low pressure and in ambient air. Other devices required either

an external blood pump which could lead to additional complications such as hemolysis and erythrocyte damage[19], [20] or had an ‘‘alveolar’’ chamber or microchannels [9], [10], [12]–[15], [17], [21] to deliver pure oxygen to the blood to enhance oxygen transfer. Polydimethylsiloxane (PDMS) has been the first choice membrane for all these microfluidic blood oxygenators due to its high permeability to oxygen and carbon dioxide. However, it is elastic and deforms easily which can lead to delamination. This characteristic is particularly detrimental in oxygenators that are exposed to ambient air [18]rather than pressurized enriched oxygen. Increasing the stiffness of the PDMS membrane which still preserving its oxygen transfer characteristics can be a potential way to improve the performance of such oxygenators. In this paper, we report on a novel composite gas-permeable membrane fabricated by embedding an ultra-thin stainless-steel mesh in PDMS. Additionally, a new design for the blood flow path (referred to as the “vascular network”) is introduced to reduce the hydraulic resistance of the single SOU devices while not affecting gas transfer capacity at low blood flow rates. We describe the characteristics and performance of the SOU and LAD in vitro and compare the LAD results of an in-vivo animal experiment

3.3 Materials and methods

3.3.1 Design

The oxygenator (also called the lung assist device -LAD) was designed to be modular to accommodate infants of various weights and consisted of several single oxygenator units (SOUs) combined in series and parallel combinations.

The SOU consisted of a microfluidic vascular network attached to a gas permeable membrane. The vascular network facilitates blood distribution and formation of a thin layer of blood adjacent to the gas permeable membrane to allow oxygenation. Two designs were considered; one in which the height of the channels (100 µm) in the vascular network was uniform (Figure 3.1.a) and the other where the height gradually decreases from the inlet (170 µm) to the center (60 µm) and then increases to the outlet with 170 µm height (Figure 3.1.b). The gradual decrease of height from the inlet to the center

ensured that there are no dead zones and that there are no sudden changes in the shear stress encountered by the blood. The vascular network was in the shape of a square (43 mm on the side) with the inlet and the outlet connections (4.1 mm ID) at two diagonally opposite corners and consists of an array of pillars (1 mm x 1mm) to support the thin gas permeable membrane attached to it.

PDMS was used as the membrane material due to its high gas permeability [22]. However, thin PDMS membrane bulges out when the microfluidic network is perfused with blood especially when the other side of the membrane is exposed to ambient conditions as in our design. Such deformation can significantly reduce the efficiency of oxygenation and lead to lower saturation levels in the oxygenated blood. Therefore, the PDMS membrane is reinforced with a thin stainless-steel mesh (MS-400/19, Asada Mesh Co. Ltd.) that increases its stiffness and prevents deformation under operating pressures.

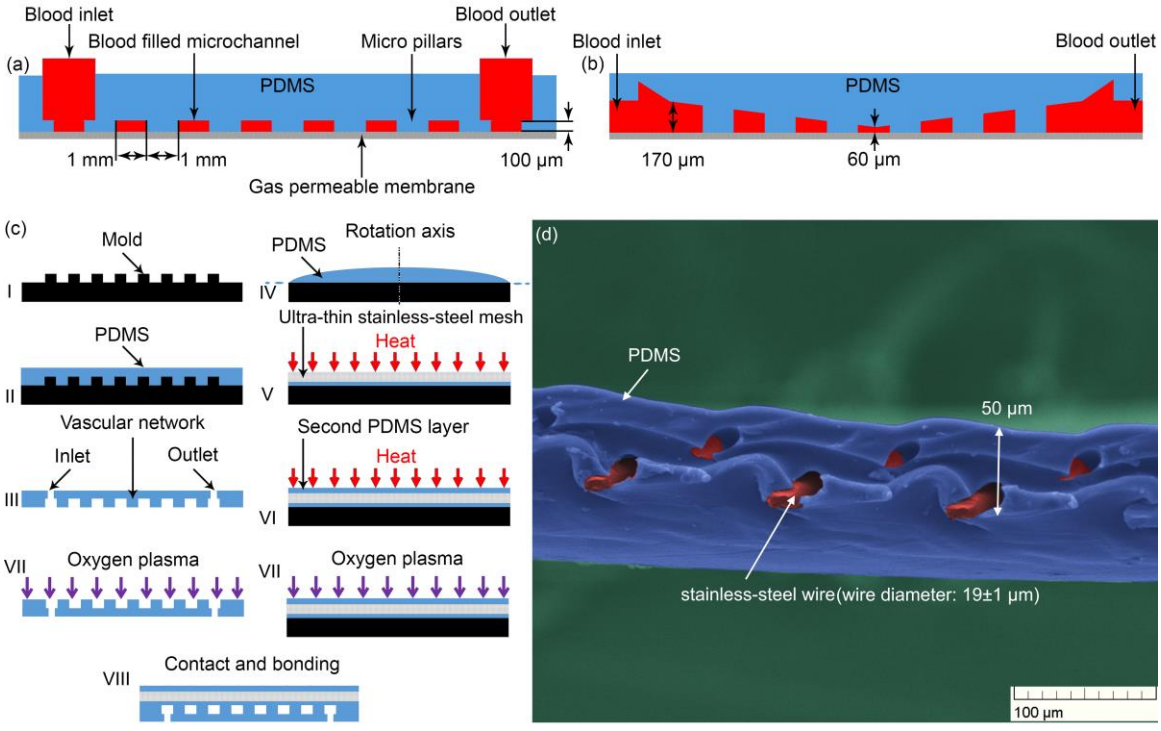

Figure 3.1: (a) Schematic cross-sectional view of a flat device, (b) schematic cross-sectional view of a sloping device, (c) device fabrication process, and (d) false colour SEM image of composite membrane.

The mesh had a thickness of 39±2 μm and composite membrane fabricated by infusing the PDMS into the mesh to completely cover it was 50 μm in thickness. The mesh has a pore size of 45 μm and a porosity of 49%.

3.3.2 Fabrication process

Fabrication of the oxygenator is a three-step process as shown in Figure 3.1.c: first the vascular network and the membrane are fabricated; the network and the membrane are bonded after treatment of the surfaces in an oxygen plasma.

The template for the network with flat profile was fabricated by etching the pattern on SU8-100 by means of photolithography [23] (Figure 3.1.c.I). The vascular network was fabricated by casting PDMS, in 10:1 base/curing agent ratio, on the negative template of the network (Figure 3.1.c.II), at 60^{o}C for 5 h. After curing, the vascular network was peeled off and residual PDMS inside the tubing was removed (Figure 3.1.c.III). The template for the network with sloping profile was fabricated on an aluminum block using a ball nose tool of diameter of 500 μm on a computer numerical control (CNC) 3-axis micro-milling machine (Matsuura LX-1)1mm^2 pockets were fabricated using a 500 μm diameter square end micro milling tool on the same machine. The features were machined within 2 μm to 5 μm accuracy.

The PDMS membrane was fabricated by spin-coating PDMS on a substrate made by bonding teflon sheet on silicon wafer. The PDMS was spun at 4000 RPM for 30 s, then cured at 60^{o}C for 5 h. The composite membrane was fabricated by spinning PDMS at 4000 RPM for 30 s on the substrate (Figure 3.1.c.IV); the steel mesh was then laid on the uncured material (Figure 3.1.c.V) and cured at 60^{o}C for 5 h; a second coat of PDMS was then spun onto the mesh (Figure 3.1.c.VI) and cured. The thickness of the resulting membrane was about 50 μm (Figure 3.1.d). A PDMS membrane without steel mesh reinforcement was also made by bonding two 25-μm-thick layers to produce a combined thickness of 50 μm and used for comparison purposes. In addition, the second 25-μm-thick layer reduced the chance of having any pinholes in PDMS membranes.

The network and the membrane were bonded together by exposing the bonding surfaces to an oxygen plasma at 50 W power for 2.5 min before bringing them into contact (Figure 3.1.c.VII). The device was dried at 60^{o}C for 5 h before peeling from the substrate (Figure 3.1c.VIII).

The LAD consisted of 32 sloping SOUs with composite membranes, and included connectors, silicone tubing (MasterFlex platinum-cured silicone tubing), PDMS flow dividers, and acrylic holders. The device included 16 parallel branches containing two SOUs in each branch as shown in Figure 3.2.a. The acrylic holders were fabricated using a laser cutter and were glued together using acrylweld (acrylic solvent). Figure 3.2.b shows the star-shaped PDMS flow divider designed for optimal blood distribution among the branches as shown in Figure 3.2.c. A mold was made using a ProJet™ HD 3000 3D printer (3D SYSTEMS Corp., Rock Hill, USA) and was used to fabricate the flow divider; oxygen plasma was applied to the surfaces for bonding to a thick flat PDMS layer to seal the channels.

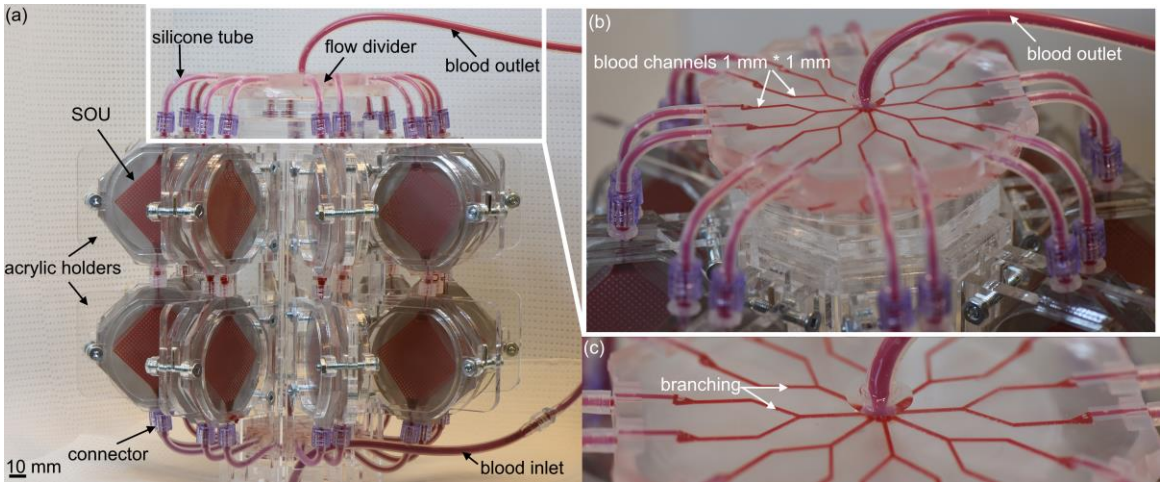

Figure 3.2: (a) Image of the LAD with 32 SOUs filled with bovine blood (10 mL total volume), (b)image of the flow divider with 16 branches filled with bovine blood, and (c) close-up view of the flow divider.

Blood enters at the center and is distributed among the branches which have square cross-section with side 1 mm and length 30 mm as depicted in Figure 3.2.b. The total priming volume of the LAD was about 10 mL.

3.3.3 Burst Pressure and Membrane Expansion Measurement

All the SOUs fabricated were tested at a pressure higher than the operating pressure to ensure that they are structurally sound before integrating them into the LAD or further testing. In order to test the devices, an experimental setup as shown in Figure 3.3.a was constructed. It consisted of a syringe which served as a pressure source attached to the inlet of the SOU. A pressure transducer (TruWave Transducer, Edwards Lifesciences LLC, Irvine, CA, USA) connected to a monitor (SpaceLabs 90369 Patient Monitor, SpaceLabs Medical Inc) was also attached to the inlet of the SOU to measure the pressure applied. The SOU was first perfused with water and then the 3-way connector at the outlet was closed to seal the system. The pressure was increased further by pumping more water while monitoring the pressure till reached the maximum of 250 mmHg. Only the devices that passed this test were used for further testing.

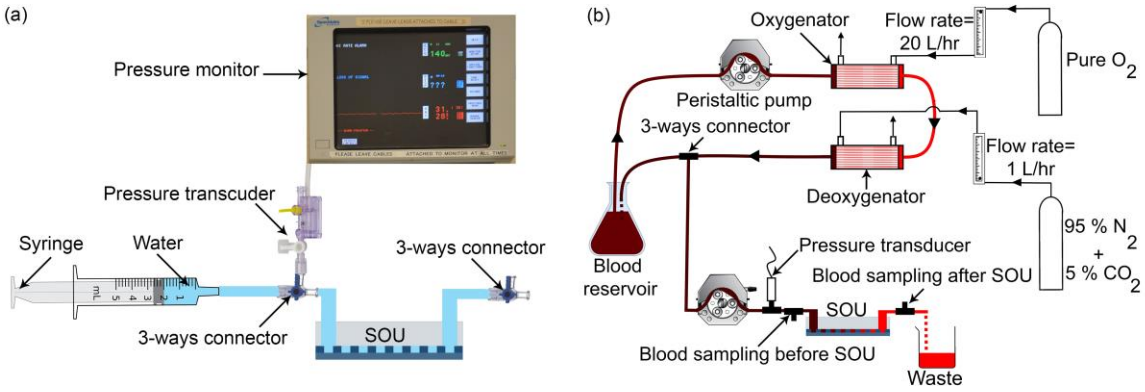

Figure 3.3: (a) Experimental setup for burst pressure measurement, (b) experimental setup to test an oxygenator and the LAD.

In addition, an optical surface profiler (Newview 5000, Zygo) was used to measure the amount of membrane expansion (deflection) for a sloping SOU with PDMS membrane at various applied pressures. After filling SOUs with water and pressuring it to 10, 40, and 70 mmHg, the topography of the top PDMS membrane was mapped using the optical surface profiler and maximum deflection of the membrane at various location, determined.

3.3.4 In-vitro oxygenation testing

The experimental setup used to characterize oxygenation performance of the SOUs is shown in Figure 3.3.b. The setup consists of two parts; the first part consists of a loop used to maintain the oxygen saturation level in blood over the duration of the experiment. It consists of a reservoir containing bovine blood, a peristaltic pump, a hollow fiber oxygenator, gas flow regulators, and a deoxygenator. Bovine blood (Bovine 7200807-500ML, Lampire Biologics) was used for the experiment and the hematocrit ranged between 28% and 32%. The oxygen saturation, partial pressure of oxygen, partial pressure of carbon dioxide and pH of the input blood were in the range of 42 – 51%, 37 – 44 mmHg, 51 – 61 mmHg and 7.07 – 7.13 respectively. The blood in the reservoir was pumped using a peristaltic pump (ISM832C, Ismatec) through two hollow fiber oxygenators connected in series at a flow rate of 4 mL/min. The first oxygenator (CAPIOX RX05, Terumo) adjacent to the pump was perfused with 20 L/h of oxygen on the gas side to completely oxygenate the blood (to 100% saturation). The deoxygenator (OXR, Living Systems Instrumentation), located downstream was used to set the desired hypoxic condition (SaO_2=46%) by flowing a controlled amount of carbon dioxide and nitrogen mixture (5%/95% v/v) through its gas side.

Once the oxygen saturation level of all the blood in the reservoir was stabilized, the blood was withdrawn from the reservoir using a second peristaltic pump (ISM832C, Ismatec) with setting flow rate ranging between 0.5 – 4 mL/min and pushed through SOUs. When LAD was tested, the blood flow rate was set between 8 – 48 mL/min. Blood was sampled both at the entry and the exit of the tested device, and analyzed using a blood gas analyzer (GEM3000, Instrumentation Laboratory). Difference between the oxygen saturation of the blood at the inlet and the outlet was used to calculate the oxygen uptake capacity of the device at the given blood flow rate. For all experiments, the pressure drop was recorded. All experiments were repeated 5 times for each set of conditions.

3.3.5 In vivo experiment

A new born piglet of ~ 2 kg weight was used to test the LAD using the experimental settings as described previously [2]. Before filling with blood, checks were carried out to ensure that the LAD was leak proof and that all SOUs were perfused equally. The LAD was first filled with isopropanol to remove any air from the device, then the isopropanol was replaced by pumping micro filtered deionized water for 30 minutes. Subsequently, the LAD was perfused and filled with a normal saline solution containing 3 units/mL heparin. The piglet was anesthetized with intraperitoneal sodium pentobarbital (30 mg/kg; MTC Pharmaceutics, Cambridge, ON, Canada). An ear vein was cannulated with a 22-G angiocatheter (Angiocath, Becton Dickinson, Sandy, UT, USA) for maintenance fluids (5% dextrose at 80 mg/kg/day; Baxter, Toronto, ON, Canada) and for administration of maintenance sodium pentobarbital (16 mg/kg) if needed. An endotracheal tube (size 3.5) was placed via tracheostomy for mechanical ventilator. Initial settings for the ventilator was set to peak inspiratory pressure (PIP) of 15 mmHg (2 kPa), positive end-expiratory pressure (PEEP) of 6 mmHg (0.8 kPa), mean airway pressure (MAP) of 8 mmHg (1.07 kPa), inspiratory time (IT) of 0.5 s, and respiratory rate (RR) of 30 breaths/min. At baseline, a humidified gas mixture (warmed to 38° C) with FiO_2 of 0.3 was delivered at 8 L/min. Body temperature was maintained constant at 39 ℃ using a heat lamp and was being monitored by using an ISC probe which was placed on abdomen. A 3.5 Fr Argyle umbilical catheter (Sherwood, Medical, St. Louis) was inserted into the right femoral artery to measure systemic blood pressure and heart rate. A bolus of 400 units/kg of heparin was injected to the extracorporeal circuit for anticoagulation, subsequently, heparin was being infused at flow rate of 30 units/kg/h. 14 Gauge 1.1” length angio-catheters (BD Catheters) was used to access the left carotid artery and right jugular vein in order to create extracorporeal bypass. Subsequently, the LAD was perfused by being connected to this extracorporeal bypass. The LAD was tested under various flow rates and two different ventilator settings. To simulate respiratory failure and test the efficiency of the LAD, the piglet was ventilated with hypoxic gas (FiO_2=0.15). Blood samples were collected before and after LAD and analyzed with a blood gas analyzer. The study

protocol was approved by the McMaster University Animal Research Ethics Board (AREB#10-03-14).

3.4 Results and Discussion

Oxygenators using the stainless-steel reinforced PDMS membrane were tested both for their mechanical performance as well as their oxygenation capabilities and compared with oxygenators of similar design but with PDMS membranes without reinforcement. The best performing design of the SOUs was chosen to then build a LAD, consisting of 32 SOUs, and the oxygenation characteristics of the LAD was also tested in-vitro at flow rate similar to those that would be required in a neonate for lung assist function. Finally, the LAD was used in an in-vivo experiment to oxygenate a piglet under normoxic and hypoxic conditions.

3.4.1 Mechanical Testing

The burst pressure test was conducted on SOUs with flat and sloping channel designs that were attached with both PDMS and composite (PDMS reinforced with stainless steel) membranes. The results, shown in Figure 3.4.a, indicate that all the oxygenators are structurally sound and do not fail at pressures that are normally encountered during use (red band in the figure). However, the margin of safety is low for oxygenators that had only the PDMS membrane. The composite membrane devices demonstrated a significantly better performance and none of the tested devices delaminated or failed in any way even at an applied pressure of 250 mmHg which is significantly higher than normal operating conditions. The superior performance of composite membrane as compared to PDMS membrane can be attributed to the strength of composite membrane. Figure 3.4.b shows schematically a cross-section of the membrane attached to the pillars under pressure ‘P’. The PDMS membrane has a low Young’s modulus and undergoes a large deflection under pressure. As a result, the delamination force at the edge of the pillars is directed at a greater angle to the bonded interface which results in peeling of the membrane from the pillars. The composite membrane has higher Young’s modulus due to the steel mesh and hence it undergoes a much lower deflection under pressure. As a

result, the delamination force is at a lesser angle to the bonded interface. Therefore, it requires a higher force/pressure for delamination making it mechanical more robust.

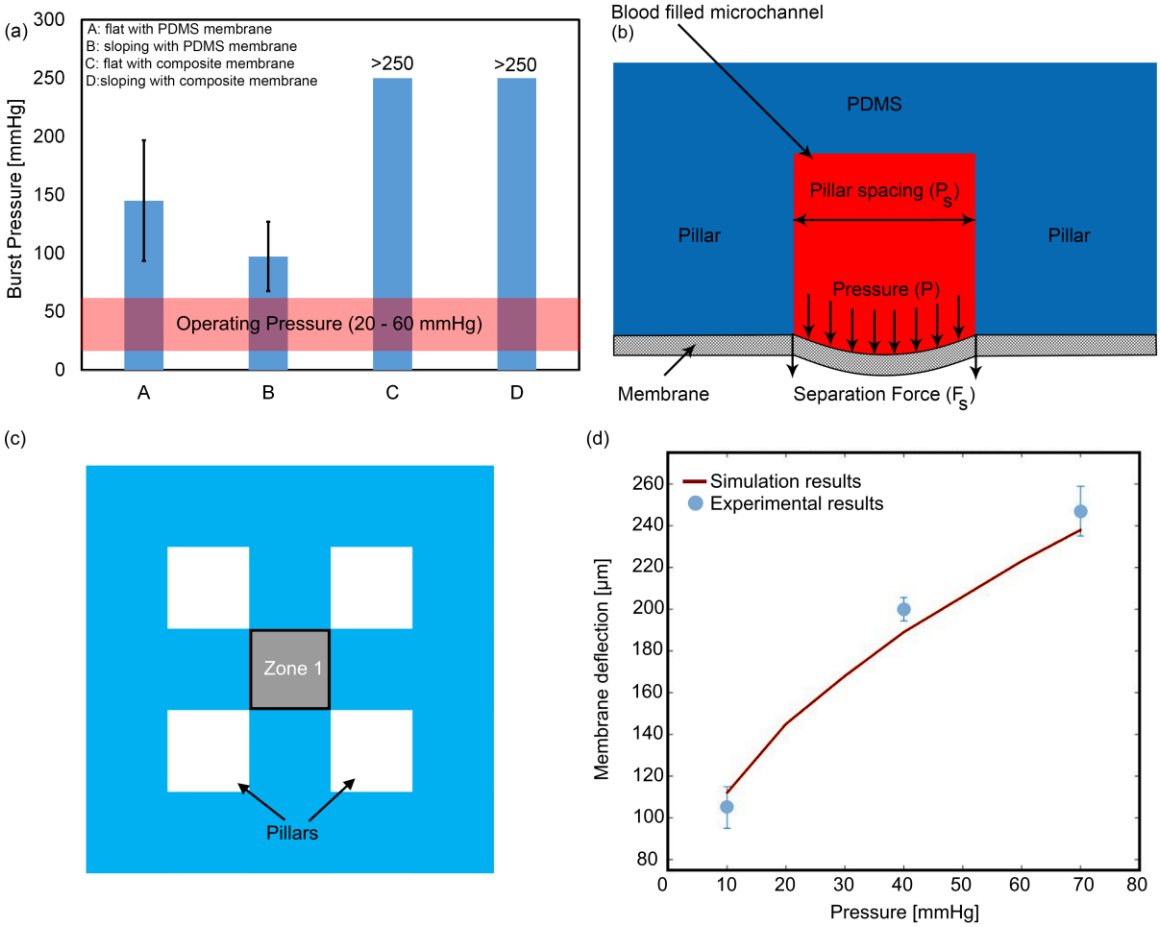

Figure 3.4: (a) Burst pressure of oxygenators with various designs. SOUs with composite membrane can sustain higher operating pressure without failure for both flat and sloping designs, (b) figure illustrating a segment of the membrane under pressure, (c)illustration of the zone at which the membrane topography was profiled. The blue regions represent the microchannel network (d) the amount of membrane expansion (deflection) for three different pressures of 10, 40, 70 mmHg for a sloping SOU with PDMS membrane.

To quantify the effect of pressure on membrane expansion (deflection), the position of the center point of the membrane in the zone (Figure 3.4.c) between the pillars were measured using the optical profilometer, before and after the application of various pressures ranging from 10-70 mmHg. The change in the position (deflection) of the center point represents the maximum deflection of the membrane in that region to the applied pressure. Zone 1 represents the area at the center of four adjacent pillars located on the corner of a square. The measured deflections are plotted in Figure 3.4.d and show an

increase with applied pressure. The deflections are substantial and will have significant effect on oxygenation. For instance, at a pressure of 40 mmHg, the effective channel height of a sloping SOU with PDMS will be increased by 200 μm. The measured deflection closely matches with the simulated (using ANSYS) deflection at those applied pressure as shown in Figure 3.4.d. Measurements for the composite membrane show negligible deflection of the membrane under these pressure conditions.

3.4.2 In-vitro Blood Oxygenation Measurements for SOUs

Performance of the SOUs was evaluated by flowing blood through them at various set flow rates of 0.5, 1, 1.5, 2, 3, and 4 mL/min while exposing them to the ambient atmosphere. The pressure drop and the increase in the oxygen saturation of the blood between the inlet and the outlet were measured and shown in Figure 3.5. The pressure drop (Figure 3.5.a) increases with flow rate for all the oxygenator designs, as expected. Devices with composite membrane showed higher pressure drop than devices with PDMS membrane. This is again in accordance with expectations since the composite membrane is stiffer and undergoes smaller deflections than the PDMS. Since hydraulic resistance varies inversely with channel height, the hydraulic resistance of devices with composite membrane are expected to be higher than devices with PDMS. The expected pressure drop was also calculated based on a previously published model [24] and was found to be higher than the experimentally obtained value. This is attributed to the expansion of the PDMS which results in a higher effective channel height, reducing the pressure drop observed experimentally. The difference between the calculated pressure drop based on the model and the experimental value is smaller for the composite membrane as compared to the PDMS membrane indicating that the deflection of the PDMS membrane was larger. The oxygen uptake by the blood (Figure 3.5.b) shows an initial increase to reach a maximum followed by a decrease, for all oxygenator designs. The initial increase can be explained by the higher flow rate of hypoxic blood that is able to acquire increasing amounts of the oxygen flux through the gas exchange membrane till it reaches the maximum. The decrease in the oxygen uptake at higher flux can be attributed to

higher deflection of the membrane at these operating pressures, which reduces the residence time of blood in the device and affects oxygenation performance.

It can also be seen that the SOUs with the composite membrane consisting of steel reinforced PDMS has a higher oxygen uptake than the unreinforced PDMS membrane. The oxygen transfer of both composite flat and sloping SOUs was same (not statistically different) at low blood flow rates (up to 1.5 mL/min). At higher blood flow rates composite flat SOUs show better performance compared to composite sloping.

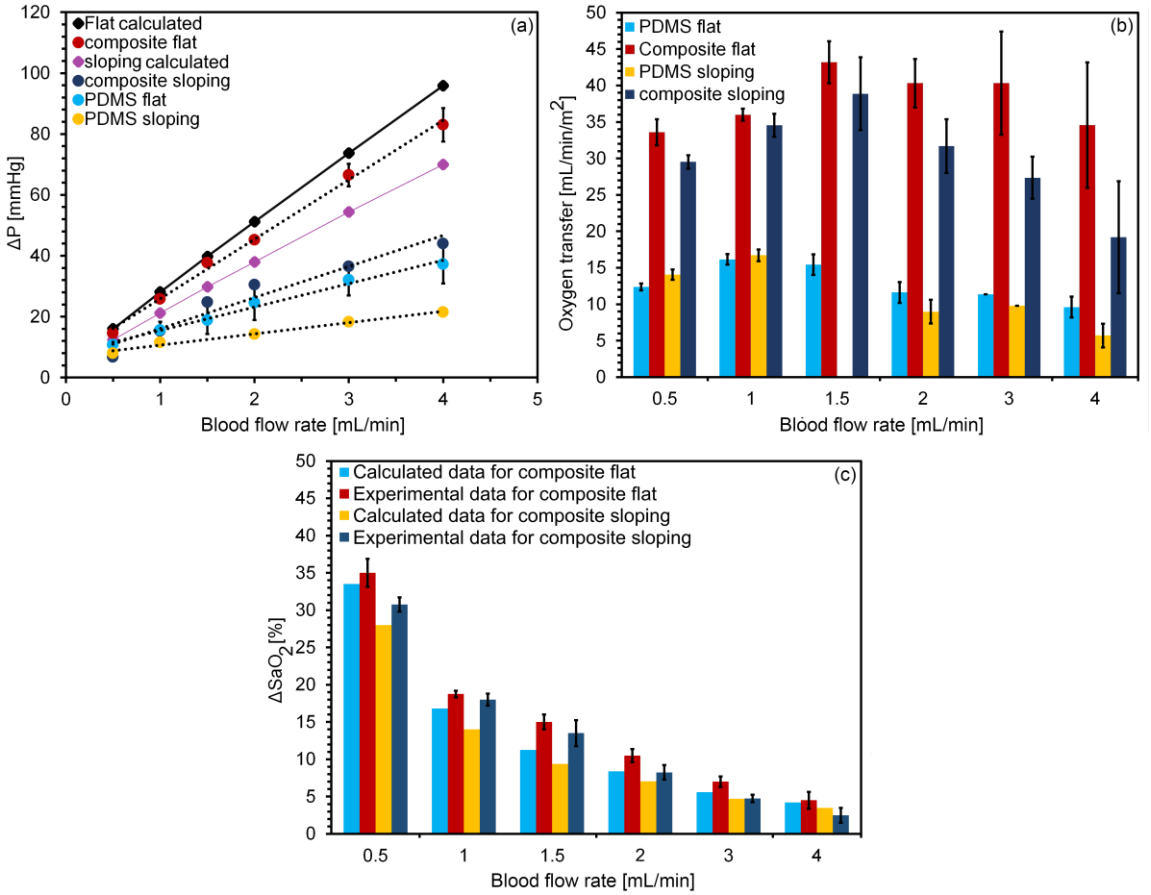

Figure 3.5: In vitro performance of SOUs: (a) pressure drop, (b) oxygen uptake at various blood flow rates, and (c) comparison of change in oxygen saturation level (ΔSaO_2) for composite flat and sloping with their calculated values. Data are means ± SD, n=5.

However, to make an illustrative comparison between composite flat and sloping designs, an estimation for the performance of each design at an operating pressure of 30 mmHg, which is the mean expected arterio venous pressure difference in a neonate, should be

made. In the case of the flat design with PDMS membrane, the total oxygen uptake was 0.018 mL/min with a flow rate of 3 mL/min. However, the flat design with composite membrane exhibited the total oxygen uptake of 0.026 mL/min at a flow rate of 1.2 mL/min at an operating pressure of 30 mmHg which is 44% higher than that of the flat design with PDMS membrane. The SOU with the sloping design and a composite membrane had a total oxygen uptake of 0.025 mL/min with a flow rate of 1.5 mL/min which was 40% higher than that of the flat design with PDMS membrane. Although the oxygen uptake of the sloping design with composite membrane was nearly the same as the flat profile, it was able to sustain a higher flow rate at the same pressure, thereby enabling oxygenation of more blood. Therefore, this design was selected for fabrication of the LAD.

In addition, the same model[24] was used to calculate the change in oxygen saturation level for both composite flat and sloping designs which were not significantly different from experimental results as shown in Figure 3.5.c.

3.4.3 In-vitro Blood oxygenation measurements for LAD

To calculate the number of required units for assembling the new LAD, the experimental results for SOUs with sloping design and composite membrane were used. The LAD was supposed to have several parallel branches which would have the same pressure drop as the LAD. In addition, it was assumed that the pressure drop for each branch would split equally between each two SOUs. Then, the number of required branches was calculated to ensure that enough oxygenation at a blood flow rate of 30 mL/min/kg of baby would achieve.

The LAD consisting of a total of 32 SOUs with sloping profile and composite membrane assembled in 16 parallel lines with 2 SOUs in series in each line was used to perform pressure drop and blood oxygenation experiments similar to the one's performed for the SOUs. Blood at various flow rates from 8 - 48 ml/min was pumped through the LAD and the change in oxygen saturation, pressure drop and CO_2 release (calculated by using change in CO_2 partial pressure) were measured and reported in Figure 3.6.

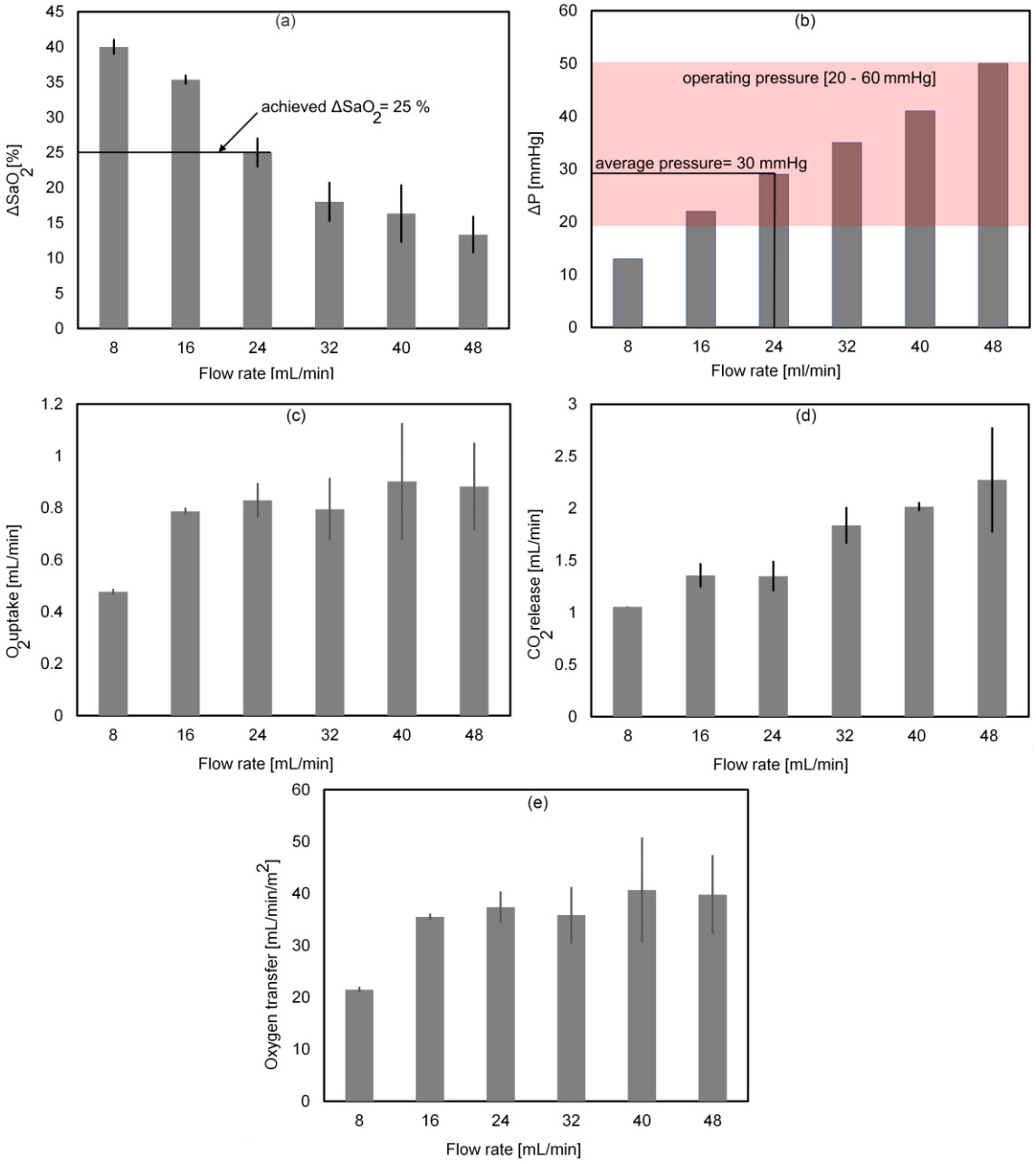

Figure 3.6: In vitro test of the LAD with bovine blood at various blood flow rates: (a) change in oxygen saturation, (b) pressure drop, (c) oxygen uptake, (d) carbon dioxide release, and (e) oxygen transfer. Data are means ± SD, n=3.

It can be seen that in this configuration, the oxygen saturation can be increased by up to 40% at 8 ml/min which reduces with increasing flow rate to ~ 13.3% at 48 ml/min (Figure 3.6.a). This is expected as higher flow rates lead to lower residence time of blood in the oxygenator and hence lesser increase in the saturation level of blood. There is a

corresponding increase in pressure drop from ~ 13 mmHg to 50 mmHg (Figure 3.6.b). The oxygen uptake, the CO2 release, and the oxygen transfer were also found to increase with the flow rate (Figure 3.6.c,d,e). At a typical operating pressure drop of 30 mmHg, the blood flow rate in this LAD will be ~ 24 mL/min, and will result in a 25 % change in oxygen saturation in ambient air, with the average oxygen uptake and CO_2 release were 0.83 mL/min and 1.35 mL/min, respectively. In comparison, Gimbel and Flores [8] reported an oxygen transfer rate of 1.2 mL/min at a blood flow rate of 25 mL/min for their microfluidic oxygen transfer device using pure oxygen. The microfluidic LAD reported here may be considered more efficient while operating in ambient air given its relatively low pressure drop.

Figure 3.7 shows oxygen uptake for flat design SOUs with composite membrane tested in ambient air and enriched oxygen atmosphere. Changing air to pure oxygen improved the oxygen uptake of flat design SOUs with composite membrane up to 7 times. Therefore, data for the flat design SOU with composite membrane suggests that in pure oxygen, the oxygen transfer capacity of the LAD would increase by up to 3-fold, meaning that it could achieve oxygen transfer of 2.4 mL/min at a blood flow rate of 24 mL/min.

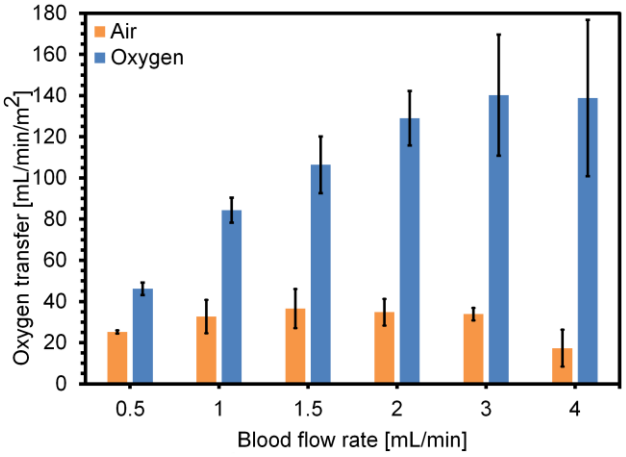

Figure 3.7: In vitro performance of flat design SOUs with composite membrane and the channel height of 110 µm tested in air and pure oxygen.

In order to identify whether the performance of the LAD met the clinical need, the oxygenation requirement was calculated as follows. A typical neonate will have a heart rate of 150 min^{-1}, a stroke volume of 2 mL/kg (body weight)[25]. To avoid cardiac

compromise, only 10 % of cardiac output volume could be sent to the LAD[26]. Therefore, an extracorporeal bypass volume of 30 mL/min/kg can be estimated by multiplying heart rate, stroke volume, and percent extracorporeal shunt. This represents the typical flow rate that the LAD has to support and oxygenate.

Assuming an average haemoglobin concentration of 0.16 g/mL[27] of blood and oxygen binding capacity of 1.34 mL(oxygen) / g (hemoglobin)[28] . Therefore, the total oxygen carrying capacity (0 to 100% saturation) of 30 mL/min/kg[18] of blood flowing through the LAD would be about 6.4 mL/min/kg. Since the typical incoming venous blood into the LAD will be already at 70% saturation in the case of neonates with RDS[29], increasing the saturation to 100% will require (30% of 6.4) 1.9 mL/min of oxygen uptake. Our current design of LAD achieves an oxygen uptake of 0.83 mL/min in ambient air which could be improved to 2.4 mL/min using pure oxygen. Therefore, if the LAD was operated in an enriched oxygen environment, it is likely to meet the desired oxygen transfer requirement for one kg preterm neonate with RDS.

3.4.4 Comparison to other microfluidic devices

Table 3.1 shows the comparison among composite flat, composite sloping and the LAD presented in this study with other microfluidic blood oxygenator devices which used air as ventilating gas [2], [16], [17], [30]. In this comparison, oxygen transfer and blood flow rate are normalized to the effective gas exchange surface area to provide a better comparison among all devices. As shown in Table 3.1, the LAD has better oxygen transfer at the same normalized blood flow rate compared to others except Potkay[16] 2011 and Rieper[17] 2015. However, it should be noted, the higher oxygen transfer in these studies were achieved at a high pressure drop of 500 mmHg and 80 mmHg, respectively, which are not suitable for using as a pumpless device in NICU for preterm and term neonates suffering from RDS.

Table 3.1: A summary of previous works of microfluidic blood oxygenator devices. This table includes only devices which were tested by air. Values in the table is from each reported work or estimated based on reported values in each work. The height of blood channels is shown by H. The oxygen transfer and pressure drop data represents the maximum reported results at achieved blood flow rates for that oxygen transfer. N/A indicates that this data was not available from the papers

	H [μm]	Surface Area [cm^2]	Priming Volume [mL]	ΔP [mmHg]	Oxygen transfer [$mL/min/m^2$]	Flow Rate [$L/min/m^2$]
Composite flat	100	7.04	0.14	83	40.32	5.68
Composite sloping	170-60	6.93	0.166	44	38.88	5.77
LAD	170-60	221.76	10	50	40.67	2.16
Potkay[16] 2011	20	2.34	0.006	500	138.9	6.41
	10	1.67	0.002	N/A	224.5	8.98
Rochow[2] 2014	80	152.6	4.8	62	31	2.62
Rieper[17] 2015	200	1200	7	80	13	0.5
Thompson[30] 2017	10	N/A	N/A	120	44	2.64

3.4.5 In-vivo Animal Experiments

The LAD was then connected to a piglet and its oxygenation performance tested under various flow rates and two different ventilator settings: i) the piglet was ventilated under standard condition (Oxygen was feeded into the mechanical ventilator) and ii) hypoxic gas was used to simulate lung failure ($FiO_2 = 0.15$) using experimental set-up shown in Figure 3.8. The oxygen partial pressure (PO_2), carbon dioxide partial pressure (PCO_2), and oxygen saturation level (SaO_2) were measured during the experiment both before and after the blood enters the LAD as reported in Table 3.2.

At baseline setting a maximum blood flow rate of 25 mL/min was achieved. The mean arterial blood pressure was 48 mmHg, and the mean pressure in the tube between carotid artery and the LAD was 32 mmHg. The LAD raised oxygen saturation from SaO_2 91-98 % to 100%. The LAD was tested for 150 minutes under this condition. Further, the LAD was tested under hypoxic ventilation of the piglet (FiO_2=0.15). A maximum flow rate of 16.7 mL/min with a mean arterial blood pressure of 29 mmHg was achieved.

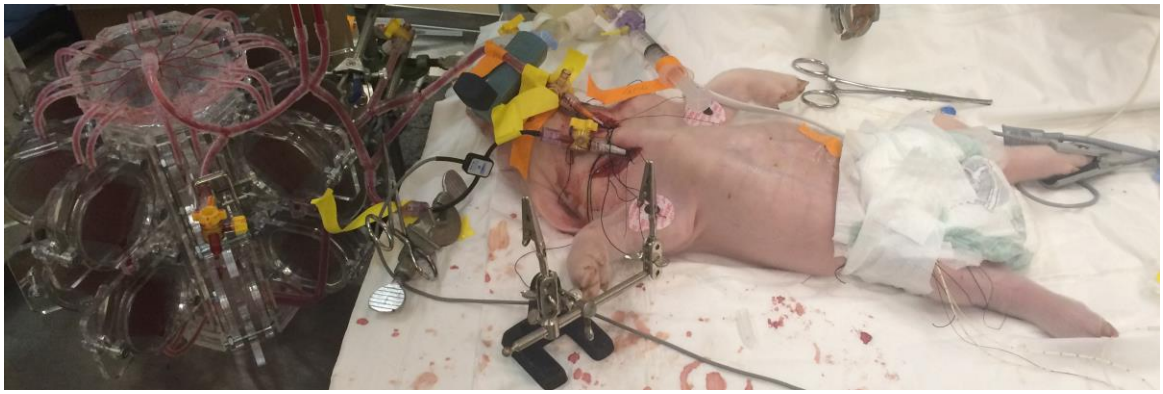

Figure 3.8: Setup of the animal experiment.

Table 3.2: Blood gases measured during the animal experiment at the inlet (blood from piglet to LAD) and the outlet of the LAD.

Normal condition							
Sample	Blood flow rate [mL/min]	Pre-LAD PCO_2 [mmHg]	Pre-LAD PO_2 [mmHg]	Pre-LAD SaO_2 [%]	Post-LAD PCO_2 [mmHg]	Post-LAD PO_2 [mmHg]	Post-LAD SaO_2 [%]
1	10	42	72	93	17	169	100
2	13.7	35	60	91	13	199	100
3	16	41	65	93	20	180	100
4	16.7	45	88	98	19	181	100
5	18.3	40	75	95	24	178	100
6	24	43	72	94	26	175	100
7	25	41	77	95	24	198	100
Hypoxic gas (FiO_2 = 0.15)							
1	11	45	33	56	27	160	98
2	15	41	33	60	25	125	99
3	16.7	39	38	69	23	105	100

It is notable that the LAD was able to raise the oxygen saturation (SaO_2) level from 56-69 % to 98-100%. In addition, at lower flow rates of 11 and 15 ml/min the oxygen saturation could be increased to near complete saturation from a lower value of 56 and 60%. The duration of the hypoxia experiment was 50 minutes. The total in-vivo experiment during which the piglet was stable lasted in total 5 hours.

The in-vivo performance of the LAD under the hypoxic conditions (SaO_2: 69% to 100% at 16.7 mL/min) is comparable to the in-vitro experiment results of the LAD (SaO_2: 58% to 93-94% at 16 mL/min).

3.5 Conclusion

In this study, a steel mesh-reinforced composite silicone membrane was introduced to improve the performance of a microfluidic blood oxygenator in terms of mechanical strength of the membrane and oxygenation. A new design with a "sloping" flow profile of the blood flow channels was developed to reduce flow resistance. In addition, a new LAD design having 32 individual oxygenator units with composite membranes and sloping profiles connected in parallel was built and tested. Composite membrane devices showed improvement in oxygenation of up to 44% compared to PDMS membrane devices. At a mean pressure of 30 mmHg, the LAD increased oxygenation by 25% at a blood flow rate of 24 mL/min. In addition, an in vivo experiment using a newborn piglet with the LAD showed significantly improved performance confirmed the blood experiments results for the LAD. The design is amenable to further reduction in form factor in order to make it more compact. These simple and passive oxygenation devices which do not require an external pump or enriched oxygen supply are likely to find broad applications for oxygenation not only with neonates but also with infants and in some cases adults.

References

[1] W. J. Watkins, S. J. Kotecha, S. Kotecha, M. Winkleby, and S. Petrou, "All-Cause Mortality of Low Birthweight Infants in Infancy, Childhood, and Adolescence: Population Study of England and Wales," *PLOS Med.*, vol. 13, no. 5, p. e1002018, May 2016.

[2] N. Rochow *et al.*, "An Integrated Array of Microfluidic Oxygenators as a Neonatal Lung Assist Device: In Vitro Characterization and In Vivo Demonstration," *Artif. Organs*, vol. 38, no. 10, pp. 856–866, Oct. 2014.

[3] R. J. Rodriguez, "Management of Respiratory Distress Syndrome: An Update," *Respir. Care*, vol. 48, no. 3, pp. 279–287, 2003.

[4] A. Polito *et al.*, "Neurologic complications in neonates supported with extracorporeal membrane oxygenation. An analysis of ELSO registry data," *Intensive Care Med.*, vol. 39, no. 9, pp. 1594–1601, Sep. 2013.

[5] R. de Vroege *et al.*, "Comparison of three commercially available hollow fiber oxygenators: gas transfer performance and biocompatibility," *ASAIO J.*, vol. 47, no. 1, pp. 37–44, 2001.

[6] N. Rochow *et al.*, "Artificial placenta -Lung assist devices for term and preterm newborns with respiratory failure," *Int J Artif Organs*, vol. 36, pp. 377–391, 2013.

[7] T. Femmer, M. L. Eggersdorfer, A. J. Kuehne, and M. Wessling, "Efficient gas-liquid contact using microfluidic membrane devices with staggered herringbone mixers," *Lab Chip*, vol. 15, no. 15, pp. 3132–3137, 2015.

[8] A. A. Gimbel, E. Flores, A. Koo, G. García-Cardeña, and J. T. Borenstein, "Development of a biomimetic microfluidic oxygen transfer device," *Lab Chip*, vol. 16, no. 17, pp. 3227–3234, 2016.

[9] D. M. Hoganson *et al.*, "Branched vascular network architecture: a new approach to lung assist device technology.," *J. Thorac. Cardiovasc. Surg.*, vol. 140, no. 5, pp. 990–995, 2010.

[10] D. M. Hoganson, H. I. Pryor, E. K. Bassett, I. D. Spool, and J. P. Vacanti, "Lung assist device technology with physiologic blood flow developed on a tissue engineered scaffold platform.," *Lab Chip*, vol. 11, no. 4, pp. 700–707, 2011.

[11] and L. F. M. J.-K. Lee, M. C. Kung, H. H. Kung, "Microchannel Technologies for Artificial Lungs: (3) Open Rectangular Channels," *ASAIO J. NIH Public Access*, vol. 54, no. 4, pp. 390–395, 2008.

[12] T. Kniazeva *et al.*, "Performance and scaling effects in a multilayer microfluidic extracorporeal lung oxygenation device," *Lab Chip*, vol. 12, no. 9, pp. 1686–1695, 2012.

[13] T. Kniazeva, J. C. Hsiao, J. L. Charest, and J. T. Borenstein, "A microfluidic respiratory assist device with high gas permeance for artificial lung applications," *Biomed. Microdevices*, vol. 13, no. 2, pp. 315–323, 2011.

[14] K. M. Kovach *et al.*, "In vitro evaluation and in vivo demonstration of a biomimetic, hemocompatible, microfluidic artificial lung.," *Lab Chip*, vol. 15, no. 5, pp. 1366–75, 2015.

[15] J. K. Lee, H. H. Kung, and L. F. Mockros, "Microchannel technologies for artificial lungs: (1) theory.," *ASAIO J.*, vol. 54, no. 4, pp. 372–82, 2008.

[16] J. A. Potkay, M. Magnetta, A. Vinson, and B. Cmolik, "Bio-inspired, efficient, artificial lung employing air as the ventilating gas.," *Lab Chip*, vol. 11, no. 17, pp. 2901–2909, 2011.

[17] T. Rieper, C. Muller, and H. Reinecke, "Novel scalable and monolithically integrated extracorporeal gas exchange device," *Biomed. Microdevices*, vol. 17, no. 5, pp. 1–10, 2015.

[18] W.-I. Wu *et al.*, "Lung assist device: development of microfluidic oxygenators for preterm infants with respiratory failure.," in *Lab on a chip*, 2013, vol. 13, no. 13, pp. 2641–50.

[19] J. Byrnes *et al.*, "Hemolysis during cardiac extracorporeal membrane oxygenation: a case-control comparison of roller pumps and centrifugal pumps in a pediatric population.," *ASAIO J.*, vol. 57, no. 5, pp. 456–61, 2011.

[20] A. D. Meyer *et al.*, "Hemolytic and thrombocytopathic characteristics of extracorporeal membrane oxygenation systems at simulated flow rate for neonates.," *Pediatr. Crit. Care Med.*, vol. 13, no. 4, pp. e255-61, Jul. 2012.

[21] M. C. Kung, J.-K. Lee, H. H. Kung, and L. F. Mockros, "Microchannel technologies for artificial lungs: (2) screen-filled wide rectangular channels.," *ASAIO J.*, vol. 54, no. 4, pp. 383–389, 2008.

[22] M. C. Bélanger and Y. Marois, "Hemocompatibility, biocompatibility, inflammatory and in vivo studies of primary reference materials low-density polyethylene and polydimethylsiloxane: A review," *J. Biomed. Mater. Res.*, vol. 58, no. 5, pp. 467–477, Jan. 2001.

[23] H. Lorenz, M. Despont, N. Fahrni, N. LaBianca, P. Renaud, and P. Vettiger, "SU-8: a low-cost negative resist for MEMS," *J. Micromechanics Microengineering*, vol. 7, no. 3, pp. 121–124, Sep. 1997.

[24] J. A. Potkay, "A simple, closed-form, mathematical model for gas exchange in microchannel artificial lungs," *Biomed. Microdevices*, vol. 15, no. 3, pp. 397–406, 2013.

[25] Y. Agata *et al.*, "Changes in left ventricular output from fetal to early neonatal life," *J. Pediatr.*, vol.

119, no. 3, pp. 441–445, Sep. 1991.

[26] Y. Takahashi, K. Harada, A. Ishida, M. Tamura, T. Tanaka, and G. Takada, “Changes in left ventricular volume and systolic function before and after the closure of ductus arteriosus in full-term infants,” *Early Hum. Dev.*, vol. 44, no. 1, pp. 77–85, Jan. 1996.

[27] W.-I. Wu *et al.*, “Lung assist device: development of microfluidic oxygenators for preterm infants with respiratory failure,” *Lab Chip*, vol. 13, no. 13, p. 2641, 2013.

[28] R. N. Pittman, *Chapter 4 - Oxygen Transport; in "The Circulatory System and Oxygen Transport."* 2011.

[29] M. Zimmermann *et al.*, “Interhospital transportation of patients with severe lung failure on pumpless extracorporeal lung assist,” *Br. J. Anaesth.*, vol. 96, no. 1, pp. 63–66, 2006.

[30] A. J. Thompson, L. H. Marks, M. J. Goudie, A. Rojas-Pena, H. Handa, and J. A. Potkay, “A small-scale, rolled-membrane microfluidic artificial lung designed towards future large area manufacturing,” *Biomicrofluidics*, vol. 11, no. 2, 2017.

4 Chapter 4

AN ARTIFICIAL PLACENTA TYPE MICROFLUIDIC BLOOD OXYGENATOR WITH DOUBLE-SIDED GAS TRANSFER MICROCHANNELS AND ITS INTEGRATION AS A NEONATAL LUNG ASSIST DEVICE

Complete citation:

Mohammadhossein Dabaghi, Gerhard Fusch, Neda Saraei, Niels Rochow, John L. Brash, Christoph Fusch, and P. Ravi Selvaganapathy. *"An artificial placenta type microfluidic blood oxygenator with double-sided gas transfer microchannels and its integration as a neonatal lung assist device."* Biomicrofluidics 12, no. 4 (2018): 044101.

Copyright:

Contribution:

My contributions include designing the experiments, planning and performing the experiments, interpretation and analysis of data and results, and writing the manuscript.

4.1 Abstract

Preterm neonates suffering from respiratory distress syndrome require assistive support in the form of mechanical ventilation or extracorporeal membrane oxygenation, which may lead to long-term complications or even death. Here we describe, a high performance artificial placenta type microfluidic oxygenator, termed as double-sided single oxygenator unit (dsSOU), that combines microwire stainless-steel mesh reinforced gas permeable membranes on both sides of a microchannel network, thereby significantly reducing the diffusional resistance to oxygen uptake as compared to previous single-sided oxygenator designs. The new oxygenator is designed to be operated in a pumpless manner, perfused solely due to the arterio-venous pressure difference in a neonate and oxygenate blood through exposure directly to ambient atmosphere without any air or oxygen pumping. The best performing dsSOUs showed up to ~ 343% improvement in oxygen transfer compared to a single-sided SOU (ssSOU) with the same height. Later, the dsSOUs were optimized and integrated to build a lung assist device (LAD) that could support the oxygenation needs for a 1-2 kg neonate under clinically relevant conditions for the artificial placenta, namely: flow rates ranging from 10 - 60 mL/min and pressure drop of 10 – 60 mmHg. The LAD provided an oxygen uptake of 0.78 – 2.86 mL/min, which corresponded to increase in oxygen saturation from 57±1 % to 93 – 100 %, under pure oxygen environment. This microfluidic lung assist device combines elegant design with new microfabrication methods to develop a pumpless, microfluidic blood oxygenator that is capable of supporting 30% of the oxygen needs of a pre-term neonate.

4.2 Introduction

Preterm infants account for about 10% of 4 million total births each year in the United States [1] which amounts to ~ 400,000 births[2]. Globally, World Health Organization reports that 15 million preterm births occur every year and this number is increasing rapidly [3]. Preterm birth complications have been recognized as the main cause of death for children aging less than 5 years, accounting for around one million deaths in 2015[4]. Additionally, the survival rate for preterm neonates that are 28 weeks or less gestational age is extremely low (less than 50%)[5].

Respiratory distress syndrome (RDS) or hyaline membrane disease has been recognized as the second major cause of mortality in neonates[6]. In 2005, the number of cases with RDS increased to 12.7 % from 11.6 % in 2003 [7]. Since lungs are among the last organs to fully develop, preterm and term neonates suffering from RDS require additional breathing support such as mechanical ventilation, until their lungs are fully developed. However, the positive pressure applied during mechanical ventilation could cause morbidities such as necrotizing bronchiolitis and alveolar septal injury with inflammation and scarring[8], [9] resulting in some long-term complications such as bronchopulmonary dysplasia (BPD) and hypoxic ischemic encephalopathy (HIE)[10],[11]. Extra-corporeal membrane oxygenation (ECMO) is the method of choice when mechanical ventilation is not sufficient and preterm neonates need external oxygenation support. However, ECMO is an invasive method and requires surgery to connect the device directly to the central blood vessels. Hollow fiber membrane based ECMO are used for this purpose to provide adequate gas exchange. Although the current oxygenators have shown promising life-saving results for treating respiratory failure in adults, they not well suited for use with preterm and term neonates suffering from RDS due to their high priming volume and considerable pressure drop. Their high priming volumes requires that they be filled with donor blood instead of saline, which can lead to complications. The high pressure drop necessitates an external pump for perfusion which can damage the blood cells [12], [13]. It should be noted that the total blood volume of a neonate is 95 – 100 mL kg^{-1} [8]. Therefore, oxygenators should have a low priming volume (~ 10 mL kg^{-1} of body weight)

in order to use saline as a filling solution and to avoid excessive dilution of blood and consequent reduction in hematocrit [8]. Such a device as well as the required extracorporeal circuit would have a priming volume which is compatible with clinical dosage of saline solution boluses of 10 – 20 mL kg^{-1} for neonates with hypotension[14], [15].

Consequently, a passive lung assist device (LAD), pumped by the baby's heart (the arterio venous pressure differential for a neonate is between 20 to 60 mmHg) and capable of gas exchange in ambient air would be ideal; a concept termed as the artificial placenta. Such a LAD could be connected to the umbilical vessels to ameliorate the poor gas exchange capability of under-developed lungs during their final stages of growth and maturation. The recent development of microfluidic technology that enables fabrication high surface to volume ratio fluidic networks [16], [17] is especially suited for an artificial placenta device with low priming volume, low hydraulic resistance (low pressure drop), and high gas transfer in ambient air. Over the past decade, many microfluidic oxygenators have been developed, yet only a few of them[9],[18],[19] could be perfused solely by the arterio venous pressure differential and work in ambient air without a need of external gas supply. Most of other microfluidic blood oxygenators were designed to be operated with the assistance of an external pump, which can cause complications such as hemolysis [20], [21], or required additional actively perfused gas supply, such as pure oxygen or compressed air to enhance to gas exchange[16], [17], [22]–[30]. One limitation of previous pumpless, ambient gas exchange oxygenators[9],[18],[19] has been that only one side of the microfluidic network, through which the blood flows, is composed of the thin gas exchange membrane. This limitation can be overcome by incorporating thin gas exchange membrane on both sides albeit with additional fabrication complexity. Indeed, oxygenators with double-sided gas exchange microfluidic channels have been previously developed [31], [29]. They have a microfluidic oxygen supply and distribution manifolds on their either side which serve to stabilize the membrane and prevent their distortion, delamination and failure under operating pressures. However, these manifolds require that the exchange gases be pumped through them and are not suited for the artificial placenta

configuration where gas exchange with the ambient atmosphere is sought. In addition, exchange of gases with air at ambient pressure is preferable to 100% oxygen at high pressure due to complications such as hyperoxemia and oxygen toxicity [32]. In this study, we report a new technique to fabricate a thin microfluidic blood oxygenator (SOU) that is capable of gas exchange from both the top and bottom sides of the blood channel network. Consequently, the gas exchange area of the device is increased to improve gas exchange capacity while its overall priming volume was not changed. Blood testing was performed to measure the performance of SOUs under realistic clinical settings. This optimized configuration was used to build a LAD by connecting several SOUs together. Blood testing was performed to measure the performance of SOUs and the LAD under realistic clinical settings. This new design, enabled by the new fabrication process, is the first pumpless artificial placenta device capable of achieving the required oxygen gas exchange to support neonates with RDS.

4.3 Methods

4.3.1 Design

A new design (Figure 4.1) of the single oxygenator unit (SOU) was developed, which consisted of two main components: i) a blood vascular network that is responsible for facilitating blood flow distribution by forming a thin blood layer close to the membranes for gas exchange and ii) two gas permeable membranes that form the top and the bottom of the vascular network to allow gas transfer. The channel layout for the blood vascular network was adapted from previous designs that had been optimized for uniform distribution of the blood over a large surface and with no dead zones, low hydraulic resistance and low shear stresses encountered by blood[18]. This design (Figure 4.1.a and b) consisted of a square-shaped chamber filled with arrays of square-shaped micropillars that formed an interconnected blood flow network. The micropillars provided mechanical support to hold large area membranes apart and maintained the blood vascular network integrity during operation. Optimal pillar size of 1x1 mm was found to be the most suitable[19] for reliable bonding of the gas exchange membrane to the blood channel

network and therefore used here. The initial size of the blood vascular network was 43 mm × 43 mm with three different depths of 75 µm, 110 µm, and 145 µm which produced pressure drops that spanned the range of arterio venous pressure differences in neonates. This layout allowed 76 % of the gas exchange membrane area to be involved in gas transfer. Two pieces of silicone tubes (3.6 mm ID) were diagonally placed on two opposite corners to serve as an inlet and outlet.

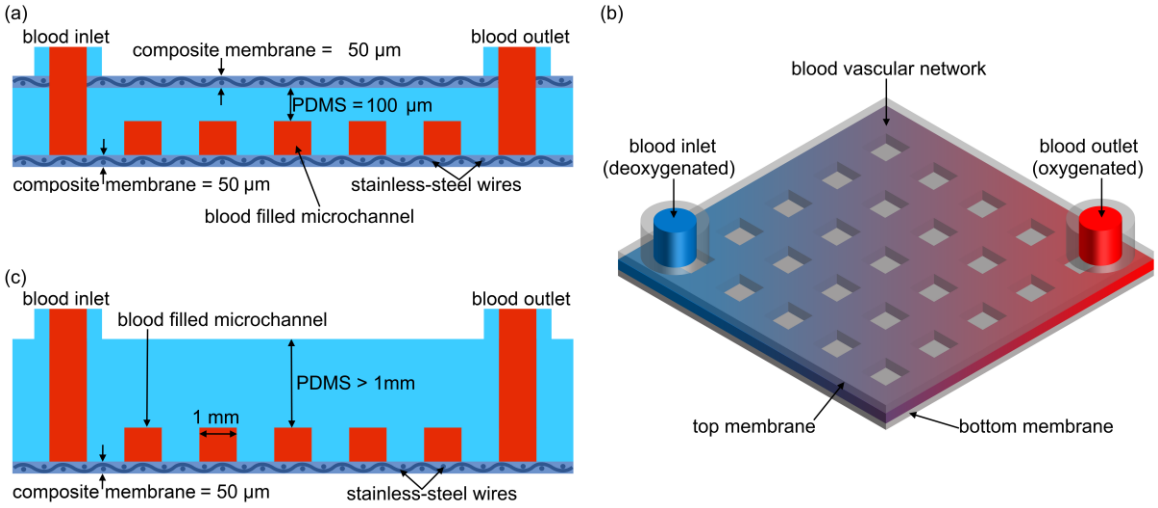

Figure 4.1: (a) Schematic cross-sectional view of a SOU with double-sided gas diffusion membrane, (b) schematic 3D view of a double-sided SOU, and (c) schematic cross-sectional view of a SOU with single-sided gas diffusion membrane.

The gas exchange membrane used consisted of a stainless-steel reinforced thin (50-µm) PDMS membrane on one side that was adapted from our previous work[19]. The composite membrane consisted of an ultra-thin stainless-steel mesh (MS-400/19, Asada Mesh Co. Ltd.) with a thickness of 39 ± 2 µm, pore size of 45 µm and a porosity of 49% which was covered with PDMS to form a 50 µm-thick membrane. Additionally, a new fabrication process was developed in this paper which facilitated the incorporation of a slightly thicker (150-µm) steel reinforced membrane on the other side of the blood channels as well, in order to facilitate higher gas exchange. The new fabrication process enabled a 100% increase in the surface area for gas exchange while maintaining the priming volume, pressure drop and other hydraulic characteristics of the device and was incorporated to increase the oxygenation performance. The older design[19] (Figure

3.1.c) consisting of thin gas exchange membrane on one side was also fabricated and tested for comparison purposes.

4.3.2 Fabrication

Previously, we had developed a microfluidic blood oxygenator with a new composite membrane and single-sided gas diffusion blood channels[19]. One side of the oxygenator was composed of a stainless-steel mesh reinforced, thin PDMS membrane that was stiff and prevented any deformation under the operating pressure while still allowing efficient gas exchange. However, the other (top) side, which contained the microchannel network embedded in it, was composed of a thick (more than 1 mm) PDMS layer which was required in the fabrication process to attach to the thin PDMS membrane firmly and peel off without any deformation or defects. In order to improve the gas exchange characteristics, attempts were made to reduce the thickness of the top side to anywhere between 50-200 μm so that gas exchange can occur on both sides. However, these attempts proved unreliable and defects were generated while peeling off a large area (~ 20 cm^2) thin PDMS membrane layer with embedded microchannel network. In this paper, we have developed a new fabrication process where the stainless-steel mesh is incorporated into both sides of a thin cast part consisting of the microfluidic network. This fabrication process also ensures that the stainless-steel mesh is firmly embedded in the PDMS and is not exposed to the blood at any location. The incorporation of the stainless-steel mesh provides structural support to the thin (250 - 500 μm) but large microfluidic layer (~ 20 cm^2). This reliable fabrication process enables for the first time, high yield manufacture of the double-sided oxygenator units that can achieve high gas exchange and better performance.

Microfluidic blood oxygenators with double-sided gas diffusion, were fabricated using a modified PDMS soft-lithography process as shown in Figure 4.2. First, the negative template of the blood vascular network for both designs (single-sided and double-sided) was fabricated by patterning on SU-8 3035 (Microchem Corp, Westborough, MA, USA) using a conventional photolithography technique[33]. PDMS (Sylgard 184, Dow Corning,

Midland, MI) was prepared by mixing the base and the curing agent together in 10:1 ratio by weight. A desiccator was used for 30 minutes to degas the mixture. PDMS was spin-coated on the microchannel mold with the speed of 500 RPM for 60 s to form the vascular network as shown in Figure 4.2.a. Subsequently, this spin coated layer was heated up to 85 ℃ in an oven to cure the PDMS while in the mold. A second layer of PDMS was spun with a speed of 4000 RPM for 40 s on top of the cured PDMS to form a 25-µm-thick PDMS layer. A piece of ultra-thin stainless-steel mesh was embedded into the wet PDMS as shown in Figure 4.2.b (To avoid exposing stainless-steel mesh to blood, two holes were cut into the mesh at the inlet and the outlet positions by a scalpel and was carefully aligned and placed on top of the vascular network). The composite reinforced microfluidic layer was placed in an oven at 85 ℃ for 10 minutes to cure the PDMS. Subsequently, a third layer of PDMS was spin-coated on top of the previous layer with the same speed and cured in an oven at 85 ℃ for 10 minutes as seen in.

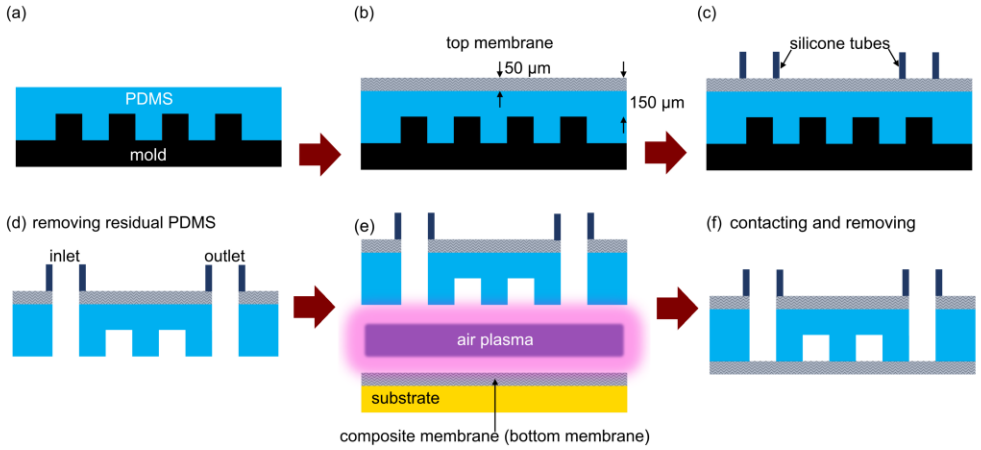

Figure 4.2: Fabrication process of a dsSOU: (a) a thin layer of PDMS was spin-coated on the top of mold and the product was placed in an oven to cure PDMS, (c) another thin layer of PDMS was spin-coated on the top of the cured PDMS and a piece of stainless-steel mesh was embedded into wet PDMS, following a third spin-coated PDMS layer (d) silicone tubes were placed on two opposite corners as the inlet and outlet, (e) the device was peeled off and residual PDMS inside inlet and outlet was removed, and (f) the bottom surface of the vascular network and the composite membrane were exposed to air plasma, the blood vascular network and the membrane were brought in contact and placed in an oven at 85 ℃ overnight, and the substrate was removed.

For the inlet and outlet, two 10-mm-silicone tubes (MasterFlex platinum-cured silicone tubing) were attached diagonally on two opposite corners of the vascular network using wet PDMS (Figure 4.2.c) and cured at 85 ℃ for an hour to strengthen gluing between

tubes and the vascular network. The device was peeled off from the mold and residual PDMS inside tubes was removed by a biopsy punch (Figure 4.2.d). This new approach of layer by layer fabrication of the microfluidic base layer enables highly reliable fabrication of pinhole free layer area thin microfluidic networks that are critical for the oxygenator.

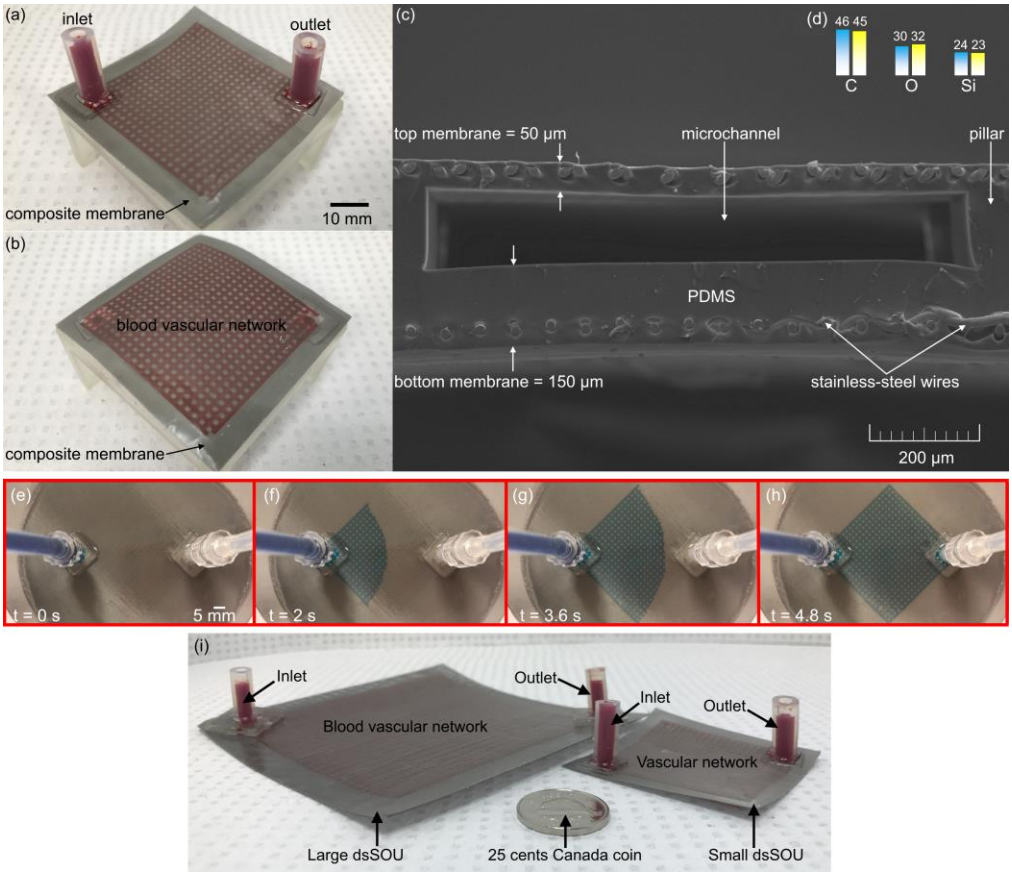

Figure 4.3: (a) image of the top-side of a double-sided SOU filled with bovine blood, (b) image of the back-side of the same SOU filled with bovine blood, (c) SEM image of a double-sided SOU, (d) the XPS analysis of both PDMS and composite membranes (blue bars represent for composite membrane and yellow ones represent for PDMS membrane), (e – h) sequence of filling a dsSOU with the height of ~110 µm with dyed water (flow rate = 2 mL/min) and (i) Image of a small dsSOU besides a large dsSOUs for size comparison (both devices were filled with bovine blood). The coin shown in the figure is a Canadian 25-cent piece (approx. 20 mm diameter).

The composite membrane was produced as previously described[19]. In short, PDMS was spin-coated on a substrate at 4000 RPM for 40 s and a piece of ultra-thin stainless-steel mesh was laid on the uncured PDMS; then it was cured in an oven at 85 °C for 30 minutes. Second layer of PDMS was spin-coated on the cured product with the same speed and time and cured in an oven at 85 °C for 30 minutes. Once the vascular network

and the membrane were ready, they were bonded to each other by using a hand held air plasma[34] (BD-20AC Laboratory Corona Treater, Electro-Technic Products, Chicago, IL, UAS) as shown in Figure 4.2.e.

Their activated surfaces were brought in contact and formed a strong bonding with each other. The device was stored in an oven at 85 ℃ overnight to strengthen the bonding. Finally, the device was removed from the substrate and was ready to use (Figure 4.2.f). Figure 4.3.a and b show a dsSOU filled with bovine blood.

Smaller dsSOUs with three different heights of 75, 110, and 145 µm for the microfluidic blood vascular network were fabricated and tested to compare their performance with single sided oxygenators. All smaller double-sided devices had the same dimensions for the blood vascular network (43 mm × 43 mm) with an effective gas exchange surface area of 14.08 cm^2 but with different priming volume of 0.106 (75 µm), 0.156 (110 µm), and 0.204 mL (145 µm) respectively.

The SEM image of the cross-section of a fabricated dsSOUs is shown in Figure 4.3.c. The top and bottom membranes have a thickness of 50 and 150 µm, respectively. Therefore, both the top and bottom surfaces can participate effectively in gas exchange between the blood flowing in the channel and the ambient air surrounding the device. Also, it can be seen that the stainless-steel wires are completely embedded in the PDMS and will not be exposed to the blood flowing inside the channels. X-ray photoelectron spectroscopy (XPS) analysis of the surface of a PDMS and a composite membrane (Figure 4.3.d) showed that the elemental compositions at the surface of the PDMS coated stainless steel mesh was similar to PDMS and did not show any Fe which would indicate any exposed steel. Filling in this device is also uniform as shown in Figure 4.3.e – h and there are no dead zones created that could promote clot initiation.

Larger SOUs (91 mm x 91 mm) with blood vascular network with a height of 200 and 245 µm and a priming volume of 1.25 and 1.53 mL was also fabricated, as shown in Figure 4.3.i, in order to be incorporated in the LAD. The large SOUs have 4-fold larger gas exchange surface area (62.56 cm^2) and only four of them are required to support the

gas exchange needs of a 1-2 kg neonate. The use of large SOUs significantly reduced the priming volume associated with the interconnects and the two interconnect designs (LAD 1 and 2) as shown in Figure 4.4, had a total priming volume of only 17 and 8 mL of blood.

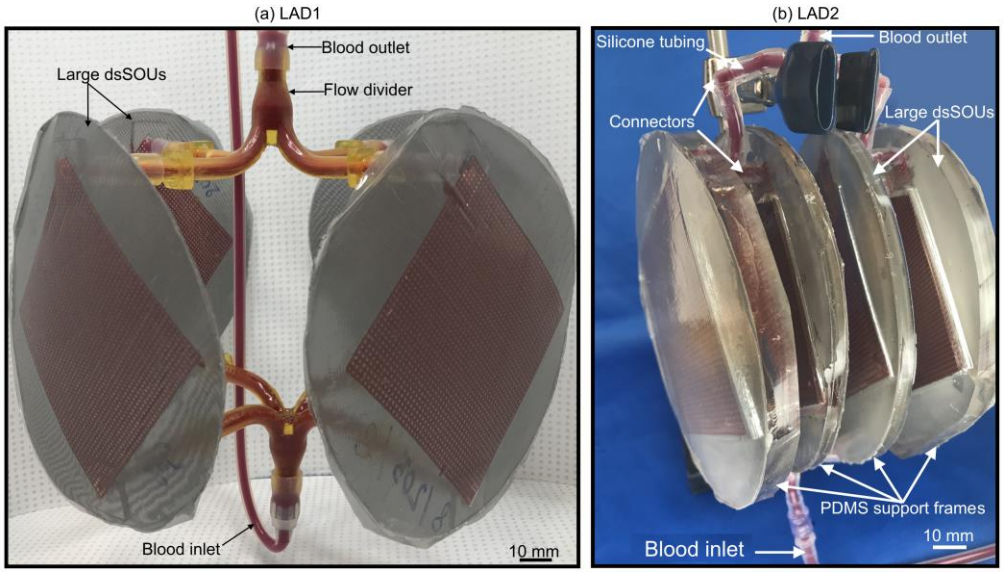

Figure 4.4: (a) image of the LAD1 with four large dsSOUs with a total priming volume of 17 mL and (b) image of the LAD2 with four large dsSOUs which were connected by connectors and silicone tubing with a total priming volume of 8 mL. Both LADs were filled with bovine blood.

4.3.3 Requirements for an artificial placenta type oxygenator

In the artificial placenta type configuration, the lung assist device (LAD) is placed in parallel to the body's systemic circulation such that the inlet is connected to an artery and the outlet to the vein. This is to ensure that the arterio-venous pressure difference that pumps blood through the body will also perfuse the device. This kind of connection is in contrast to other commonly used ECMO devices that use external pumps which are usually connected to the body in venous-artery or venous-venous configuration[35]. The arterio-venous connection places specific constraints on the design of the devices. Blood which enters the LAD is arterial blood. As a result, the blood has already passed through the lungs where it has been oxygenated before it enters the LAD. Under lung failure and/or pulmonary hypertension, the arterial blood may only be 10-30% below full saturation. Therefore, compared to current ECMO oxygenator our LAD is designed to

work at the upper end of the oxygen binding curve of haemoglobin[8]. Further, the LAD should have a low dead volume (typically 10-20% of the 100 mL/kg body weight) so that it could be filled with saline and not require blood transfusion. The LAD should also not induce high cardiac output failure due to excessive bypass blood flow from the systemic circulation. As a result, the LAD should operate under flow rates of 20 to 30 mL min^{-1} kg^{-1} of a baby. The oxygen saturation of the incoming blood is estimated at 70%[36]. Blood with an average haemoglobin concentration of 16 g dL^{-1} and oxygen binding capacity of 1.39 mL oxygen per one gram of haemoglobin is considered in this calculation[37], [38]. At blood flow rates from 20 to 30 mL min^{-1} kg^{-1} of a baby, the LAD would need to deliver 1.3 to 1.9 mL of O_2 min^{-1} kg^{-1} of a baby. This is the maximum amount of oxygen which could be taken up by the blood with a blood flow of 20 to 30 mL min^{-1} kg^{-1} of a baby[8], [9], [18]. Consequently, during testing, the oxygen saturation level in blood before the LAD was adjusted to 59 ± 3% (lower than the physiological values) so that it could be increased to 90% or higher to determine the maximum gas transfer capability of the LAD that is designed to support neonates weighing up to 2 kg.

4.3.4 Gas exchange testing in blood

In vitro gas exchange testing was performed on these oxygenators using blood to assess their performance. Before perfusing the device with blood, deionized water was used to prime the device so as to ensure a uniform blood flow and prevent trapping of air bubbles. Then, heparinized (3 units mL^{-1}) bovine blood (Bovine 7200807-1L, Lampire Biologicals Laboratories, Pipersville PA) was used to evaluate oxygen transfer in the device. The oxygen concentration in blood was adjusted to venous conditions to mimic in vivo oxygenation provided by the natural lungs. In order to achieve a target saturation level, a hollow fiber oxygenator (PDMSXA-1.0, PermSelect®, Ann Arbor, MI, USA) was used. Blood was pumped through the shell of the hollow fiber membrane by a peristaltic pump (Ismatec model ISM832C, Ismatec, Glattbrugg, Switzerland) at 15-25 mL min^{-1} while a carbon dioxide/nitrogen gas mixture (5%/95% v/v) was introduced through fibers at 20 L h^{-1} to reach a desired oxygen saturation level of 63% ± 5%. Then, blood was stored in a sealed bottle and placed in a fridge at 4 °C overnight to minimize the oxygen metabolism

by cells and maintain the set oxygen saturation level. The next day, blood was transferred to 140-mL syringes (Monoject™) and a cap was used to tightly close the syringe for further use. Before transferring blood to syringes, a stir bar was placed inside of each syringe.

A 140-mL syringe filled with heparinized blood was loaded to a syringe pump (22 syringe pump, Harvard Apparatus, Holliston, MA, USA) and magnetic stirrer was located under the syringe (Figure 4.5). The stir bar inside the syringe provided sufficient mixing in blood to keep it homogeneous throughout the experiment. The blood was perfused through the microfluidic oxygenator. The flow rate was varied from 0.5 mL min^{-1} to 4 mL min^{-1} for dsSOUs and ssSOU.

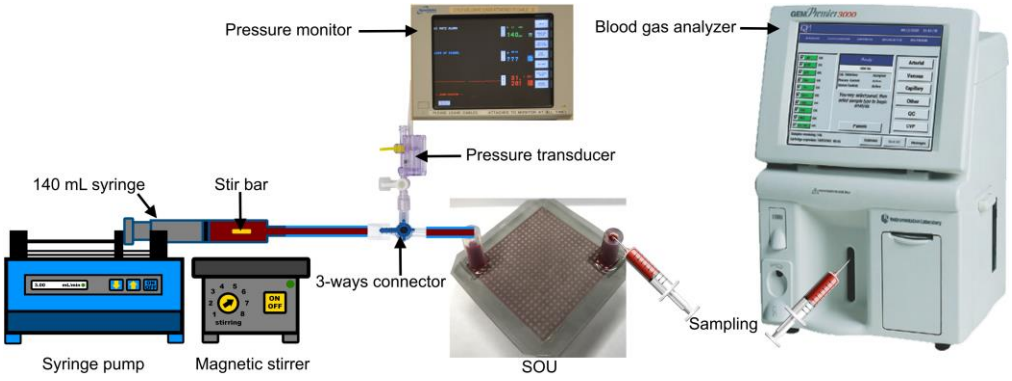

Figure 4.5: Experimental set-up for gas exchange testing in blood.

A TruWave Pressure Transducer (Edwards Lifesciences LLC, Irvine, CA, USA) was placed before the device and connected to a Spacelabs 90369 Patient Monitor (SpaceLabs Medical Inc., Redmond, WA, USA) to monitor the pressure drop during the experiment. Blood was analyzed by a point-of-care blood gas analyzer (GEM Premier 3000, Instrumentation Laboratory, Lexington, MA, USA) before and after the device to assess the oxygen content in blood and determine the rate of oxygen uptake by the device. Also, the hematocrit content was measured by a Complete MicroHematocrit System (StatSpin CritSpin, Norwood, MA, USA). The total concentration of oxygen in the blood was calculated by taking the sum of the amount of dissolved oxygen and the hemoglobin-bound oxygen[18].

To evaluate the maximum oxygen transfer capacity of oxygenators, an enriched oxygen environment was created around oxygenators by placing them inside of an airtight chamber (200 mm × 300 mm × 120 mm) made of acrylic. Once the oxygenator was placed inside of the chamber, it was filled with pure oxygen so that it completely fills the chamber and sealed at atmospheric pressure.

4.4 Results and Discussion

4.4.1 Comparison between the performance of single and double sided single oxygenator units

dsSOUs with three heights of 75 µm, 110 µm, and 145 µm were fabricated and tested with blood to select the appropriate height that could produce pressure drop in the operational regime (20 – 60 mmHg). The devices were tested at various blood flow rates of 0.5, 1, 1.5, 2, 3, and 4 mL min^{-1} (Figure 4.6). For all tested devices, pressure drop linearly increased with blood flow rates as shown in Fig. 5. Also, it was observed that the pressure drops decreased with increasing channel height from 75 µm to 145 µm as expected. The gray region in Figure 3.4 shows the operation regime for successful pumpless operation of the artificial placenta device. It can be seen that devices with a channel height of 75 µm was not suitable as the pressure drop is higher than the operational regime.

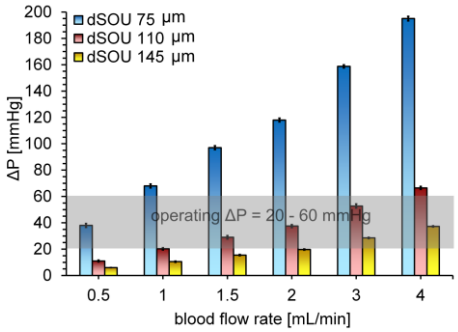

Figure 4.6: Pressure drop of dsSOUs at various blood flow rate for different heights. Data are mean ± SD, n=4.

However, both devices with channel height of 110, 145 µm had lower pressure drops than 60 mmHg over a significant range of blood flow rates and could be considered for this

application. As a result, dsSOUs with the channel height of 110 µm was chosen as the optimum device for further experiments. Then, both ssSOUs and dsSOUs (with channel height of 110 µm) were fabricated and their gas exchange performance measured in order to characterize the improved performance. In vitro gas exchange testing was conducted flowing blood at various flow rates of 0.5, 1, 1.5, 2, 3, and 4 mL min^{-1} while simultaneously measuring the increase in partial pressure of oxygen (pO_2) and oxygen saturation level (SaO_2) between the inlet and outlet of the oxygenator.

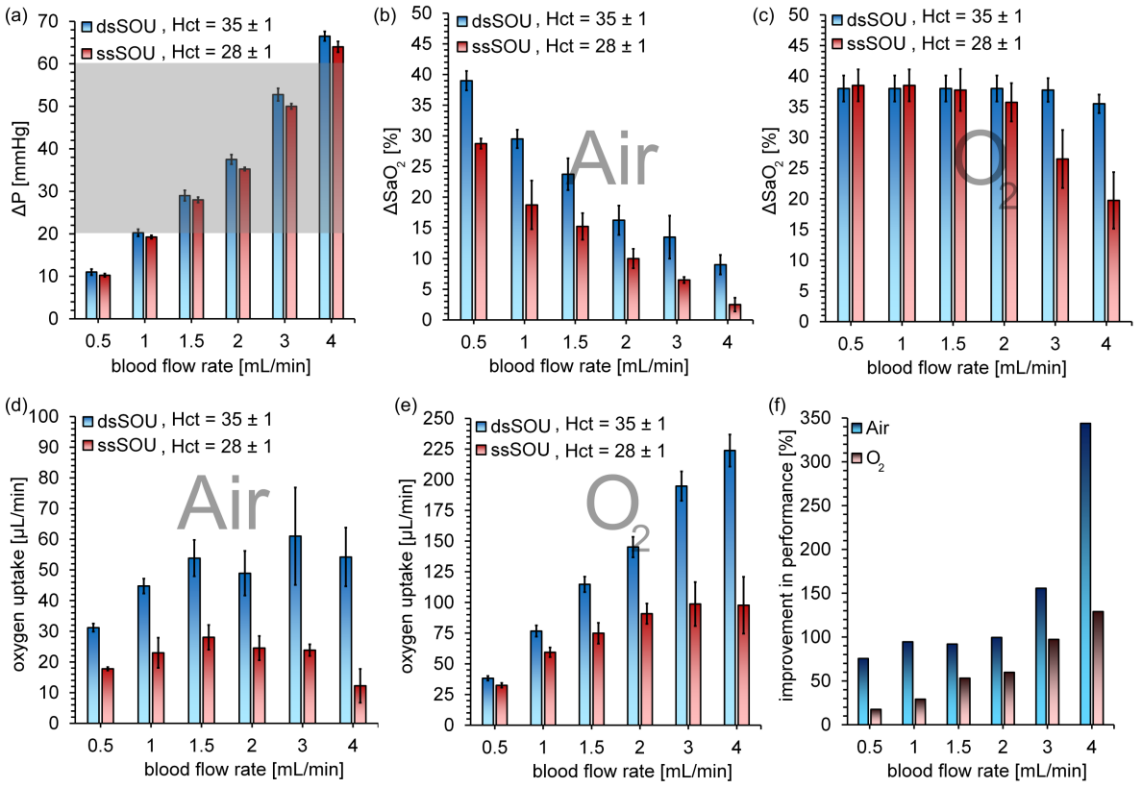

Figure 4.7: In vitro comparison between ssSOUs and dsSOUs: (a) pressure drop, (b) the increase in oxygen saturation level in room air, (c) the increase in oxygen saturation level in an enriched oxygen environment with atmospheric pressure, (d) the oxygen uptake for room air, (e) the oxygen uptake in an enriched oxygen environment with atmospheric pressure, and (f) the improvement in performance for dsSOUs compared to ssSOUs. Hematocrit (Hct) level is shown for both ssSOUs and dsSOUs. Data are means ± SD, n=4.

The experiment for each type of devices was repeated 4 times and the average was calculated for each condition. Each device was first tested in ambient air and then in an enriched oxygen environment. The results shown in Figure 4.7 demonstrate that the oxygenation of blood is always better when dsSOUs are used as compared to ssSOUs.

Simultaneously, the pressure drops of both ssSOU and dsSOUs were measured with flow of blood and no significant difference was observed as shown in Figure 4.7.a. This result confirmed that the dsSOU, despite being thin, is stiff and does not undergo any structural change under the operating pressure that could affect its performance. It also confirmed that the differences in performances observed was solely due to the higher gas transfer area enabled by exposure of the blood to oxygen from both sides and not due to any other factors. Gas exchange tests showed that the ssSOU increased the oxygen saturation of the blood. This effect decreased gradually with increase in blood flow rate, as shown in Figure 4.7.b when exposed to air at atmospheric pressure. Exposure to pure oxygen environment at atmospheric pressure allowed the increase in oxygen saturation to be stable till flow rates were less than 3 mL min^{-1} before falling at higher flow rates, as shown in Figure 4.7.c. Additionally, the experimental results for ssSOUs showed that increasing blood flow rate, especially at lower blood flow rates (0.5 – 1.5 mL min^{-1}), resulted in a gradual increase of oxygen uptake (Figure 4.7.d). However, at higher blood flow rates (1.5 – 3 mL min^{-1}) the oxygen uptake remains constant and even decreased at a blood flow rates > 3 mL min^{-1}. This behaviour could be a result of the competing effects of increased volume of blood flowing in the device and the reduced residence time of each of the red blood cells in it. Alternatively, at higher flow rates, the membranes are flexed which could increase the effective channel height and a lower oxygen uptake. At high flow rates only the layers close to the gas exchange membrane have sufficient flux of oxygen molecules to attain saturation and a significant amount of blood away from the membrane remained unsaturated as it leaves the device. The results also show that the oxygen uptake of ssSOUs was enhanced in an enriched oxygen environment (Figure 4.7.e). The oxygen uptake increased steadily with flow rate until 3 mL/min, and then stabilizes. No further reduction in oxygen uptake was observed at higher flow rate. This behaviour can be attributed to the higher oxygen flux through the membrane due to the higher concentration gradient across it under enriched conditions.

The dsSOUs were found to perform better than the ssSOUs under all flow conditions as shown in Figure 4.7. The change in oxygen saturation (ΔSaO_2) also decreased for

dsSOUs when the flow rate was increased which was similar to the ssSOUs. However, the rate of the decrease was smaller compared to ssSOUs in room air (Figure 4.7.b). Interestingly, in pure oxygen environment the blood was fully saturated at flow rates below 3 mL min^{-1} and consequently the ΔSaO_2 was found to remain constant at these flow rates (Figure 4.7.c) and decrease at higher flow rates. It should be noted that the superior performance of dsSOUs was also under conditions when the hematocrit (Hct) of the blood used for testing is higher as compared to ssSOU. Blood with lower hematocrit value can be saturated with lesser amount of oxygen and if both were tested with blood with same Hct values, the difference in performance will be even larger.

Consequently, the oxygen uptake for dsSOUs was found to be significantly higher compared to ssSOUs, especially at higher blood flow rates (Figure 4.7.d). For instance, at a blood flow rate of 4 mL min^{-1}, the dsSOU produced an oxygen uptake of 54.2 µL min^{-1} while it was only 12.2 µL min^{-1} for the ssSOU operating under the same conditions. This represents a 343% (Figure 4.7.f) improvement in oxygenation due to exposure of both sides of blood vascular network to ambient air. The oxygen uptake of dsSOUs was also found to increase with the increase in blood flow rate and stabilize at higher flow rates (Figure 4.7.d). Unlike the ssSOU exposed to ambient air, no drop in oxygen uptake was observed at the highest tested flow rate of 4 mL min^{-1}. The access to oxygen from both sides of the blood vascular network in dsSOUs reduces the effective diffusion length for the oxygen to travel by half thereby providing a more stable oxygen uptake at higher flow rates. Like ssSOUs, dsSOUs were also tested in an enriched oxygen environment (Figure 4.7.e). The oxygen uptake was found to continuously increase with increasing blood flow rate. It was also found to be higher as compared with ssSOUs. For instance, the oxygen uptake at a blood flow rate of 4 mL min^{-1} was 223.8µL min^{-1} for dsSOUs which shows 129% (Figure 4.7.f) improvement in oxygen uptake over the ssSOU under similar conditions. This behaviour can also be attributed to the higher concentration gradient across the membrane that produces a high flux of oxygen which is able to sustain the continued increase in oxygen uptake.

Finally, dsSOUs with different heights were tested with bovine blood to evaluate their performance under the same conditions (Figure 4.8). As seen in Figure 4.8.a, oxygen uptake of dsSOUs with different heights were not significantly different, especially at higher blood flow rates. This could be because of lower resistance time for blood in microchannels which limits the gas exchange to the regions close to both membranes. Although the oxygen uptake was improved by exposing oxygenators to pure oxygen, they still had the same behaviour (Figure 4.8.b). These results reveal that decreasing the height of blood channel would increase gas exchange but not significantly. Therefore, pressure drop and its suitability for pumpless operation would be the key factor in determining the suitable height of the oxygenator for artificial placenta application.

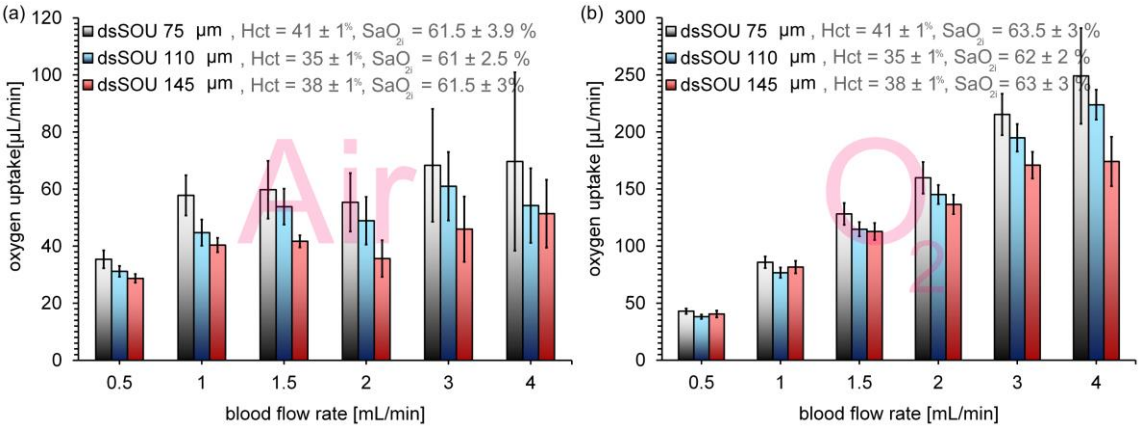

Figure 4.8: In vitro gas exchange testing in blood for dsSOU with three different heights at various blood flow rates: (a) tested in room air, and (b) tested in in an enriched oxygen environment with atmospheric pressure. Oxygen saturation level at the inlet (SaO_{2i}). Data are mean ± SD, n=4.

4.4.2 Scaling of double-sided SOUs

Very few microfluidic oxygenators have been shown to be capable sustaining a large blood flow (~10 mL/min) at reasonable pressure drop (20-60 mmHg) and oxygenating blood sufficiently. This is primarily due to the small size of the microchannels (which causes high resistance to blood and increasing pressure drop) and the inability to fabricate large area devices (which limits the residence time for sufficient oxygenation). Instead of stacking multiple smaller SOUs, larger SOUs can be used as they would reduce the number of interconnections between the devices when the LAD is assembled and serve to

reduce the overall priming volume of the oxygenator. For instance, by increasing size of the SOU to 91 mm × 91 mm, the gas exchange surface area will have the same total gas exchange surface area as 4 smaller devices with the size of 43 mm × 43 mm. This larger configuration will eliminate several interconnections needed and reduce the overall priming volume of the LAD. Therefore, larger dsSOUs (91 mm in length) were fabricated with 200 and 245 µm in height to optimize to produce a pressure drop lower than 60 mmHg under the operating blood flow rates and were tested with blood over a wider range of blood flow rates from 1 mL min^{-1} to 12 mL min^{-1} in ambient air and under pure oxygen environment. The pressure drop of both large dsSOUs was found to linearly increase with blood flow rates as shown in Figure 4.9.

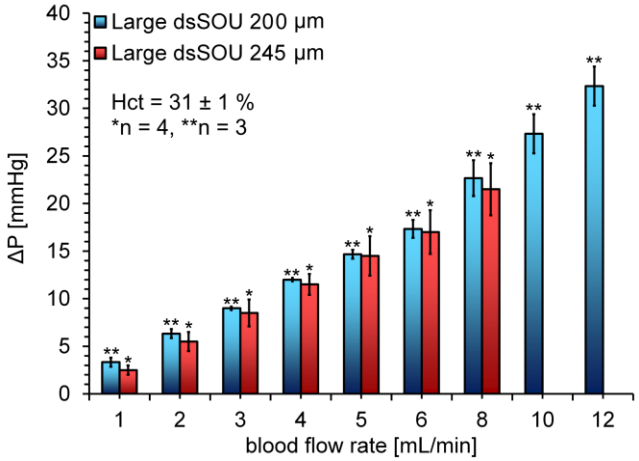

Figure 4.9: Pressure drops of large dsSOUs tested with bovine blood at various blood flow rates. Data represents the mean ± SD.

As seen in Figure 4.9, there was no significant difference in the pressure drop of the two dsSOUs of different heights at various flow rates. It remains between 20-35 mmHg for flow rates between 8-12 mL/min. These results indicate that gas exchange characteristics should determine the optimal height of the device. The larger SOUs allow a much longer residence time of blood in the device as compared to the smaller SOUs although they operate at nearly the same pressure drop.

Subsequently, gas exchange experiments were performed on large dsSOUs with a height of 200 µm and 245 µm. The oxygen uptake of the blood perfused through the dsSOUs

was found to gradually increase with increasing blood flow rates up to 7.5 mL min^{-1} and 12 mL min^{-1} in ambient air as shown in Figure 4.10.a and c. Similar to the smaller dsSOUs, a better oxygen uptake was also achieved when exposed to pure oxygen in the ambient instead of room air for the large dsSOUs. The oxygen uptake at a blood flow rate of 8 mL min^{-1} was 0.44 and 0.52 mL min^{-1} for large dsSOUs with the height of 245 and 200 µm, respectively while the corresponding pressure drops were 21.5 and 22.7 mmHg. The higher flow rate, lower pressure drop and the higher oxygen uptake obtained make the large dsSOUs suitable for integration into an LAD. In addition, the CO_2 release (Figure 4.10.b and d) was also measured.

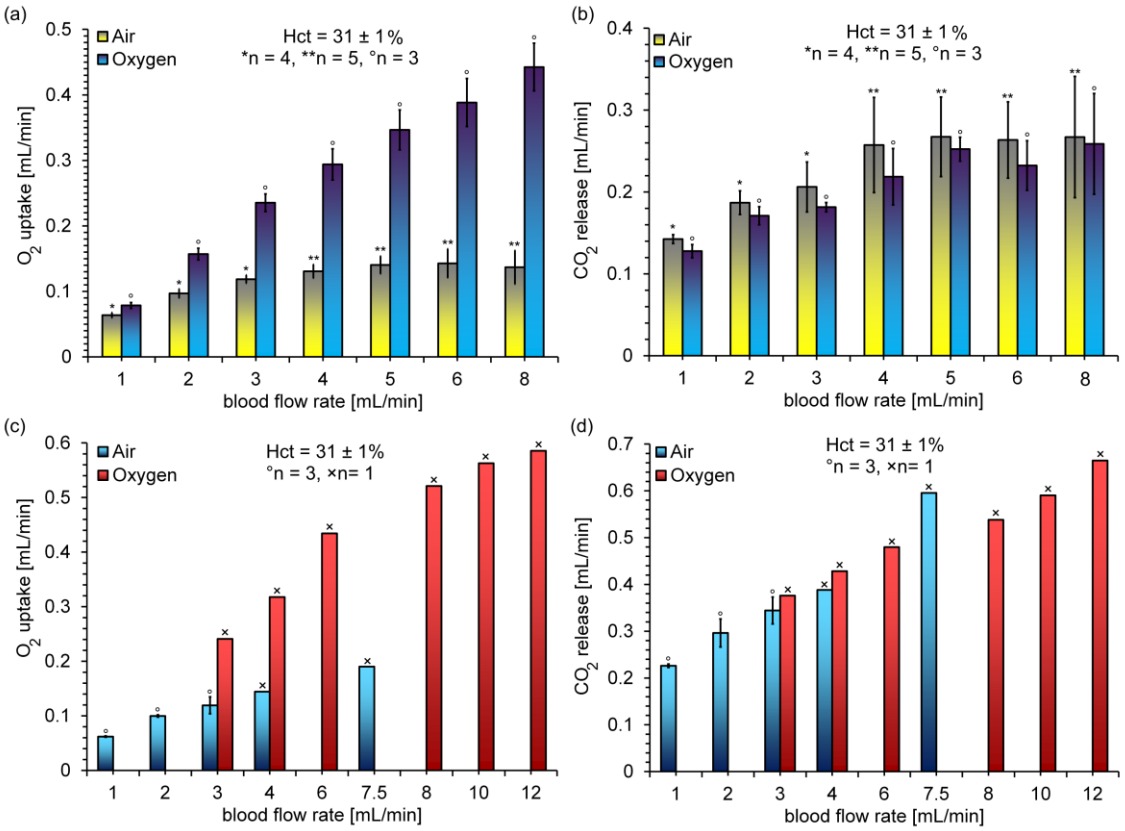

Figure 4.10: In vitro performance of large dsSOUs: (a) oxygen uptake and (b) CO_2 release for devices with a height of 245 µm, (c) oxygen uptake and (d) CO_2 release for devices with a height of 200 µm at various blood flow rates. Data represents the mean ± SD.

The CO_2 release was not significantly impacted by changing ambient atmosphere from air to pure oxygen. For example, large dsSOUs with the height of 245 µm could release CO_2

at a rate of 0.27 mL min^{-1} and 0.26 mL min^{-1} in room air and pure oxygen environment, respectively. However, the height of the channels had a significant impact on the CO_2 release. For instance, at a blood flow rate of 8 mL min^{-1} and in a pure oxygen environment, the amount of CO_2 release was 0.26 mL min^{-1} in for dsSOU with a height of 245 µm as compared to 0.66 mL min^{-1} for dsSOU with a height of 200 µm. Due to its superior performance in both oxygen and CO_2 exchange, large dsSOU with the height of 200 µm was chosen as the optimum configuration for using in LAD development.

It should be noted that a single large dsSOU could achieve an oxygen uptake as high as 0.59 mL min^{-1} at a blood flow rate of 12 mL min^{-1} and with a pressure drop of 32 mmHg when exposed to pure oxygen environment, which corresponds to a volume % transfer of 4.9%. In comparison, the small dsSOUs achieved an oxygen uptake of 0.17 mL min^{-1} at a blood flow rate of 3 mL min^{-1} with the same pressure drop. If four smaller dsSOUs were connected in parallel, an oxygen uptake of 0.68 mL min^{-1} can be achieved at a blood flow rate of 12 mL min^{-1} which is 14 % more compared to the oxygen uptake of a single large dsSOU. The slightly poorer performance of the single large dsSOU can be attributed to the increased height of the fluidic channels which was required to ensure that the pressure drop was in the optimal range (~30 mmHg). Nevertheless, the combination of four smaller SOUs will have a significantly higher priming volume due to interconnections. Therefore, the larger dsSOUs, which had lower priming volume compared to a stack of smaller of SOUs, were used in the construction of the LAD and in subsequent testing.

4.4.3 Development of a compact LAD

The LAD was constructed by assembling 4 larger dsSOUs in parallel to meet the design requirements and to satisfy the estimated oxygenation needs of a neonate weighing up to 2 kgs. A parallel design enabled a modular increase in the amount of flow that could be handled without changing the pressure drop or the oxygenation characteristics of the SOUs. Blood flow dividers were designed with symmetrical flow paths to connect the inlets of all the large dsSOUs to a central line (LAD1). In addition, the LAD was also reorganized into a different configuration by replacing flow dividers with connectors and

silicone tubing (LAD2). First, the pressure drop of both LADs was measured with bovine blood with the same haematocrit level of 31 ± 1 % to ensure both were operating in the same pressure drop range. Finally, the LAD1 was tested with bovine blood at blood flow rates of 10 – 60 mL min^{-1} in an enriched oxygen environment. Then, blood properties at the inlet and the outlet of the LAD were measured to determine the gas transfer capacity of the LAD.

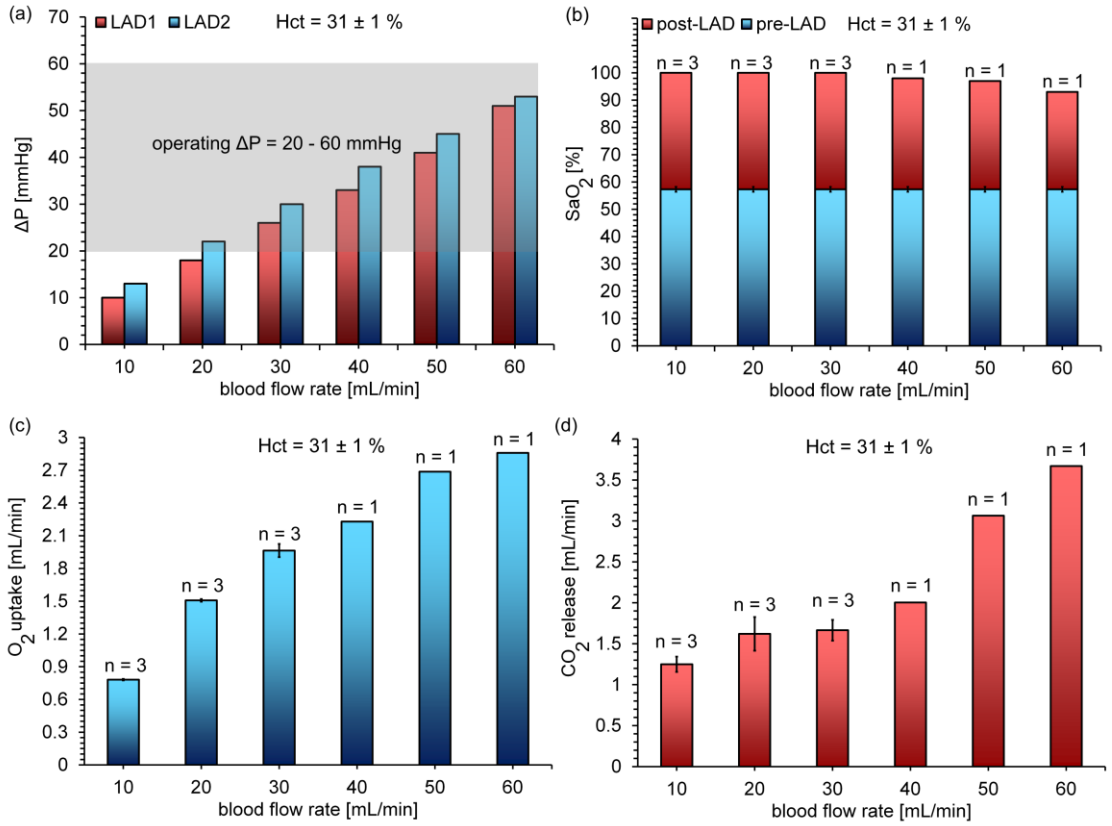

Figure 4.11: In vitro test of the LADs with bovine blood at various blood flow rates: (a) pressure drop comparison between LAD1 and LAD2, (b) oxygen saturation level before and after the LAD1, (c) oxygen uptake for the LAD1, and (d) CO_2 release for the LAD1. Data are means ± SD.

Pressure drop of the LADs were measured at various blood flow rates from 10 – 60 mL min^{-1} as shown in Figure 4.11.a. The pressure drop linearly increased with the blood flow rate and stayed within the optimum operating range (20 – 60 mmHg, the grey box shown in Figure 4.11.a) for all tested blood flow rates. The measured pressure drop of the LADs was the sum of pressure drops in large dsSOUs, flow dividers, connector, and tubing. To

estimate the pressure drop contribution of the flow dividers, connector, tubing, and large dsSOUs; we calculated the difference between the LAD (flow 10 mL min^{-1} through each large dsSOU; 33 mmHg for LAD1 and 38 mmHg for the LAD2) and a single larger dsSOU (flow 10 mL min^{-1}, 27.3 mmHg), resulting as 5.7 mmHg and 10.7 or 17% and 28 % of the total pressure drop, respectively. This showed the significant impact of flow dividers and connector tubing in the total pressure drop which would have been significantly higher if smaller double-sided SOUs were used.

The gas transfer of the LAD was measured when it was exposed to pure oxygen at atmospheric pressure. Figure 4.11.b shows the oxygen saturation level in blood achieved at the outlet of devices by operating at various flow rates. The results showed that the blood exiting the LAD was fully oxygenated (100 % saturation) for blood flow rates up to 30 mL min^{-1} which indicates that the LAD provided sufficient residence time and oxygen flux to completely saturate the incoming unsaturated blood (at 57 ± 1 % saturation). However, beyond 30 mL min^{-1} flow rate, the oxygen saturation level at the outlet decreased but never dropped below 90% saturation. This behaviour was expected as the residence time of blood in the oxygenator reduced at higher flow rates. Nevertheless, the oxygen uptake continued to increase with flow rate even up to 60 mL min^{-1} as the larger volume of blood flowing through the oxygenator assists in carrying larger amount of oxygen. For instance, the oxygen uptake at blood flow rates of 30 and 60 mL min^{-1} was 1.96 and 2.85 mL min^{-1} (Figure 4.11.c). Moreover, the CO_2 transfer was calculated and shown in Figure 4.11.d which showed a steady increase in CO_2 release over blood flow rates. This was expected as the thickness of boundary layer adjacent to membranes was reduced at higher blood flow rates resulting in better CO_2 exchange. In addition, as the same large dsSOUs were used to build the LAD2, it would be expected to see the same gas exchange properties without repeating the blood testing. These results demonstrate that this design of the LAD can provide the desired amount of oxygen delivery under proposed flow rates for preterm and term neonates with RDS.

The performance of the same LAD configuration when exposed to ambient air was also calculated using the experimental results obtained earlier for the larger double-sided

SOUs and plotted. The LAD could achieve an estimated ~ 20% increase in oxygen saturation level (equal to an oxygen uptake of 0.8 mL min^{-1}) at a typical blood flow rate of 30 mL min^{-1} and a pressure drop of 26 mmHg for LAD1 or 30 mmHg for LAD2 in ambient air. In summary, compared to the previous LAD[19] design developed for the artificial placenta, the new LAD with larger double-sided SOUs could achieve higher increase in oxygen saturation of blood, using lesser number of SOUs (and consequently lower priming volume) and at lower pressure drop.

4.4.4 Comparison to other microfluidic blood oxygenators

In summary, the performance of dsSOUs was found to be superior to the ssSOU design.

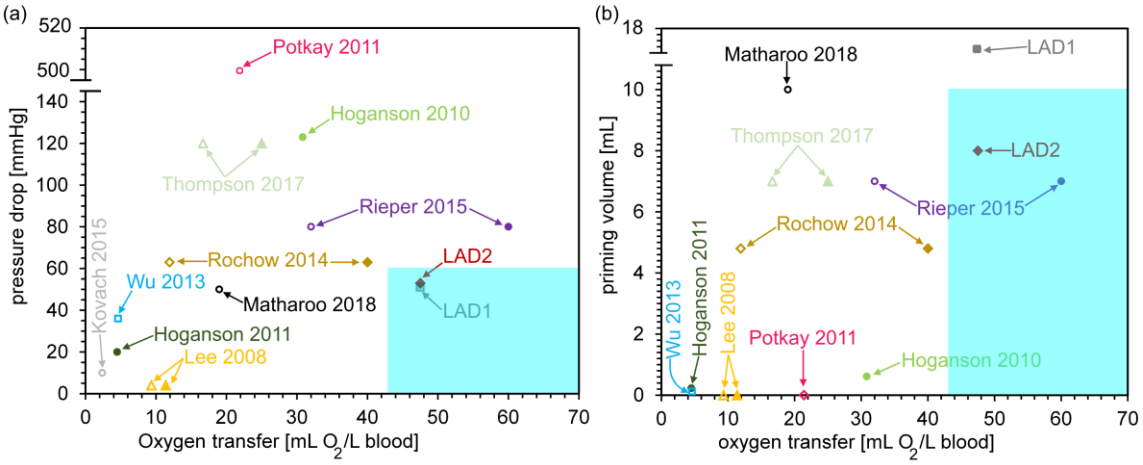

Figure 4.12: Comparison of various oxygenators based on their oxygen transfer versus: (a) pressure drop and (b) priming volume (all data are extracted directly from each paper or calculated based on data reported). The same color and shape is used to show data from the same work. Only works that reported priming volume and pressure drop are included in these graphs. Open and filled shapes represent oxygen transfer in ambient air and enriched oxygen environment, respectively. The blue boxes show required oxygen transfer for an artificial placenta without the need of an external pump and a priming volume less than 10 mL. Single oxygenator units have low priming volume and are clustered on the x-axis.

In order to compare its performance with other microfluidic blood oxygenators[9], [16], [28]–[30], [17]–[19], [22], [23], [25]–[27], the reported oxygen transfer rate and blood flow rate could be normalized to the gas exchange surface area. So, the amount of oxygen uptake per one litre of blood was calculated and defined as “oxygen transfer” to show the capacity of each device. This term also represents the amount of normalized oxygen transfer rate at a normalized blood flow rate of 1 L min^{-1} m^{-2}, which can be used for

comparison purposes. Among all microfluidic blood oxygenators[9], [10], [27]–[30], [39], [16], [18], [19], [22]–[26], the device developed by Rieper et al.[29] has the highest oxygen transfer of 60 mL of O_2 per liter of blood using oxygen as the perfusion gas. In comparison, the newly developed dsSOUs with a height of 75 µm exposed to a pure oxygen environment (without any gas pumping) achieved a higher oxygen transfer of 62.3 mL of O_2 per liter of blood. Even the dsSOUs with a height of 110 µm could achieve an oxygen transfer of 56 mL of O_2 per liter of blood in a pure oxygen environment which is comparable to the device made by Rieper et al.[29] It should be noted that this performance was also achieved at a lower pressure drop of 66 mm Hg compared to the device made by Rieper et al.[29] with a pressure drop of 80 mm Hg.

For the ideal pumpless implementation of the artificial placenta, the design criteria will be i) an operating pressure drop of 20 – 60 mmHg, ii) a minimum oxygen transfer of 1.3 mL of O_2 min^{-1} kg^{-1} body weight and iii) a blood flow rate of 30 mL min^{-1} kg^{-1} of a body weight. This corresponds to an oxygen transfer of 43 mL of O_2 L^{-1} of blood kg^{-1} body weight to provide the required oxygen transfer for a baby. Figure 4.12 shows both pressure drop and priming volume versus the corresponding oxygen transfer for all microfluidic devices. Only those devices which are within the blue boxes fulfil the above stated criteria and have therefore the capability to be used as a pumpless oxygenator with low priming volume for the artificial placenta application using either oxygen or ambient air. To best of our knowledge, the LAD described in this paper which was operated in a pure oxygen environment is so far the only microfluidic-based oxygenator that meets all the requirements for an artificial placenta as indicated by the blue boxes. Ongoing efforts are underway to increase the number of SOUs in the LAD to achieve a similar level of oxygen transfer in ambient air environment.

4.5 Conclusion

In this study, a new microfabrication technique for microfluidic blood oxygenators was established with double-sided gas transfer in blood channels, thereby improving gas exchange. Different heights of the blood vascular network were tested with bovine blood and the best one was compared to the device with single-sided gas transfer channels. Oxygen uptake of the double-sided device was increased up to 343% compared to the single-sided device. The dsSOUs would be ideal to fabricate a LAD which could fulfill all design criteria of an artificial placenta including required gas exchange, low priming volume, and capable of being operated by a baby's heart due to low pressure drop. Further, the size of dsSOUs was increased to be able to support higher blood flow rates with minimizing the priming volume of blood by using less connectors and tubing. Gas exchange properties of the large dsSOUs were not compromised significantly compared to the smaller dsSOUs. Subsequently, four large dsSOUs were fabricated and used to build a lung assist device (LAD) as an artificial placenta for preterm and term neonates suffering from RDS. The LADs consisted of 4 large dsSOUs with a low priming volume of 8 mL and 17 mL could provide enough oxygen to blood ranging from 1.96 mL min^{-1} to 2.86 mL min^{-1} using pure oxygen as ventilation gas. This LAD fulfills all design criteria of an artificial placenta including required gas exchange, low priming volume, and capable of being operated by a baby's heart due to low pressure drop. In the future, the design of the blood vascular network can be modified in a way to reduce hydraulic resistance in regions where have less contribution in gas transfer to achieve the same oxygen uptake at lower pressure drop. Additionally, antithrombin-heparin (ATH)[40], [41] or polyethylene glycol (PEG)[42] can be coated on the surface of dsSOUs to improve anticoagulation properties of PDMS surfaces in which are contact with blood. Finally, newer designs that have higher gas exchange can be used to provide the sufficient oxygenation in ambient air.

References

[1] J. A. Martin, B. E. Hamilton, M. J. K. Osterman, S. C. Curtin, and T. J. Mathews, "Births: Final Data for 2015," *Natl. Vital Stat. Reports*, vol. 66, no. 1, pp. 1–70, 2017.

[2] B. E. Hamilton, J. A. Martin, and M. J. K. S. Osterman, "Births: Preliminary Data for 2015 National Vital Statistics Reports," *Natl. Vital Stat. Reports*, vol. 65, no. 3, pp. 1–15, 2015.

[3] "World Health Organization. Preterm birth fact sheet.," *World Health Organization*, 2017. [Online]. Available: http://www.who.int.libaccess.lib.mcmaster.ca/mediacentre/factsheets/fs363/en/. [Accessed: 22-Dec-2017].

[4] L. Liu *et al.*, "Global, regional, and national causes of under-5 mortality in 2000–15: an updated systematic analysis with implications for the Sustainable Development Goals," *Lancet*, vol. 388, no. 10063, pp. 3027–3035, 2016.

[5] B. Bryner *et al.*, "An extracorporeal artificial placenta supports extremely premature lambs for 1 week," *J. Pediatr. Surg.*, vol. 50, no. 1, pp. 44–49, 2015.

[6] R. Ramanathan, J. J. Bhatia, K. Sekar, and F. R. Ernst, "Mortality in preterm infants with respiratory distress syndrome treated with poractant alfa, calfactant or beractant: A retrospective study," *J. Perinatol.*, vol. 33, no. 2, pp. 119–125, 2013.

[7] DE Schraufnagel, *"Respiratory Distress Syndrome of the Newborn," in Breathing in America: diseases, progress, and hope. New York: American Thoracic Society*, no. 3. 2010.

[8] N. Rochow *et al.*, "Artificial placenta -Lung assist devices for term and preterm newborns with respiratory failure," *Int J Artif Organs*, vol. 36, pp. 377–391, 2013.

[9] N. Rochow *et al.*, "An Integrated Array of Microfluidic Oxygenators as a Neonatal Lung Assist Device: In Vitro Characterization and In Vivo Demonstration," *Artif. Organs*, vol. 38, no. 10, pp. 856–866, Oct. 2014.

[10] R. J. Rodriguez, "Management of respiratory distress syndrome: an update.," *Respir. Care*, vol. 48, no. 3, pp. 279–287, Mar. 2003.

[11] K. Fletcher, R. Chapman, and S. Keene, "An overview of medical ECMO for neonates," *Semin. Perinatol.*, vol. 42, no. 2, pp. 68–79, 2018.

[12] A. Polito *et al.*, "Neurologic complications in neonates supported with extracorporeal membrane oxygenation. An analysis of ELSO registry data," *Intensive Care Med.*, vol. 39, no. 9, pp. 1594–

1601, Sep. 2013.

[13] R. de Vroege *et al.*, “Comparison of three commercially available hollow fiber oxygenators: gas transfer performance and biocompatibility,” *ASAIO J.*, vol. 47, no. 1, pp. 37–44, 2001.

[14] J. E. Palmer, “Fluid therapy in the neonate: Not your mother’s fluid space,” *Vet. Clin. North Am. - Equine Pract.*, vol. 20, no. 1, pp. 63–75, 2004.

[15] J. Brierley *et al.*, “Clinical practice parameters for hemodynamic support of pediatric and neonatal septic shock: 2007 update from the American College of Critical Care Medicine,” *Crit. Care Med.*, vol. 37, no. 2, pp. 666–688, 2009.

[16] M. C. Kung, J.-K. Lee, H. H. Kung, and L. F. Mockros, “Microchannel technologies for artificial lungs: (2) screen-filled wide rectangular channels.,” *ASAIO J.*, vol. 54, no. 4, pp. 383–389, 2008.

[17] and L. F. M. J.-K. Lee, M. C. Kung, H. H. Kung, “Microchannel Technologies for Artificial Lungs: (3) Open Rectangular Channels,” *ASAIO J. NIH Public Access*, vol. 54, no. 4, pp. 390–395, 2008.

[18] W.-I. Wu *et al.*, “Lung assist device: development of microfluidic oxygenators for preterm infants with respiratory failure.,” in *Lab on a chip*, 2013, vol. 13, no. 13, pp. 2641–50.

[19] H. Matharoo *et al.*, “STAINLESS STEEL REINFORCED COMPOSITE SILICONE MEMBRANE AND ITS INTEGRATION INTO MICROFLUIDIC OXYGENATORS FOR HIGH PERFORMANCE GAS EXCHANGE,” *Biomicrofluidics*, vol. 12, no. 1, p. 014107, 2018.

[20] A. D. Meyer *et al.*, “Hemolytic and thrombocytopathic characteristics of extracorporeal membrane oxygenation systems at simulated flow rate for neonates.,” *Pediatr. Crit. Care Med.*, vol. 13, no. 4, pp. e255-61, Jul. 2012.

[21] J. Byrnes *et al.*, “Hemolysis During Cardiac Extracorporeal Membrane Oxygenation: A Case-Control Comparison of Roller Pumps and Centrifugal Pumps in a Pediatric Population,” *ASAIO J.*, vol. 57, no. 5, pp. 456–461, Sep. 2011.

[22] A. J. Thompson, L. H. Marks, M. J. Goudie, A. Rojas-Pena, H. Handa, and J. A. Potkay, “A small-scale, rolled-membrane microfluidic artificial lung designed towards future large area manufacturing,” *Biomicrofluidics*, vol. 11, no. 2, 2017.

[23] D. M. Hoganson *et al.*, “Branched vascular network architecture: a new approach to lung assist device technology.,” *J. Thorac. Cardiovasc. Surg.*, vol. 140, no. 5, pp. 990–995, 2010.

[24] T. Kniazeva, J. C. Hsiao, J. L. Charest, and J. T. Borenstein, “A microfluidic respiratory assist device with high gas permeance for artificial lung applications,” *Biomed. Microdevices*, vol. 13, no.

2, pp. 315–323, 2011.

[25] J. A. Potkay, M. Magnetta, A. Vinson, and B. Cmolik, “Bio-inspired, efficient, artificial lung employing air as the ventilating gas.,” *Lab Chip*, vol. 11, no. 17, pp. 2901–2909, 2011.

[26] D. M. Hoganson, H. I. Pryor, E. K. Bassett, I. D. Spool, and J. P. Vacanti, “Lung assist device technology with physiologic blood flow developed on a tissue engineered scaffold platform.,” *Lab Chip*, vol. 11, no. 4, pp. 700–707, 2011.

[27] T. Kniazeva *et al.*, “Performance and scaling effects in a multilayer microfluidic extracorporeal lung oxygenation device,” *Lab Chip*, vol. 12, no. 9, pp. 1686–1695, 2012.

[28] K. M. Kovach *et al.*, “In vitro evaluation and in vivo demonstration of a biomimetic, hemocompatible, microfluidic artificial lung.,” *Lab Chip*, vol. 15, no. 5, pp. 1366–75, 2015.

[29] T. Rieper, C. Muller, and H. Reinecke, “Novel scalable and monolithically integrated extracorporeal gas exchange device,” *Biomed. Microdevices*, vol. 17, no. 5, pp. 1–10, 2015.

[30] A. A. Gimbel, E. Flores, A. Koo, G. García-Cardeña, and J. T. Borenstein, “Development of a biomimetic microfluidic oxygen transfer device,” *Lab Chip*, vol. 16, no. 17, pp. 3227–3234, 2016.

[31] K. A. Burgess, H. H. Hu, W. R. Wagner, and W. J. Federspiel, “Towards microfabricated biohybrid artificial lung modules for chronic respiratory support,” *Biomed. Microdevices*, vol. 11, no. 1, pp. 117–127, 2009.

[32] J. A. Potkay, “The promise of microfluidic artificial lungs.,” *Lab Chip*, vol. 14, no. 21, pp. 4122–4138, 2014.

[33] B. Loechel, C. Lin, G. Lee, C. Ho, and W. Hsu, “su-8 a low-cost negative resist for MEMs.pdf,” vol. 7, pp. 121–124, 1997.

[34] K. Haubert, T. Drier, and D. Beebe, “PDMS bonding by means of a portable, low-cost corona system,” *Lab Chip*, vol. 6, no. 12, pp. 1548–1549, 2006.

[35] E. P. Rivers, D. S. Ander, and D. Powell, “Central venous oxygen saturation monitoring in the critically ill patient.,” *Curr. Opin. Crit. Care*, vol. 7, no. 3, pp. 204–211, 2001.

[36] W. Tin, “Pulse oximetry, severe retinopathy, and outcome at one year in babies of less than 28 weeks gestation,” *Arch. Dis. Child. - Fetal Neonatal Ed.*, vol. 84, no. 2, pp. F106–F110, 2001.

[37] O. Siggaard-Andersen, P. D. Wimberley, N. Fogh-Andersen, and I. H. Gøthgen, “Measured and derived quantities with modern ph and blood gas equipment: Calculation algorithms with 54

equations," *Scand. J. Clin. Lab. Invest.*, vol. 48, no. S189, pp. 7–15, 1988.

[38] S. Vashisht, "Clinical governance in pain management.," *Anaesthesia*, vol. 59, no. 1, pp. 88–99, 2004.

[39] L. M. JK Lee, MC Kung, HH KUng, "Microchannel Technologies for Artificial Lungs: (3) Open Rectangular Channels," *ASAIO J. NIH Public Access*, vol. 54, no. 4, pp. 390–395, 2008.

[40] J. M. Leung, L. R. Berry, A. K. C. Chan, and J. L. Brash, "Surface modification of polydimethylsiloxane with a covalent antithrombin-heparin complex to prevent thrombosis," *J. Biomater. Sci. Polym. Ed.*, vol. 25, no. 8, pp. 786–801, 2014.

[41] J. M. Leung *et al.*, "Surface modification of poly(dimethylsiloxane) with a covalent antithrombin–heparin complex for the prevention of thrombosis: use of polydopamine as bonding agent," *J. Mater. Chem. B*, vol. 3, no. 29, pp. 6032–6036, 2015.

[42] K. M. Kovach, J. R. Capadona, A. Sen Gupta, and J. A. Potkay, "The effects of PEG-based surface modification of PDMS microchannels on long-term hemocompatibility," *J. Biomed. Mater. Res. - Part A*, vol. 102, no. 12, pp. 4195–4205, 2014.

5 Chapter 5

AN ULTRA-THIN, ALL PDMS-BASED MICROFLUIDIC LUNG ASSIST DEVICE WITH HIGH OXYGENATION CAPACITY

Complete citation:

Mohammadhossein Dabaghi, Neda Saraei, Gerhard Fusch, Niels Rochow, John L. Brash, Christoph Fusch, and P. Ravi Selvaganapathy. *"An ultra-thin, all PDMS-based microfluidic lung assist device with high oxygenation capacity."* Under review for submission.

Contribution:

My contributions include designing the experiments, planning and performing the experiments, interpretation and analysis of data and results, and writing the manuscript.

5.1 Abstract

Preterm neonates with immature lungs require a lung assist device (LAD) to maintain oxygen saturation at normal levels. Over the last decade, microfluidic blood oxygenators have attracted considerable interest due to their ability to incorporate unique biomimetic design and to oxygenate in a physiologically relevant manner. Polydimethylsiloxane (PDMS) has become the main material choice for these kinds of devices due to its high gas permeability. However, fabrication of large area ultrathin microfluidic devices that can oxygenate sufficient blood volumes at clinically relevant flow rates, entirely made of PDMS, have been difficult to achieve primarily due to failure associated with stiction of thin PDMS membranes to each other at undesired locations during assembly. Here, we demonstrate the use a modified fabrication process to produce large area ultrathin oxygenators entirely made of PDMS and robust enough to withstand the hydraulic conditions that are encountered physiologically. We also demonstrate that a LAD assembled from these ultra-thin double-sided microfluidic blood oxygenators can increase oxygen saturation level by 30 % at a flow rate of 30 mL/min and a pressure drop of 21 mm Hg in room air which is adequate for one-kg preterm neonates. In addition, we demonstrated that our LAD could withstand high blood flow rate of 150 mL/min and increase oxygen saturation by 26.7 % in enriched oxygen environment which is the highest gas exchange reported so far by any microfluidic-based blood oxygenators. Such performance makes this LAD suitable to provide support to one kg neonate suffering from respiratory distress syndrome (RDS).

5.2 Introduction

Mechanical ventilation and extracorporeal membrane oxygenation (ECMO) are the two main options to provide additional oxygenation for preterm neonates with RDS. Both methods are invasive and lead to long-term complications such as bronchopulmonary dysplasia[1], [2]. In the first method, positive applied pressure in mechanical ventilation can cause damage to the baby's fragile lung tissues. Alternatively, current ECMO devices require a high blood volume to be primed (usually more than 20 mL),external pump and oxygen supply[3]. An external pump could damage red blood cells and therefore lead to hemolysis[4], [5]. Moreover, using oxygen as a sweep gas can limit the device portability. Therefore, a pump-less device, capable of being operated solely by the baby's heart (20 - 60 mmHg) and with ability of oxygenation in ambient air would be the best solution to minimize post-treatment side effects[3], [5], [6] (such a concept is known as an artificial placenta). Over the last years, several microfluidic-based devices have been introduced for blood oxygenation[5], [7]–[21], but only few of them[5], [11], [12], [20] could be operated without any pump and have sufficient gas exchange capability in room air.

Fabrication of microfluidic blood oxygenators with double-sided gas exchange [12], [21] have led to promising improvement in performance lately. Two different approaches have been taken to fabricate such oxygenators, namely: 1) use of gas perfusion channels on each side of the microfluidic blood network microchannels which provide mechanical support during operation[21] or 2) use of a stiffer material such as stainless-steel mesh to reinforce the PDMS gas exchange membrane[12] such that they could be directly exposed to the ambient atmosphere[4]. The first approach needs an external gas supply and pumps to perfuse the gases which is not desired, while the second approach reduces the effective gas exchange surface area due to the reinforcement that does not have the same permeation characteristics as PDMS. The reinforcement helps maintain the integrity of the gas exchange membrane both during fabrication as well as operation and makes the device more reliable. Nevertheless, gas exchange efficiency can be considerably improved if the reinforcement were eliminated. It would be ideal to reliably fabricate large area, all PDMS, thin microfluidic device with gas exchange membrane on two sides

that could be sufficient to provide the oxygenation capacity for one kg neonate while still reliably operating under physiological conditions. In this paper, we have adapted a technique to form conformal slippery surfaces [22]–[27] to coat the molds in order to form and release large area ultra-thin PDMS layers embedded with microfluidic channel network. Using this method, we demonstrate the manufacture of a free standing double-sided single oxygenator unit (dsSOU) with a large surface area of 62.56 cm^2.Subsequently, we assembled 8 dsSOUs together as a LAD with minimum connectors and two flow distributors with biomimetic design. Consequently, this LAD showed a high gas exchange capacity, even in room air which meets the minimum requirements for one-kg preterm neonates. The experimental results demonstrated that this configuration is well suited for passive pumpless operation for artificial placenta type application in room air or oxygen-enriched environment.

5.3 Methods

5.3.1 Design of dsSOU

The design for the dsSOUs consisted of the blood vascular network which is a layer of interconnected microchannels made by two thin non-porous PDMS membranes as shown in Figure 5.1.a. The top and the bottom membranes had a thickness of 120 and 30 µm, respectively. The blood vascular network was square-shaped with a length of 91 mm (Figure 5.1.b) and a height of 160 µm (determined to be optimal for pumpless operation by numerical simulation described in supplementary section - Supplementary Figure. 1.1.a). An array of pillars with a dimension of 1 × 1 mm was placed (a spacing of 1 mm) inside the chamber to support the large area membranes, holding them apart (Figure 5.1.b) and thus forming the microchannel network. The pillar dimension and channel height were optimized in such a way to achieve a uniform velocity profile, low pressure drop, and low shear stress as demonstrated in Supplementary Figure 1.1.b, c, and d. The thickness of the top membrane was optimized to provide sufficient structural strength for handling the device and to minimize membrane deflection while the bottom membrane was optimized for high gas exchange which resulted in the different thicknesses chosen.

As pressure drop is one of the key factors for designing an artificial placenta-type oxygenator[12], we developed a new inlet configuration (Figure 5.1) for our devices to ameliorate the loss of pressure and shear stress generated at these locations. Inlets perpendicular to the microfluidic layer is typically used in many oxygenator designs as it is convenient and simple to fabricate. However, this particular type of access results in a significant redirection of blood which can introduce a large pressure drop. To address this issue, a tapered inlet configuration was designed which provided an access to the blood vascular network from the side of the blood channels. Moreover, a numerical simulation was performed to study the impact of the new inlet configuration on shear stress and pressure drop using the model which shows significant reduction in pressure drops and shear stress (explained in supplementary, Supplementary Figure 1.1.e and f).

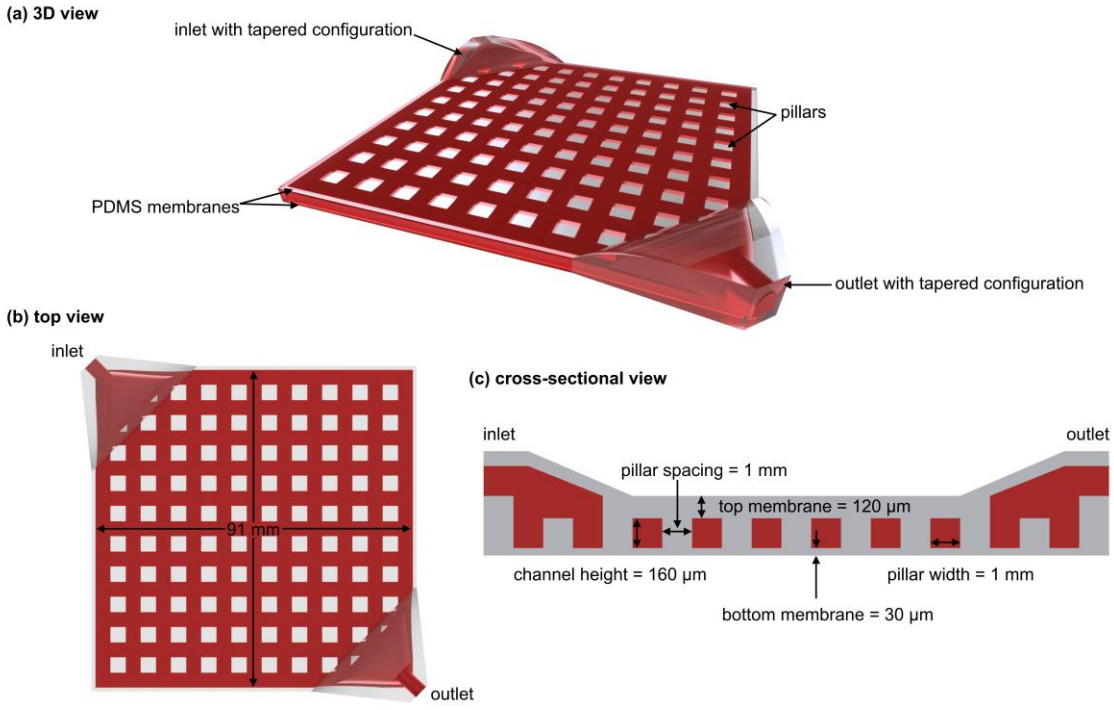

Figure 5.1: (a) 3D schematic drawing of dsSOU with tapered inlet configuration, (b) top view of dsSOU and (c) the cross-sectional view of the device.

5.3.2 Mold fabrication and coating

The negative mold for the blood vascular network was fabricated by the conventional photolithography using SU8 (3035, MicroChem). Chemical vapor deposition (CVD) methods was used to coat a thin and uniform layer of a silane-based compound on a silicon-mold to reduce stickiness of PDMS to the mold. First, the microfabricated mold was soaked in acetone for a minute (Figure 5.2.a) following by soaking in isopropanol for another minute (Figure 5.2.b) and then rinsing with DI water (Figure 5.2.c). Then, it was dried with compressed air and placed on a hot-plate at 150 °C for 15 minutes (Figure 5.2.d). Next, it was exposed to oxygen plasma (900 mTorr, Harrick Plasma cleaner) for 2 minutes to activate its surface (Figure 5.2.e). Then, it was placed under a desiccator besides a petri-dish containing a piece of kimwipe tissue which was wetted with 200 µL of trichloro (1H,1H,2H,2H-perfluorooctyl) silane (Sigma Aldrich) vacuumed to ~ 50 mm Hg (Figure 5.2.f). After 1 hour, it was taken out and placed on a hot plate at 100 °C for 3 hours to let unbonded silane molecules evaporate (Figure 5.2.g). As a result, a uniform perfluoro-silane was coated on the mold which resulted in increasing the hydrophobicity of the surface to ~ 115 ° from 28 ° (shown in supplementary, Supplementary Figure. 1.2).

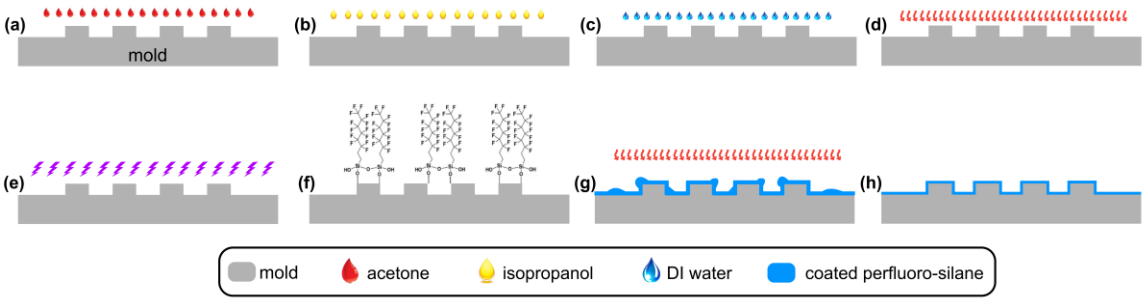

Figure 5.2: Coating process for trichloro (1H 1H 2H 2H-perfluorooctyl) silane on the mold by CVD.

5.3.3 Device fabrication process

To produce an ultra-thin PDMS-based microfluidic blood oxygenator with double-sided microchannels, we modified our pervious device fabrication technique[4], [12]. PDMS monomer and its curing agent was mixed with a ratio of 10:1 and desiccated to remove all

air bubbles. PDMS was spin coated on top of the mold at a speed of 850 RPM for a minute and placed under a desiccator to removed air-trapped inside hollow pillars' features in the mold (Figure 5.3.a).

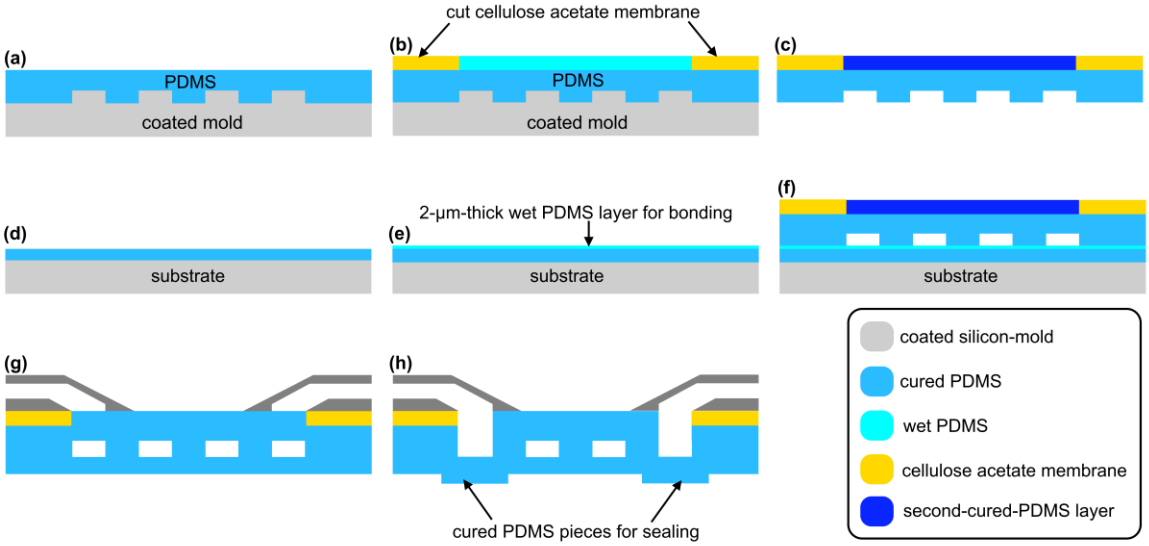

Figure 5.3: Fabrication process for dsSOU with tapered inlet configuration: a) spin coating of first PDMS layer and its cure, b) spin coating an additional thin PDMS layer and embedding cellulose acetate membrane, c) cure of additional layer and peeling from the mold, d) spin coating of the bottom PDMS membrane layer and its cure, e) spin coating of a thin adhesive layer, f) Integration of the bottom membrane with the top channel, (g) placement of inlet and outlet using half-cured PDMS, and (h) removal of residual PDMS and sealing the bottom side of each inlet/outlet.

It should be noted that this step was repeated few times till all hollow pillars' features in the mold filled with PDMS. An additional PDMS layer was spin coated at 1500 RPM for a minute and a frame of cellulose acetate membrane (to provide an annular support) was embedded into wet PDMS (Figure 5.3.b). It was placed on a hot-plate at 85 °C for 30 minutes to cure PDMS and the membrane was peeled off from the mold (Figure 5.3.c). In a next step, the bottom PDMS membrane was fabricated by spin coating PDMS on a substrate with a speed of 2000 RPM for a minute and was cured in an oven at 85 °C for 15 minutes (Figure 5.3.d). An additional thin layer of PDMS (a thickness of ~ 2 µm) was spin coated on the cured PDMS membrane at a speed of 8000 RPM for a minute (Figure 5.3.e) to function as an adhesive layer. The blood vascular network and PDMS membrane were brought in contact and left at room temperature overnight (Figure 5.3.f). Overnight

curing let PDMS diffuse to both sides and formed a very strong bonding. Pre-manufactured, PDMS-made inlets with a tapered configuration were placed on two opposite corners using wet PDMS as a glue (Figure 5.3.g). Residual PDMS was removed from the other side to open the inlet by a scalpel and a biopsy punch and two 1-mm-thick pieces of cured PDMS were used to seal the other sides (Figure 5.3.h).

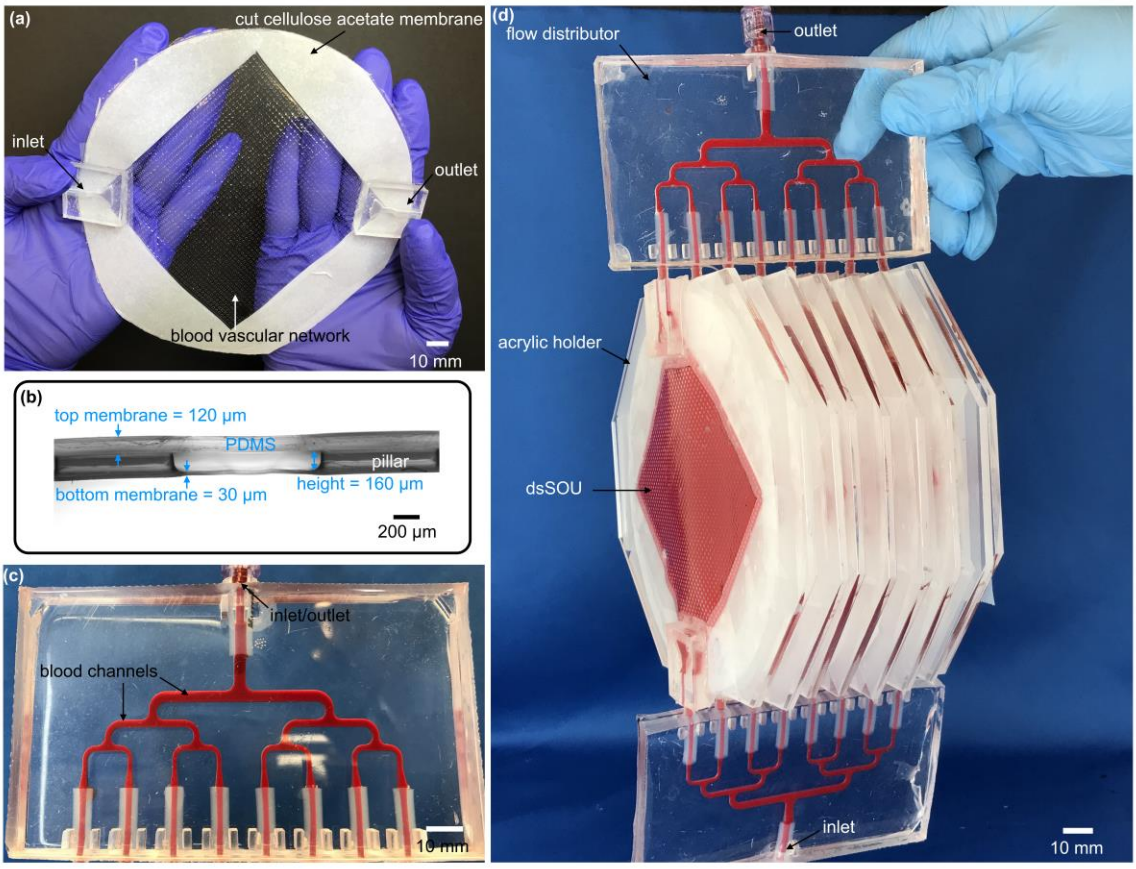

Figure 5.4: (a) an image of dsSOU with tapered inlet and outlet configuration, (b) a microscopic image cross-sectional view of the device, (c) the flow distributor filled with bovine blood, (d) the assembled LAD with 8 dsSOUs and two flow distributors which is filled with bovine blood.

The fabricated device with tapered inlet/outlet configuration is shown in Figure 5.4.a. This configuration spreads out the incoming blood into a larger area of the thin blood vascular network and hence produces a much smaller pressure drop and significantly smaller shear stress. In addition, its transparency can also be used to monitor any potential clot formation that may occur at this region. The cross-section of one of the

microchannels is shown in Figure 5.4.b in which the top and bottom membranes (thickness of 120 and 30 µm) can been seen clearly.

Burst pressure testing was performed on individual oxygenators to ensure that the bonding and PDMS membranes were strong enough. The fabricated oxygenators were found to withstand the operating pressure of 20-60 mm Hg easily and no failure was observed below 300 mm Hg. The process and the burst pressure results are shown in Supplementary Figure 1.3 in the supplementary section.

5.3.4 Design Criteria for LAD and its Assembly

It should be noted that our LAD (an artificial placenta-type blood oxygenator) is designed for a parallel arterio-venous connection to the human circulatory system as opposed to conventional ECMO devices that are designed for a venous-artery or venous-venous configuration [28]. Therefore, in our configuration, blood entering the LAD is already partially-oxygenated by the lung (arterial blood). As a result, our LAD is expected to operate at the upper end of the oxygen binding curve of haemoglobin compared to current ECMO devices and a typical increase in oxygen saturation by 30% would be sufficient to fully saturate the incoming blood[29]. In addition, the priming volume of the LAD should be low enough so that no blood transfusion is needed. To avoid cardiac output failure because of excessive bypass blood flow to the systemic circulation, the LAD should not be operated at very high blood flow rates. Consequently, blood flow rates should range from 20 to 30 mL min^{-1} kg^{-1} of a baby[3], [12],[29,30]. Therefore, LADs were tested with incoming blood saturation levels well below 70% (typically ~55%) in order to determine the full capacity of the oxygenator in increasing the saturation level at various operational flow rates.

In the construction of the LAD, eight dsSOUs were attached in parallel to meet the design criteria and to meet the estimated gas exchange needs of a preterm neonate weighing up to two kg. A parallel configuration was chosen here to increase the overall gas exchange capacity by operating the LAD at higher blood flow without making any discernible impact on the pressure drop or the oxygenation characteristics of devices. Flow

distributors could provide symmetrical and biomimetic flow paths to blood without any damage to red blood cells (the hematocrit was measured before and after and did not change during the experiment). The branching channel design uses the Murray's Law[32] which ensures a gentle flow distribution among channels without producing high pressure drop and shear stress and damaging red blood cells. To fabricate this flow distributor, the flow distributor was cast out of a 3D-printed mold (Formlab Form 2) and bonded to a cured PDMS using flame-activation technique[33] as depicted in Figure 5.4.c. Numerical simulations were performed to investigate the flow distribution uniformity, pressure drop and shear stress profiles inside the flow distributors as seen in Supplementary Figure. 1.3.g, h, and i in supplementary. These results illustrate that the flow distributors had a uniform velocity profile, a low pressure drop of ~ 2 mm Hg at a blood flow rate of 60 mL/min, and a maximum shear stress of ~ 6 Pa at the same blood flow rate. Attaching the dsSOUs to the flow distributors by connectors, the LAD was ready to test (Figure 5.4.d). First, the LAD was perfused with normal saline solution and ran for 1 hour to ensure that no device had a leakage.

5.3.5 Experimental Setup for Gas Exchange Testing with Blood

Bovine blood (Bovine blood, sterile Citrated, CL1700-1000C) was purchased from Cedarlane and heparinized (3 units/mL). To be able to simulate partially saturated arterial blood conditions in the natural lungs, the oxygen saturation (SaO_2) level in blood was adjusted using a hollow fiber membrane oxygenator (PDMSXA-1.0, PermSelect®, Ann Arbor, MI, USA) which was supplied by a carbon dioxide/nitrogen gas mixture (5%/95% v/v) in the fibers at 20 L h^{-1}. The blood was circulated with a flow of 15 – 25 mL min^{-1} through the oxygenator to reduce the oxygen saturation level to around 55 ± 5 %. Once, the blood had reached the desired SaO_2, it was transferred to a bottle with a sealed lid and was stored in a fridge overnight to reduce the oxygen consumption by red blood cells (RBC) and achieve equilibrium.

The experimental set-up is shown in supplementary (Supplementary Figure. 1.4). A TruWave Pressure Transducer (Edwards Lifesciences LLC, Irvine, CA, USA) and a

Spacelabs 90369 Patient Monitor (SpaceLabs Medical, Inc., Redmond, WA, USA) were used to report the pressure drop during the experiment by installing the pressure transducer before the LAD. A point-of-care blood gas analyzer (GEM Premier 3000, Instrumentation Laboratory, Lexington, MA, USA) was used in this study to measure blood properties before and after the device to evaluate the gas exchanges by the device. In addition, a Complete MicroHematocrit System (StatSpin CritSpin, Norwood, MA, USA) was used to measure the hematocrit level. To calculate the total content of oxygen in the blood, the amount of dissolved oxygen and the hemoglobin-bound oxygen were measured and summed[20]. For testing in room air, the LAD was exposed directly to ambient without any manifolds and the gas exchange measurements were done. For testing in an enriched oxygen environment at atmospheric pressure, the LAD was placed inside a Ziploc® bag and the bag was perfused with oxygen at a flow of 20 L/hr (the bag was not fully sealed to let excess gases leave the bag).

5.4 Results and Discussion

The performance of the LAD was assessed with bovine blood at blood flow rates between 10 to 60 mL/min in room air and 30 to 150 mL/min in an enriched oxygen environment. The pressure drop of the LADs were also measured at various flow rates from 10 to 150 mL/min in two configurations: 1) only for the LAD and 2) the LAD with the extracorporeal circuit (the extracorporeal circuit includes all tubes before and after the LAD and all connectors used in the line) as shown in Figure 5.5.a and b. The increase in pressure drop with flow rates was found to be linear as expected and was within the operating pressure drop range (20–60mmHg, the gray box depicted in Figure 5.5.a and b) for blood flow rates below 60 mL/min, which satisfies the conditions for pumpless operation of an artificial placenta-type oxygenator[12] while meeting the flow rates needed to support a 2 kg neonate.

Figure 5.5.c shows the oxygen saturation level (SaO_2) in blood before and after the LAD at different blood flow rates in room air.

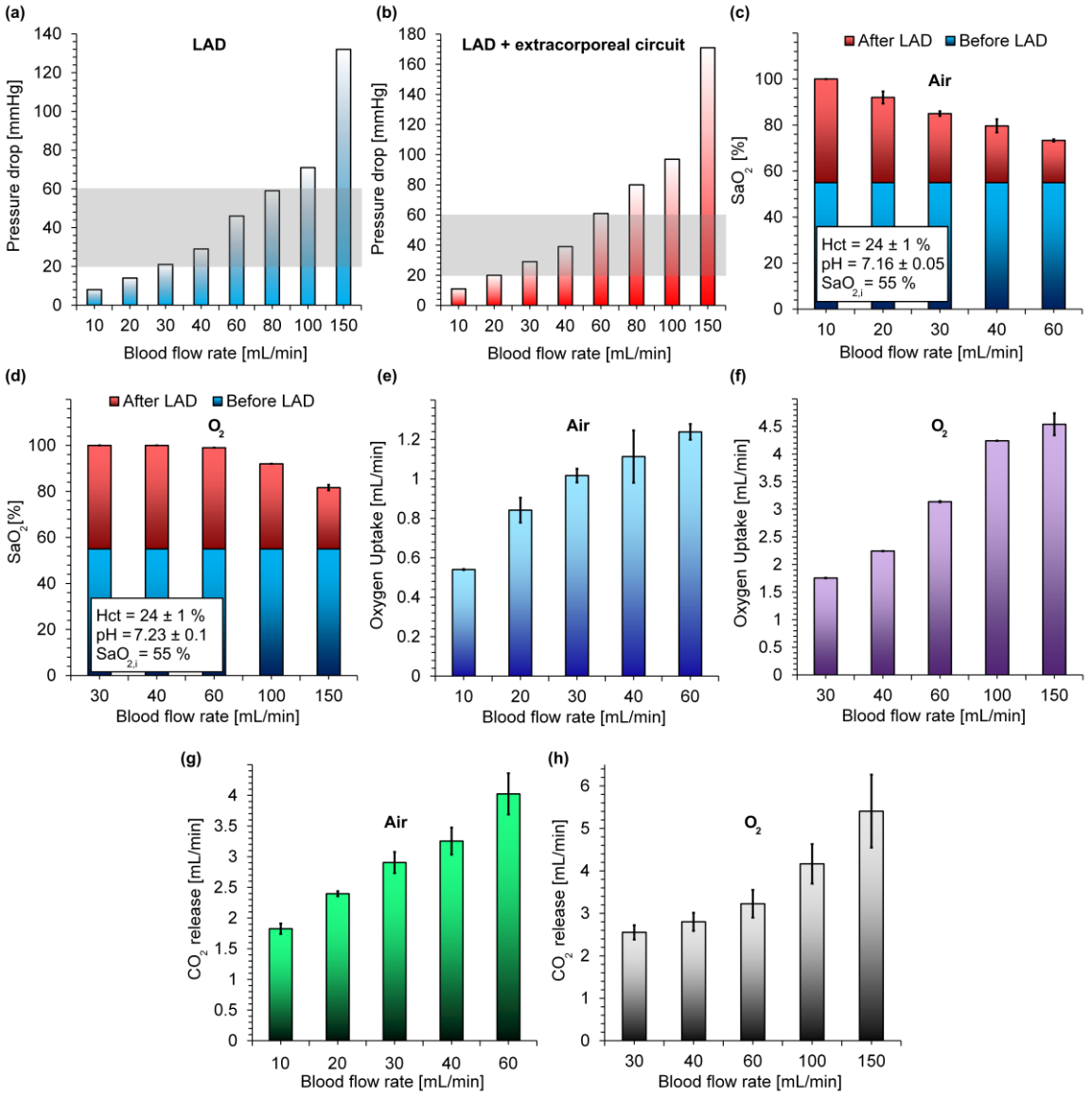

Figure 5.5: In vitro performance of the LAD: (a) pressure drops of the LAD at various blood flow rates, (b) the pressure drop of the LAD plus the extracorporeal circuit at various blood flow rates, (c) oxygen saturation level before and after the LAD in room air oxygen at various blood flow rates, (d) oxygen saturation level before and after the LAD in an enriched oxygen environment at various blood flow rates,(e) oxygen uptake of the LAD in room air at various blood flow rates, (f) oxygen uptake of the LAD in an enriched oxygen environment at various blood flow rates, (g)CO_2 release of the LAD in room air at various blood flow rates, and (h) CO_2 release of the LAD in an enriched oxygen environment at various blood flow rates. Data represents the mean ± SD, n = 3.

The results showed that the oxygen saturation level of blood can be increased by 45 to 30% when the blood flow rate is between 10 to 30 mL/min. The level of saturation achieved is inversely correlated to the blood flow rate due to the fact that blood had

smaller residence time in the LAD, and the red blood cells have a lower chance to adsorb oxygen molecules. In particular, the LAD was able to increase the oxygen saturation level by 30 % at a blood flow rate of 30 mL/min and a low pressure drop of 21 mm Hg (29 mm Hg, including the extracorporeal circuit) which would satisfy the oxygenation need of a one-kg preterm neonates with RDS[5], [12], [20]. In the case when the LAD was exposed to pure oxygen, it fully oxygenated blood (~ 100 %) from 55% up to a flow rate of 60 mL/min as shown in Figure 5.5.d. This level of increase in oxygen saturation level would be sufficient to support preterm neonates with RDS up to 2 kg in an artificial placenta format. It should be noted that, the LAD could achieve an oxygen saturation level of 92 % (an increase in saturation of 37%) even at a blood flow rate of 100 mL/min. These results suggest that this LAD configuration can support preterm neonates with various weights up to 2 kg with an oxygen ambient. The oxygen uptake in both conditions (room air and enriched oxygen environment) increased with blood flow rate even up to 150 mL/min as more oxygen was carried by blood passing the LAD as shown in Figure 5.5.e and f. For example, the oxygen uptake of the LAD at a blood flow rate of 30 mL/min was 1.01and 1.75 mL/min in room air and oxygen, respectively. As the blood used in this experiment had low hematocrit content (as compared to that in neonate's blood), the calculated oxygen transfer underestimates the amount that would be transferred under similar conditions when a neonate’s blood (with higher hematocrit) were used.

In addition, the carbon dioxide release that was calculated also increased with blood flowrates in both conditions as shown in Figure 5.5.g and h. This behaviour could be attributed to the decrease in the thickness of boundary layer close to both membranes at higher blood flow rates and to the increase in the total volume of CO_2 containing flowing across the membrane. Moreover, exposing the LAD to pure oxygen as compared to air did not have a significant effect on CO_2 release which is typical of many blood oxygenators. For instance, the CO_2 release of the LAD was 2.9 ± 0.17 mL/min and 2.55 ± 0.16 mL/min at a typical blood flow rate of 30 mL/min for an artificial placenta type oxygenator.

Previous artificial placenta type microfluidic-based oxygenator[12] have reported oxygen uptake of up to 2.86 mL/min (with a corresponding oxygen saturation level increased from 57 % to 93 %) at a blood flow rate of 60 mL/min using pure oxygen as the ambient environment. In comparison, the new LAD in this work could achieve an oxygen uptake of 3.14 mL/min (raised oxygen saturation level from 55 % to 99 %) at the same blood flow rate but at a lower pressure drop (decreased by 13 %). To be able to compare other microfluidic blood oxygenators[4], [5], [13], [18] with the LAD developed in this study, their performance at a blood flow rate of ~ 30 mL/min (which is required for a one-kg preterm [5], [12]) was determined and reported in Table 5.1. An ideal device should increase oxygen saturation level by ~ 30 % at a maximum pressure drop of ~ 30 mm Hg and a minimum blood flow rate of 30 mL min^{-1} in room air[5], [12], [20]. On this basis, the number of required single oxygenator units, total gas exchange surface area, priming volume, increase in oxygen saturation level, oxygen transfer, and blood flow rate has been calculated. The LAD in this study, achieves the highest increase in saturation (45%) with the lowest pressure drop (21 mm Hg) among all designs with oxygen as the exchange gas.

Table 5.1: Comparison between this work and previous microfluidic blood oxygenator. All devices have been scaled to meet the requirement of an artificial placenta type oxygenator in a pumpless manner (having a pressure drop of ~ 30 mm Hg). Number of single oxygenator units required to make an artificial placenta type oxygenator is represented as N_t. Priming volume for only single oxygenator units and the total priming volume are shown by PV_o and PV_t, respectively.

Source	H [µm]	N_t	Surface area [cm^2]	PV_o [mL]	PV_t [mL]	ΔSaO_2 [%]	O_2 transfer [mL/min]	Blood flow [mL/min]	ΔP [mmHg]	Gas
Hoganson[18] 2011	100	5	115	N/A	N/A	N/A	0.48	31.5	20	O_2
Rochow[5] 2014	80	20	305	2.5	10	N/A	1.04	30	32	O_2
	80	20	305	2.5	10	N/A	0.61	30	32	Air
Dabaghi[12] 2018	200	4	250	5	8	42	1.96	30	30	O_2
Thompson[13] 2018	30	6	189	2.8	N/A	38	1.13	30	33	O_2
Dabaghi[4] 2018	160	3	300	3	N/A	40	1.89	30	30	O_2
This LAD	160	8	800	8	12.5	30	1.01	30	21	Air
	160	8	800	8	12.5	45	1.8	30	21	O_2
	160	8	800	8	12.5	45	2.24	40	29	O_2

Even using air as the exchange gas, it is able to demonstrate superior performance and achieves 30% increase in saturation at the lowest pressure drop of 21 mm Hg. Finally, the new LAD could achieve an oxygen transfer of 2.24 mL min^{-1} at a pressure drop of ~ 30 mm Hg which is the highest among the listed devices in Table 5.1 operating in conditions to support a 1-kg neonate in the artificial placenta format.

5.5 Conclusion

In this paper, a LAD with eight microfluidic double-sided blood oxygenators was introduced which was capable of supporting higher blood flow rates with minimizing the priming volume of blood by using less connectors compared to other microfluidic blood oxygenators for preterm neonates with RDS. The device was made of two thin PDMS membranes on the top and the bottom of the blood flow path and had a high surface area for gas exchange. Use of perfluoro silane coating allowed the fabrication of an ultra-thin PDMS-based microfluidic device for oxygenation purposes with high reliability. Gas exchange properties of this LAD was found to be better than other microfluidic-based oxygenators and were sufficient for preterm neonates. In the LAD construction, a biomimetic approach was taken to enhance the blood distribution and eliminate introducing dead zones and high shear stress regions. This LAD had a low priming volume of 12.5 mL and could provide a maximum oxygen transfer of 1.24 mL/min in room air and 4.54 mL/min using pure oxygen as ventilation gas. This LAD meets all design parameters of an artificial placenta-type device by having low priming volume, capable of being operated without the need of a pump, and capable of sufficient gas transfer in room air to support one kg neonate in the artificial placenta configuration.

References

[1] R. J. Rodriguez, "Management of respiratory distress syndrome: an update.," *Respir. Care*, vol. 48, no. 3, pp. 279–287, Mar. 2003.

[2] K. Fletcher, R. Chapman, and S. Keene, "An overview of medical ECMO for neonates," *Semin. Perinatol.*, pp. 1–12, 2018.

[3] N. Rochow *et al.*, "Artificial placenta -Lung assist devices for term and preterm newborns with respiratory failure," *Int J Artif Organs*, vol. 36, pp. 377–391, 2013.

[4] M. Dabaghi *et al.*, "An Ultra-thin Highly Flexible Microfluidic Device for Blood Oxygenation," *Lab Chip*, vol. 18, no. 24, pp. 3780–3789, 2018.

[5] N. Rochow *et al.*, "An integrated array of microfluidic oxygenators as a neonatal lung assist device: In vitro characterization and in vivo demonstration," *Artif. Organs*, vol. 38, no. 10, pp. 856–866, 2014.

[6] J. Peng *et al.*, "Postnatal dilatation of umbilical cord vessels and its impact on wall integrity: Prerequisite for the artificial placenta," *Int. J. Artif. Organs*, vol. 41, no. 7, pp. 393–399, Jul. 2018.

[7] L. M. JK Lee, MC Kung, HH KUng, "Microchannel Technologies for Artificial Lungs: (3) Open Rectangular Channels," *ASAIO J. NIH Public Access*, vol. 54, no. 4, pp. 390–395, 2008.

[8] K. M. Kovach *et al.*, "In vitro evaluation and in vivo demonstration of a biomimetic, hemocompatible, microfluidic artificial lung.," *Lab Chip*, vol. 15, no. 5, pp. 1366–75, 2015.

[9] A. A. Gimbel, E. Flores, A. Koo, G. García-Cardeña, and J. T. Borenstein, "Development of a biomimetic microfluidic oxygen transfer device," *Lab Chip*, vol. 16, no. 17, pp. 3227–3234, 2016.

[10] A. J. Thompson, L. H. Marks, M. J. Goudie, A. Rojas-Pena, H. Handa, and J. A. Potkay, "A small-scale, rolled-membrane microfluidic artificial lung designed towards future large area manufacturing," *Biomicrofluidics*, vol. 11, no. 2, 2017.

[11] H. Matharoo *et al.*, "Steel reinforced composite silicone membranes and its integration to microfluidic oxygenators for high performance gas exchange," *Biomicrofluidics*, vol. 12, no. 1, 2018.

[12] M. Dabaghi *et al.*, "An artificial placenta type microfluidic blood oxygenator with double-sided gas transfer microchannels and its integration as a neonatal lung assist device," *Biomicrofluidics*, vol. 12, no. 3, 2018.

[13] A. J. Thompson, L. J. Ma, T. J. Plegue, and J. A. Potkay, "Design Analysis and Optimization of a Single Layer PDMS Microfluidic Artificial Lung," *Trans. Biomed. Eng.*, 2018.

[14] K. A. Burgess, H. H. Hu, W. R. Wagner, and W. J. Federspiel, "Towards microfabricated biohybrid artificial lung modules for chronic respiratory support," *Biomed. Microdevices*, vol. 11, no. 1, pp. 117–127, 2009.

[15] D. M. Hoganson *et al.*, "Branched vascular network architecture: a new approach to lung assist device technology.," *J. Thorac. Cardiovasc. Surg.*, vol. 140, no. 5, pp. 990–995, 2010.

[16] J. A. Potkay, M. Magnetta, A. Vinson, and B. Cmolik, "Bio-inspired, efficient, artificial lung employing air as the ventilating gas.," *Lab Chip*, vol. 11, no. 17, pp. 2901–2909, 2011.

[17] T. Kniazeva, J. C. Hsiao, J. L. Charest, and J. T. Borenstein, "A microfluidic respiratory assist device with high gas permeance for artificial lung applications," *Biomed. Microdevices*, vol. 13, no. 2, pp. 315–323, 2011.

[18] D. M. Hoganson, H. I. Pryor, E. K. Bassett, I. D. Spool, and J. P. Vacanti, "Lung assist device technology with physiologic blood flow developed on a tissue engineered scaffold platform.," *Lab Chip*, vol. 11, no. 4, pp. 700–707, 2011.

[19] T. Kniazeva *et al.*, "Performance and scaling effects in a multilayer microfluidic extracorporeal lung oxygenation device," *Lab Chip*, vol. 12, no. 9, pp. 1686–1695, 2012.

[20] W.-I. Wu *et al.*, "Lung assist device: development of microfluidic oxygenators for preterm infants with respiratory failure," *Lab Chip*, vol. 13, no. 13, p. 2641, 2013.

[21] T. Rieper, C. Muller, and H. Reinecke, "Novel scalable and monolithically integrated extracorporeal gas exchange device," *Biomed. Microdevices*, vol. 17, no. 5, pp. 1–10, 2015.

[22] A. Tuteja, W. Choi, J. M. Mabry, G. H. Mckinley, and R. E. Cohen, "Robust omniphobic surfaces," vol. 2008, 2008.

[23] X. Li, D. Reinhoudt, and M. Crego-calama, "What do we need for a superhydrophobic surface ? A review on the recent progress in the preparation of superhydrophobic surfaces," no. 1995, 2007.

[24] D. C. Leslie *et al.*, "A bioinspired omniphobic surface coating on medical devices prevents thrombosis and biofouling," *Nat. Biotechnol.*, vol. 32, no. 11, pp. 1134–1140, 2014.

[25] A. K. Epstein, T. Wong, R. A. Belisle, E. Marie, and J. Aizenberg, "Liquid-infused structured surfaces with exceptional anti-biofouling performance," vol. 109, no. 33, 2012.

[26] M. Villegas, Z. Cetinic, A. Shakeri, and T. F. Didar, "Analytica Chimica Acta Fabricating smooth PDMS micro fl uidic channels from low-resolution 3D printed molds using an omniphobic lubricant-infused coating," *Anal. Chim. Acta*, vol. 1000, pp. 248–255, 2018.

[27] T. Wong *et al.*, "Bioinspired self-repairing slippery surfaces with pressure-stable omniphobicity," *Nature*, vol. 477, no. 7365, pp. 443–447, 2011.

[28] E. P. Rivers, D. S. Ander, and D. Powell, "Central venous oxygen saturation monitoring in the critically ill patient.," *Curr. Opin. Crit. Care*, vol. 7, no. 3, pp. 204–211, 2001.

[29] W. Tin, "Pulse oximetry, severe retinopathy, and outcome at one year in babies of less than 28 weeks gestation," *Arch. Dis. Child. - Fetal Neonatal Ed.*, vol. 84, no. 2, pp. F106–F110, 2001.

[30] W.-I. Wu *et al.*, "Lung assist device: development of microfluidic oxygenators for preterm infants with respiratory failure.," in *Lab on a chip*, 2013, vol. 13, no. 13, pp. 2641–50.

[31] N. Rochow *et al.*, "An Integrated Array of Microfluidic Oxygenators as a Neonatal Lung Assist Device: In Vitro Characterization and In Vivo Demonstration," *Artif. Organs*, vol. 38, no. 10, pp. 856–866, Oct. 2014.

[32] C. D. Murray, "The Physiological Principle of Minimum Work: I. The Vascular System and the Cost of Blood Volume.," *Proc. Natl. Acad. Sci. U. S. A.*, vol. 12, no. 3, pp. 207–14, Mar. 1926.

[33] R. Ghaemi, M. Dabaghi, R. Attalla, A. Shahid, H.-H. Hsu, and P. R. Selvaganapathy, "Use of flame activation of surfaces to bond PDMS to variety of substrates for fabrication of multimaterial microchannels," *J. Micromechanics Microengineering*, vol. 28, no. 8, p. 087001, Aug. 2018.

6 Chapter 6

AN ULTRA-THIN HIGHLY FLEXIBLE MICROFLUIDIC DEVICE FOR BLOOD OXYGENATION

Complete citation:

Mohammadhossein Dabaghi, Neda Saraei, Gerhard Fusch, Niels Rochow, John L. Brash, Christoph Fusch, and P. Ravi Selvaganapathy. *"An Ultra-thin Highly Flexible Microfluidic Device for Blood Oxygenation."* Lab on a Chip 18, no. 24 (2018): 3780 – 3789.

Copyright:

Contribution:

My contributions include designing the experiments, planning and performing the experiments, interpretation and analysis of data and results, and writing the manuscript.

6.1 Abstract

Many neonates who are born premature suffer from respiratory distress syndrome (RDS) for which mechanical ventilation and extracorporeal membrane oxygenation (ECMO) device are used in treatment. However, the use of these invasive techniques results in higher risk of complications like bronchopulmonary dysplasia or require surgery to gain vascular access. An alternative biomimetic approach is to use the umbilical cord as a vascular access and to connect a passive device to the baby that functions like a placenta. This concept, known as the artificial placenta, provides enough oxygenation and causes minimal distress or complications. Herein, we have developed a new artificial placenta-type microfluidic blood oxygenator (APMBO) with high gas exchange, low priming volume and low hydraulic resistance such that it can be operated only by pressure differential provided by a baby's heart. Mimicking the placenta, we have made our new device ultra-thin and flexible so that it can be folded in a desired shape without losing its capability for gas exchange and achieve a compact form factor. The ability to fold allowed optimization of connectors and reduced the overall priming volume to sub-milliliter while achieving a high oxygen uptake which would be sufficient for preterm neonates with birth-weight around 0.5 kg.

6.2 Introduction

Low birth-weight neonates with respiratory distress syndrome (RDS) need external support such as mechanical ventilation to meet their oxygenation needs. Mechanical ventilation can cause long-term complications such as bronchopulmonary dysplasia[1], [2]. Under severe respiratory failure, extracorporeal membrane oxygenation (ECMO) can be used to provide sufficient oxygen uptake and carbon dioxide removal. Nonetheless, current ECMO devices have high priming volume (>20 mL), most of them need external pump and therefore are not suited for preterm and term neonates (<2 kg)[3]. A passive device pumped solely by the baby's heart (20 - 60 mmHg) and capable of oxygenating in ambient air would be ideal (a concept termed as the artificial placenta (AP)) [3]. Over the past decade, several microfluidic oxygenators have been developed[4]–[28], but only few of them[4], [5], [26] could be perfused solely by the pressure differential of a baby's heart or work in air ambient.

The development of microfabrication methods for blood oxygenators led to the design of gas exchange micro channels with dimensions comparable to capillaries in lungs[20], [29]. Consequently, promising oxygen transfer rates were achieved albeit at low blood flow rate. Over the last decade, the main focus of research has been on the scaling of the capacity of these microfabricated devices to be able to support sufficient blood flow with sufficient oxygenation. Two different approaches have been taken. The first approach is to scale up the size of the microfluidic blood oxygenators by fabricating a device which had higher surface area for gas exchange[4], [22] . Several large area single layer device that are exposed to the ambient air on both sides[4], [5], [26], [28] have been developed. However, such devices are rigid, do not have a compact form factor and can take up significant space. The second approach is to connect several smaller units together to increase the total capacity[4]–[6], [13], [22], [23], [26]. Although promising, this approach requires significant number of external interconnections that greatly increase the total priming volume of the device. Higher capacity is achieved in this approach by stacking planar (due to the intricacies of microfabrication using photolithography) oxygenator units one on top of another and establishing fluidic interconnections between

the layers[6], [9], [12], [13], [15], [16], [20], [22]–[24]. However, such stacking eliminates access of layers in the middle to the ambient air for gas exchange and necessitates integration of a channel network for perfusion of air or oxygen, further complicating the design. A biomimetic approach would be to fabricate a thin film oxygen exchange device in 2D and fold it into a compact 3D shape similar to the structure of the alveolar layers present in the lungs. However, this requires the construction of the oxygenator from flexible materials that can be bent and folded into a 3D shape.

Although flexible and stretchable microfabricated devices have been developed for applications such as flexible electronics[30]–[33] to wearable sensing[33]–[35] and soft robotics[36]–[39], they have rarely been used in microfluidics for the purposes of gas exchange. This is primarily due to complexity of fabrication as well as the ability of the device to recover the ability to perfuse and exchange gases even after significant mechanical deformation. Nevertheless, realization of flexible and foldable microfluidic device that could be employed for gas exchange can lead to development of large area yet compact oxygenators that are portable and wearable. In this paper, we describe a new ultra-thin oxygenator composed of polymer reinforced PDMS membrane that is flexible, can be folded to achieve a compact form without loss of functionality and gas exchange properties. We demonstrate three configurations that use the flexibility of the ultra-thin oxygenators to reduce the form factor and the priming volume of the ECMO unit. First, we demonstrate that a flat oxygenator (of the APMBO design) can be folded into a compact form factor easily without it leaking or rupturing. Oxygen exchange was performed to show that there is negligible difference between the flat and the curved profiles. Next, a flower shaped configuration that consists of four of the APMBO units with a common inlet is demonstrated. This design was used to demonstrate that several oxygenators units could be integrated with a single inlet thereby reducing the overall priming volume and the foldability of the oxygenator is a key element that enables this to occur. Finally, a larger size of the APMBO unit was used and rolled in such a way that the inlet and the outlet are adjacent to each other. This way the external interconnects to the oxygenator are minimized and the total priming volume reduced. In almost all the

other oxygenators, the inlet and the outlet are placed far apart and the connectors that link the oxygenator to the vasculature carry a significant priming volume. This configuration uses the foldability of this oxygenator elegantly to significantly reduce this volume and address this issue. We show that these configurations minimize the priming volume required for the connectors and reduce it significantly as compared to other such configurations.

6.3 Materials and Design

6.3.1 Microfluidic device design and characterization

The artificial placenta-type microfluidic blood oxygenator (APMBO) was designed to supplement the gas exchange already occurring in underdeveloped lungs of the neonate [3]. The device (Figure 6.1.a) consisted of two nonporous gas-permeable membranes that sandwich a blood distribution (vascular) network, and was fabricated using modified microfabrication and soft lithography technique[4] . The blood vascular network consisted of crossing microchannels that are 1 mm in width and 130 μm in height as shown in Figure 6.1.b. This design has been optimized previously[4], [5], [28] for uniform flow distribution. A channel height of 130 μm was chosen to produce pressure drop in the operating range of 20 – 60 mm Hg over a range of applicable flow rates. The gas permeable membranes sandwiching the vascular network on the top and the bottom is held apart by 1 x 1 mm pillars[5], [28]. Gas permeable membranes are made of polydimethylsiloxane (PDMS) because its high gas permeability and biocompatibility, which allows high rate of gas transfer and porous polytetrafluoroethylene (PTFE) membranes deployed as a scaffold to reinforce PDMS. As demonstrated before[5], PDMS alone is elastic (Tensile strength of 0.8 MPa) and compliant and therefore will stretch out under the operating conditions causing poor oxygenation performance. Reinforcement using a PTFE (Tensile strength of 25 MPa) scaffold improves the mechanical stiffness considerably which can lead to improved oxygenation. Gas exchange membranes on both the sides of the vascular network have been shown previously to significantly enhance the oxygenation characteristics [5].

Porous PTFE membranes with a pore size of 1 µm (porosity of 83 % and thickness of ~35 µm) and 0.2 µm (porosity up to 90 % and thickness of ~25 µm) were used for the bottom and top membranes resulting in 110 µm-thick and 25 µm-thick composite membranes, respectively (composite membrane 1, 2) as shown in Figure 6.1.c. The optimum thickness of the membranes was chosen based on flow characterization of the fabricated oxygenators (Supplementary Figure 2.1). The blood vascular network has a surface area of 29.19 cm^2 and a height of 130 µm which corresponds to a priming volume of ~ 0.38 mL. We have recently developed a layer-by-layer soft-lithography technique[4] which is facile and scalable to fabricate large area ultra-thin microfluidic devices. Our novel fabrication technique has been adapted to integrate porous PTFE membranes as a reinforcement for ultra-thin PDMS layers which confers flexibility and foldability to the entire device as well as improving mechanical properties of the entire device (Supplementary Figures 2.3 ,2.4, and 2.5).

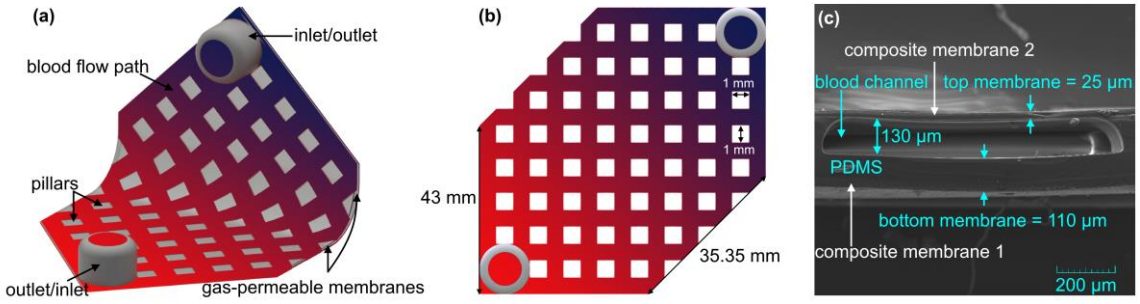

Figure 6.1: (a) schematic 3D-view of APMBO, (b) schematic top-view of APMBO, and (c) a SEM image of the cross-section of the device.

6.3.2 Fabrication process of APMBO

The fabrication process for ultra-thin flexible APMBOs is depicted in Figure 6.2. The conventional photolithography technique was used to make the negative template of the blood vascular network using SU-8 photoresist (SU-8 3035, Microchem Corp, Westborough, MA, USA). PDMS (Sylgard 184, Dow Corning, Midland, MI) with a ratio of 10:1 (the base and the curing agent) was mixed, spin-coated on the mold with the speed of 750 RPM for 60 s, and cured on a hot-plate at 85 °C (Figure 6.2.a). Then, the

second layer of PDMS was spin-coated with the speed of 2000 RPM for 40 s on the previous layer, a piece of PTFE membrane with pore size of 1 µm and a porosity of 83 % (PTU103001H, Sterlitech, Kent, WA, US) was embedded into wet PDMS and cured in an oven at 85 °C (Figure 6.2.b). The device was peeled off from the mold (Figure 6.2.c). Next, a piece of PTFE membrane with pore size 0.2 µm and a porosity of up to 90 % (PTU023001, Sterlitech, Kent, WA, US) was placed on a substrate and fully covered with PDMS for 15 minutes to let PDMS diffuse through pores (Figure 6.2.d). Subsequently, the PDMS was spun with the speed of 8000 RPM for 60 s to form a thin PDMS layer which would be used later as a glue for bonding the vascular network (Figure 6.2.e).

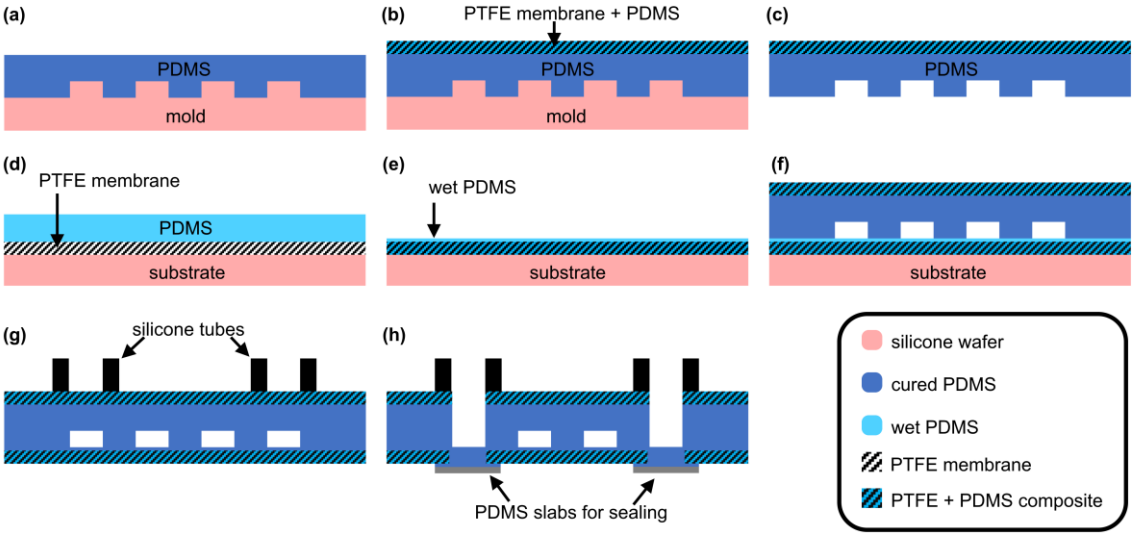

Figure 6.2: Fabrication process of a APMBO: (a) spin-coating a thin layer of PDMS on the top of mold and it was placed on a hot plate to cure PDMS, (b) spin-coating the second PDMS layer on the previous layer and the PTFE membrane with pore size of 1 µm was embedded into wet PDMS, (c) peeling off the device from the mold, (d) the PTFE membrane with pore size of 0.2 µm was placed on the substrate and fully covered with PDMS for 15 minutes, (e) the wet PDMS was spun and formed a thin PDMS layer, (f) a contact made between the vascular network and the wet PDMS layer on the PTFE membrane and the product was placed in an oven, (g) silicone tubes were placed on the designated locations for the inlet and outlet and the device was removed from the substrate, and (h) PDMS inside the inlet and outlet was removed with a biopsy punch and a piece of cured PDMS was used as sealing.

As the thin PDMS layer was still wet, the blood vascular network was brought in contact with wet PDMS layer and the product was left on a leveled surface in room temperature

overnight to let PDMS fully cure (Figure 6.2.f). Then, two 15-mm-silicone tubes (MasterFlex platinum-cured silicone tubing) were placed on the designated locations of the vascular network by applying wet PDMS and cured at 85 °C for an hour the device was removed from the substrate (Figure 6.2.g). Finally, residual PDMS inside the inlet and outlet was removed using a biopsy punch and a small piece of cured PDMS was glued to the bottom side by applying half-cured PDMS (Figure 6.2.h).

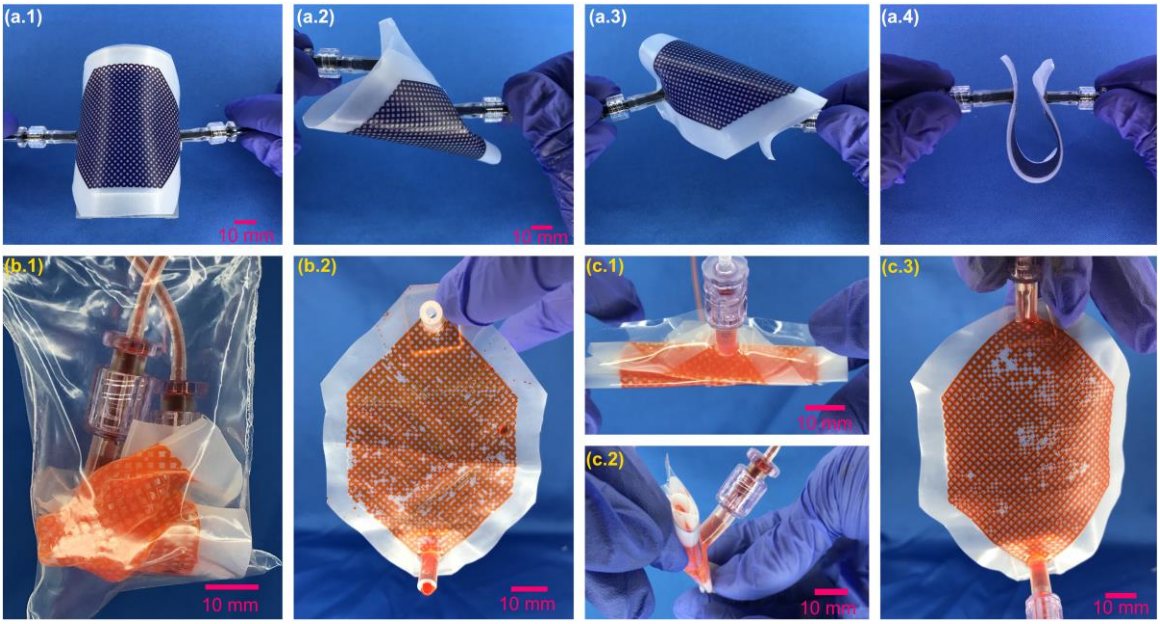

Figure 6.3: APMBO made of PDMS and PTFE membranes capable of being bent and rolled while being perfused. (a.1-4) bending APMBOs while being perfused, (b.1) crumpling and inserting APMBO in a small plastic bag while perfused with water, (b.2) unfolded the crumpled APMBO, (c.1-2) folding APMBO in a zig-zag shape and perfused with water, and (c.3) unfolded the zig-zag shaped APMBO after perfusion.

After device fabrication, APMBOs were perfused with dyed water while they were bent in different shapes to ensure a perfect and leakage-free operation (Video1 in supplementary). As shown in Figure 6.3.a1 - 4, an APMBO was twisted to different shapes while perfusing with dyed water and could sustain the deformation without any failure nor introducing any air bubbles to the vascular network. To show the flexibility of APMBO, a more complex deformation was applied by crumpling an APMBO into a small plastic bag in an irregular way as depicted in Figure 6.3.b1 (Video2 in supplementary). Then, APMBO was perfused with dyed water and unfolded again to

observe its filling. Figure 6.3.b2 shows the device after unfolding was leakproof and had more than 90 % of the vascular network that was still perfusable. Finally, another APMBO was folded back and forth into a shape like an accordion (Figure 6.3.c1) and packed to form a very compact microfluidic device (Figure 6.3.c2) (Video3 in supplementary). Subsequently, the device was perfused with dyed water and unfolded to investigate filling inside the vascular network which was more than 90 % (Figure 6.3.c3). APMBO is versatile enough to be folded or rolled to different shapes while maintains its integrity and functionality which was a proof-of-concept that flexible APMBOs could undergo bending and rolling even very complicated shapes without failure. It is also interesting to note that infused solution is able to perfuse around pinched off locations and reach the outlet, indicating the robustness of the channel network.

6.3.3 Experimental set-up for gas exchange testing

Heparinized (3 units ml^{-1}) bovine blood (Bovine 7200807–1L, Lampire Biologicals Laboratories, 245 Pipersville, PA) was used to assess the gas exchange efficiency of devices. Prior to any experiment, oxygen saturation level (SaO_2) of blood was adjusted to the desired level using the method developed previously[4]. Briefly, heparin (3 units ml^{-1}) was added to blood and stored in the fridge overnight. Then, blood was passed through a hollow fiber membrane oxygenator to bring oxygen saturation down 60 % while being perfused by a mixture of N_2 and CO_2 (95%/5% v/v). Then, blood was stored again in the fridge, and transferred to 140 mL-syringes prior to each experiment. All devices were tested in room air and a pure oxygen environment at atmospheric pressure (and room temperature) and blood properties including oxygen saturation level, pH, partial pressure of oxygen (pO_2), partial pressure of carbon dioxide (pCO_2) and hematocrit level (Hct) were measured using a blood gas analyzer for each condition. Also, hematocrit level was measured before and after each experiment to ensure that blood was not hemolyzed. Moreover, the pressure drop was monitored during experiment and no significant increase in pressure drop was observed.

6.4 Results and Discussion

6.4.1 Gas exchange performance of APMBO

The devices were tested at various blood flow rates of 0.5 – 5 mL min^{-1} in room air and 0.5 – 8 mL min^{-1} in an atmospheric pressure pure oxygen environment. Although most of the oxygenators are typically tested in pure oxygen, the ability to provide sufficient oxygenation in air will enable a simpler and more elegant device that is more suited for artificial placenta application[3]. Therefore, testing was performed under both these conditions.

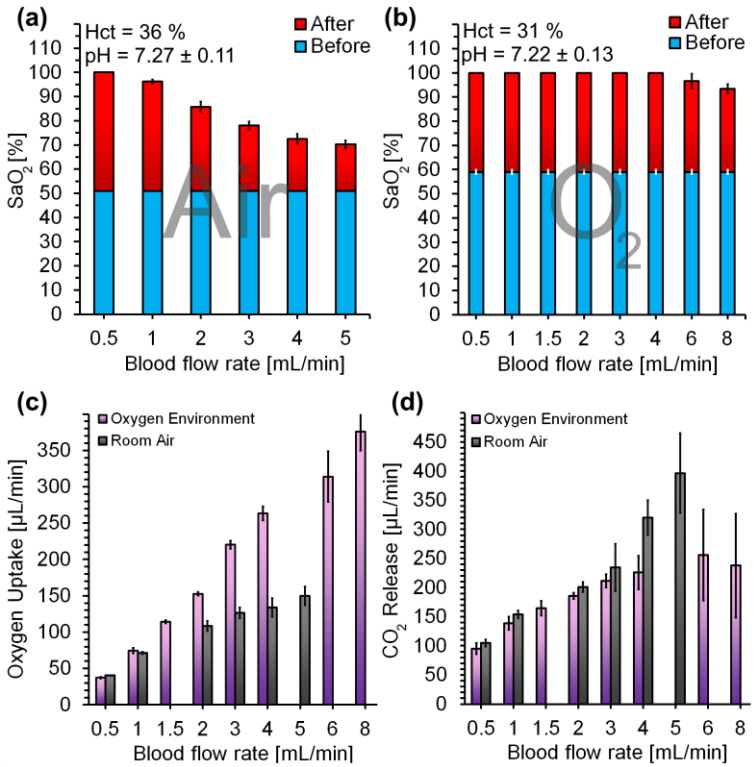

Figure 6.4: In vitro performance of APMBO: (a) oxygen saturation level measurement before and after each device in room air, (b) oxygen saturation level measurement before and after each device in an enriched oxygen environment with atmospheric pressure, (c) oxygen uptake, and (d) carbon dioxide release at various blood flow rates. Data are means ± SD, n=4 and n=5 for air and oxygen, respectively.

The SaO_2 of APMBOs was found to decrease with the increase of blood flow rates in room air (Figure 6.4.a) as red blood cells (RBCs) have a smaller residence time in the

device for gas exchange. However, in an atmospheric pure oxygen environment, full saturation of the incoming blood was achieved at flow rates up to 4 mL min^{-1} with slightly decreased saturation at higher flow rates (Figure 6.4.b), due to shorter resistance time. Figure 6.4.c shows oxygen uptake for different flow rates which was calculated by summing the amount of oxygen molecules bound to hemoglobin and those dissolved oxygen in blood[28]. In both, room air and oxygen environment, oxygen uptake was increased with the increase in blood flow rates. The devices tested in oxygen had higher oxygen transfer compared to those tested in room air, as a consequence of the increased flux across the gas permeable membrane due to the higher oxygen concentration in the ambient. A second critical parameter in evaluation of any oxygenator is the rate of carbon dioxide release. Similar to oxygen transfer, the rate of CO_2 release for all devices increased with an increase of blood flow rates as indicated in Figure 6.4.d. Interestingly, the devices tested room air had higher CO_2 release as compared to the device exposed to pure oxygen. This may be because of the accumulation of released carbon dioxide in the chamber producing a higher level of carbon dioxide in the chamber. This issue could be overcome by introducing a continuous perfusion of oxygen to the chamber and exhausting the exhaled gases.

6.4.2 The Effect of Bending and Rolling on APMBO Performance

To investigate the effect of folding and rolling on APMBO and ensure that their performance would not be compromised, these devices were bent and primed with dyed water to trace their filling pattern. The distribution of flow in devices that was laid flat (Figure 3.5.a 1 – 4) were compared with ones that were bent (Figure 6.5.b 1 – 4) by observing the flow path and measuring filling time. Figure 6.5.a and b show that APMBO in both flat and bent (using the holder seen in Figure 6.5.c with a diameter curvature of 50 mm) geometry behaved similarly and filled the blood vascular network uniformly with the same pattern. Moreover, the filling time for APMBO in both positions did not change and was 25 seconds at a flow rate of 1 mL min^{-1}. The priming volume was found to be ~ 0.42 mL which was slightly larger than the designed priming volume (~ 0.38 mL). This difference could be because of pressure induced deflection in both membranes, as water

flowed into the microchannels. In addition, pressure drop and gas exchange of APMBOs were measured in both flat and bent positions using blood to investigate whether deformation would affect the flow characteristics in the APMBOs. As shown in Figure 6.5.d, pressure drop increased with blood flow rates for both geometries but there was insignificant difference in the characteristics between the two geometries. The other critical parameter, the effect of bending on oxygen uptake, also did not change significantly compared to flat devices as seen in Figure 6.5.e. With the aforementioned observations, it can be concluded that the APMBOs can be reshaped in a desired form without losing their characteristics of uniform flow distribution and gas exchange.

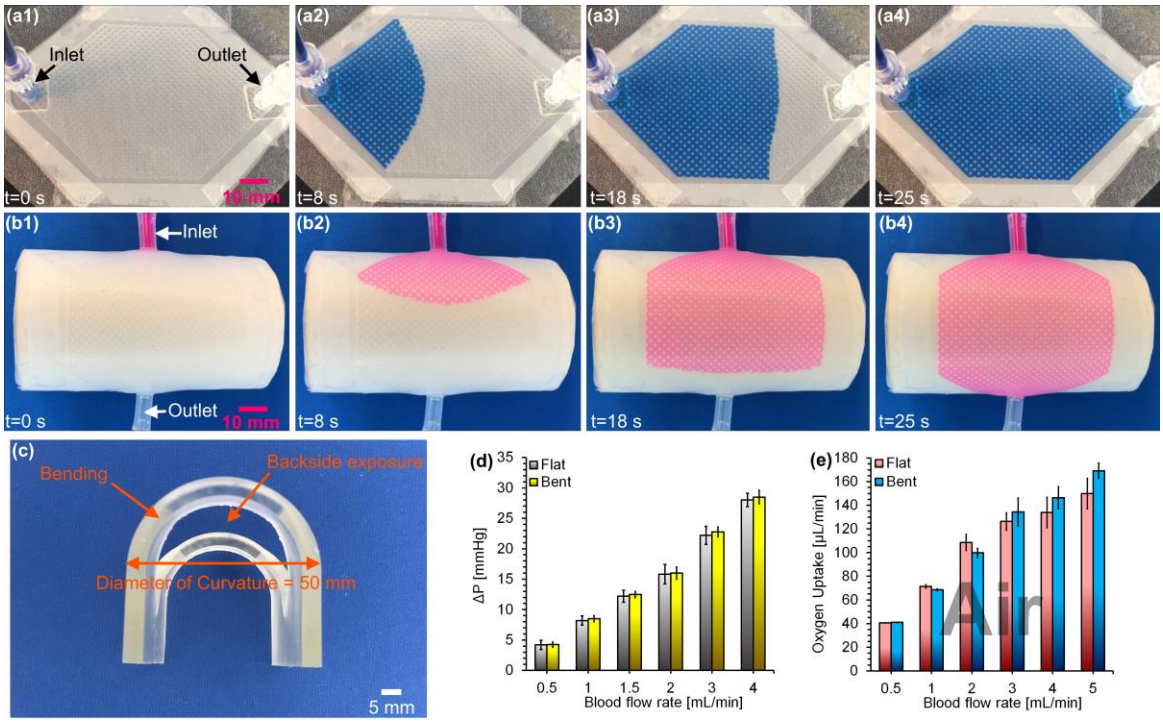

Figure 6.5: Filling of devices with dyed water: (a1) – (a4) APMBO in flat position, (b1) – (b4) APMBO in bent position (bending does not affect the filling time and the flow path), (c) the 3D-printed holder for bending APMBOs with positioning inlet and outlet in 180 ° of each other, (d) pressure drops measured at different blood flow rates, and (e) the oxygen uptake of APMBOs in both flat and bent positions. Data are means ± SD, n=4.

6.4.3 The Effect of Curvature Dimension on Flow Characteristics

As discussed earlier, APMBOs had the ability to be bent or folded in a desired shape to reduce the form factor. An experiment was performed using the experimental set-up shown in Figure 6.6.a, to investigate the effect of different diameter of curvature on pressure drop. We tested the pressure drop for two factors: (1) the flow rate and (2) the geometry of the device. First, APMBOs were bent using a 3D-printed holder (Supplementary Figure 2.6) at different curvature ranging from 10 – 50 mm, then flow rates were swept from 4 – 20 mL min^{-1} while the pressure drop was measured. Isopropanol was used to ensure a bubble-free filling during perfusing as introducing air bubbles could impact flow distribution and subsequently the pressure drop. No discernible change in the pressure drop at a constant flow rate was observed, as shown in Figure 6.6.b. Even at a high flow rate of 20 mL min^{-1}, there was only 1 mm Hg increase in pressure drop at the smallest curvature compared to other diameter of curvature and the flat position.

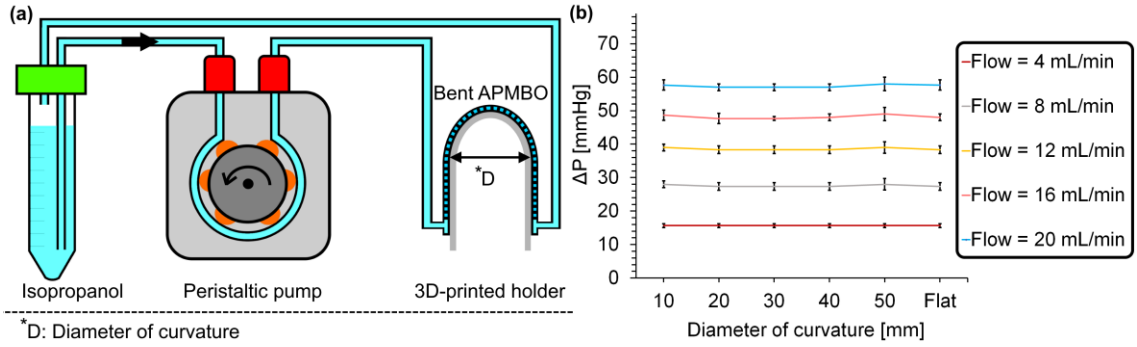

Figure 6.6: (a) the experimental set-up for measuring pressure drop of APMBOs for different curvature at different flow rates and (b) the pressure drops results versus the diameter of the curvature at different flow rates. Data are means ± SD, n=3.

This observation suggests that the hydraulic resistance of the channels was unaffected due to bending and the design of the microfluidic network prevented any local collapse that could affect flow distribution.

6.4.4 A Foldable Integrated Lung Assist Device

Lung assist devices are typically fabricated by assembling several oxygenator modules in parallel in order to accommodate the total volumetric flow required for sufficient oxygenation of the neonate's blood. Such oxygenators with parallel modules typically use tubing and connectors to interconnect them together. The interconnects that are used for the assembly of the device usually take up more than 50% of the priming volume and also prevent the device from being more compact[4][40].

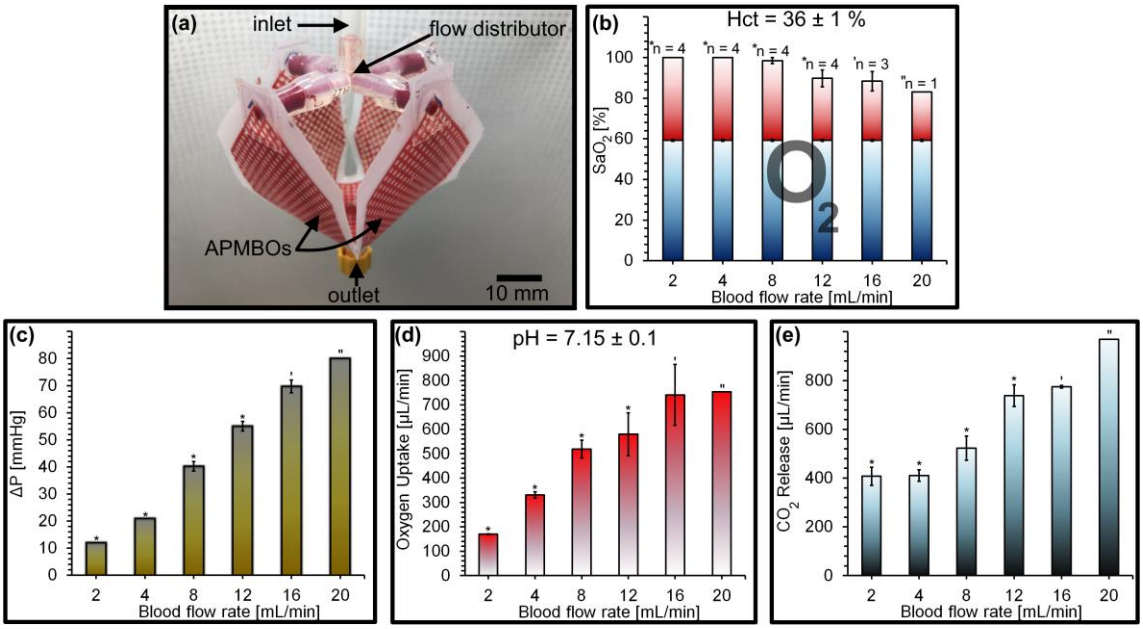

Figure 6.7: (a) A flower-shaped compact LAD consisting of 4 APMBO units in parallel (b) Oxygen saturation level measurement before and after the LAD in an enriched oxygen environment at atmospheric pressure (c) Pressure drop in the LAD, (d) Oxygen uptake, and (e) Carbon dioxide release at various operating blood flow rates. Data are Mean ± SD.

The flexibility of our device enabled us to design interesting configurations that not only reduced the form factor but also minimized the priming volume at the same time. A flower shaped configuration was designed such that each of the four "petals" of the flower correspond to a single oxygenator unit (Figure 6.7.a– the cutting lines of the device fabrication was shown in Supplementary Figure 2.7). The outlets of the oxygenator are integrated into one thereby minimizing the priming volume of the connections. The

foldability of the device allows the petals to be folded into a bud shape so that the inlet connectors are also brought closer together and connected to a 3D printed flow distributor while still allowing all sides of the oxygenators to be exposed to ambient air or an environment filled with oxygen. The height of blood vascular network was 100 μm and the total surface area was 41.81 cm^2 with ~ 83% of which was effective in gas exchange. The priming volume of the blood vascular network was only 0.42 mL and the total priming volume including the flow distributor and tubing was ~ 0.84 mL. As a comparison, LADs made using parallel assembly of individual oxygenator units[4], [5] will have a total priming volume that is higher by at least 50 %. In addition, the folded design also makes it more compact.

A measure of compactness could be made by calculating the projected area of the device which is the area of the image that a 3D object projects on to a plane. The projected surface area of the flower shaped device decreased by 82 % from 153.9 cm^2 in the flat position to 27.4 cm^2 for the flower shaped one. Bovine blood with SaO_2 around 59 % was flowed to the LAD which was placed in an enriched pure oxygen environment with atmospheric pressure and the blood properties were measured at the outlet. With increase in the blood flow rate, lower oxygen saturation level was achieved down to 83 % at the blood flow rate of 20 mL/min (Figure 6.7.b). This level of increase may be sufficient enough for preterm neonates with very low birth-weight suffering from RDS as the arterial blood would be partially oxygenated by a preterm baby's underdeveloped lungs more than 70 %[4], [28]. In this case, if the arterial blood has a SaO_2 of ~ 70 %, this flower shaped compact LAD can increase the oxygen saturation level at least to ~ 90 % using pure oxygen. The pressure drops in this configuration also increased linearly with increasing the blood flow rate (Figure 6.7.c) as expected. The oxygen uptake and carbon dioxide release were also calculated from the measured saturation data. The oxygen uptake was found to gradually increase up to the blood flow rate of 16 mL/min and became steady at the blood flow rate of 20 mL min^{-1} as shown in Figure 6.7.d which suggested that the flower-shaped APMBO may reached its maximum capacity for oxygen transfer. The carbon dioxide release also showed an increase with increasing the blood

flow rate (Figure 6.7.e). The maximum oxygen uptake of 754.2 µL min^{-1} (115 mL min^{-1} m^{-2}) and a carbon dioxide release of 969.9 µL min^{-1} were achieved at a blood flow rate of 20 mL min^{-1}.

6.4.5 Large Rolled APMBO with Compact Cylindrical Geometry

Another interesting configuration that was designed and fabricated was a large area oxygenator that could support the entire oxygenation needs of a ~0.5 kg neonate. This oxygenator was rolled into a cylinder so that the inlet and the outlets were positioned adjacent to each other. In this format, the length of the external connectors needed are significantly reduced, producing a configuration with the smallest priming volume (Supplementary Figure 2.8). Large APMBO (91 mm x 91 mm) with a surface area of 62.56 cm^2 and a channel height of 160 µm that was optimized for pumpless operation (pressure drop between 20-60 mmHg), were fabricated (Figure 6.8.a).

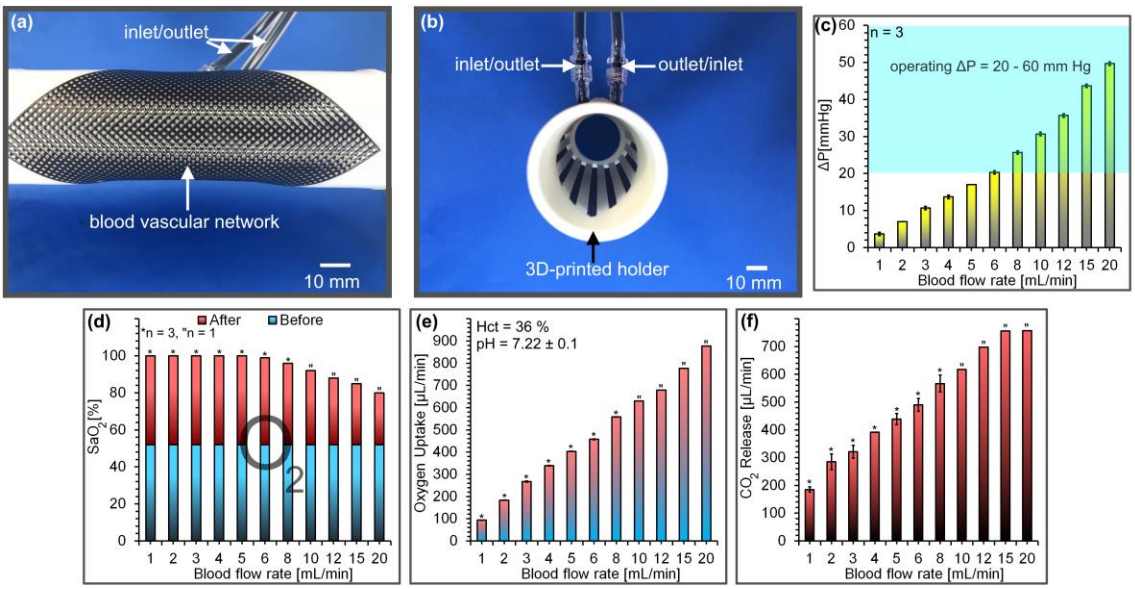

*Figure 6.8: (a) Top-view of the rolled APMBO, (b) Axial view of rolled APMBO, In vitro performance of rolled APMBO: (c) pressure drop, (d) oxygen saturation level measurement before and after the rolled APMBO in an enriched oxygen environment with atmospheric pressure, (e) oxygen uptake, and (f) carbon dioxide release. Data are Mean ± SD, *n=3, "n=1.*

The fabricated APMBO was rolled around a 3D-printed holder in such way that both sides of the blood vascular network would be exposed to the ambient as shown in Figure

6.8.b. This device has a priming volume of 1 mL and a total priming volume (including the interconnects) of only 1.25 mL. This represents a significant reduction in volume from other oxygenator designs and makes it ideal for extremely low weight pre-term babies. This APMBO had a projected surface area of 182.4 cm^2 in a flat position which was reduced by 65 % to 64 cm^2 by rolling around the 3D-printed holder. The rolled APMBO was then tested with blood at various flow rates ranging from 1 mL min^{-1} to 20 mL min^{-1} under an atmospheric pure oxygen environment to determine its oxygenation performance.

The pressure drop was found to linearly increase with increasing blood flow rates and was always in the operating pressure drop range for preterm neonates (between 20-60 mmHg) as seen in Figure 6.8.c. The measured pressure drop was the summation of the rolled APMBO and the external circuit. The blood was found to be fully oxygenated up to a blood flow rate of ~ 6 mL min^{-1} and the outlet SaO_2 was gradually decreased with increase in flow rate, to 80 % at a blood flow rate of 20 mL min^{-1} (Figure 6.8.d) which is associated with the reduced residence time of the blood in the device under high flow rates.

The oxygen uptake (Figure 6.8.e) and the carbon dioxide (Figure 6.8.f) release were calculated. As expected, the oxygen uptake always increased with increasing blood flow rates due to the higher oxygen flux at higher blood flow rates. The rate of carbon dioxide release also increased at higher blood flow rates. The maximum oxygen uptake and carbon dioxide release were 877.0 µL min^{-1} and 757.5 µL min^{-1}, respectively. For a preterm baby with RDS, an artificial placenta device is expected to provide an oxygen transfer of 1.3 – 1.9 mL min^{-1} kg^{-1} of a baby weight[4]. Here, the maximum oxygen uptake of 877 µL min^{-1} (88.2 mL min^{-1} m^2) was achieved which would be sufficient enough for preterm neonates with extremely low birth-weight[4], [26] up to 675 g. In addition, such a device would not need any additional blood transfusion owing to its low priming volume which is 1.25 mL. Additionally, this rolled APMBO does not require very long tubing for connection to the vessels because of its unique design.

6.5 Conclusion

In this paper, we introduced a highly flexible artificial placenta-type microfluidic blood oxygenator (APMBO) which can be used to reduce the form factor and the overall priming volume of a LAD for preterm neonates. First, the gas exchange performance of this flexible device was measured in room air and an atmospheric pure oxygen environment. Subsequently, we showed that our flexible device could undergo bending without losing its functionality by observing the flow pattern, measuring the filling time and investigating the gas exchange properties. Later, a more advanced design that consisted of 4 smaller APMBOs was used to make a flower shape LAD that utilized the flexibility to achieve a compact form. By folding the petals of this flower shape and bringing the inlets together, several connecters were eliminated, and this LAD had a low priming volume of ~ 0.84 mL. Finally, a large APMBO was fabricated and rolled onto a 3D-printer holder so that both inlet/outlet accesses were placed in the adjacent of each other. This configuration can reduce the need of external tubing for connecting the LAD to the vessels resulting lower priming volume. All the three configurations exploit the flexibility of the oxygenator to reduce its form factor and its priming volume. This approach for oxygenator fabrication is scalable and paves the way for fabricating a large area multi modular oxygenator with integrated flow distributors on a single sheet and folding it into a compact form post fabrication.

References

[1] R. J. Rodriguez, "Management of respiratory distress syndrome: an update.," *Respir. Care*, vol. 48, no. 3, pp. 279–287, Mar. 2003.

[2] K. Fletcher, R. Chapman, and S. Keene, "An overview of medical ECMO for neonates," *Semin. Perinatol.*, pp. 1–12, 2018.

[3] N. Rochow *et al.*, "Artificial placenta -Lung assist devices for term and preterm newborns with respiratory failure," *Int J Artif Organs*, vol. 36, pp. 377–391, 2013.

[4] M. Dabaghi *et al.*, "An artificial placenta type microfluidic blood oxygenator with double-sided gas transfer microchannels and its integration as a neonatal lung assist device," *Biomicrofluidics*, vol. 12, no. 3, 2018.

[5] H. Matharoo *et al.*, "Steel reinforced composite silicone membranes and its integration to microfluidic oxygenators for high performance gas exchange," *Biomicrofluidics*, vol. 12, no. 1, 2018.

[6] T. Kniazeva *et al.*, "Performance and scaling effects in a multilayer microfluidic extracorporeal lung oxygenation device," *Lab Chip*, vol. 12, no. 9, pp. 1686–1695, 2012.

[7] T. Rieper, B. Wehrstein, A. N. Maurer, C. Mueller, and H. Reinecke, "Evaluation model of an extracorporeal gas exchange device made of silicone rubber," *Biomed. Eng. / Biomed. Tech.*, vol. 57, no. SI-1 Track-I, pp. 1109–1112, 2012.

[8] N. Rochow *et al.*, "Integrated microfluidic oxygenator bundles for blood gas exchange in premature infants," *Proc. IEEE Int. Conf. Micro Electro Mech. Syst.*, no. February, pp. 957–960, 2012.

[9] D. M. Hoganson, H. I. Pryor, E. K. Bassett, I. D. Spool, and J. P. Vacanti, "Lung assist device technology with physiologic blood flow developed on a tissue engineered scaffold platform.," *Lab Chip*, vol. 11, no. 4, pp. 700–707, 2011.

[10] E. K. Bassett, D. M. Hoganson, J. H. Lo, E. J. N. Penson, and J. P. Vacanti, "Influence of vascular network design on gas transfer in lung assist device technology.," *ASAIO J.*, vol. 57, no. 6, pp. 533–8, 2011.

[11] R. Sreenivasan, E. K. Bassett, D. M. Hoganson, J. P. Vacanti, and K. K. Gleason, "Ultra-thin, gas permeable free-standing and composite membranes for microfluidic lung assist devices," *Biomaterials*, vol. 32, no. 16, pp. 3883–3889, 2011.

[12] J. A. Potkay, M. Magnetta, A. Vinson, and B. Cmolik, "Bio-inspired, efficient, artificial lung

employing air as the ventilating gas.," *Lab Chip*, vol. 11, no. 17, pp. 2901–2909, 2011.

[13] T. Kniazeva, J. C. Hsiao, J. L. Charest, and J. T. Borenstein, "A microfluidic respiratory assist device with high gas permeance for artificial lung applications," *Biomed. Microdevices*, vol. 13, no. 2, pp. 315–323, 2011.

[14] W. Wu *et al.*, "Development of Microfluidic Oxygenators as Lung Assisting Devices for Preterm Infants," in *15th International Conference on Miniaturized Systems for Chemistry and Life Sciences*, 2011, pp. 550–552.

[15] D. M. Hoganson *et al.*, "Branched vascular network architecture: a new approach to lung assist device technology.," *J. Thorac. Cardiovasc. Surg.*, vol. 140, no. 5, pp. 990–995, 2010.

[16] A. J. Thompson, L. H. Marks, M. J. Goudie, A. Rojas-Pena, H. Handa, and J. A. Potkay, "A small-scale, rolled-membrane microfluidic artificial lung designed towards future large area manufacturing," *Biomicrofluidics*, vol. 11, no. 2, 2017.

[17] K. A. Burgess, H. H. Hu, W. R. Wagner, and W. J. Federspiel, "Towards microfabricated biohybrid artificial lung modules for chronic respiratory support," *Biomed. Microdevices*, vol. 11, no. 1, pp. 117–127, 2009.

[18] J. A. Potkay and D. Ph, "a High Efficiency Micromachined Artificial Lung," in *The 15th International Conference on Solid-State Sensors, Actuators and Microsystems (Transducers 2009)*, 2009, pp. 2234–2237.

[19] J. K. Lee, H. H. Kung, and L. F. Mockros, "Microchannel technologies for artificial lungs: (1) theory.," *ASAIO J.*, vol. 54, no. 4, pp. 372–82, 2008.

[20] and L. F. M. J.-K. Lee, M. C. Kung, H. H. Kung, "Microchannel Technologies for Artificial Lungs: (3) Open Rectangular Channels," *ASAIO J. NIH Public Access*, vol. 54, no. 4, pp. 390–395, 2008.

[21] L. M. JK Lee, MC Kung, HH KUng, "Microchannel Technologies for Artificial Lungs: (3) Open Rectangular Channels," *ASAIO J. NIH Public Access*, vol. 54, no. 4, pp. 390–395, 2008.

[22] A. A. Gimbel, E. Flores, A. Koo, G. García-Cardeña, and J. T. Borenstein, "Development of a biomimetic microfluidic oxygen transfer device," *Lab Chip*, vol. 16, no. 17, pp. 3227–3234, 2016.

[23] T. Rieper, C. Muller, and H. Reinecke, "Novel scalable and monolithically integrated extracorporeal gas exchange device," *Biomed. Microdevices*, vol. 17, no. 5, pp. 1–10, 2015.

[24] K. M. Kovach *et al.*, "In vitro evaluation and in vivo demonstration of a biomimetic, hemocompatible, microfluidic artificial lung.," *Lab Chip*, vol. 15, no. 5, pp. 1366–75, 2015.

[25] T. Femmer, M. L. Eggersdorfer, A. J. Kuehne, and M. Wessling, “Efficient gas-liquid contact using microfluidic membrane devices with staggered herringbone mixers,” *Lab Chip*, vol. 15, no. 15, pp. 3132–3137, 2015.

[26] N. Rochow *et al.*, “An integrated array of microfluidic oxygenators as a neonatal lung assist device: In vitro characterization and in vivo demonstration,” *Artif. Organs*, vol. 38, no. 10, pp. 856–866, 2014.

[27] J. a Potkay, “The promise of microfluidic artificial lungs.,” *Lab Chip*, vol. 14, no. 21, pp. 4122–4138, 2014.

[28] W.-I. Wu *et al.*, “Lung assist device: development of microfluidic oxygenators for preterm infants with respiratory failure,” *Lab Chip*, vol. 13, no. 13, p. 2641, 2013.

[29] M. C. Kung, J.-K. Lee, H. H. Kung, and L. F. Mockros, “Microchannel technologies for artificial lungs: (2) screen-filled wide rectangular channels.,” *ASAIO J.*, vol. 54, no. 4, pp. 383–389, 2008.

[30] S. Xu *et al.*, “Soft Microfluidic Assemblies of for the Skin,” *Science (80-.).*, vol. 344, no. April, pp. 70–74, 2014.

[31] M. Kaltenbrunner *et al.*, “An ultra-lightweight design for imperceptible plastic electronics,” *Nature*, vol. 499, no. 7459, pp. 458–463, 2013.

[32] J. C. Yeo, Kenry, J. Yu, K. P. Loh, Z. Wang, and C. T. Lim, “Triple-State Liquid-Based Microfluidic Tactile Sensor with High Flexibility, Durability, and Sensitivity,” *ACS Sensors*, vol. 1, no. 5, pp. 543–551, 2016.

[33] X. Pu *et al.*, “Ultrastretchable, transparent triboelectric nanogenerator as electronic skin for biomechanical energy harvesting and tactile sensing,” *Sci. Adv.*, vol. 3, no. 5, pp. 1–11, 2017.

[34] A. Chortos, J. Liu, and Z. Bao, “Pursuing prosthetic electronic skin,” *Nat. Mater.*, vol. 15, no. 9, pp. 937–950, 2016.

[35] J. Kim *et al.*, “Stretchable silicon nanoribbon electronics for skin prosthesis,” *Nat. Commun.*, vol. 5, pp. 1–11, 2014.

[36] S. Li, D. M. Vogt, D. Rus, and R. J. Wood, “Fluid-driven origami-inspired artificial muscles,” *Proc. Natl. Acad. Sci.*, vol. 114, no. 50, p. 201713450, 2017.

[37] T. Ranzani, S. Russo, N. W. Bartlett, M. Wehner, and R. J. Wood, “Increasing the Dimensionality of Soft Microstructures through Injection-Induced Self-Folding,” *Adv. Mater.*, vol. 1802739, p. 1802739, 2018.

[38] S. I. Rich, R. J. Wood, and C. Majidi, "Untethered soft robotics," *Nat. Electron.*, vol. 1, no. 2, pp. 102–112, 2018.

[39] W. Hu, G. Z. Lum, M. Mastrangeli, and M. Sitti, "Small-scale soft-bodied robot with multimodal locomotion," *Nature*, vol. 554, no. 7690, pp. 81–85, 2018.

[40] A. J. Thompson, L. J. Ma, T. J. Plegue, and J. A. Potkay, "Design Analysis and Optimization of a Single Layer PDMS Microfluidic Artificial Lung," *Trans. Biomed. Eng.*, 2018.

7 Chapter 7

A PUMPLESS MICROFLUIDIC NEONATAL LUNG ASSIST DEVICE FOR ARTIFICIAL PLACENTA APPLICATIONS

Complete citation:

Mohammadhossein Dabaghi, Niels Rochow, Neda Saraei, Gerhard Fusch, Shelley Monkman, Kevin Da, Alireza Shahin-Shamsabadi, Devon Jones, John L. Brash, Dragos Predescu, Kathleen Delaney, Christoph Fusch, and P. Ravi Selvaganapathy. *"A Pumpless Microfluidic Neonatal Lung Assist Device for Artificial Placenta Applications."* Under preparation to be submitted.

Contribution:

My contributions include designing and fabricating the lung assist device for in vitro and in vivo experiments, planning and performing the related experiments, interpretation and analysis of data and results, and writing the manuscript.

7.1 Abstract

Premature neonates have severe morbidity and fatality as their lungs are immature and current supportive treatment such as mechanical ventilation or extracorporeal membrane oxygenation (ECMO) cause iatrogenic damages. Therefore, a non-invasive and biomimetic concept called as artificial placenta would be beneficial to overcome complications and challenges associated with the current standard of care for respiratory support of these preterm infants. In this configuration, a pumpless device is connected to the umbilical cord to access the systematic circulation for gas exchange purposes. In this study, we have introduced a pumpless neonatal lung assist device (LAD) which can be used as an artificial placenta device. Our new LAD has high oxygenation capability in both pure oxygen or room air as the sweep gas. To investigate the applicability of this LAD in clinical use, it was connected to a newborn piglet of the same weight as a typical neonate and showed that it was capable of achieving high gas exchange in room air and an enriched oxygen environment in passive operation. These findings indicate that this LAD has potential application as a biomimetic artificial placenta type device to support the oxygenation needs of a preterm neonate.

7.2 Introduction

Premature births are associated with significant morbidity and mortality. Neonates, especially those with very low birth-weights and born at less than 28 weeks of gestational age[1], [2] have a very low survival rate, with those born earlier 24 weeks of gestational age[3] having more than 50 % mortality. One among the leading causes of morbidity associated with preterm birth is respiratory distress caused by lack of surfactants in underdeveloped and immature lungs. [4]–[7]. Mechanical ventilation is often used for respiratory support of such premature neonates[8] who are in respiratory distress. Nonetheless, this method is invasive and could lead to severe complications such as pulmonary injury, chronic lung disease, and retinopathy of prematurity which would lead to several long-term side effects[9]–[11]. In more severe cases, extracorporeal membrane oxygenation (ECMO) is used. This procedure is also invasive and requires vascular access and therefore, surgery. Current hollow fiber based blood oxygenators that are used in ECMO are not suitable for neonatal application due to their high priming volume (> 20 mL), high pressure drop which requires an external pump for perfusion, and their gas exchange dependency to oxygen[8], [12]. Moreover, other complications such as cerebral injury with intracranial hemorrhage or infarction, poor somatic growth, and chronic lung disease could be caused by this technology[13].

Microfabrication technologies have been employed to fabricate blood oxygenators that can address the limitations of current ECMO devices by applying a biomimetic architecture to their design similar in size to capillaries in the lung in order to enhance gas transfer efficiency, increase effective surface area for transfer as well as reduce shear stress in blood flow and avoid stagnation [14], [15]. Several microfluidic blood oxygenators[12], [16]–[32] have been introduced aimed at improving gas exchange efficiency; however, only a few of them[12], [16], [21]–[23] were explicitly designed to be used as an artificial placenta device.

The artificial placenta (AP) approach where blood is circulated through a passive device pumped solely by the arteriovenous pressure difference of the neonate's heart and capable

of exchanging blood gases with the ambient is physiologically similar to in-utero conditions and overcomes some of the issues associated with traditional ECMO devices. [8], [12], [16]. Previous AP type microfluidic blood oxygenators could not fulfill all requirements, especially achieving sufficient oxygenation in room air. Besides, most artificial placenta-type microfluidic blood oxygenators[12], [21], [22] have been examined in vitro and even those[16], [23] tested in vivo could not provide adequate oxygenation in room air.

Here, we develop a high-performance, pumpless, neonatal lung assist device and perform in-vivo experiments on newborn piglets to demonstrate its ability to meet the clinical need. The LAD was assembled from high-performance microfluidic blood oxygenators (MBOs) [22] in a parallel configuration to enable sufficient flow of blood through it as it was pumped by the pressure generated by the piglet's heart. The entire LAD was also coated with heparin to reduce its systemic infusion and the performance of this coating was also evaluated. We report the in-vitro gas exchange performance of the LAD as well as its in-vivo performance when the piglet was intentionally put in respiratory distress by putting it under hypoxic conditions. Systemic blood gas measurements as well as cardiovascular conditions were monitored during repeated cycles of hypoxic and normoxic conditions over a period of 200 minutes. Our results show that this passive pumpless LAD could provide adequate oxygenation in room air to restore near normoxic condition and has the potential for meeting the clinical need to support neonates under respiratory distress.

7.3 Results

7.3.1 Microfluidic blood oxygenator device

The microfluidic blood oxygenator (MBO) was constructed entirely out of polydimethylsiloxane (PDMS) and comprised of three components: a blood vascular network that spreads the incoming blood into a thin uniform layer suitable for fast gas exchange, enclosed by two thin composite membranes made of polytetrafluoroethylene (PTFE) and PDMS with high permeability for blood gases and sufficient stiffness to

withstand the physiological pressure encountered, and a tapered shaped inlet/outlet to access the blood vascular network. The blood vascular network was a microchamber with a height of 180 µm containing an array of 1x1 mm square-shaped micropillars. The design which is shown in Figure 7.1 was optimized to ensure that a uniform blood distribution was achieved and had a surface area of 29.19 $cm^{2,}$ and a priming volume of 0.52 mL. Tapered inlet and outlet were integrated on top of the blood vascular network to ensure smooth distribution of blood from a cylindrical inlet connection into the vascular network. It also minimizes shear stress that could lead to hemolysis, platelet activation, and clot formation.

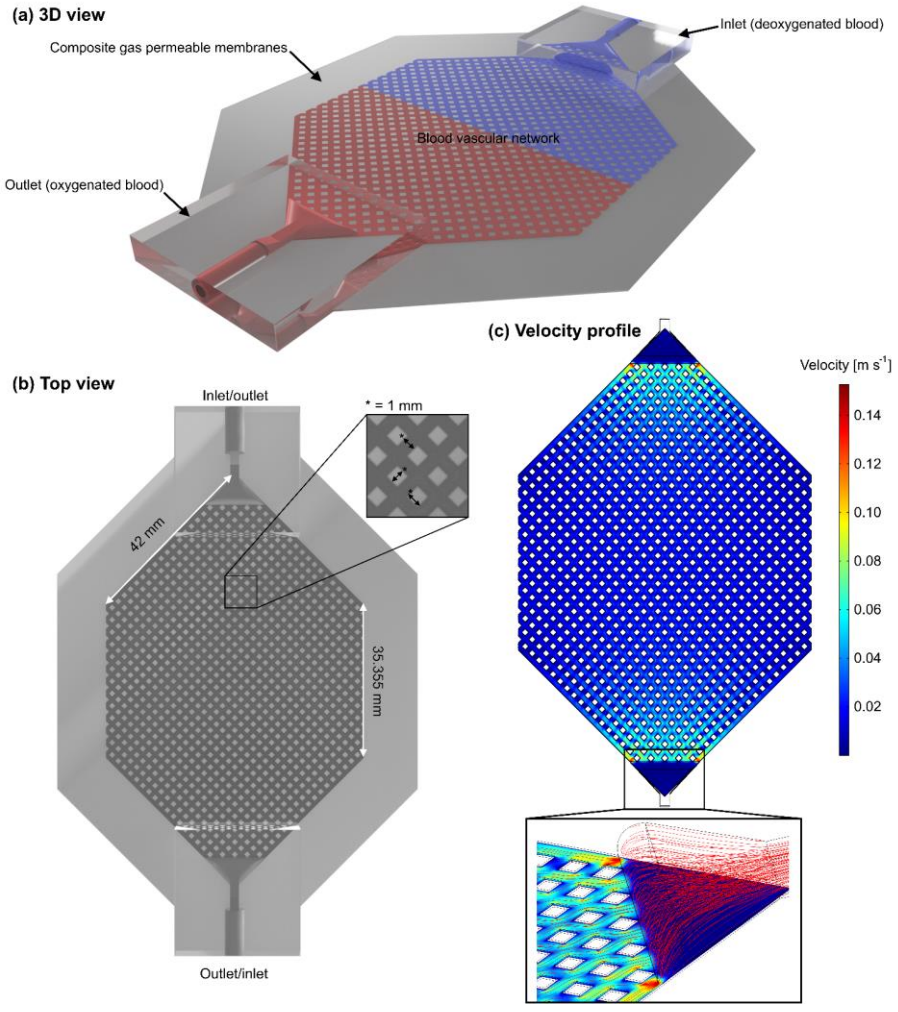

Figure 7.1: (a) 3D schematic drawing of MBO with tapered inlet/outlet configuration, (b) top view of MBO and (c) the velocity profile of MBO at a blood flow rate of 5 mL min-1 showing a uniform distribution with a gentle change in flow direction and no deal zone.

7.3.2 A compact neonatal lung assist device

A single MBO cannot provide enough oxygenation to support preterm neonates with RDS with different weights. As a result, a lung assist device (LAD) was constructed by assembling 16 MBOs in a parallel configuration (Figure 7.2). The frame was 3D printed to arrange the MBOs in a compact form and consisted of several fixtures to hold MBOs along with a top and bottom holder to maintain fixed gaps between the MBO holders.

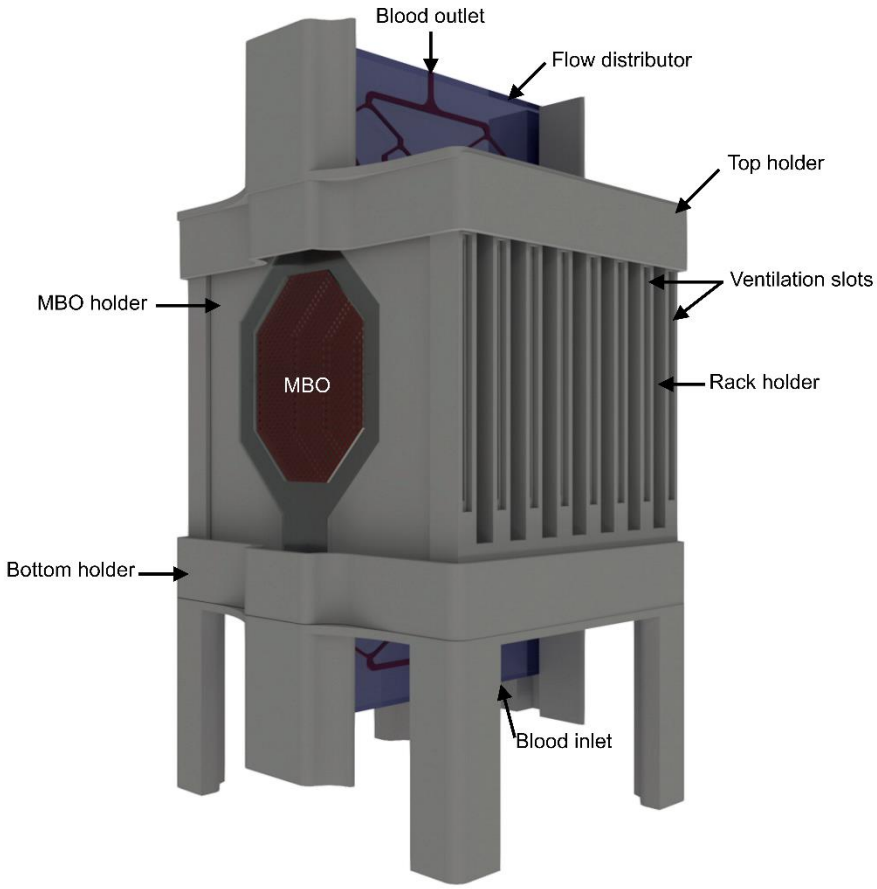

Figure 7.2: 3D drawing of the LAD showing all 3D-printed components, MBOs, and flow distributors. There is fixed gaps among all MBOs for air to flow convectively. Blood is fed to the LAD from the bottom flow distributor and leaves the LAD from the top one to ensure that no air bubble is trapped inside.

Each MBO holder was designed to hold two MBOs at a fixed distance apart from each other to facilitate convective gas flow on all sides of the MBO, naturally. Then, eight such MBO holders were inserted into the appropriate slots in the top and bottom holders to form the compact LAD. Blood flow distributors were designed based on Murray's Law[33], [34] to minimize shear stresses while efficiently distributing blood and connected with the assembled MBOs using a 10-mm-piece of silicone tube and connectors.

7.3.3 In vitro testing of LAD using bovine blood

The gas exchange performance of the LAD in-vitro was investigated in enriched oxygen environment as well as in room air using heparinized bovine blood The oxygen saturation level (Sa O_2) of the blood introduced into the LAD was adjusted to 58 ± 2 % in experiments performed in an enriched oxygen environment and 63 ± 1 % in experiments conducted in room air and the oxygen saturation in the outlet was measured. The LAD could fully oxygenate (Sa O_2 = ~ 100 %) blood up to a flow rate of 80 mL min^{-1} in an enriched oxygen environment and increase to ~ 95 % at a blood flow rate of 100 mL min^{-1}(Figure 7.3.a). The oxygen uptake was calculated by summing the amount of dissolved oxygen and adsorbed oxygen to red blood cells[12]. The oxygen uptake was between 0.92 to 5.71 mL min^{-1} with a linear increase showing the superior oxygen transfer capacity of the LAD using oxygen as the sweep gas (Figure 7.3.b). The LAD had a different gas transfer behavior in room air as oxygen concentration was lower. Consequently, oxygen saturation level achieved was lower and the blood was fully oxygenated only up to a blood flow rate of 20 mL min^{-1}. The outlet saturation level started to drop and was 87 % at a blood flow rate of 60 mL min^{-1}(Figure 7.3.c). The oxygen uptake linearly increased with blood flow rates and was 1.82 mL min^{-1} at a blood flow rate of 60 mL min^{-1} in room air (Figure 7.3.d). The pressure drop of the LAD (Figure 7.3.e), as well as the LAD (Figure 3.f) with the extracorporeal circuit, was measured over a range of flow rates from 10-100 mL min^{-1}.

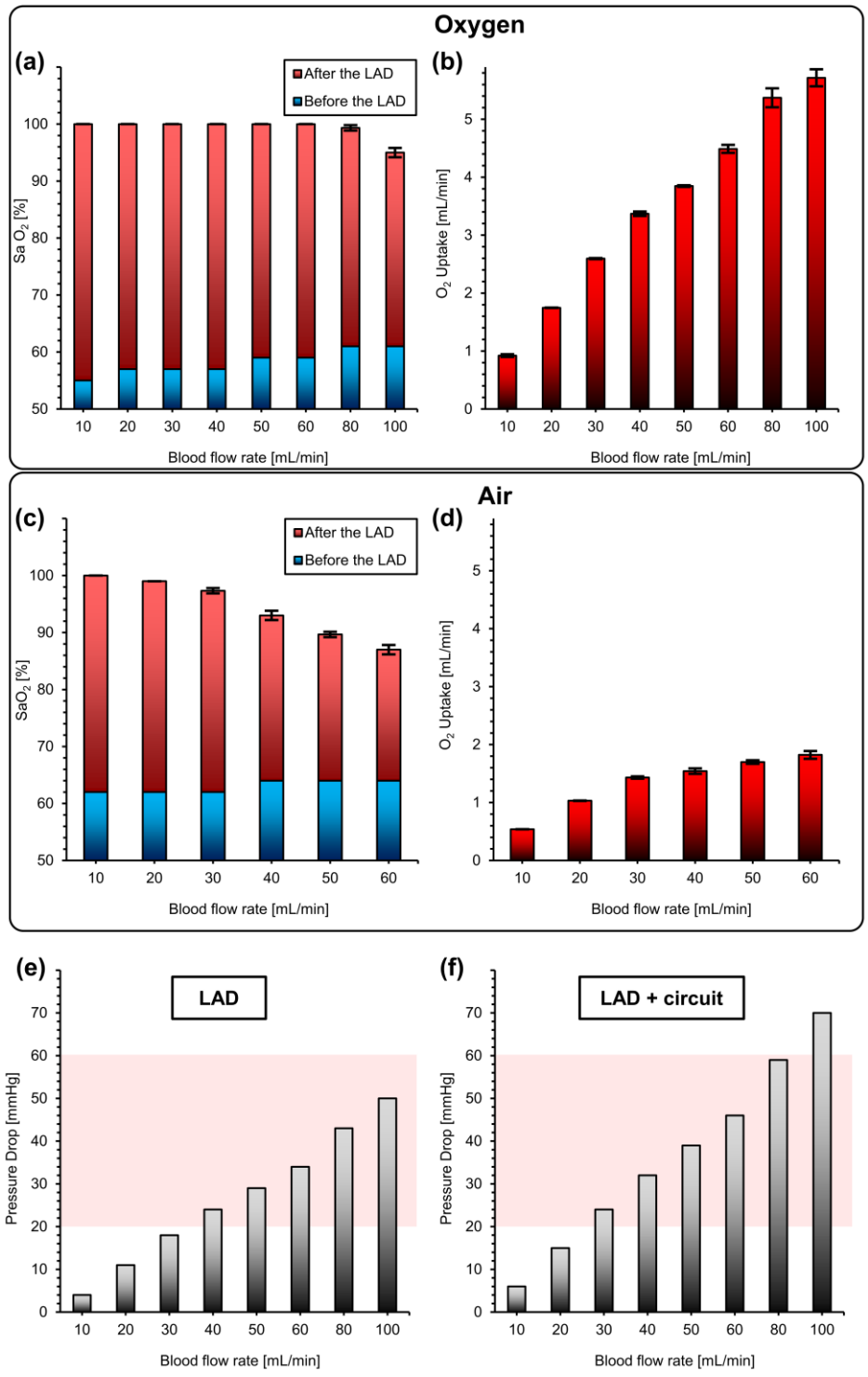

Figure 7.3: In vitro test of the LAD with heparinized bovine blood at various blood flow rates: (a) oxygen saturation level before and after the LAD in oxygen, (b) oxygen uptake in oxygen (c) carbon dioxide release in oxygen, (d) oxygen saturation level before and after the LAD in room air, (e) oxygen uptake in room air,

(f) carbon dioxide release in room air, (g) pressure drops for the LAD (the shaded region indicates the operational pressure drops range for a pumpless operation), and (h) the pressure drops for the LAD with the extracorporeal circuit. Data are means ± SD, n = 3. Hematocrit was 38 % and 29 % for oxygen and air conditions, respectively.

7.3.4 Modification of blood-in-contact surfaces with heparin

To minimize the chance of clot formation, platelet activation, and thrombosis, all blood-in-contact surfaces were coated with heparin prior to the main experiment. Heparin with a concentration of 100 units mL^{-1} was added to normal saline solution and perfused to the LAD in a closed-loop configuration for 4 – 5 hours followed by washing with normal saline solution (Figure 7.4.a1). FITC-heparin was used to assess the stability and quality of the coating. After coating an MBO with FITC-heparin for 4 – 5 hours, the MBO has rinsed with PBS solution for 15 min to wash away the uncoated heparin while the fluorescent intensity was monitored (Figure 7.4.a2). The results confirmed that 15 minutes was sufficient to remove uncoated heparin from MBOs. PDMS has a hydrophobic nature turning its surface into a suitable place for adsorbing different proteins such as Fibrinogen which can potentiate the coagulation process[35]. Therefore, a hydrophilic surface modification on PDMS may reduce the risk of protein adsorption. Coating PDMS with heparin decreased the contact angle from 120 ° to 66 ° and the surface became hydrophilic which is beneficial in reducing protein adsorption and preventing the activation of the coagulation cascade (Figure 7.4.b). More importantly, heparin is an anti-coagulant and its presence on the surface also mitigates the thrombotic effect of blood exposure to other surfaces. An MBO was coated with FITC-heparin using the same process, and a wide-angle fluorescence image was taken which showed the uniformity of the coating inside the blood vascular network (Figure 7.4.c). Subsequently, PBS solution was perfused in the MBO at a flow rate of 3 mL min^{-1} for 20 hours to investigate the stability of coated heparin on PDMS surfaces (Figure 7.4.d). The strong heparin coating on PDMS could be because of the formation of hydrogen bonding between hydroxyl groups of heparin and the available oxygen atoms in PDMS backbone chains[36]. Furthermore, PBS samples were collected during the first 3-hours run to look for FITC-heparin in solution which could have shown that some heparin was detached

from the surface showing no discernable change in fluorescence intensity (Figure 7.4.e). These results suggested that the heparin coating was stable enough at the operating flow range.

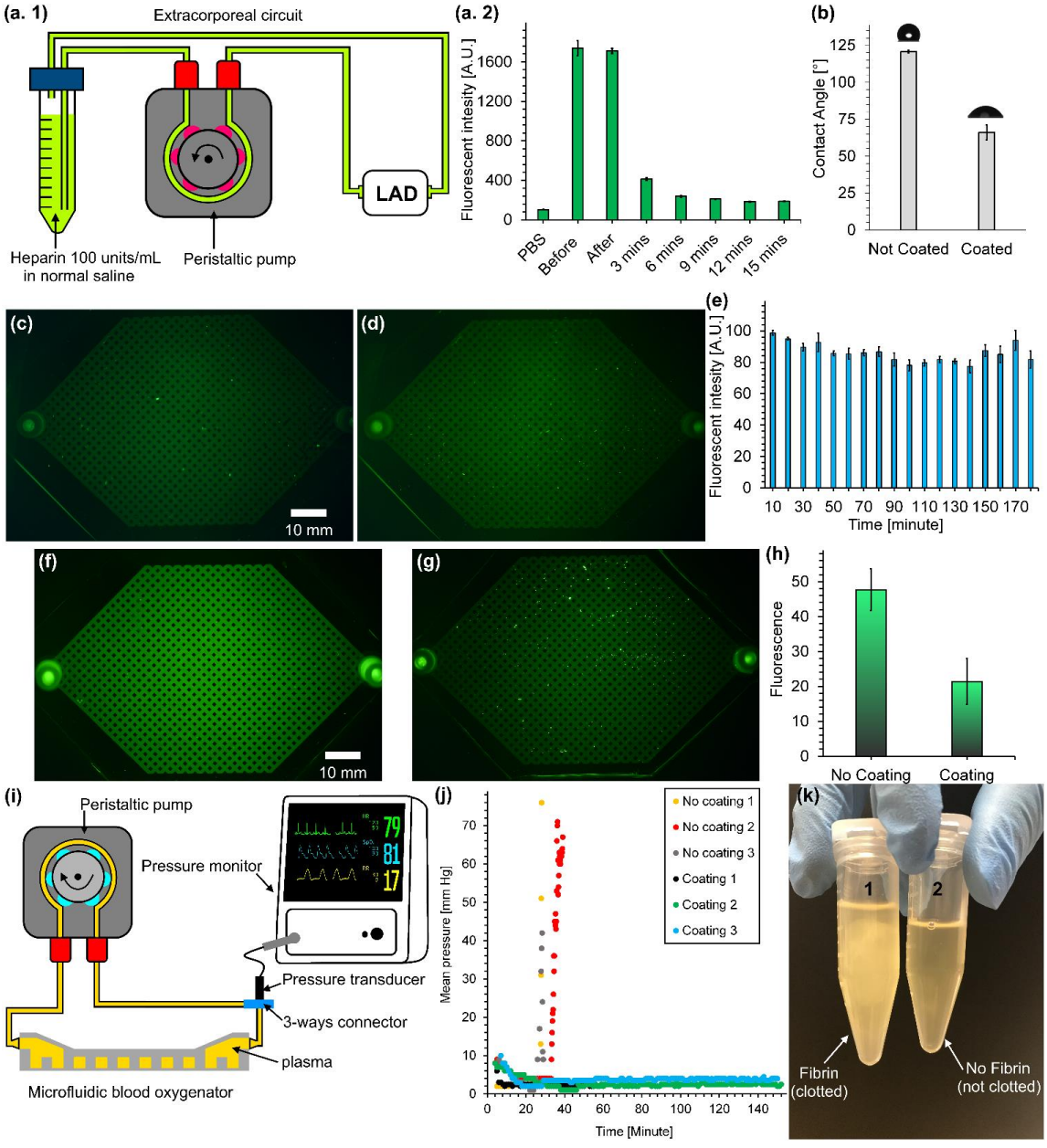

Figure 7.4: In vitro results for surface modification of PDMS with heparin: (a. 1) the experimental setup for coating, (a. 2) fluorescent intensity of collected samples after PBS washing a coated MBO with FITC-heparin, (b) contact angle measurements for not coated and coated surfaces, (c) a wide-angle view of an MBO coated with FITC-heparin, (d) a wide-angle view of a MBO coated with FITC-heparin after flowing

with PBS for 20 hours, (e) fluorescent intensity of collected samples after flowing a coated MBO with FITC-heparin for 3 hours, (f) a wide-angle view image of FITC−fibrinogen adhesion inside a non-coated MBO, (g) a wide-angle view image of FITC−fibrinogen adhesion inside a coated MBO with heparin, (h) fluorescent intensity comparison between non-coated and coated surfaces using ImageJ software, (i) the experimental setup for plasma coagulation pressure test, (j) a representative trace of pressure change in coated and non-coated MBOs, and (k) collected plasma after running the closed-loop for clotting test.

7.3.5 FITC−fibrinogen adhesion test

Fibrinogen adsorption experiments were conducted by adding FITC-fibrinogen to PBS buffer with a pH of 7.4 to investigate the antithrombotic property of the non-coated and coated surfaces. Coated and non-coated MBOs were perfused in a separate closed-loop containing 2 mg mL^{-1} FITC-fibrinogen for 3 hours and washed later by PBS (pH = 7.4) for 30 minutes. Then, MBOs (filled with PBS) were visualized by a wide-angle view fluorescence imaging setup to observe fibrinogen adsorption (Figure 7.4.f and g). The fluorescent intensity of each MBO was quantified using ImageJ software which showed a significant difference in fibrinogen adsorption between coated and non-coated MBOs suggesting that the heparin coating was effective in reducing fibrinogen adsorption (Figure 7.4.h). Antithrombin (AT) is a protein present in plasma which inhibits several factors involved in coagulation cascades, most importantly thrombin. Circulating AT in plasma can be bonded to immobilized heparin molecules on PDMS surface and form an AT-heparin complex which inhibits thrombin at higher rates, thereby preventing the conversion of soluble fibrinogen to insoluble fibrin strands. As a result, the chance of fibrinogen adsorption on PDMS surface and the fibrin formation was reduced significantly.

7.3.6 Accelerated Plasma coagulation test in MBOs

Formation of any micro-clots can impact the oxygenator's performance, especially one with microchannels that could be easily occluded by micro-clots resulting in mal-flow-distribution, a decrease of gas transfer rate, and finally device failure[37], [38]. Therefore, the plasma coagulation test was performed for both coated and non-coated MBOs using citrated plasma which was activated by adding $CaCl_2$. To activate the plasma, 5 mL 25 mM $CaCl_2$ was added to 5 mL human plasma and was transferred immediately to the

closed loop where the inlet and the outlet of the oxygenator were connected without leaving any air bubbles inside (Figure 7.4.i). Then, the plasma was pumped in the loop, and clotting was monitored by the increase in pressure at the inlet of the oxygenator. Mean pressure of non-coated MBOs increased after ~ 29 ± 3.5 minutes (as a comparison activated plasma samples with $CaCl_2$ stored in a falcon tube clotted around 20 minutes) while no perceptible change in pressure was observed in coated MBOs up to 150 minutes demonstrating that the heparin coating was sufficient enough to extend the clotting time (Figure 7.4.j). After the experiment, plasma collected from the uncoated devices showed precipitates in the form of clots while those from the coated devices were clear and had no precipitates (Figure 7.4.k).

7.3.7 Experimental setup of the newborn piglet model

The animal experiment model to perform in vivo studies was adopted from Rochow et. al[16] (Figure 7.5). A newborn piglet was first weighted (1.78 kg) and anesthetized by intraperitoneal injection of sodium pentobarbital (30 mg kg^{-1}, MTC Pharmaceutics, Cambridge, ON, Canada). To monitor the body temperature and maintain it at 39 °C during the experiment, an infant servo control (ISC) probe was placed on the piglet's abdomen. To provide controlled mechanical ventilation, an endotracheal tube (3.5 mm inner diameter, Portex, Keene, NH, USA) was placed via tracheostomy and connected to a Servo 300 ventilator (Siemens, Mississauga, ON, Canada). The ventilator was adjusted in a way to assure that the newborn piglet experienced a physiologic gas exchange at the beginning: peak inspiratory pressure (PIP) of 14 cm H_2O, positive end-expiratory pressure (PEEP) of 5 cm H_2O, inspiratory time (IT) of 0.33 s, and respiratory rate (RR) of 31 breaths min^{-1}. A mixture of oxygen (30 %) and nitrogen (70 %) was humidified and warmed up to 38 °C for delivering to the piglet (at a flow rate of 8 L min^{-1}). 22-G angio-catheters were used to cannulate femoral and abdominal veins for maintenance fluids: sodium pentobarbital (16 mg/kg), 5% dextrose (80 mg kg^{-1} day^{-1}), hydrocortisone and dopamine infusion (2 µg kg^{-1} min^{-1}). The dopamine was adjusted (2 to 20 µg kg^{-1} min^{-1}) to maintain the mean systematic blood pressure in a range of 68 – 80 mmHg. During the

experiment, the piglet was paralyzed using a muscle relaxant Pancuronium with an initial bolus 0.2 mg kg^{-1} and continuous infusion of 20 µg kg^{-1} min^{-1}.

Two 14-G 1.1-inch angio-catheters (Angiocath) were used to cannulate left carotid artery and right jugular vein for creating an extracorporeal circuit in which the LAD was attached. This circuit consisted of two loops: 1) shortcut bypass and 2) the LAD bypass. Once one of the bypasses was opened, the other one was closed. A flow sensor (in the main line) with a monitor and a pressure transducer (in a branching line connected to the main line) with a blood pressure monitor were installed in the circuit to report the extracorporeal blood flow rate and blood pressure.

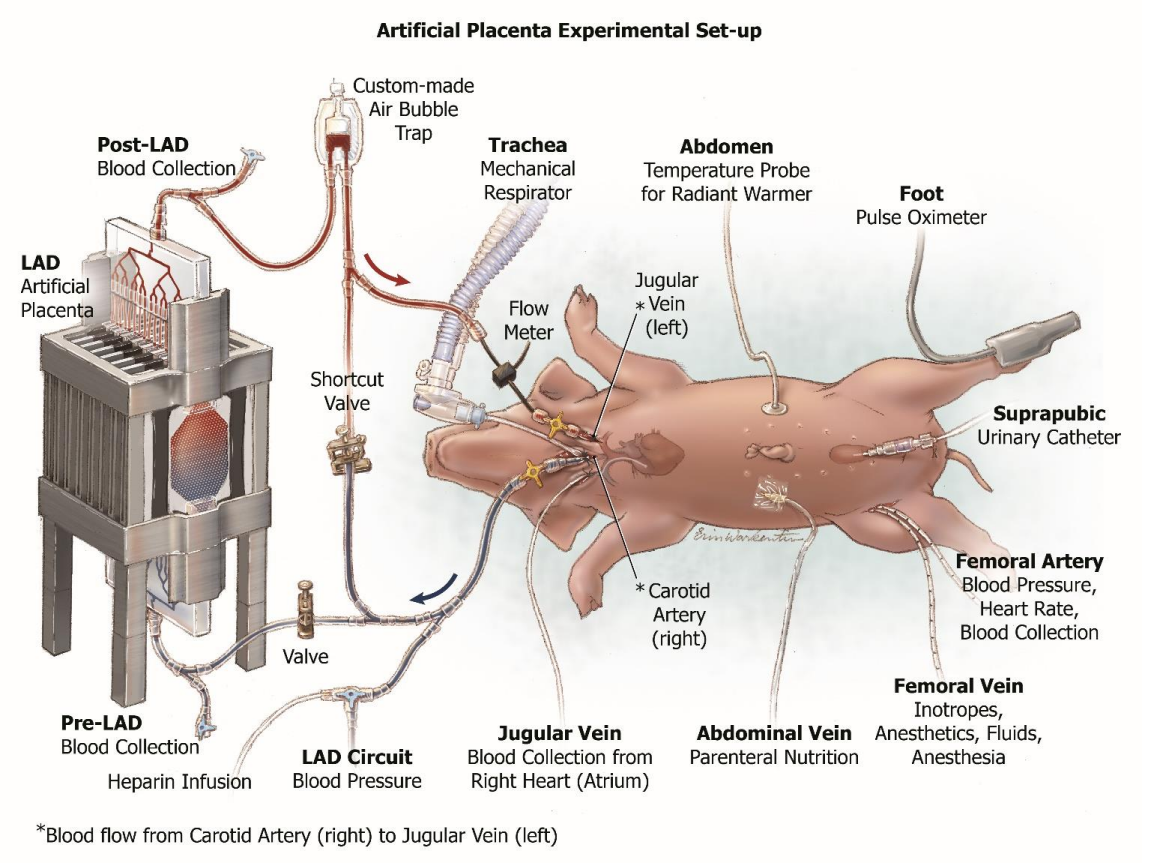

Figure 7.5: Experimental setup of the newborn piglet model for testing a pumpless neonatal lung assist device for artificial placenta application.

While the extracorporeal circuit was connected, a bolus of 400 units kg^{-1} of heparin as an anticoagulant was delivered to the piglet and maintained at an infusion rate of 30 units kg^{-}

^{1} h^{-1}. Access to the right femoral artery was achieved by insertion of a 3.5 Fr Argyle umbilical catheter. This vascular access was used to measure systemic blood pressure, heart rate, and for blood collections. An effort was made to secure the catheter in the place, and it was being perfused by a heparinized normal saline solution with a concentration of 3 units mL^{-1} at a perfusion rate of 1.5 mL h^{-1}. A pressure transducer with a blood pressure monitor was attached to the catheter to monitor systemic blood pressure during the experiment. Another vascular access was established via right internal jugular vein using a 3.5 Fr Argyle umbilical catheter which was advanced under ultrasound into the right atrium of the heart which allows measuring the mixed blood (systemic venous blood and LAD oxygenized). Peripheral oxygen saturation was also monitored using a pulse oximeter which was placed on one of the feet.

The study protocol was approved by the McMaster University Animal Research Ethics Board (AREB #10-03-14).

7.3.8 The animal experiment procedure for artificial placenta application

The LAD was tested in vivo using oxygen as the sweep gas or exposing the LAD directly to room air. Once the extracorporeal circuit was constructed and perfused by pressure differential provided by the piglet's heart, the LAD's bypass was closed, and blood flowed through the shortcut line under a normoxic condition to ensure that all vital parameters were steady (termed Shortcut Normoxic). Next, a hypoxic condition was simulated for the piglet by adjusting the ventilator to the following settings: PIP of 10 cm H_2O, PEEP of 5 cm H_2O, IT of 0.33 s, and RR of 15 – 19 breaths min^{-1}. While under hypoxic conditions, the piglet was tested with the blood flowing through the shortcut (termed Shortcut Hypoxic) and also when the shortcut was closed and the blood flowed through the LAD (termed LAD Hypoxic). Figure 7.6 shows the sequence of conditions that the piglet was exposed to over the time frame for the in-vivo experiment. Initially, baseline measurements were made by exposing the piglet to normoxic condition with the blood flowing through the shortcut. Then, hypoxic condition was initiated, and blood flow switched between the shortcut and through the LAD in three cycles each when the

LAD is exposed to pure oxygen and air. Multiple blood samples were taken under each of these conditions and at various time points as shown in Figure 7.6**.** The blood samples were collected from the femoral artery, right atrium, before the LAD, and after the LAD to conduct blood gas analysis. At the end of the experiment, shortcut normoxic condition was established (control) and a final set of blood samples were taken for measurement of blood gas levels.

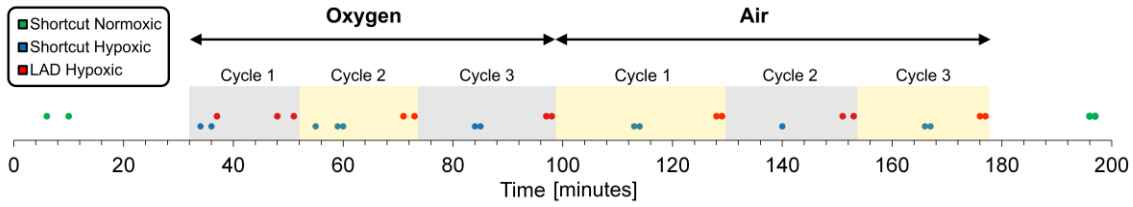

Figure 7.6: Time sequence of in-vivo measurements indicating the conditions that the piglet was exposed and the timepoints where blood samples where extracted.

7.3.9 Systematic blood measurements

It is vital to discern the effect of the extracorporeal circuit on systematic blood parameters such as blood flow rate, heart rate, mean LAD/shortcut pressure, and mean blood pressure. Since the LAD was connected to the systemic circulation (an arteriovenous connection) in a parallel configuration, the resistance to blood flow would reduced which would result in a higher systemic blood flow rate (under short cut normoxic condition). When the piglet is made hypoxic, the systemic blood flow rate was found to increase as it compensates for the lower oxygen saturation level in blood (Figure 7.7.a and e). However, when the extracorporeal blood circulation is switched from the shortcut to the LAD, it adds not only oxygen to the blood but also increases the resistance in this parallel circuit. This results in the observed lowering of the systemic blood flow rate when the LAD is connected. Heart rate was found to be elevated under the hypoxic condition to pump blood faster and increase the rate of gas exchange, but it dropped back to normal levels when the LAD became active indicating that the LAD was successful in alleviating the hypoxic condition (Figure 7.7.b and f).

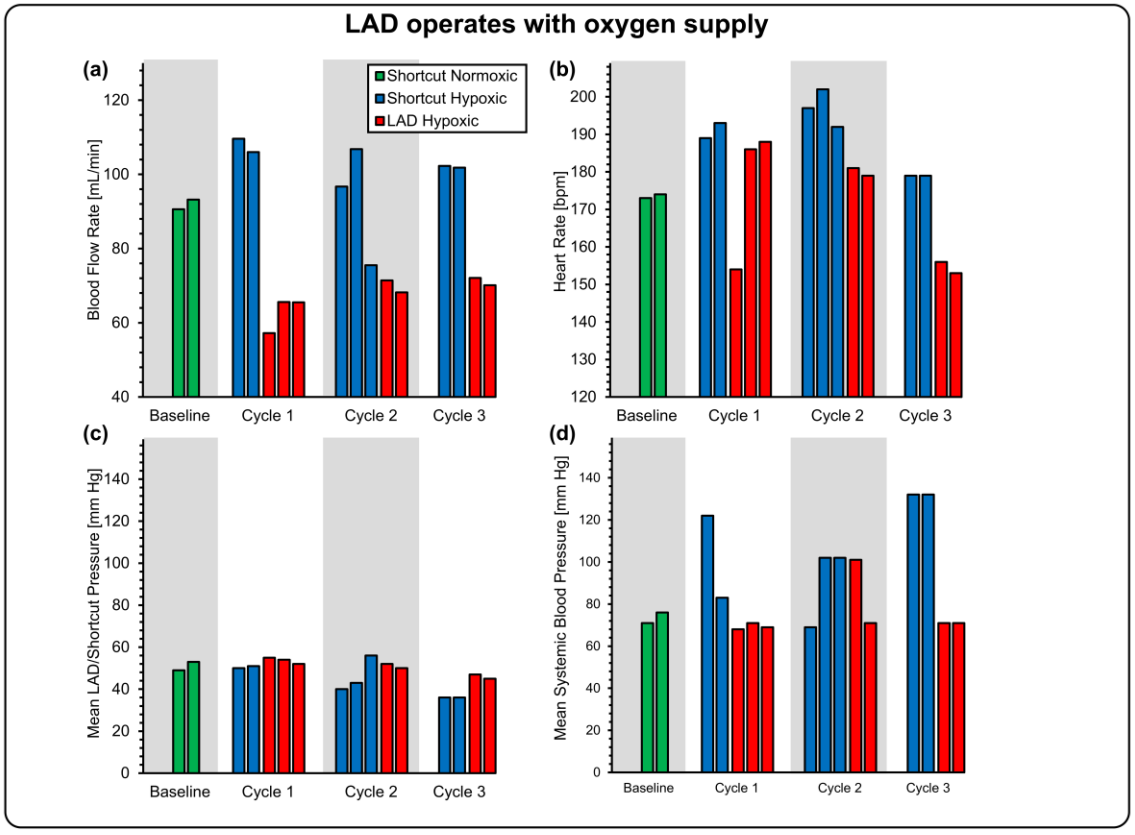
LAD operates with oxygen supply
(a)
Shortcut Normoxic
Shortcut Hypoxic
LAD Hypoxic
Blood Flow Rate [mL/min]
120
100
80
60
40
Baseline
Cycle 1
Cycle 2
Cycle 3
(b)
Heart Rate [bpm]
200
190
180
170
160
150
140
130
120
(c)
Mean LAD/Shortcut Pressure [mm Hg]
140
120
100
80
60
40
20
0
(d)
Mean Systemic Blood Pressure [mm Hg]

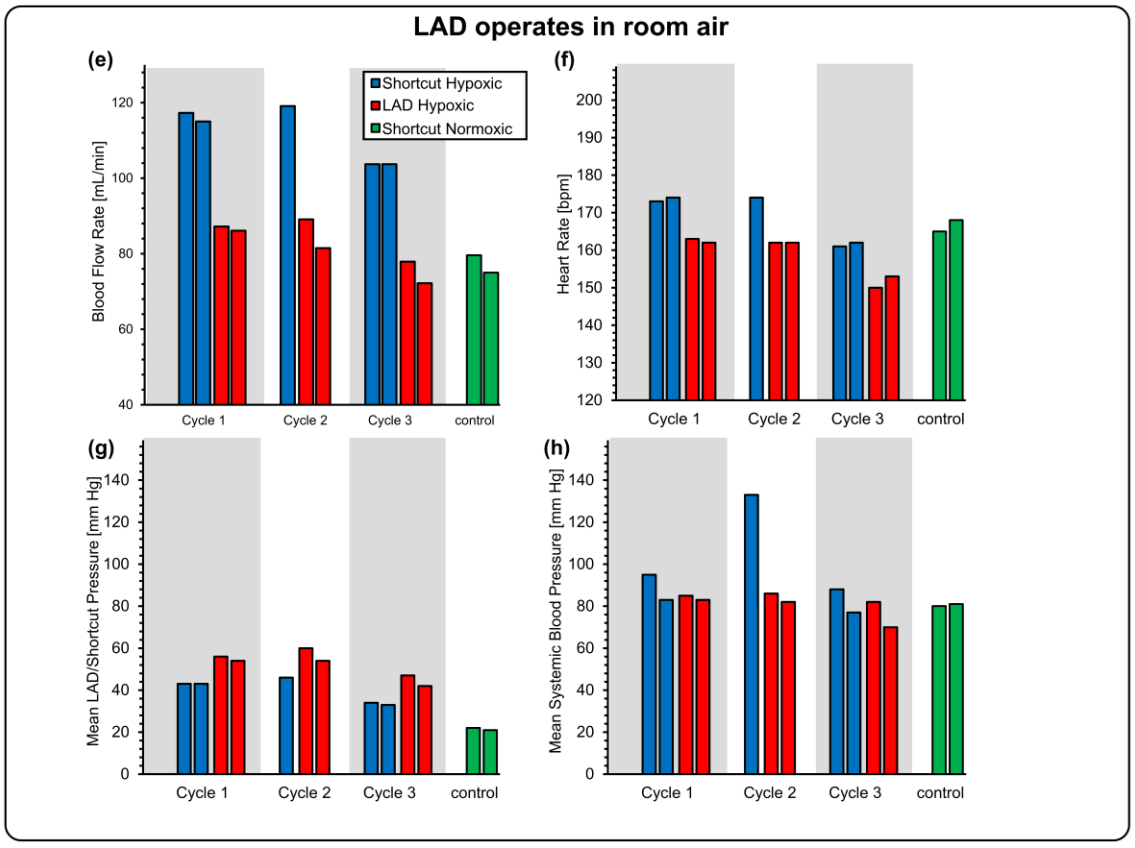
LAD operates in room air
(e)
Shortcut Hypoxic
LAD Hypoxic
Shortcut Normoxic
Blood Flow Rate [mL/min]
120
100
80
60
40
Cycle 1
Cycle 2
Cycle 3
control
(f)
Heart Rate [bpm]
200
190
180
170
160
150
140
130
120
(g)
Mean LAD/Shortcut Pressure [mm Hg]
140
120
100
80
60
40
20
0
(h)
Mean Systemic Blood Pressure [mm Hg]

Figure 7.7: Effect of extracorporeal bypass on cardiovascular parameters: (a) blood flow rate while the LAD was using oxygen as the sweep gas, (b) heart rate while the LAD was using oxygen as the sweep gas, (c) mean LAD/shortcut pressure while the LAD was using oxygen as the sweep gas, (d) mean systemic arterial blood pressure measured at the femoral artery while the LAD was using oxygen as the sweep gas, (e) blood flow rate when the LAD was exposed to room air, (f) heart rate when the LAD was exposed to room air, (g) mean LAD/shortcut pressure when the LAD was exposed to room air, and (h) mean systemic arterial blood pressure measured at the femoral artery when the LAD was exposed to room air.

The mean blood pressure at the location where the blood emerges extracorporeally (Figure 7.7.c and g) was always lower in the shortcut hypoxic condition compared to the LAD hypoxic confirming that the LAD line achieved lower flow rates. Moreover, mean systemic blood pressure (at the femoral artery) (Figure 7.7.d and h) was elevated under the hypoxic conditions and returns to normal levels when oxygenation through the LAD is initiated.

7.3.10 In vivo gas exchange testing

At the end of each cycle, blood samples were collected extracorporeally before and after the LAD as well as from the femoral artery and the jugular vein from the right cardiac atrium to determine systemic blood gas levels. The saturation of oxygen (SaO_2), partial pressure of oxygen (pO_2), and partial pressure of carbon dioxide (pCO_2) were measured in these samples by a blood gas analyzer. Under the shortcut hypoxic condition, the blood flow rate was stable and ranged from 102 mL min^{-1} to 110 mL min^{-1}. When the LAD (LAD hypoxic condition) was connected, its hydraulic resistance was low enough for it to be perfused solely by the piglet's heart and generate a stable blood flow rate from 65 mL min^{-1} to 72 mL min^{-1} (37 – 41 mL min^{-1} kg^{-1}), clearly demonstrating that the design was able to support clinically relevant flow rates in a pumpless manner. When the LAD was placed in an enriched oxygen environment (a chamber with slight oxygen flow of ~ 15 L hr^{-1}), the LAD was able to fully oxygenate the blood at these relevant flow rates in all experiments. In one instance, it was able to increase the Sa O_2 from a low 78 % to 100% at a high blood flow rate of ~ 70 mL min^{-1} (Figure 7.8.a). The LAD also could significantly increase the pO_2 up to 473 mm Hg (as compared to 68 mm Hg at its inlet) resulting in highly oxygenated blood leaving the LAD outlet **(**Figure 7.8.b**)**. pCO_2 was

also decreased at this condition with a maximum drop of 81 mm Hg to 50 mm Hg at a blood flow rate of 70 mL min^{-1} (Figure 7.8.c).

When the LAD was exposed to ambient air, the gas exchange performance was lower but still significant. For instance, in one cycle, the LAD was capable of increasing the SaO_2 from 73 % to 90 % at a high blood flow rate of 85 mL min^{-1} (Figure 7.8.d**)** demonstrating a clinically relevant performance during pumpless operation. pO_2 was significantly enhanced after the LAD and a maximum value of 66 mm Hg was reached at a blood flow rate of 85 mL min^{-1} **(**Figure 7.8.e**)**. pCO_2 was also reduced after the LAD **(**Figure 7.8. f).

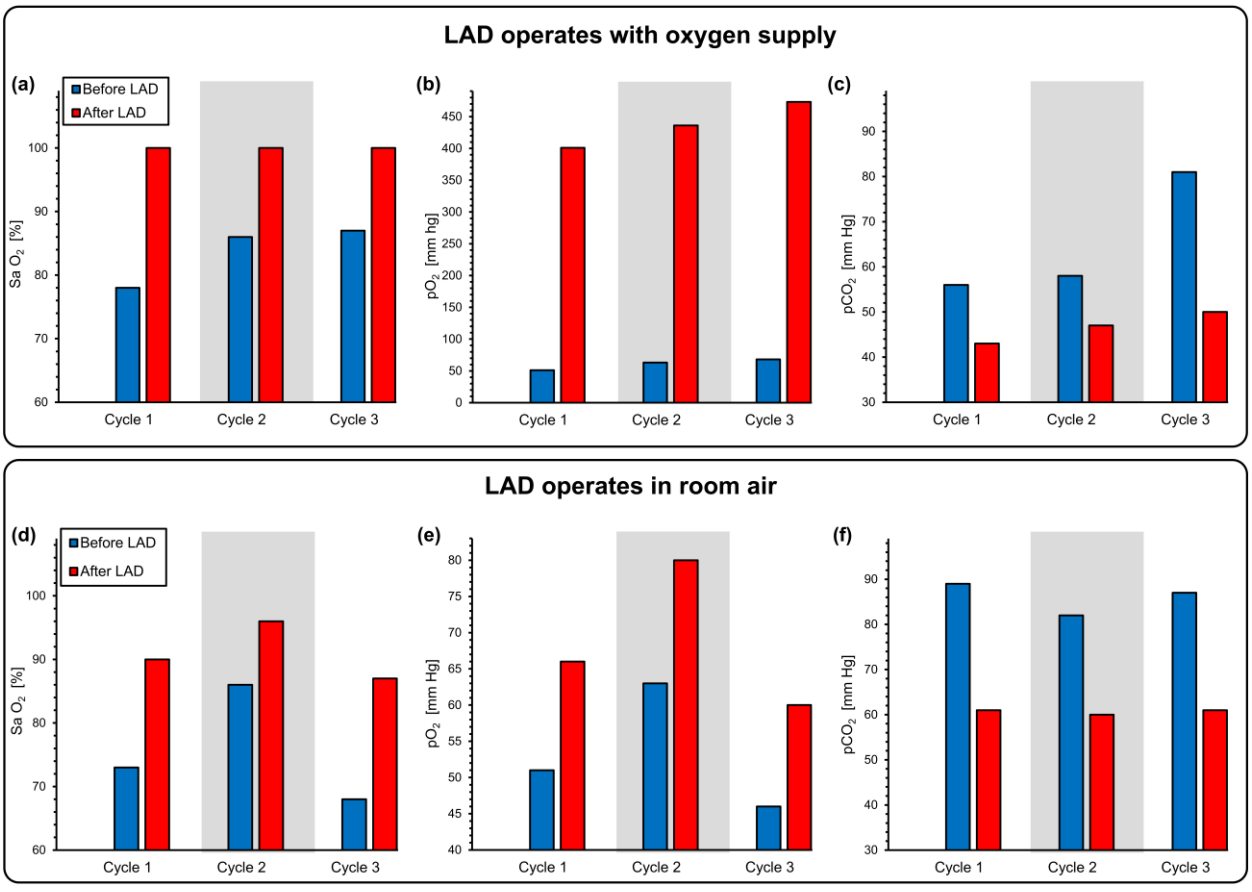

Figure 7.8: Gas exchange at the LAD when connected in-vivo to a piglet. Measurements were of the blood at the inlet and outlet of the LAD when it is connected to the piglet and pumped by the arterio-venous pressure difference: (a) pO_2,(b) Sa O_2, (c) pCO_2 before and after the LAD using oxygen as the sweep gas, and (d) pO_2, (e) Sa O_2, (f) pCO_2 before and after the LAD exposed directly to room air.

All these parameters (pO_2, SaO_2, and pCO_2) were also measured at the femoral artery and right atrium (mixed deoxygenated blood after being consumed by the body) to determine the impact of the LAD on systemic oxygenation for the piglet. All measurements were performed when the piglet was under the hypoxic condition. Both systemic pO_2 and SaO_2 (femoral) increased when the LAD exposed to pure oxygen environment was connected with the hypoxic piglet with a maximum increase of 41 mm Hg to 66 mm Hg in pO_2 and 52 % to 86 % in SaO_2 (Figure 7.9.a and b). When the LAD was exposed to room air, the increase in systemic pO_2 and SaO_2 was lower but a promising increase of pO_2 from 42 mm Hg to 63 mm Hg and Sa O_2 from 56 % to 84 % at a blood flow rate 88 mL min^{-1} was achieved (Figure 7.9.d and e). pCO2 was also decreased in both oxygen environment and room air (Figure 7.9.c and f).

Similar behavior was observed when measurements were performed at the right heart (atrium). Systemic pO_2 and Sa O_2 significantly increased when connected to the LAD but their values at the atrium (Figure 7.9.g and h) were lower than levels immediately after the LAD as blood in the atrium is a mixture of the venous blood from the systemic circulation which is usually rich in carbon dioxide and poor in oxygen with the oxygenated blood from the LAD. During each cycle, pCO_2 was also a little elevated after connecting the LAD which was placed under an oxygen-rich hood (Figure 7.9.i). When the LAD was exposed to room air, pO_2 and Sa O_2 measured from right atrium also showed an improvement in oxygen content in blood (Figure 7.9.j and k). This time, pCO_2 was slightly lower after switching from the shortcut to the LAD extracorporeal connection under hypoxic conditions suggesting that the LAD could be more effective in removing carbon dioxide while exposed to room air (Figure 7.9.l). As expected, the oxygen saturation level was dropped in both the femoral artery and the right atrium when the piglet was in hypoxic state and the LAD was inactive (Figure 7.9). However, the saturation level significantly increased when the LAD was connected. For instance, when exposed to the hypoxic condition the oxygen saturation level in the right atrium dropped to 19 % but increased to 57 % after connecting the LAD (Figure 7.9.h).

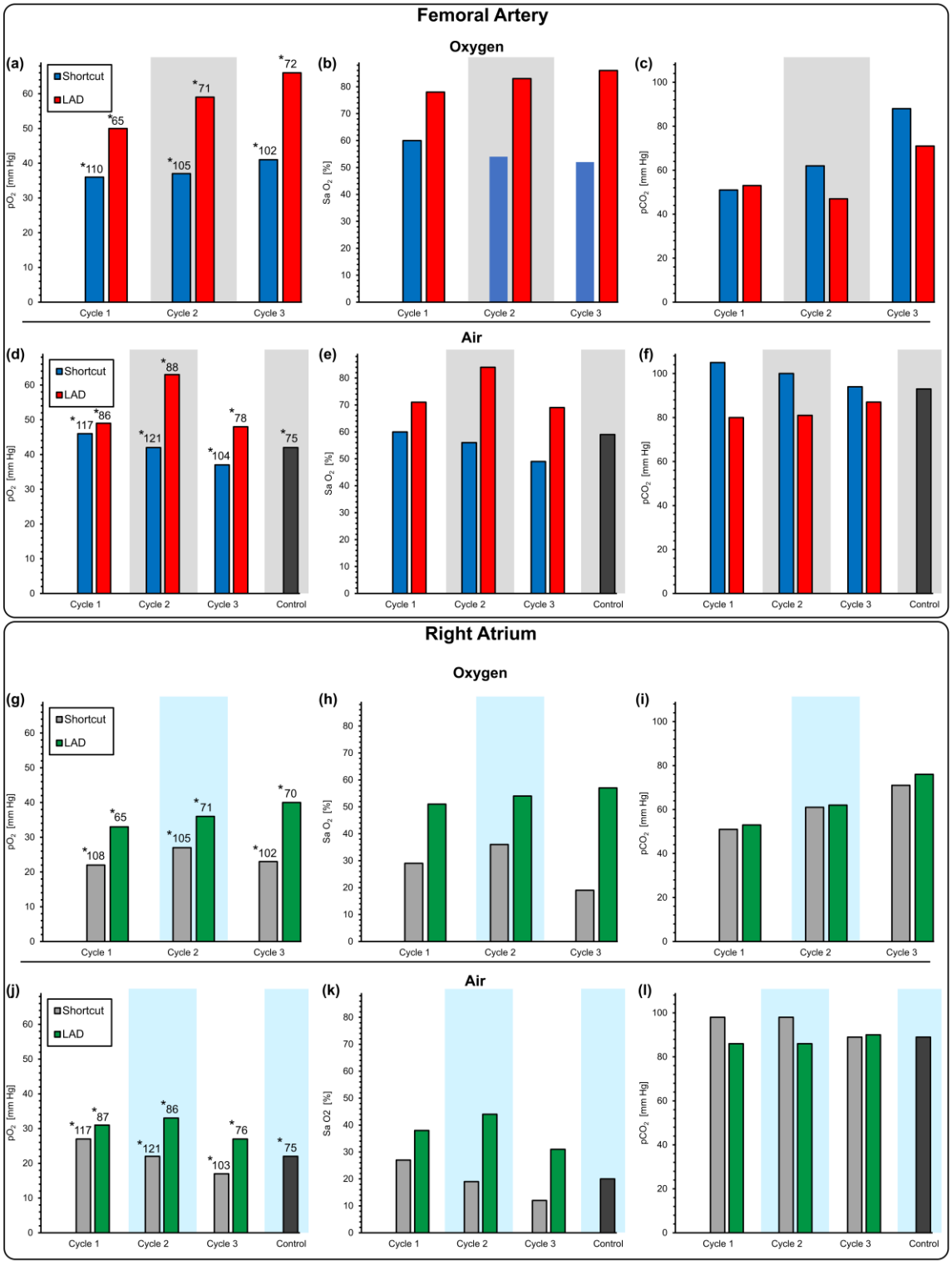

Figure 7.9: Gas exchange at the femoral artery and the right atrium when connected in-vivo to a piglet. Measurements were of the blood at the femoral artery and the right atrium when the LAD is connected to

*the piglet and pumped by the arterio-venous pressure difference (a) pO_2,(b) Sa O_2 ,(c) pCO_2 for femoral artery using oxygen as the sweep gas, (d) pO_2 ,(e) Sa O_2 ,(f) pCO_2 for femoral artery exposed directly to room air, and (g) pO_2,(h) Sa O_2 ,(i) pCO_2 for right atrium using oxygen as the sweep gas, (j) pO_2 ,(k) Sa O_2 ,(l) pCO_2 for right atrium exposed directly to room air. * values are flow rates (mL min^{-1}) in the shortcut or the LAD.*

Also, this effect was observed when the LAD operated in room air with a maximum rise from 31 % to 59 % in Sa O_2 (Figure 7.9.k). These results indicate that that LAD has a significant effect in increasing the blood gas levels even in systemic circulation and performs effectively as a lung assist device.

7.3.11 Metabolic analysis by sampling from the femoral artery

For each cycle, blood samples were collected from the femoral artery to analyze the pH of blood, bicarbonate content, and base excess (BE) (Figure 7.10).

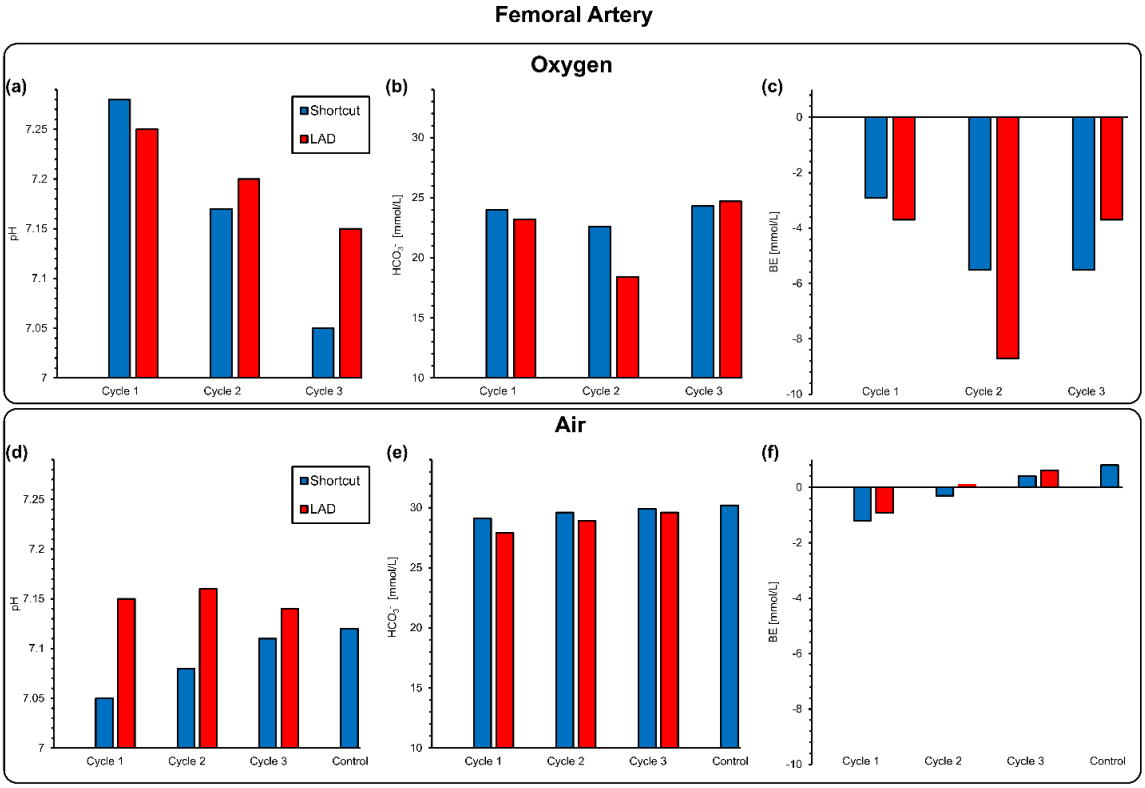

Figure 7.10: The metabolic analysis: (a) pH measurement, (b) bicarbonate content, (c) base excess pCO_2 for femoral artery using oxygen as the sweep gas, and (d) pH measurement, (e) bicarbonate content, and (f) base excess for femoral artery exposed directly to room air.

7.4 Discussion

We tested a new LAD which was constructed of 16 stacked MBOs and designed to support preterm and term infants with respiratory failure in a newborn piglet model. In this study, the LAD provided significant gas exchange throughout a period of ~ 200 minutes. The current extracorporeal circuit achieves blood flow rates through the LAD comparable with one-third of the cardiac output which was adequate to maintain the piglet cardiovascularly stable throughout the experiment. Our concept of the LAD includes the features of an artificial placenta which allows the newborn to continue to breathe while a partial fetal circulation via the umbilical artery, LAD circuit, and the umbilical vein is established [16]. The idea, however, is that the newborn will continue to breathe while the LAD provides additional gas exchange and allows the lungs to heal. Although our concept of the artificial placenta is designed to be connected to the umbilical vessels[16], at this developmental stage, we used vascular access via carotid artery and jugular vein. This is a compromise of the piglet model. We found that in a one-day-old piglet, the lumen of the umbilical vessels became fibrotic and using a Seldinger wire technique, catheters not bigger than an outer diameter of 1.2 mm could be placed. Other researchers used lamb models which have umbilical vessels with large diameters[1]–[3], [39]. Two approaches have been taken for artificial placenta applications. The first is to develop a womb like configuration where the entire oxygenation occurs extracorporeally[1], [2], [39]–[41]. In this approach, they use a commercial, high priming volume, hollow fiber oxygenator and an external pump for blood perfusion as preterm lamb models that match the appropriate gestational age are heavier (up to ~ 5 kgs) as compared with humans (1-2 kgs). The second is where partial extracorporeal support is provided[16] to compensate the loss in gas exchange capacity of lungs. As a result, a fully extracorporeal oxygenation is not needed, therefore, we specifically designed and optimized our microfluidic LAD for human preterm neonates and to facilitate pumpless extracorporeal support with the minimum possible priming volume. The ability to custom fabricate the microfluidic oxygenator allowed us to achieve the specific design criteria for the priming volume, hydraulic resistance and oxygen

uptake for human preterm neonates. By using the piglet of the same birthweight, rather than the same gestational age, as the neonate, we were able to accurately test the extracorporeal system for oxygenation performance. The smaller priming volume of this oxygenator also mitigated the effect of hemodilution when the saline that was used to fill it was mixed with the venous blood. The custom and modular design was also critical for pumpless operation as hydraulic resistance of the oxygenator could be tailored to produce adequate blood perfusion and oxygen uptake based on the baby's weight and an external pump could be eliminated.

Since the arteriovenous pressure difference in a neonate is typically between 20 – 60 mm Hg[12], [16], [21]–[23], such a pressure head applied to this LAD would generate a flow rate between 65 - 86 mL min^{-1} in this LAD which meets the requirement of a blood flow rate of 20 – 30 mL min^{-1} kg^{-1} of a neonate typically needed to provide lung assist function (Figure 7.7.a and e). In this range of flow rates and under in-vitro conditions, this LAD was able to increase the oxygen saturation level from ~ 75 % to ~ 100 % which would be sufficient to fulfill oxygenation need for these preterm babies[12], [16], [21]–[23].

Of note, the hemoglobin of the piglet was at a lower level (hematocrit: 23 to 27%) in this experiment. A preterm infant has usually considerably higher hematocrit level (40 to 60%)[42], and as a result, the oxygen-carrying capacity of the blood would allow higher amounts of gas exchange and oxygen delivery. As the hematocrit level in preterm neonates is higher an elaborate calculation is performed in the supplementary to predicate the amount of oxygen transfer by the LAD when blood would have higher hemoglobin content. In this calculation, it is assumed that the hemoglobin content decreases[42] and the blood flow rate increases[43] as a neonate is growing. Then, the amount of oxygen transfer was calculated for preterm neonates with different weights up to 1 kg over a period of 96 hours after birth (Shown in supplementary Figure 3.5). As a result, the current configuration of the LAD would allow a gas exchange of 4.2 mL min^{-1} kg^{-1} using oxygen as the sweep gas or 3.1 mL min^{-1} kg^{-1} while the LAD would be exposed to room air for a one-kg preterm at 96 hours postnatal age which would be sufficient to replace 50 to 75 % of the oxygen requirements for the resting energy expenditure of a preterm

infant[44], [45] (≤ 1 kg). The oxygen consumption by a one-kg preterm neonate after 96 hours was estimated to be ~ 7 mL min^{-1} kg^{-1} that an artificial placenta type oxygenator would need to provide ~ 30 % of this value[8], [16]. Our approach provides an arteriovenous connection for the LAD. A portion of the blood which has left the lungs and has been partially oxygenated will subsequently directed extracorporeally into the LAD. The LAD provides an assist function by further increasing the saturation of the blood entering it so that systemic levels could be improved. In addition, results from in vitro testing using blood suggests that the LAD used in this study had the potential to raise oxygen saturation level by ~ 25 % in room air with a corresponding blood flow rate of 50 mL min^{-1} which is suitable for supporting a body weight of up to 1.5 kg[8].

Further, the decrease of the hematocrit by 4% points from 27% to 23% would require a transfusion of approximately 4 mL/kg of packed red blood cells to replace this loss. This is considered a low amount and proves that our LAD circuit has a minimized filling volume which makes it feasible for micro-preemies.

The piglet was cardiovascularly stable throughout the entire in-vivo experimentation that occurred over a period of ~ 200 minutes. We did not observe bradycardia or tachycardia, or arrhythmia and the blood pressure was in the desired range. Our LAD was connected in parallel to the systemic circulation and considerable amounts of blood bypassing the systemic circulation extracorporeally. The bypassed blood flow (65 – 86 mL min^{-1}) compromises up to one-third of the cardiac output. This clinical condition is similar to a large patent ductus arteriosus or a ventricle septum defect and could pose a risk to the heart of high cardiac output failure. Clinical signs would be tachycardia, low systemic blood pressure, and lactacidemia. We found that blood pressure of the piglet remained stable (Figure 7.7.d and h), no significant increase of the heart rate (Figure 7.7.b and f) was noted, and no metabolic acidosis could be observed (Figure 7.10).

The oxygen saturation level in preterm neonates with respiratory failure should be maintained in an acceptable range. A pulse oximeter is a typical method to monitor the oxygen saturation in a neonatal intensive care unit. Although the optimal pulse oxygen

saturation (SpO_2) is still uncertain, this measurement can be used to balance the oxygen needs of preterm neonates[46]–[50]. Here, we decreased the respiratory rate in the ventilator aiming for a SpO_2 of lower levels similar to the condition that a preterm neonate may experience. The goal was to raise and maintain SpO_2 in the range of 85 – 95 % after administrating our LAD. This importance was achieved in all three cycles while the LAD was supplied by pure oxygen (SpO_2) (results are shown in Supplementary Figure. 3.9). In the third cycle, SpO_2 was 57 % under shortcut hypoxic and improved significantly to 91 once the LAD became active. After switching the ventilation gas to room air, the LAD was still able to increase SpO_2 during all cycles. Only in the second cycle, SpO_2 was raised and maintained to the suggested values (it raised from 69 % to 90 %). However, lower oxygenation level (81 %) in the first cycle could happen because of very hypoxic condition in the piglet (SpO_2 was 42 % at the end of shortcut hypoxic) which seems to be an unrealistic situation in the case of preterm neonates. In the third cycle, entering blood to the LAD was at a lower level of 68 % compared to other cycles (73 % and 86 % for the first and second cycles) suggesting that the piglet did not reach to a stable condition or incur a very undesirable hypoxic condition. In overall, the LAD could ameliorate poor oxygenation either using oxygen or room air as the ventilation gas when the piglet was under an acceptable hypoxic condition. Moreover, SpO_2 in healthy newborn piglets with a weight of 1.77 ± 0.13 kg varies from 84 to 96 %[51].

The piglet was exposed to significant insensible water losses. There are two main contributing factors: first, the piglet is exposed to a radiant warmer to maintain a body temperate of 39°C and promotes evaporation of water. Studies of ventilated ill newborns under a radiant warmer showed that these infants lose $28.04 \cdot e^{-1.73(Weight\ in\ kg)}$ ml/kg/hr[52]. Second, the LAD is composed of PDMS which is permeable to water. Water from the circulating blood could have evaporated as a result. Throughout the experiment, the piglet received more than 15 ml/kg/hr of normal saline. The blood gases did not show signs of metabolic acidosis, the hydrogen carbonate remained in desired range, as well as the urine output was stable indicating sufficient hydration. As a result, a

possible future modification to minimize evaporation and prevent heat loss can be to surround the LAD by humified air.

We used low dose hydrocortisone and dopamine in this study to allow sufficient stress response, to minimize inflammatory responses and to provide vascular tone. In our experimental setting, the piglet underwent surgery for the establishment of the tracheostomy and catheters are placed invasively. Further, exposing the piglet's blood to the extracorporeal tubes and LAD can potentially induce inflammation including mild capillary leak syndrome. An increase in vascular tone by dopamine as well as the effects of hydrocortisone on the reduction of inflammation and blood pressure provide a stable condition for this experiment.

A key feature of our LAD is the coating of inner surfaces to prevent blood clotting and to establish hemocompatibility. In our experiment, we primed the LAD with a normal saline and heparin solution. It could be hypothesized that some of the heparin is absorbed by the PDMS. This bonding could be explained by the formation of hydrogen bonding or electrostatic interaction between heparin molecules and PDMS chains[36]. However, this approach alone was not sufficient to prevent blood clotting and we used it in conjunction with a typical systemic dose of heparin for systemic anticoagulation. Nevertheless, coating was important in preventing any deleterious clot formation on the surfaces of the oxygenators and critical for smooth operation of the LAD in in-vivo experiments. In preterm infants, this approach of systemic anticoagulation may not be feasible. Preterm infants are at high risk for intraventricular hemorrhage (IVH); in particular, those infants who are born preterm from mothers with chorioamnionitis, HELLP, or preeclampsia. Systemic anticoagulation would elevate this risk significantly. Initial work to achieve hemocompatibility of the LAD has been done by our group. The coating of inner surfaces of the LAD, the tubes, and the catheter with the novel antithrombin-heparin-complex are promising[38], [53]. This type of coating could be applied to all internal surfaces to enhance hemocompatibility.

Sixteen MBOs are sufficient for a body weight of 500 to ~1500 gram while the LAD is exposed to room air (in the case of using oxygen as the sweep gas, this number of MBOs in our LAD would support a body weight of up to 2000 gram). Bigger newborns would require a stacked LAD with more MBO units.

7.5 Conclusion

In this study, a pumpless LAD using microfluidic blood oxygenators for preterm neonates suffering from RDS was developed. In vitro assessments were done by blood to investigate the gas exchange capacity of this LAD resulting in an acceptable gas transfer in room air and ample oxygenation in an oxygen-rich environment. A simple coating technique was developed to coat blood-in-contact surfaces. The functionality and stability of this coating were evaluated in vitro suggesting that the coating was effective and stable enough to be used in further animal studies. In the next step, the LAD was tested in a pumpless operation connecting to a newborn piglet. Results from the piglet experiments revealed the effectiveness of this LAD in gas exchange without complications and agreed with in vitro results. Further steps in the development of the LAD include the installation of hemocompatibility and biocompatibility as well as the development of the vascular access via umbilical vessels.

References

[1] E. A. Partridge *et al.*, "An extra-uterine system to physiologically support the extreme premature lamb," *Nat. Commun.*, vol. 8, p. 15112, 2017.

[2] J. T. Church *et al.*, "The artificial placenta: Continued lung development during extracorporeal support in a preterm lamb model," *J. Pediatr. Surg.*, vol. 53, no. 10, pp. 1896–1903, 2018.

[3] B. Bryner *et al.*, "An extracorporeal artificial placenta supports extremely premature lambs for 1 week.," *J. Pediatr. Surg.*, vol. 50, no. 1, pp. 44–9, Jan. 2015.

[4] B. J. Stoll *et al.*, "Trends in Care Practices, Morbidity, and Mortality of Extremely Preterm Neonates, 1993-2012," *JAMA*, vol. 314, no. 10, p. 1039, Sep. 2015.

[5] B. N. Manktelow, S. E. Seaton, D. J. Field, and E. S. Draper, "Population-based estimates of in-unit survival for very preterm infants.," *Pediatrics*, vol. 131, no. 2, pp. e425-32, Feb. 2013.

[6] M. Laughon *et al.*, "Chronic lung disease and developmental delay at 2 years of age in children born before 28 weeks' gestation.," *Pediatrics*, vol. 124, no. 2, pp. 637–48, Aug. 2009.

[7] B. J. Stoll *et al.*, "Neonatal outcomes of extremely preterm infants from the NICHD Neonatal Research Network.," *Pediatrics*, vol. 126, no. 3, pp. 443–56, Sep. 2010.

[8] N. Rochow *et al.*, "Artificial placenta -Lung assist devices for term and preterm newborns with respiratory failure," *Int J Artif Organs*, vol. 36, pp. 377–391, 2013.

[9] A. G. S. Philip, "Bronchopulmonary dysplasia: then and now.," *Neonatology*, vol. 102, no. 1, pp. 1–8, 2012.

[10] H. M. Chambers and D. van Velzen, "Ventilator-related pathology in the extremely immature lung," *Pathology*, vol. 21, no. 2, pp. 79–83, Jan. 1989.

[11] M. A. Attar and S. M. Donn, "Mechanisms of ventilator-induced lung injury in premature infants," *Semin. Neonatol.*, vol. 7, no. 5, pp. 353–360, Oct. 2002.

[12] W.-I. Wu *et al.*, "Lung assist device: development of microfluidic oxygenators for preterm infants with respiratory failure.," in *Lab on a chip*, 2013, vol. 13, no. 13, pp. 2641–50.

[13] A. F. J. Van Heijst, A. C. De Mol, and H. IJsselstijn, "ECMO in neonates: Neuroimaging findings and outcome," *Semin. Perinatol.*, vol. 38, no. 2, pp. 104–113, 2014.

[14] W. J. Federspiel and K. A. Henchir, "Lung, Artificial: Basic Principles and Current Applications," *Encyclopedia of Biomaterials and Biomedical Engineering, edited by G.L. Bowlin and G. Wnek*

(Marcel 49 Dekker, New York, 2004). Marcel Dekker, Inc, New York, pp. 910–921, 2004.

[15] J. K. Lee, H. H. Kung, and L. F. Mockros, "Microchannel Technologies for Artificial Lungs: (1) Theory," *ASAIO J.*, vol. 54, no. 4, pp. 372–382, Jul. 2008.

[16] N. Rochow *et al.*, "An Integrated Array of Microfluidic Oxygenators as a Neonatal Lung Assist Device: In Vitro Characterization and In Vivo Demonstration," *Artif. Organs*, vol. 38, no. 10, pp. 856–866, Oct. 2014.

[17] K. M. Kovach *et al.*, "In vitro evaluation and in vivo demonstration of a biomimetic, hemocompatible, microfluidic artificial lung.," *Lab Chip*, vol. 15, no. 5, pp. 1366–75, 2015.

[18] T. Rieper, C. Muller, and H. Reinecke, "Novel scalable and monolithically integrated extracorporeal gas exchange device," *Biomed. Microdevices*, vol. 17, no. 5, pp. 1–10, 2015.

[19] A. A. Gimbel, E. Flores, A. Koo, G. García-Cardeña, and J. T. Borenstein, "Development of a biomimetic microfluidic oxygen transfer device," *Lab Chip*, vol. 10, no. 17, p. 1047, 2016.

[20] A. J. Thompson, L. H. Marks, M. J. Goudie, A. Rojas-Pena, H. Handa, and J. A. Potkay, "A small-scale, rolled-membrane microfluidic artificial lung designed towards future large area manufacturing," *Biomicrofluidics*, vol. 11, no. 2, p. 024113, 2017.

[21] M. Dabaghi *et al.*, "An artificial placenta type microfluidic blood oxygenator with double-sided gas transfer microchannels and its integration as a neonatal lung assist device," *Biomicrofluidics*, vol. 12, no. 4, p. 044101, 2018.

[22] M. Dabaghi *et al.*, "An Ultra-thin Highly Flexible Microfluidic Device for Blood Oxygenation," *Lab Chip*, vol. 18, no. 24, pp. 3780–3789, 2018.

[23] H. Matharoo *et al.*, "Steel reinforced composite silicone membranes and its integration to microfluidic oxygenators for high performance gas exchange," *Biomicrofluidics*, vol. 12, no. 1, p. 014107, 2018.

[24] A. J. Thompson, L. J. Ma, T. J. Plegue, and J. A. Potkay, "Design Analysis and Optimization of a Single Layer PDMS Microfluidic Artificial Lung," *Trans. Biomed. Eng.*, 2018.

[25] M. C. Kung, J.-K. Lee, H. H. Kung, and L. F. Mockros, "Microchannel technologies for artificial lungs: (2) screen-filled wide rectangular channels.," *ASAIO J.*, vol. 54, no. 4, pp. 383–9, 2008.

[26] J.-K. Lee, M. C. Kung, H. H. Kung, and L. F. Mockros, "Microchannel technologies for artificial lungs: (3) open rectangular channels.," *ASAIO J.*, vol. 54, no. 4, pp. 390–5, 2008.

[27] T. Kniazeva, J. C. Hsiao, J. L. Charest, and J. T. Borenstein, "A microfluidic respiratory assist device with high gas permeance for artificial lung applications," *Biomed. Microdevices*, vol. 13, no. 2, pp. 315–323, 2011.

[28] D. M. Hoganson, H. I. Pryor, E. K. Bassett, I. D. Spool, and J. P. Vacanti, "Lung assist device technology with physiologic blood flow developed on a tissue engineered scaffold platform.," *Lab Chip*, vol. 11, no. 4, pp. 700–707, 2011.

[29] R. Sreenivasan, E. K. Bassett, D. M. Hoganson, J. P. Vacanti, and K. K. Gleason, "Ultra-thin, gas permeable free-standing and composite membranes for microfluidic lung assist devices," *Biomaterials*, vol. 32, no. 16, pp. 3883–3889, 2011.

[30] J. a Potkay, M. Magnetta, A. Vinson, and B. Cmolik, "Bio-inspired, efficient, artificial lung employing air as the ventilating gas.," *Lab Chip*, vol. 11, no. 17, pp. 2901–2909, 2011.

[31] T. Kniazeva *et al.*, "Performance and scaling effects in a multilayer microfluidic extracorporeal lung oxygenation device," *Lab Chip*, vol. 12, no. 9, pp. 1686–1695, 2012.

[32] J. H. Lo, E. K. Bassett, E. J. N. Penson, D. M. Hoganson, and J. P. Vacanti, "Gas Transfer in Cellularized Collagen-Membrane Gas Exchange Devices," *Tissue Eng. Part A*, vol. 21, no. 15–16, pp. 2147–2155, 2015.

[33] C. D. Murray, "The physiological principle of minimum work.I. The vascular system and the cost of blood volume," *Proc.Natl. Acad. Sci. U. S. A.*, vol. 12, no. 3, pp. 207–214, 1926.

[34] C. D. Murray, "the Physiological Principle of Minimum Work Applied To the Angle of Branching of Arteries," *J. Gen. Physiol.*, vol. 9, no. 6, pp. 835–841, 1926.

[35] W. I. Wu, K. N. Sask, J. L. Brash, and P. R. Selvaganapathy, "Polyurethane-based microfluidic devices for blood contacting applications," *Lab Chip*, vol. 12, no. 5, pp. 960–970, 2012.

[36] S. Thorslund, J. Sanchez, R. Larsson, F. Nikolajeff, and J. Bergquist, "Functionality and stability of heparin immobilized onto poly (dimethylsiloxane)," *Colloids Surfaces B Biointerfaces*, vol. 45, pp. 76–81, 2005.

[37] J. a Potkay, "The promise of microfluidic artificial lungs.," *Lab Chip*, vol. 14, no. 21, pp. 4122–4138, 2014.

[38] J. M. Leung *et al.*, "Surface modification of poly(dimethylsiloxane) with a covalent antithrombin-heparin complex for the prevention of thrombosis: Use of polydopamine as bonding agent," *J. Mater. Chem. B*, vol. 3, no. 29, pp. 6032–6036, 2015.

[39] J. L. Reoma *et al.*, "Development of an artificial placenta I: pumpless arterio-venous extracorporeal life support in a neonatal sheep model," *J. Pediatr. Surg.*, vol. 44, no. 1, pp. 53–59, 2009.

[40] B. W. Gray *et al.*, "Development of an artificial placenta IV: 24 hour venovenous extracorporeal life support in premature lambs," *ASAIO J.*, vol. 58, no. 2, pp. 148–154, 2012.

[41] B. Bryner *et al.*, "An extracorporeal artificial placenta supports extremely premature lambs for 1 week," *J. Pediatr. Surg.*, vol. 50, no. 1, pp. 44–49, Jan. 2015.

[42] J. Jopling, E. Henry, S. E. Wiedmeier, and R. D. Christensen, "Reference Ranges for Hematocrit and Blood Hemoglobin Concentration During the Neonatal Period: Data From a Multihospital Health Care System," *Pediatrics*, vol. 123, no. 2, pp. e333–e337, 2009.

[43] J. E. Jones and P. A. Jose, "Neonatal Blood Pressure Regulation," *Semin. Perinatol.*, vol. 28, no. 2, pp. 141–148, 2004.

[44] K. Bauer, C. Uhrig, P. Sperling, K. Pasel, C. Wieland, and H. T. Versmold, "Body temperatures and oxygen consumption during skin-to-skin (kangaroo) care in stable preterm infants weighing less than 1500 grams," *J. Pediatr.*, vol. 130, no. 2, pp. 240–244, 1997.

[45] J. Bauer, K. Maier, G. Hellstern, and O. Linderkamp, "Longitudinal evaluation of energy expenditure in preterm infants with birth weight less than 1000 g," *Br. J. Nutr.*, vol. 89, no. 04, p. 533, 2003.

[46] T. M. Raffay and M. C. Walsh, "Pulse Oximetry Targets in Extremely Premature Infants and Associated Mortality : One-Size May Not Fit All," *J. Nat. Sci.*, vol. 4, no. 6, p. e508, 2018.

[47] V. Manja, O. D. Saugstad, and S. Lakshminrusimha, "Oxygen Saturation Targets in Preterm Infants and Outcomes at 18–24 Months: A Systematic Review," *Pediatrics*, vol. 139, no. 1, p. e20161609, 2017.

[48] M. Chang, "Optimal oxygen saturation in premature infants," *Korean J. Pediatr.*, vol. 54, no. 9, pp. 359–362, 2011.

[49] A. Kayton, P. Timoney, L. Vargo, and J. A. Perez, "A Review of Oxygen Physiology and Appropriate Management of Oxygen Levels in Premature Neonates," *Adv. Neonatal Care*, vol. 18, no. 2, pp. 98–104, 2018.

[50] M. J. Huizing, E. Villamor-Martínez, M. Vento, and E. Villamor, "Pulse oximeter saturation target limits for preterm infants: a survey among European neonatal intensive care units," *Eur. J. Pediatr.*, vol. 176, no. 1, pp. 51–56, 2017.

[51] A. L. Solevåg, I. Dannevig, B. Nakstad, and O. D. Saugstad, “Resuscitation of severely asphyctic newborn pigs with cardiac arrest by using 21% or 100% oxygen,” *Neonatology*, vol. 98, no. 1, pp. 64–72, 2010.

[52] S. Baumgart, C. B. Langman, R. Sosulski, W. W. Fox, and R. A. Polin, “Fluid, Electrolyte, and Glucose Maintenance in the Very Low Birth Weight Infant,” *Clin. Pediatr. (Phila).*, vol. 21, no. 4, pp. 199–206, 1982.

[53] J. M. Leung, L. R. Berry, A. K. C. Chan, and J. L. Brash, “Surface modification of polydimethylsiloxane with a covalent antithrombin–heparin complex to prevent thrombosis,” *J. Biomater. Sci. Polym. Ed.*, vol. 25, no. 8, pp. 786–801, May 2014.

8 Chapter 8

Conclusion and Recommendations for Future Work

8.1 Conclusion

This thesis reports on the development and improvement of various microfluidic blood oxygenators to overcome the main challenges associated with the conventional microfluidic blood oxygenators in the literature. Low throughput, low gas exchange capacity especially in room air, complex blood channel geometries, scale-up, and large form factor (build-up volume) are the main challenges with these devices which have been addressed in this thesis.

Previously, conventional microfluidic blood oxygenators could handle only a few mL min^{-1} of blood (less than 10 mL min^{-1} usually) and were not efficient at high blood flow rates, especially when they are using air as their sweep gas. Therefore, the initial focus of this thesis was to assemble the oxygenators into a modular lung assist device (LAD), in order to meet the flow requirements necessary in clinical conditions. This effort demonstrated that larger volumetric flow rates of ~ 30 mL min^{-1} could be handled successfully using a series-parallel combination of oxygenators. In addition, it also developed the first iteration of the flow distributor that could distribute the large flow to several oxygenator modules. Despite these achievements, the gas exchange efficiency of the individual oxygenator units used in this part (with gas exchange on only one side) was low, and therefore a large number of oxygenators had to be used to achieve the clinically required flow rates and oxygenation levels.

It should be noted that all modular LADs introduced in this thesis have been designed based on the physics of hydraulic circuits. Therefore, each device in a LAD acts as a resistance to the blood flow and follows the same analogy and principles. In this concept,

oxygenators can be arranged in a parallel or series configuration. The parallelization is more desirable as the overall resistance would be decreased and a lower pressure drop would be generated. However, the series format was used once to enhance the oxygenation and it did not impact the overall resistance since the devices used in this work had relatively low resistance. Each particular type of oxygenator (that has the same design and geometry) could provide a certain amount of oxygenation at a given blood flow rate (and it was supposed to have a fixed resistance). Then, the number of oxygenators could be calculated by dividing the required oxygen transfer by the oxygen transfer of the device. These rules and calculations were applied to designing of all LADs mentioned in this thesis.

In order to address the issue associated with the first LAD, new double-sided oxygenators, that had gas exchange membranes on both sides of the blood flow network were designed, and new manufacturing methods were developed to fabricate them. The main innovations were to develop a layer-by-layer softlithography technique to fabricate microfluidic blood oxygenators with double-sided gas transfer channels with high precision in repeatability and robustness which are considered as vital factors for constructing a modular-based device. Moreover, the scalability of this technique was demonstrated by manufacturing devices with greater gas exchange surface area without making any discernable compromise in their gas transfer capacities. Besides design improvements, the second iteration of a modular LAD was presented here by connecting four of these enlarged double-sided blood oxygenators in a parallel configuration using two 3D-printed flow dividers. Even though this LAD could reach significantly higher gas transfer and blood flow rates (up to 60 mL min^{-1}) in an enriched oxygen environment, the number of oxygenator units were not enough to provide adequate oxygenation in room air.

In an attempt to overcome this challenge and achieve oxygenation in room air, the effective gas exchange surface area of a double-sided microfluidic blood oxygenator was increased by manufacturing all PDMS-based double-sided devices. The significant achievements were to design of a new tapered-shape inlet/outlet to minimize shear stress

and pressure drop, to develop a flow distributor with a branching network following physiological rules to gently distribute blood from the main line to single oxygenator units, to construct the third iteration of a modular LAD by assembling eight oxygenator units. The LAD was efficient enough in room air to provide the required oxygenation at a blood flow rate of 30 mL min^{-1} and a low pressure drop. Besides, this LAD could handle higher blood flow rates (even up to 150 mL min^{-1}) and produced significantly improved oxygenation when exposed to pure oxygen. Despite of these improvements, the size of the LAD was too bulky for a portable application, and it could not provide the needed oxygenation for preterm neonates weighing greater than 1 kg.

To address this issue and decrease the form factor of a microfludic blood oxygenator, an advanced flexible microfluidic device capable of being folded or rolled was developed. Such a flexible device was realized by introducing a new composite material made of PDMS and PTFE for microfluidic blood oxygenators. The flexibility of this device was demonstrated by its deformation into complex shapes without losing its functionality. The main focus here was to demonstrate the benefits of flexibilty in reducing the form factor, combing several components required in a LAD construction in one integrated device for minimizing the priming volume, and bringing the inlet and the outlet very close to each other to decrease the priming volume of the extracorporeal line. Moreover, the developed devices in this work had high mechanical strength and desired compliance which are essential factors for designing and constructing a modular LAD. Despite the design and performance improvements, a single oxygenator unit would not be enough to reach the required oxygenation for babies with various birth weight.

In order to address this limitation, 16 single oxygenator units and two flow distributors featuring a biomimetic blood branching network were assembled in a parallel format to support preterm neonates with different weights. In addition, the inlet with tapered-shaped design was integrated to these devices to minimize shear stresses encountered by blood. The main contributions were to develop a compact modular LAD with biomimetic blood flow paths, modify blood contacting surfaces with heparin for improving hemocompatibility and perform comprehensive in vitro and in vivo experiments for

evaluating the gas transfer of this LAD. The results revealed that this LAD had auspicious performance in room air (an increase in oxygen saturation level from 64 % to 90 % at a blood flow rate of 50 mL min^{-1} and very low pressure drop of 29 mm Hg). Furthermore, this LAD underwent an in vivo study using a 1.75 kg newborn piglet. Results from the piglet experiment confirmed in vitro experiments suggesting that this LAD could be operated passively and reach high blood flow rates. This LAD could increase the oxygen saturation level of blood in the femoral artery from 56 % (hypoxic and without LAD) to 84 % (hypoxic and with LAD) even by bypassing only ~ 30 % of the cardiac output to the LAD. Therefore, such a LAD can support preterm neonates weighing up to 1.5 kg in room air or up to 2 kg using pure oxygen as the sweep gas.

8.2 Recommendations for future work

Although the microfluidic blood oxygenators developed in this thesis could satisfy required oxygenation for preterm neonates with RDS in an artificial placenta configuration, they are not still at the stage to be applied in clinics for adults' patients. In addition to the increase in oxygenation capacity, ability to prevent clotting and improve hemocompatibility and developing catheters to connect the LADs to the body with minimal pressure drop have been considered as other challenges in the past. This thesis focused on the improvement of gas exchange capacity of microfluidic blood oxygenators so that it was sufficient enough to meet the requirements of a 2 kg neonate. Other groups have been active in the development of blood compatible surfaces and in development of vascular access to connect the oxygenator to the body. Despite the improvements in this thesis, there are several avenues that are possible to further improve oxygenation capacity so that they can be made more compact. In addition, new manufacturing techniques could be introduced so that large scale and reliable fabrication of these devices can be made possible.

8.2.1 Scale-up and design improvement using photolithography

Photolithography technique has been used to fabricate microfluidic blood oxygenators because this method can control precisely the size and shape of micro featured desired for these devices. Furthermore, the final mold has very smooth surface finishing meaning the casted PDMS out of the mold will be completely flat. Although few microfluidic blood oxygenators with different designs have been developed and exhibited promising enhancement in gas transfer efficiencies, these devices can still undergo some design modifications and charecterization to reach better performance. Therefore, the initial improvement in the future can be focused on design improvement using the photolithography method.

8.2.2 Design improvements

There are different geometries available in the literature for blood flow paths such as an array of parallel straight channels, a branching network of channels, and a square-shaped chamber with micro pillars. The performance of these device can be improved by reducing the blood flow path's height regardless of its geometry. Nonetheless, this would come at a price of increasing pressure drops with a great risk of occlusion. Therefore, there is always a trade-off between the size of channels and the pressure drop. Moreover, the low gas exchange surface area is another area of concern for the most of these geometries. Among all these geometries, the square-shaped micro chamber with an array of micro pillars is the one with the highest active gas exchange surface area. However, the specific anatomy of square-shaped devices results in high resistance to blood in regions which are less effective in oxygenation.

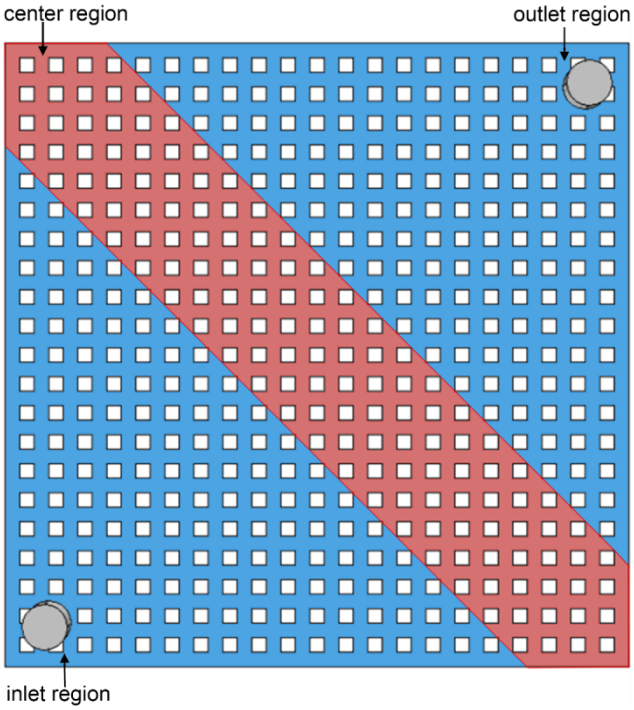

Figure 8.1: a conventional design division to smaller regions based on their contributions in pressure drop and oxygenation.

As shown in Figure 8.1, a conventional design developed in this thesis can be divided to three zones: inlet and outlet regions which have high resistance to blood flow and low

contribution in oxygenation, and the center part of the device which has a low resistance to blood and the main contribution in oxygenation. To address this shortcoming, the center region can be elongated in the direction of the diagonal vertices of the chamber with lower channels height while the inlet and the outlet regions can have a greater height to decrease the resistance to blood flow (Figure 8.2). However, such a change in the height could lead to the creation of dead zones which may lead to blood coagulation. In order to capture the benefit of this design improvement while overcoming the complication of blood coagulation, a blood flow path with a sloping region can be applied for an elongated device. This device can include three regions: 1) the inlet and outlet regions with higher height for blood distribution, 2) the sloping region for a smooth blood transfer to the effective gas transfer channels, and 3) the center region with the lowest height for the best gas exchange.

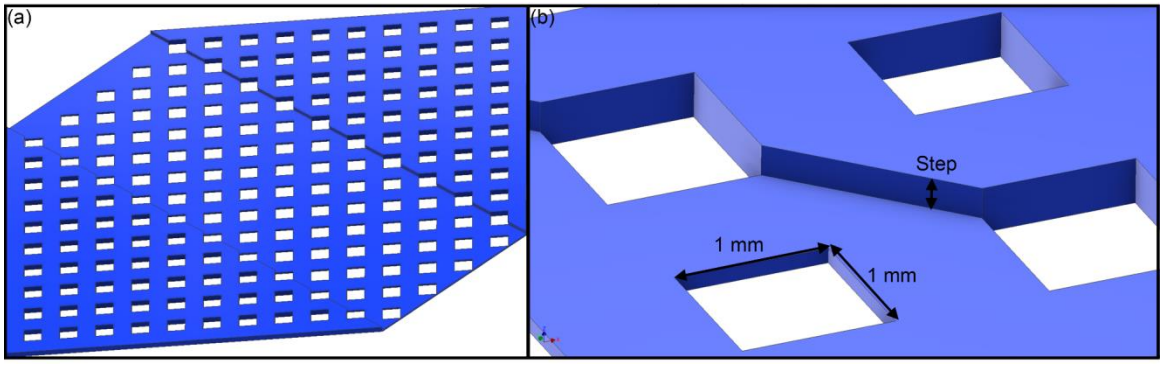

Figure 8.2: the illustration of an elongated device with two different heights to decrease the pressure drop and increase oxygenation.

It should be noted that the mold for such a device with a sloping profile cannot be made with the conventional photolithography technique. Then, an alternative fabrication method such as CNC machining can be used to fabricate this mold. High precision, reliability, more capability, uniformity in production, lower cost, design retention, and versatility are the main advantages of CNC machining. In addition, this method can enable to fabricate a larger mold with sloping features without any stagnation zones that are prone to clot formation.

8.2.3 Blood channels with four-sided gas diffusions

The performance of microfluidic blood oxygenators has been significantly enhanced by the introduction of the double-sided gas transfer channels due to the increase in the gas exchange surface area and reduction in the diffusion resistance for oxygen molecules. Another interesting approach to improve the efficiency of such a device is to have microchannels which can transfer gases from all sides of their walls. As a result, the gas exchange surface will be increased without making any change in the channel's geometry and its fluid characteristics. Moreover, the diffusion path for oxygen molecules will be decreased, thereby red blood cells at the center of the blood channel (they are the furthest cells from walls) will adsorb oxygen molecules faster. Figure 8.3 depicts the schematic cross-sectional view of single-sided, double-sided, and four-sided channels.

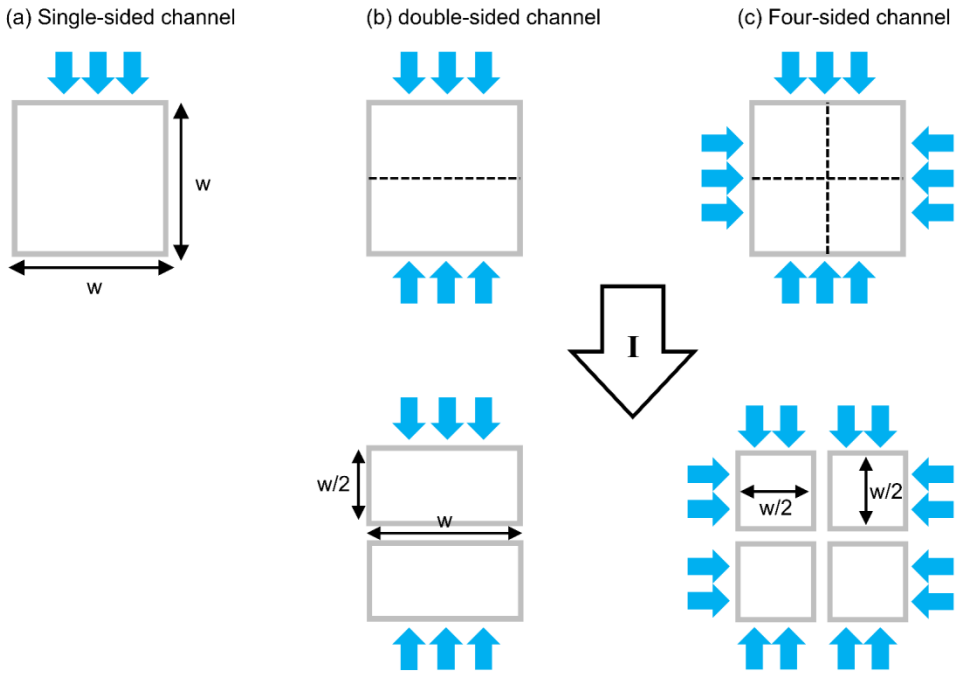

Figure 8.3: the schematic cross-sectional view of (a) a single-sided channel, (b) a double-sided channel, (c) a four-sided channel, and (I) simplified equivalent channels.

A square-shaped double-sided channel with a width of *w* can be divided into two equivalent channels with the width of *w* and the height of *w/2*. The same simplification can be done for a four-sided channel resulting in four square-shaped channels with the width of *w/2*. A device with four-sided gas transfer microchannels allows gas exchange from all the walls where blood comes in contact. Therefore, a new design is proposed here to fabricate a four-sided gas diffusion device with having some air chambers (cavities) inside of the device and adjacent to blood channels to enhance the gas exchange capacities. The initial design can have a branching network of microchannels as shown in Figure 8.4.a. One possible way to fabricate such a device is to design a microfluidic blood oxygenator with a branching network which is responsible for uniformly distributing blood to microchannels with four-sided gas diffuions.

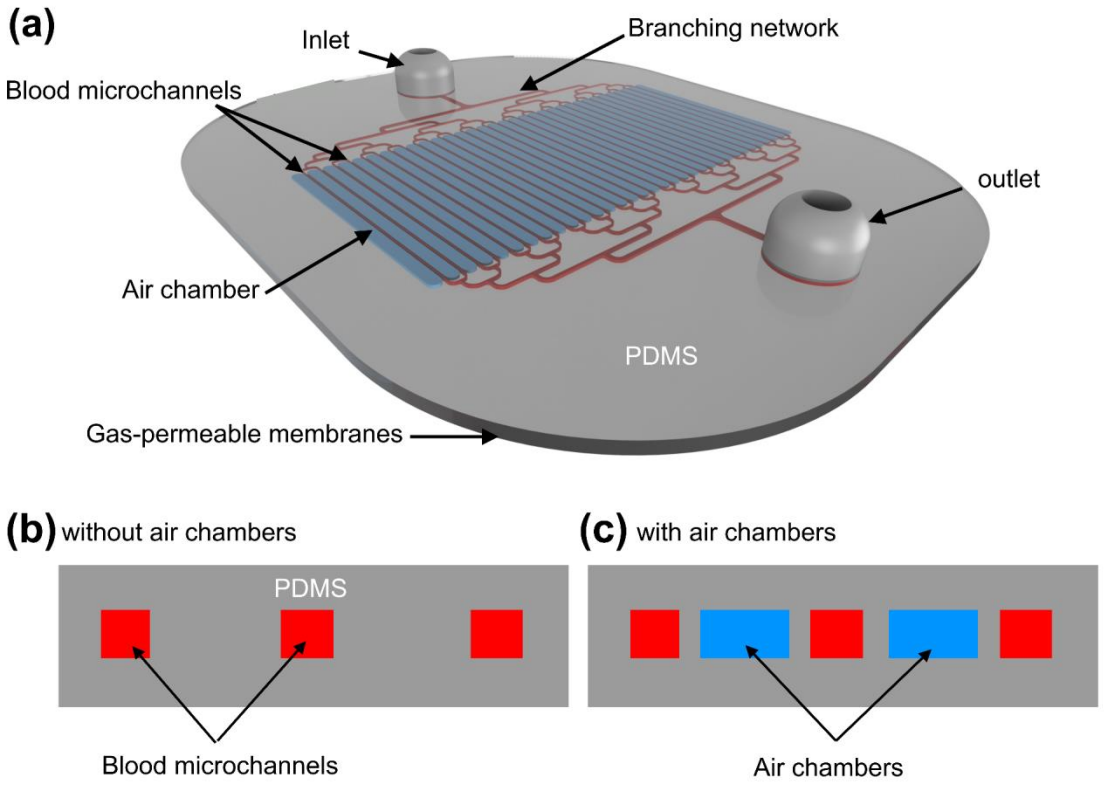

Figure 8.4: (a) a 3D schematic view of the device, (b) the cross-sectional view of a device without air chambers, and (c) the cross-sectional view of a device with air chambers.

In order to find the optimum geometry for a device with four-sided gas transfer channels, the dimension of the microchannels should be characterized based on blood flow rates to meet the design criteria, especially the pressure drop criterion. Then, the number of microchannels needed should be determined. Furthermore, the dimension of air chambers should be optimized to ensure the maximum gas transfer efficiency achieved. The air chambers can be left in a closed cell format as shown in Figure 8.4 or could be opened to the outside environment to reduce the gas transfer diffusion resistance.

8.2.4 Fabricating an integrated device using additive manufacturing

The photolithography technique is limited in size and 2D designs. Then, other fabrication methods such as additive manufacturing can be used to make devices at larger scale with higher gas transfer capacity and 3D features.

Additive manufacturing can be employed in two ways: 1) to fabricate a larger mold with 3D features and 2) to build an integrated double-sided oxygenator using a sacrificial material printing.

Additive manufacturing is capable of fabricating 3D features with more complicated geometries with a high resolution of 10 – 20 µm which can help with the manufacturing a large-scale microfluidic blood oxygenator with sloping profile. The other possible solution is to use a sacrificial material to make an integrated LAD. First, a 3D-printer can be used to print features (the blood vascular network or blood microchannels) by a sacrificial material, which is dissolvable by water or a chemical, then, PDMS will be poured or spun around the printed parts to form the entire device. Finally, a solvent or water will be used to wash away the sacrificial material, and the device will be ready without applying any further bonding. This method has several advantages such as eliminating the need for bonding and being able to fabricate any size of the device. Besides, there is no need for integrating single oxygenators units and connectors, thereby reducing the priming volume.

9 Appendix 1

Supplementary Information

An ultra-thin, all PDMS-based microfluidic lung assist device with high oxygenation capacity

Mohammadhossein Dabaghi[1], Neda Saraei[2], Gerhard Fusch[3], Niels Rochow[3], John L. Brash[1,4], Christoph Fusch[1,3,5] and P. Ravi Selvaganapathy[1,2]

[1]School of Biomedical Engineering, [2]Department of Mechanical Engineering, [3]Department of Pediatrics, [4]Department of Chemical Engineering, McMaster University, Hamilton, ON, Canada, [5]Paracelsus Medical University, Salzburg, Department of Pediatrics, University Hospital Nuremberg, Germany

9.1 Numerical modeling of pressure drops and shear stress

Numerical modelling was done to optimize the design of the blood vascular network regrading uniform velocity profile, low pressure drops, which fits in the operating pressure drops range, and shear stress. The blood flow distribution in the blood vascular network was numerically simulated in a 2D model by COMSOL® Multiphysics software. Laminar flow physics were used here to investigate the blood flow distribution inside the blood vascular network. In this simulation, the momentum conservation and the mass conservation were solved together to find velocity profile, pressure distribution and shear stress distribution inside the blood vascular network by using the Navier-Stokes equations. In this simulation, blood was assumed to have a density of 1050 kg/m^3 and a viscosity of 2.9 cP.

Numerical modelling was also used to model velocity profile, pressure drop and shear stress distribution inside the flow distributor and the inlets. In this simulation, it was assumed that the blood was a shear thinning non-Newtonian fluid and a 3D model was used. As a result, the Carreau model[1], [2], as it is shown below, was used to model the dynamic viscosity μ as a function of the shear rate.

$$\mu = \mu_\infty + (\mu_0 - \mu_\infty)[1 + (\lambda\dot{\gamma})^2]^{\frac{n-1}{2}}$$

In this equation, $\mu_\infty$is the viscosity of the blood at the infinite shear rate, which taken as 0.0345 P[1], [2]. μ_0=0.56 P[1], [2] and is defined as the viscosity of the blood at the zero shear rate. Also, λ and n are the time constant and the power-law index, respectively, with the values of 3.313 s and 0.3568[1], [2].

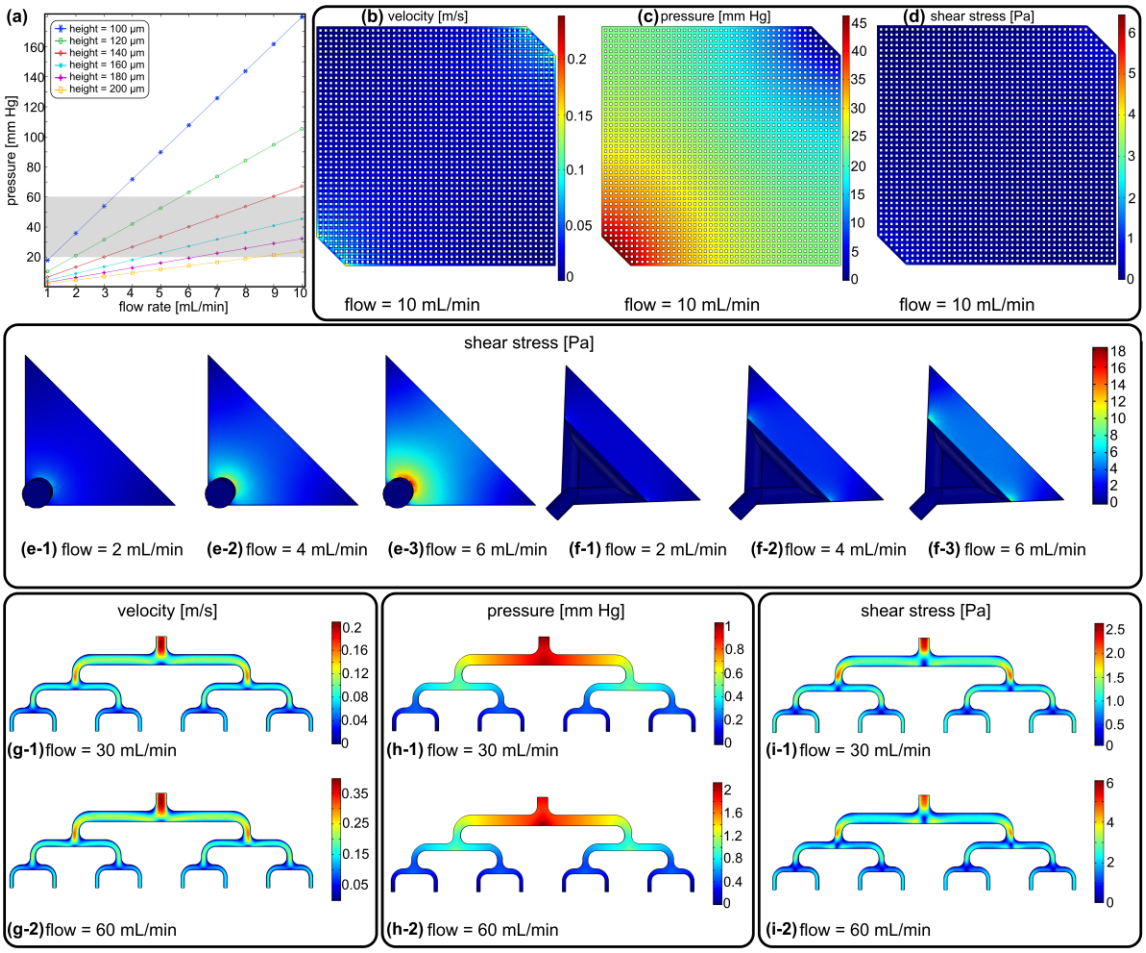

Supplementary Figure 1.9.1: Simulation results: (a) pressure drops versus blood flow rates for different channel heights (b) velocity profile, (c) pressure distribution, (d) shear stress distribution for the blood vascular network at a flow rate of 10 mL/min, , (e1-3) shears stress distribution for perpendicular inlet configuration at different blood flow rates of 2, 4, and 6 mL/min, (f1-3) shears stress distribution for tapered inlet configuration at different blood flow rates of 2, 4, and 6 mL/min, (g1,2) velocity profile in the flow distributor at blood flow rates of 30 and 60 mL/min, (h1,2) pressure distribution in the flow distributor at blood flow rates of 30 and 60 mL/min, and (i1,2) shear stress distribution in the flow distributor at blood flow rates of 30 and 60 mL/min.

9.2 Water Contact Angle Measurement for Trichloro(1H,1H,2H,2H-perfluorooctyl) Silane Coating

The water contact angle (2-µL droplet) was measured to ensure the surface of silicon-mold became hydrophobic as shown in Supplementary Figure.1.2. The water contact angle was increased from 28.47° to 114.77° which shows that the surface became more

hydrophobic resulting in reducing in surface energy. As a result, thin PDMS layer would be released easier from the coated surface.

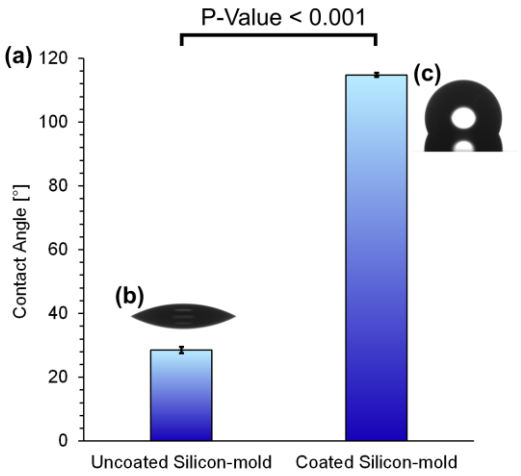

Supplementary Figure 1.9.2: (a) Water contact angle measurement, (b) water droplet on a noncoated surface, and (c) water droplet on a coated surface. Data are mean ± SD, n = 4.

9.3 Burst Pressure

To evaluate the bonding quality and the device stability under applied pressure, the burst pressure test was performed. We used the below experimental set-up to measure the burst pressure for dsSOUs and compared it with those we introduced before with stainless-steel mesh[3]. Therefore, we tested all dsSOU devices at a higher pressure compared to the operating pressure (20 – 60 mm Hg) to make sure that they were robust enough and could stand at high pressure without failure and then were integrated into the LAD or further testing. The experimental set-up (Supplementary Figure 9.3.a) consisted of a syringe pump, which was used to build up the pressure inside the loop, connected to the inlet of the dsSOU. A pressure transducer (TruWave Transducer, Edwards Lifesciences LLC, Irvine, CA, USA) was connected to a cardiac monitor or pressure monitor (SpaceLabs 90369 Patient Monitor, SpaceLabs Medical, Inc.) was also installed before the dsSOU by a 3-ways connector to report the applied pressure. The dsSOU was first filled with DI water and ensured that there was no air bubble, subsequently, the 3-way connector at the outlet of the device was closed to seal the system and build up the pressure. The pressure was raised by pumping more water in the closed loop while the pressure drops of which

the device failed was reported as the burst pressure (300 mmHg was the maximum pressure that the pressure monitor could measure and none of the devices failed below that value as seen in Supplementary Figure 9.3.b).

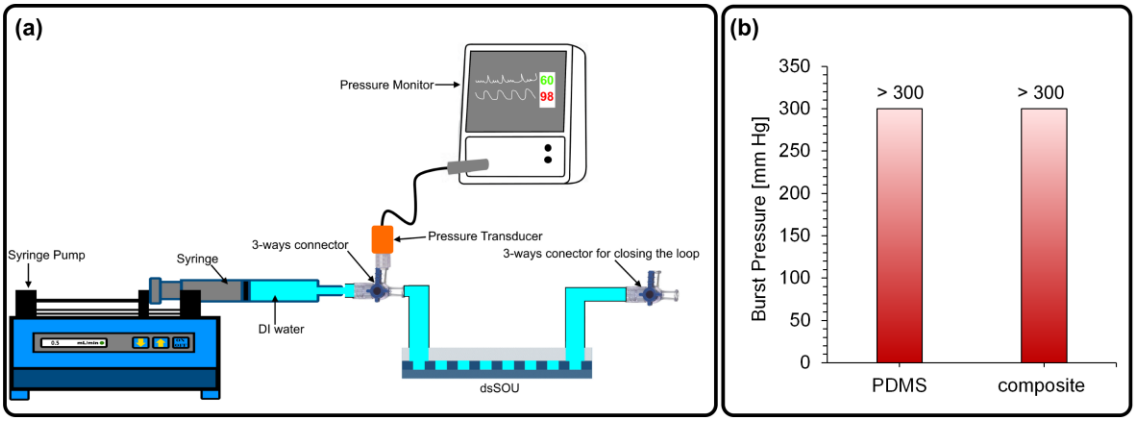

Supplementary Figure 9.3: Experimental set-up for burst pressure and (b) burst pressure comparison between dsSOUs with PDMS and composite membrane made of stainless-steel[3].

9.4 Experimental setup for Gas Exchange Testing in Blood

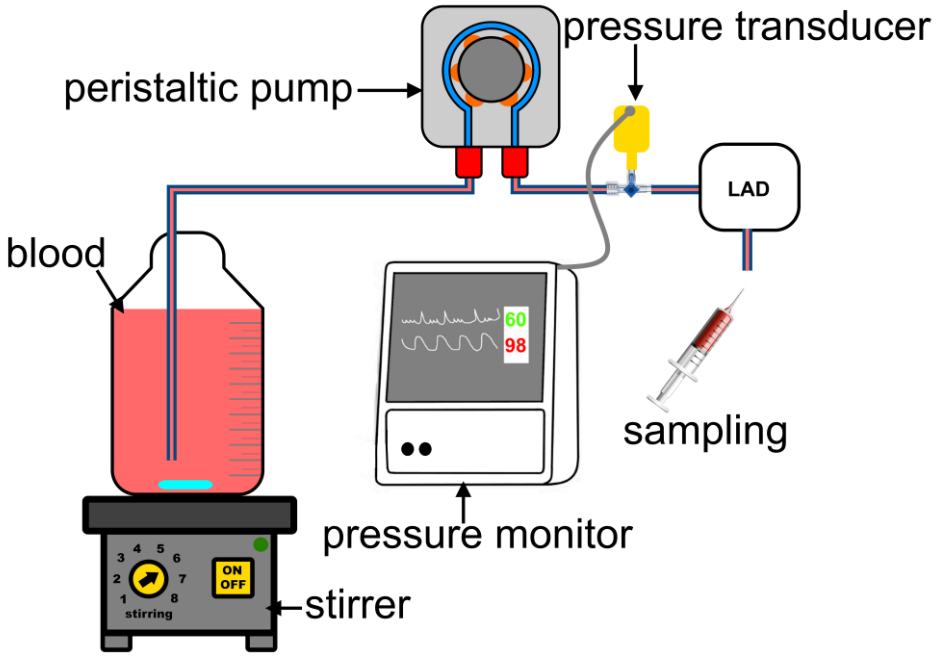

Supplementary Figure 9.4: the experimental setup to test the LAD.

10 Appendix 2

Supplementary Information

An Ultra-thin Highly Flexible Microfluidic Device for Blood Oxygenation

Mohammadhossein Dabaghi[1], Neda Saraei[2], Gerhard Fusch[3], Niels Rochow[3], John L. Brash[1,4], Christoph Fusch[1,3,5] and P. Ravi Selvaganapathy[1,2]

[1]School of Biomedical Engineering, [2]Department of Mechanical Engineering, [3]Department of Pediatrics, [4]Department of Chemical Engineering, McMaster University, Hamilton, ON, Canada, [5]Paracelsus Medical University, Salzburg, Department of Pediatrics, University Hospital Nuremberg, Germany

10.1 Pressure drop modeling

Numerical modeling (using COMSOL Multiphysics software, COMSOL Inc., Burlington, MA) was done to investigate pressure drop over different flow rates to find an optimum channel height.

In this simulation, it was assumed that the blood has a density of 1060 kg m^{-3} and a dynamic viscosity of 0.0035 Pa.s. The pressure drop over different flow rates is shown in Supplementary Figure 10.1.a. The simulation showed that the pressure drops increases by reducing the channel height as expected due to the fact that irreversible relationship between pressure drop and channel height. As operating pressure drop is from 20 – 60 mm Hg, 130 µm would be the best option because its pressure drop fits in a wide range of flow rate from 1 – 6 mL min^{-1}.

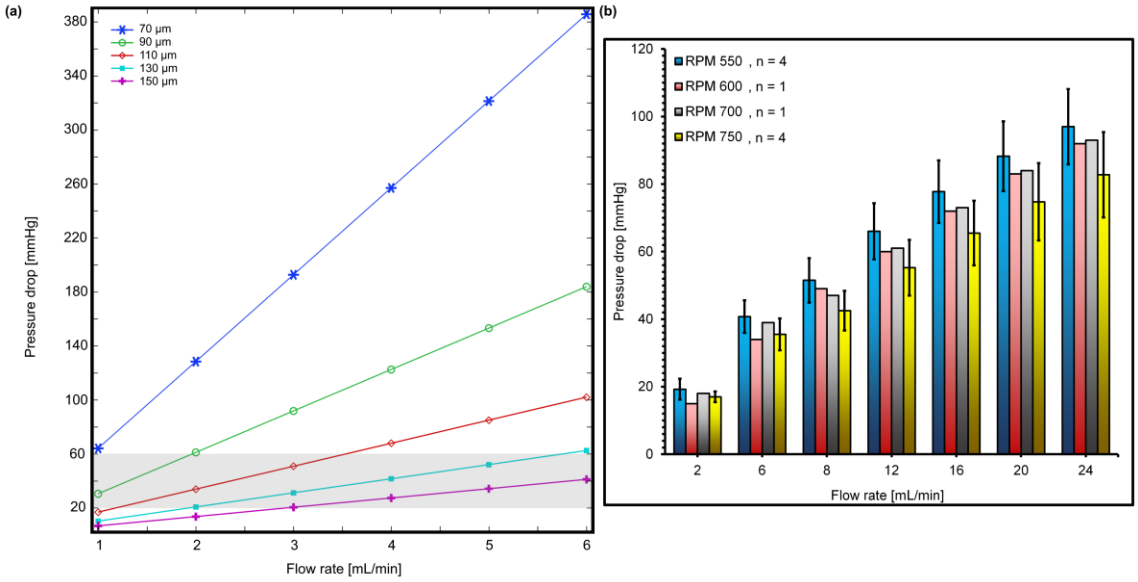

Supplementary Figure 10.1: (a) numerical simulated pressure drops at different flow rates for different channel heights (gray box shows the operating pressure drop range) and (b) pressure drop versus flow rates for devices made of different RPMs with a channel height of 130 µm.

10.2 Characterizing PDMS thickness for the bottom membrane

PDMS was spin-coated on the mold with different RPM to optimize this layer thickness. Later, the pressure drop of each device was measured by flowing water through channels

under different flow rates. Lower pressure drop means that the membrane underwent higher deflection which increases the height of the blood channel and would reduce the gas exchange. However, higher RPM would decrease the membrane thickness and increase the gas exchange. Therefore, the best RPM was selected based on these parameters.

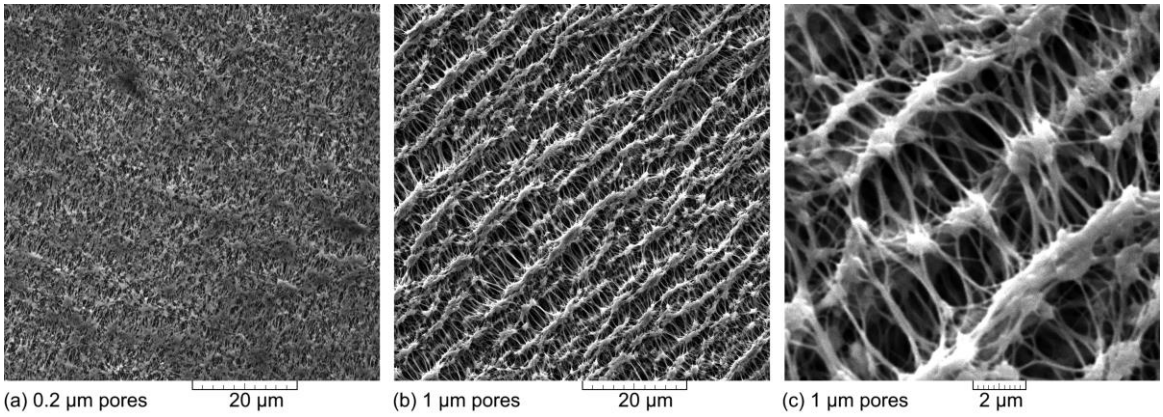

Supplementary Figure 10.2: SEM images of PTFE membranes.

10.3 Tensile Test for composite and PDMS membrane

A tensile testing machine (Shimadzu, Inc) was used to measure the mechanical properties of our new composite membrane (PTFE and PDMS) and make a comparison with PDMS membranes.

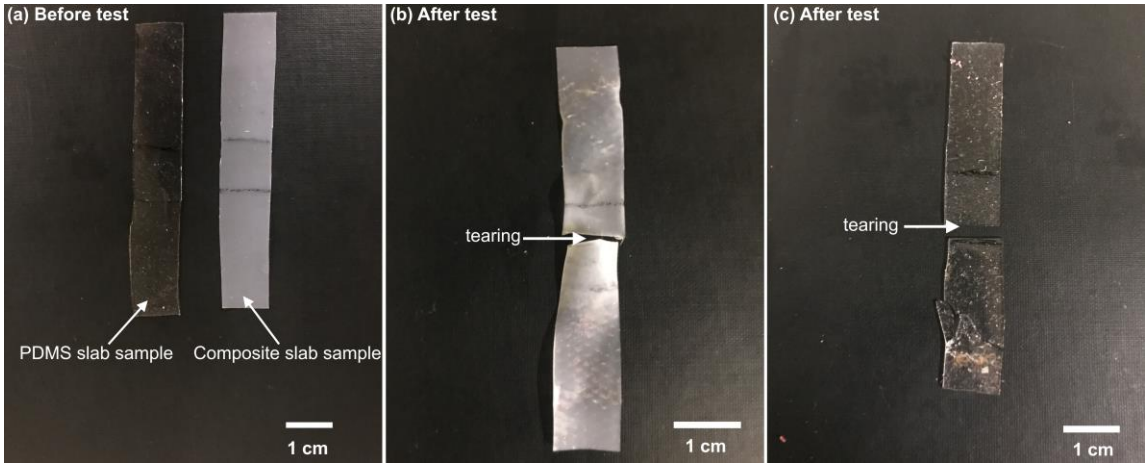

Supplementary Figure 10.3: PDMS and composite samples for tensile testing: (a) before test, (b) a composite sample after testing, and (c) a PDMS sample after testing.

Composite and PDMS membranes for tensile testing were spin-coated at a thickness of ~ 300 µm and cut into smaller pieces with rectangular sections measuring 1 cm in width and 6 cm in length as seen in Supplementary Figure 10.3.a. Then, these samples were mounted in the grips of the machine at a gauge length of 1 cm.

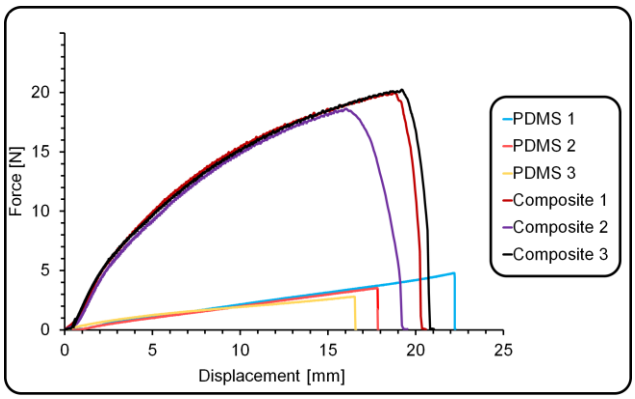

Supplementary Figure 10.4: Sample force-displacement curve for composite and PDMS membranes. The slope for Composite samples is greater than PDMS ones which shows a higher Young's modulus for composite membranes meaning that reinforcing PDMS with porous PTFE membranes improved mechanical prosperities while maintaining the flexibility prosperities of PDMS.

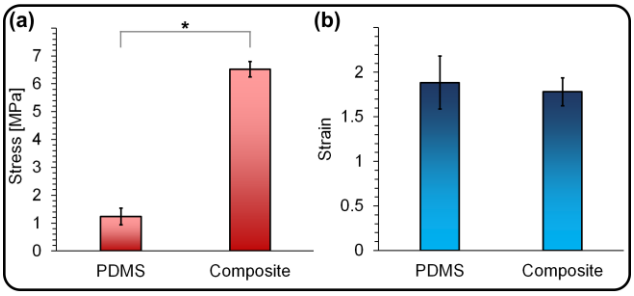

Supplementary Figure 10.5: Tensile tests of PDMS and composite samples: (a) stress at failure point and (b) strain at failure point. Embedding porous PTFE membrane in PDMS appeared to reinforce PDMS and increase the mechanical properties.

10.4 Bending Test

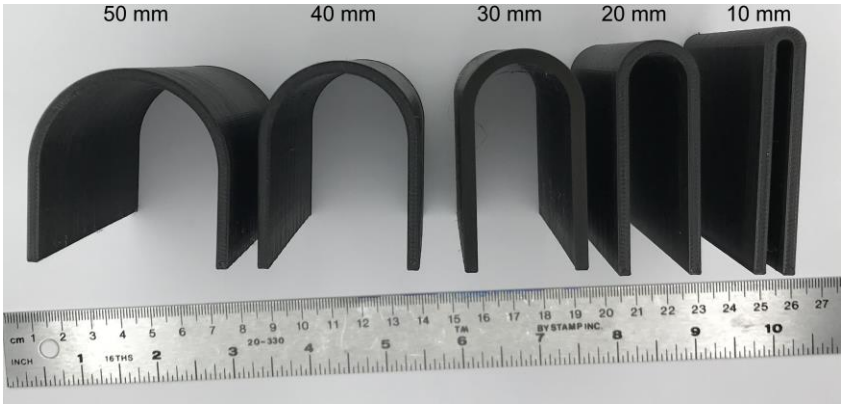

Supplementary Figure 10.6: 3D-printed holders for bending APMBOs at different curvatures.

10.5 The Origami-shaped Compact LAD Preparation

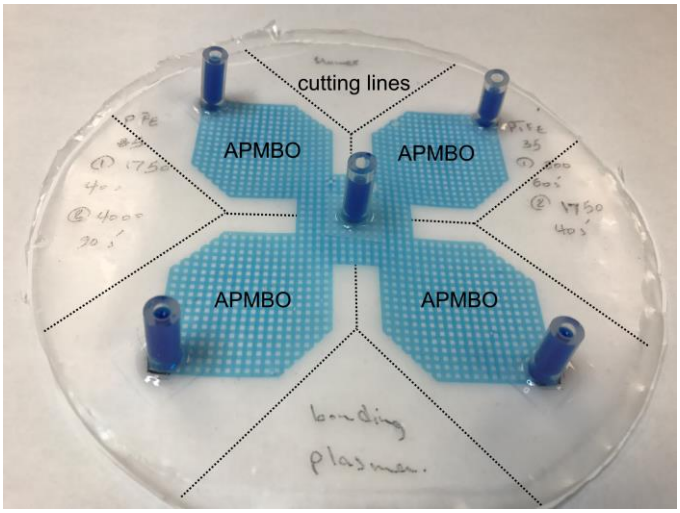

Supplementary Figure 10.7: the origami-shaped compact LAD before being fully assembled.

10.6 Extracorporeal circuit

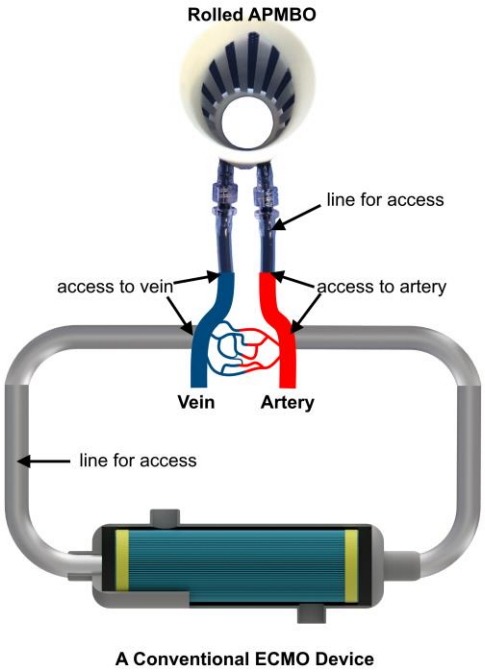

Supplementary Figure 10.8: the required extracorporeal circuit for connecting a blood oxygenator to the vessels: comparison between Rolled APMBO and a conventional ECMO device.

11 Appendix 3

Supplementary Information

A Pumpless Microfluidic Neonatal Lung Assist Device for Artificial Placenta Applications

Mohammadhossein Dabaghi[1], Niels Rochow[2], Neda Saraei[3], Gerhard Fusch[2], Shelley Monkman[2], Kevin Da[4], Alireza Shahin-Shamsabadi[1], Devon Jones[1], John L. Brash[1,4], Dragos Predescu[2], Kathleen Delaney[5], Christoph Fusch[1,2,6,] and P. Ravi Selvaganapathy[1,3]

[1]School of Biomedical Engineering, [2]Department of Pediatrics, [3]Department of Mechanical Engineering, [4]Department of Chemical Engineering, [5]Central Animal Facility Department McMaster University, Hamilton, ON, Canada, [6]Paracelsus Medical University, Nuremberg, Department of Pediatrics, University Hospital Nuremberg, Germany

11.1 Carbon dioxide release

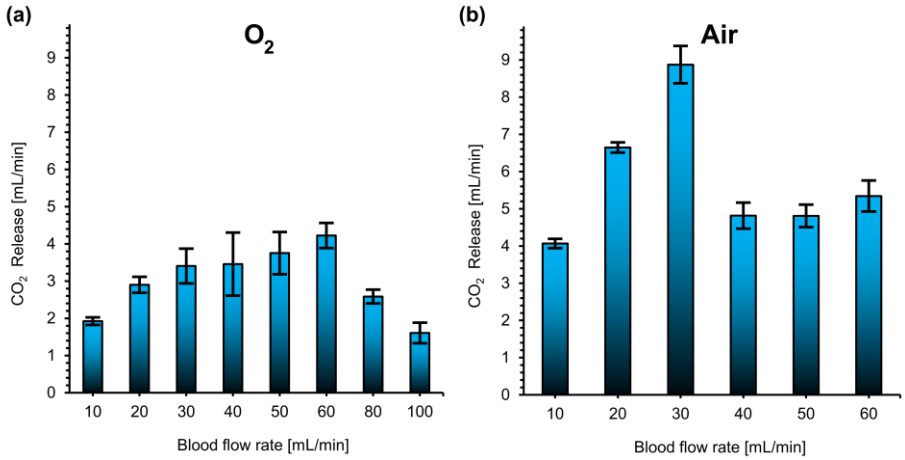

Supplementary Figure 11.1: (a) CO_2 release at various blood flow rates while the LAD was consuming oxygen as the sweep gas and (b CO_2 release at various blood flow rates while the LAD was exposed to room air.

11.2 Access to the right atrium of the heart

A 3.5 Fr Argyle umbilical catheter was used to access the right atrium of the heart via right internal jugular vein. To guide the catheter to the designated location and ensure that the catheter is not clogged, ultrasonography was used.

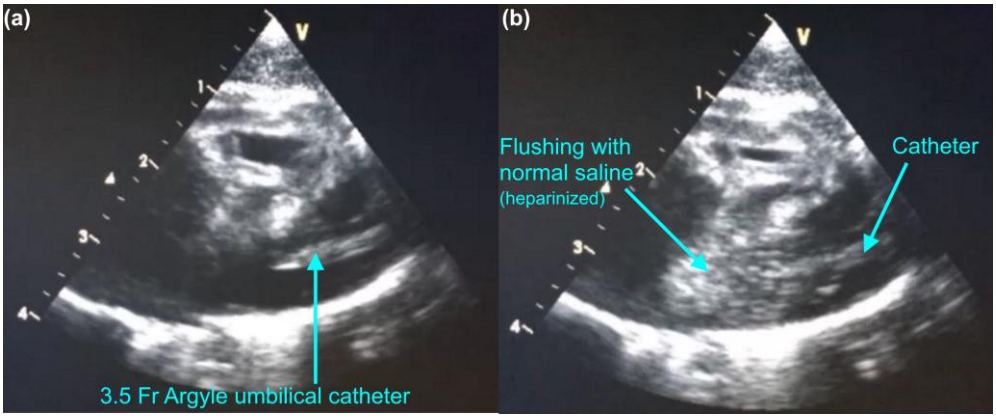

Supplementary Figure 11.2: Ultrasonography of the right atrium of the heart: (a) securing a 3.5 Fr Argyle umbilical catheter and (b) flushing the line with heparinized normal saline solution.

Error! Reference source not found.2.a shows that the catheter was placed in the right a trium of the heart. And it was flushed with heparinized normal saline showing that it was not clogged.

Achieved blood flow rates and pressure drops over time

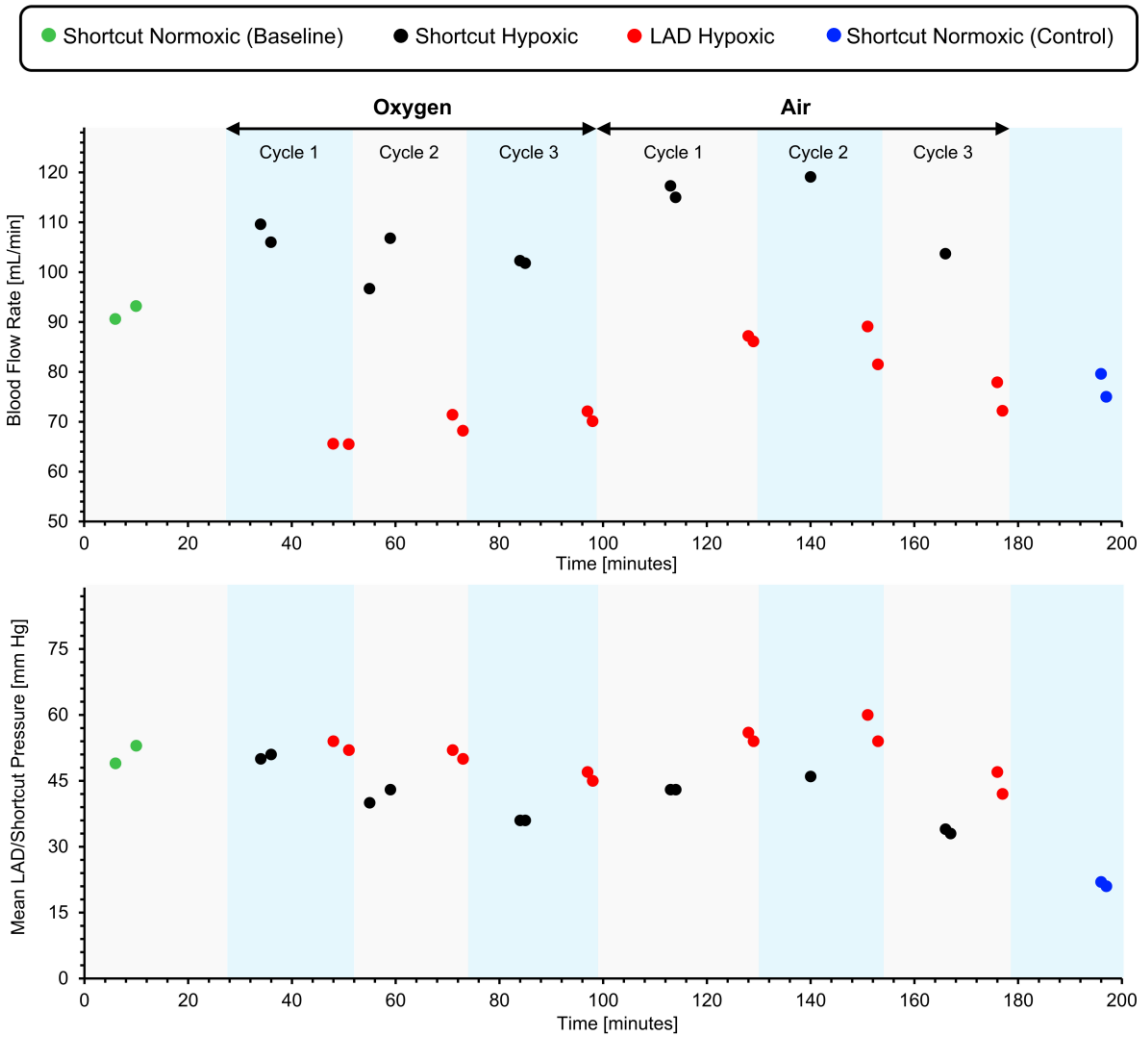

Supplementary Figure 11.3: (a) measured blood flow rates over the period of the experiment and (b) the shortcut or the LAD's pressure during the experiment.

11.3 Estimated oxygen transfer by the LAD

In this study, the piglet had a lower hematocrit levels compared to preterm neonates. Therefore, to evaluate the real capacity of the developed LAD, we estimated the amount

of oxygen transfer for different weights up 1000 grams for both oxygen and air as the sweep gas.

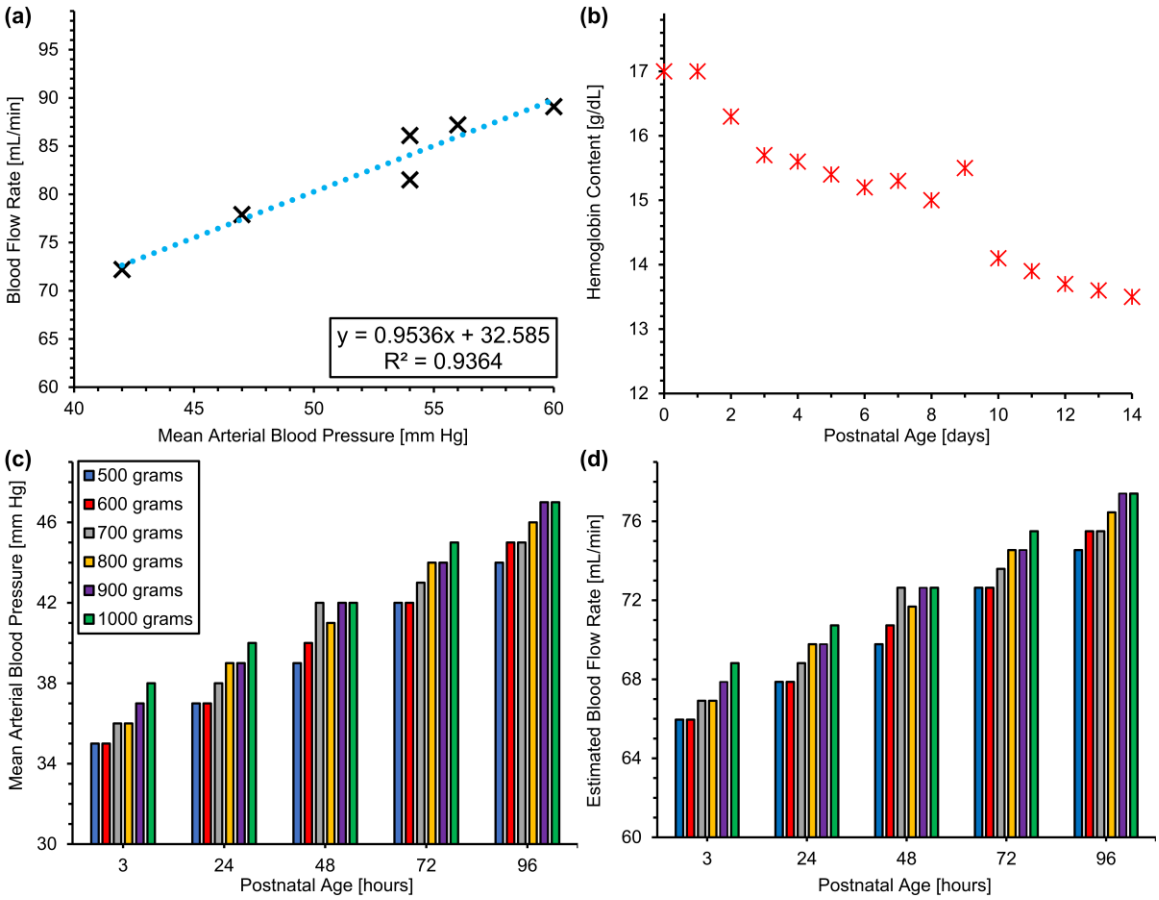

Supplementary Figure 11.4: (a) measured blood flow rates versus mean arterial blood pressure in the piglet experiment, (b) measured hemoglobin contents for preterm infants with a gestational age of 29 – 34 weeks[4], (c) measured mean arterial blood pressure for newborns with different weights over 96 hours after birth[5], and (c) estimated blood flow rates based.

First, the correlation between mean arterial blood pressure (MABP) and blood flow rates (BFR) were found using the data gathered from the piglet experiment (**Error! Reference s ource not found.**.a). A linear relationship between MABP and BFR was established which can be used to estimate BFR for other MABP values. As hematocrit level in human infants are higher, we used the measured values by Jopling et al.[4]. They measured the hematocrit level for neonates at different gestational age (GA) from 22 weeks to 42

weeks. Data used in this calculation belonged to the group with a GA of 29 – 34 weeks (**Error! Reference source not found.**4.b).

Supplementary Figure 11.5: (a) estimated oxygen transfer by the LAD while consuming oxygen as the sweep gas for preterm neonates with different birth-weights over 96 hours after births and (b) estimated oxygen transfer by the LAD while the LAD is exposed to room air for preterm neonates with different birth-weights over 96 hours after births. AP shows the reference values for different weights in an artificial placenta configuration when the LAD is supposed to provide 30 % of oxygen consumption[6].

As seen here, hematocrit level decreases after birth which would affect on the overall amount of oxygenation. Moreover, MABP values for different postnatal age (up to 96 hours after birth) and various weights (500 – 1000 grams) were borrowed from the study conducted by Jones et. al.[5] Then, the blood flow rates for each weight was estimated using these MBAP values. It was assumed that the initial value of oxygen saturation level was 75 % for an artificial placenta application and it would be raised to 100 % in an ideal scenario. This means that the maximum increase in oxygen saturation level would be 25 %. Next, the amount of increase in oxygen saturation level was estimated for each flow rate using in vitro data. For instance, the oxygen saturation level after the LAD would be always 100 % for all flow rates while oxygen is assumed to be used as the sweep gas. Under room air condition, the increase in oxygen saturation level was 25.7 % and 23 % at blood flow rates of 50 and 60 mL min^{-1}. Finally, the amount of oxygen transfer was calculated for different hours and weights considering the fact the hematocrit level decreases and blood flow rate increases while the baby is growing.

Also, it was assumed that the LAD would provide 30 % of the oxygen consumption which corresponding values are shown in **Error! Reference source not found.** as r eferences (AP). Based on this calculation, the LAD would be able to provide the required oxygenation in an artificial placenta configuration while using oxygen or air as the sweep gas.

11.4 Systemic blood circulation

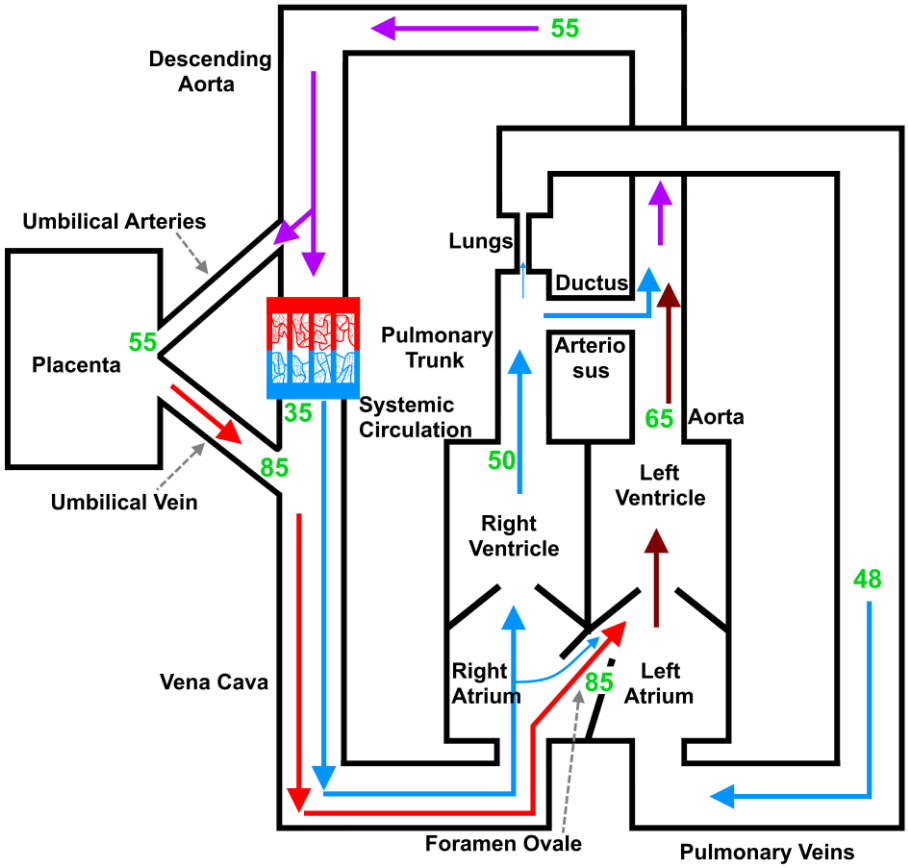

Supplementary Figure 11.6: diagram of the blood circulation in a healthy fetus, representing the directions of blood flow with the oxygen saturation levels.

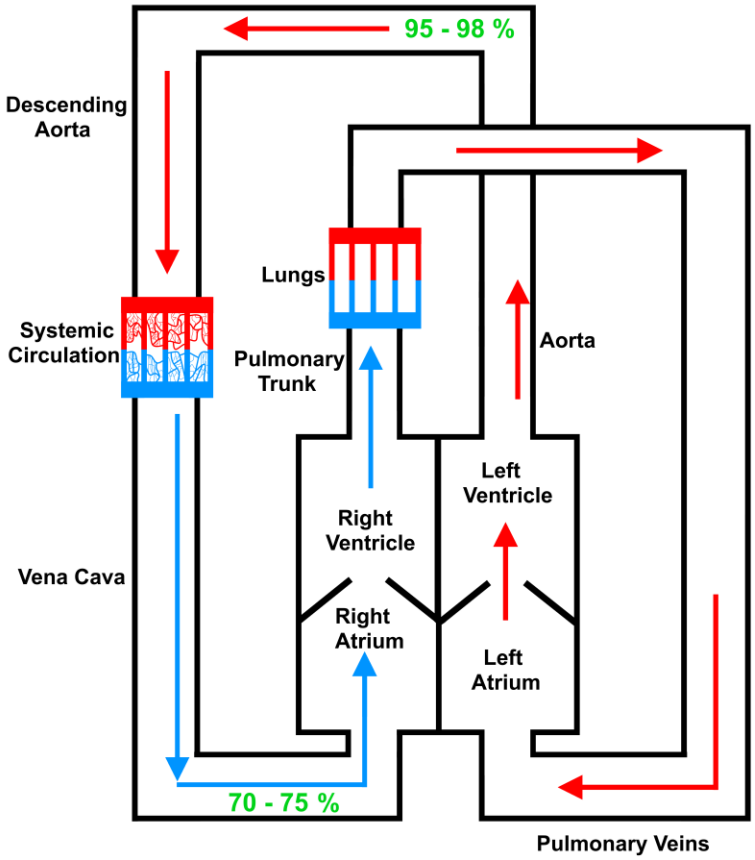

Supplementary Figure 11.7: diagram of the blood circulation in a healthy newborn, representing the directions of blood flow with the oxygen saturation levels.

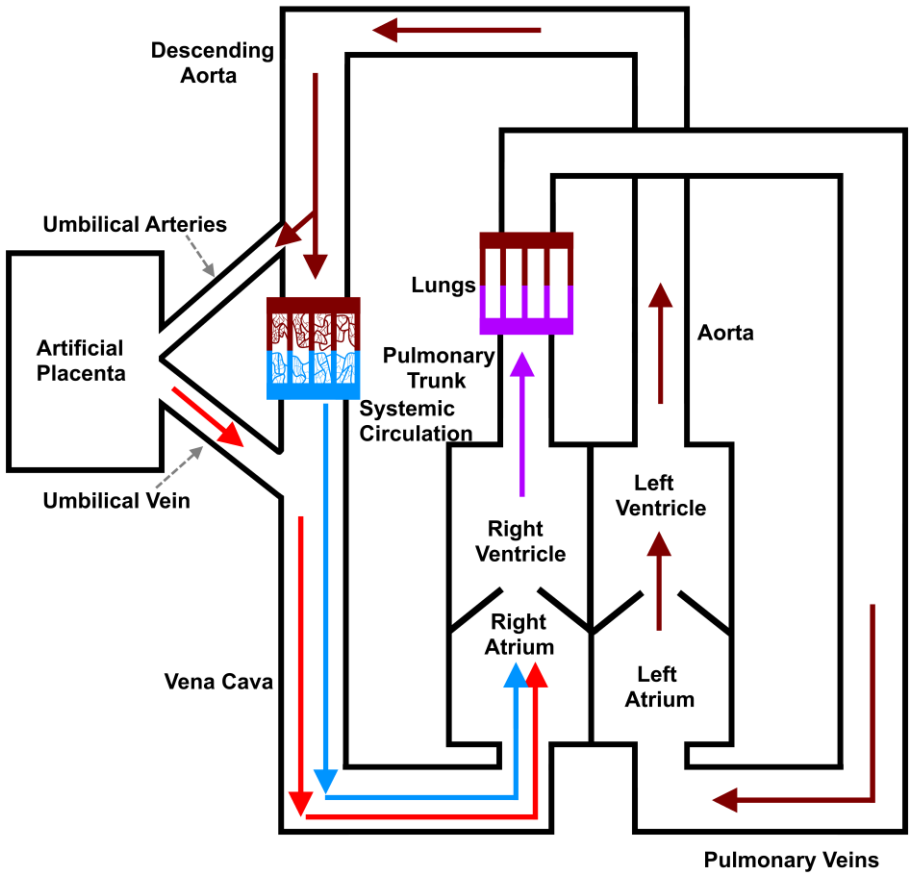

Supplementary Figure 11.8: diagram of the blood circulation in a preterm newborn connected to an artificial placenta device for oxygenation, representing the directions of blood flow with the oxygen saturation levels.

11.5 Systemic oxygen saturation measured by pulse oximeter

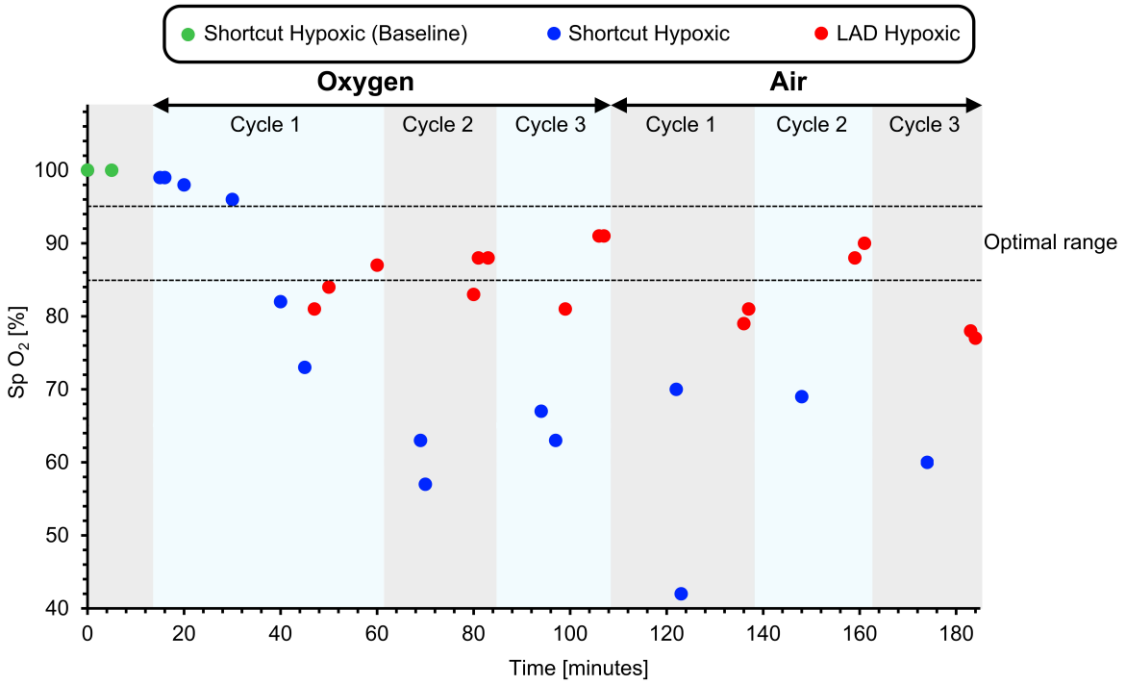

Supplementary Figure 11.9: systemic oxygen saturation level measured by a pulse oximeter placed on the left foot.

References

[1] Y. I. Cho and K. R. Kensey, "Effects of the non-Newtonian viscosity of blood on flows in a diseased arterial vessel. Part 1: Steady flows," *Biorheology*, vol. 28, no. 3/4, pp. 241–262, 1991.

[2] B. M. Johnston, P. R. Johnston, S. Corney, and D. Kilpatrick, "Non-Newtonian blood flow in human right coronary arteries: steady state simulations," *J. Biomech.*, vol. 37, no. 5, pp. 709–720, 2004.

[3] M. Dabaghi *et al.*, "An artificial placenta type microfluidic blood oxygenator with double-sided gas transfer microchannels and its integration as a neonatal lung assist device," *Biomicrofluidics*, vol. 12, no. 3, 2018.

[4] J. Jopling, E. Henry, S. E. Wiedmeier, and R. D. Christensen, "Reference Ranges for Hematocrit and Blood Hemoglobin Concentration During the Neonatal Period: Data From a Multihospital Health Care System," *Pediatrics*, vol. 123, no. 2, pp. e333–e337, 2009.

[5] J. E. Jones and P. A. Jose, "Neonatal Blood Pressure Regulation," *Semin. Perinatol.*, vol. 28, no. 2, pp. 141–148, 2004.

[6] K. Bauer, C. Uhrig, P. Sperling, K. Pasel, C. Wieland, and H. T. Versmold, "Body temperatures and oxygen consumption during skin-to-skin (kangaroo) care in stable preterm infants weighing less than 1500 grams," *J. Pediatr.*, vol. 130, no. 2, pp. 240–244, 1997.